XIX RUSSIAN PARTICLE ACCELERATOR CONFERENCE

Proceedings of the Conference

Joint Institute for Nuclear Research

XIX RUSSIAN PARTICLE ACCELERATOR CONFERENCE

Dubna, October 4–8, 2004

Proceedings of the Conference

Oral and Invited Contributions

Dubna • 2005

УДК 621.384.6(063)
ББК 22.381.1я.431
R95

CONFERENCE ORGANIZATION

ORGANIZED BY

Russian Academy of Sciences
Ministry for Industry and Energy of the Russian Federation
Ministry for Science and Education of the Russian Federation
Russian Foundation for Basic Research
Joint Institute for Nuclear Research

PROGRAMME COMMITTEE

Chairman *A. N. Skrinsky*, INP SB RAS
Vice-Chairman *I. N. Meshkov*, JINR
Scientific Secretary *G. V. Trubnikov*, JINR

A. I. Ageev, SSC RF IHEP; *A. N. Lebedev*, PI RAS; *V. V. Parkhomchuk*, INP SB RAS; *A. V. Pheshchenko*, INR RAS; *V. A. Romanov*, SSC RF IPPE; *B. Yu. Sharkov*, SSC RF ITEP; *Yu. M. Shatunov*, INP SB RAS; *G. D. Shirkov*, JINR; *E. M. Syresin*, JINR; *E. F. Troianov*, SSC RF IHEP; *N. A. Vinokurov*, INP SB RAS; *M. F. Vorogushin*, NIIEPA; *N. V. Zavyalov*, VNIIEF, Sarov

ORGANIZING COMMITTEE

Chairman *V. G. Kadyshevsky*, JINR
Vice-Chairmen *I. N. Meshkov*, JINR; *G. D. Shirkov*, JINR
Scientific Secretary *G. V. Trubnikov*, JINR
Secretary *V. K. Novikova*, JINR

E. V. Akhmanova, JINR; *N. I. Balalykin*, JINR; *G. G. Gulbekyan*, JINR; *Yu. V. Kozlov*, Ministry for Science and Education of the Russian Federation; *L. A. Kalmykova*, JINR; *A. D. Kovalenko*, JINR; *S. O. Lukyanov*, JINR; *V. M. Maximov*, Ministry for Industry and Energy of the Russian Federation; *V. V. Petrov*, BINP SB RAS; *A. V. Philippov*, JINR; *G. G. Sandukovskaya*, JINR; *E. E. Shirkova*, JINR; *L. V. Soboleva*, JINR; *T. A. Stepanova*, JINR; *E. V. Strekalovskaya*, JINR; *E. M. Syresin*, JINR; *N. A. Tokareva*, JINR

The contributions are reproduced directly from the originals presented by the Organizing Committee.

ISBN 5-9530-0079-0

PREFACE

The XIX Russian Particle Accelerator Conference (RuPAC-2004) was held from 4 to 8 October at the Joint Institute for Nuclear Research. The conference was supported by JINR, the Russian Academy of Sciences (RAS), the Russian Federal Atomic Energy Agency, Ministry for Education and Science of the Russian Federation, and the Russian Foundation for Basic Research. Chairman of the Programme Committee Academician A.N. Skrinsky made a salutatory talk at the opening ceremony.

The All-Union (now the All-Russian) RuPAC conferences have a long history. Academician Alexander Mints raised the flag of these conferences and first four of them were held in Moscow. Since 1976 the conferences took the title of All-Union and were held in Dubna for a period of time. Later they were held in Protvino at the Institute for High Energy Physics. In 2002 the accelerator forum moved to Obninsk to the Institute of Physics and Energy and was held as the All-Russian particle accelerator conference. The abbreviation RuPAC was established there which is traditional for accelerator conferences in the world, like the European EPAC, Asian APAC and American PAC events.

The present conference RuPAC is integrated into the international system, which is called the Joint Accelerator Conferences Website (JACoW), – a world accelerator community, which formally exists under the aegis of international physics unions, has a site with a free access to the library of proceedings of accelerator conferences.

The fact that the number of the conference participants has grown much recently indicates that the scientific potential of the Russian accelerator physicists is on a high level, and the interest to the RuPAC conference increases. 268 officially registered participants attended the conference plenary sessions, and, besides, free listeners arrived (as a rule, students and graduate students from Moscow universities and institutes). It is a pleasure to note a considerable amount of young attendees – about one third of all participants.

Physicists and engineers, working in the field of physics and technology of accelerators, from many scientific, educational and industrial centres of Russia took part in the conference: they were from Moscow, Saint Petersburg, Novosibirsk, Protvino, Obninck, Sarov, Troitsk, Nizhnii Novgorod, Dubna, and also from the world leading accelerator laboratories such as DESY, Forschungzentrum Jülich, GSI (Germany), CERN (Switzerland), FNAL (USA), ORNL (USA), NIRS and KEK (Japan), University of Sannio (Italy), the Kharkov Physics and Technology Institute (Ukraine), the Institute for Nuclear Research of NAS (Kiev, Ukraine), the Physics and Technology Institute, Sukhum (Georgia).

A total of 79 oral reports and 129 posters gave the full representation of the modern status of the accelerator science and technology at the conference. They covered a wide spectrum of the directions of the scientific studies: from problems of the development of new accelerators at ultra high energy, improvement and reconstruction of already existing accelerators up to the trend of the development and wide use of the accelerators in industry and medicine. The main topics of the conference were:

- Modern trends in accelerator development, colliders;
- Particle dynamics in accelerators and storage rings, cooling methods, new methods of acceleration;
- High-intensity cyclic and linear accelerators;
- Heavy-ion accelerators;
- Synchrotron-radiation sources and free-electron lasers;

Designations

The first and second letters denote the weekday (**MO** – Monday, **TU** – Tuesday, **WE** – Wednesday, **TH** – Thursday, **FR** – Friday).
The third letter classify the session (see the **List of Classifications**).
The last two ciphers are the number of the report.

List of Classifications

A Modern Trends Of Accelerator Development, Colliders
B Beam Dynamics In Accelerators And Storage Rings, Cooling Methods, New Methods Of Acceleration
C High Intensity Cyclic And Linear Accelerators
D Heavy Ion Accelerators
E Synchrotron Radiation Source And Free Electron Lasers
F Superconducting Accelerators And Technology Of Cryogenics
G Accelerating Structures And Powerful Electronics
H Control And Diagnostic System
I Ion Sources, Electron Guns, Injectors
J Accelerators For Medical And Industrial Purpose
K Radiation Problem In Accelerators
L Magnetic Systems, Power Supply And Vacuum Systems For Accelerators
M Injectors
N Cyclotron Session

CONTENTS

ELECTROPHYSICAL SYSTEMS BASED ON CHARGED PARTICLE ACCELERATORS

M.F. Vorogushin,
FSUE "D.V. Efremov Scientific Research Institute of Electrophysical Apparatus",
St. Petersburg, Russia

INTRODUCTION

The advancement of the charged particle accelerator engineering affects appreciably the modern tendencies of the scientific and technological progress in the world. In a number of advanced countries, this trend is one of the most dynamically progressing in the field of applied science and high-technology production. Such internationally known firms as VARIAN, SIEMENS, PHILIPS, ELECTA, IBA, HITACHI, etc., with an annual budget of milliards of dollars and growth rate of tens of percent may serve as an example. Although nowadays the projects of new large-scale accelerators for physical research are not implemented so quickly and frequently as desired, accelerating facilities are finding ever-widening application in various fields of human activities.

The contribution made by Russian scientists into high-energy beams physics is generally known. High scientific and technical potential in this field, qualified personnel with a high creative potential, modern production and test facilities and state-of-the-art technologies give grounds for us to aim to be among the world leaders in the designing and construction of applied accelerators.

ELECTROPHYSICAL SYSTEMS DEVELOPED IN NIIEFA

The complete process of the accelerating equipment manufacturing is implemented in the D.V. Efremov Institute, NIIEFA starting from the development of new acceleration principles and designing of new models of accelerating equipment and up to its small-scale production, on-site installation, personnel training, offering warranty/after-warranty service and supervision services practically through the whole operating lifetime of the equipment. Recently special attention is paid to the designing of electrophysical systems based on charged particle accelerators with complete production cycle. Further we shall consider the current status of the main systems.

Diagnostic Radiotherapy System

The main purpose of radiotherapy is suppression of tumor growing with a minimal effect on adjacent healthy tissues. With this aim in view, the radiotherapy treatment approach should provide radical effect on pathologic process with minimized dangerous consequences for patient.

The efficiency of radiotherapy treatment depends on clinical and biological factors, such as tumor radiosensibility, radiation tolerance of adjacent tissues involved in the treatment process, stage of disease, etc. These factors are mostly revealed in the process of patient's diagnostics. If radiotherapy is prescribed, a treatment approach is planned: areas to be treated are chosen, critical organs are found out, levels of radiation doses on the target and allowable doses in critical points are specified. The treatment approach is presented in the form of clinical prescriptions for radiotherapy treatment.

The experience of world-advanced radio-therapeutic centers shows that the required quality level of treatment can be achieved only by implementation of integrated computer-based technology, which covers all the stages of radiotherapy treatment.

Rradiotherapy system and clinical diagnostic means should have the following functions. Examination of patients and choice of treatment strategy should be done in clinics using their available diagnostic facilities. In the process of examination the data about patient will be input in the information system. As diagnostic means available in clinics differ greatly, implementation of inexpensive specialized soft-hardware systems seems highly expedient at the initial stage to load diagnostic data in the database.

When a clinic is equipped with modern anatomic and topometric means ensuring direct data exchange with the computer of such a system, there appears a possibility to involve these means in the computerized radiotherapy process.

With this aim in view, works on the development of a prototype of a double-detector gamma-tomograph has been performed in NIIEFA since 2003 in the framework of the "Nuclear Medicine "program [1].

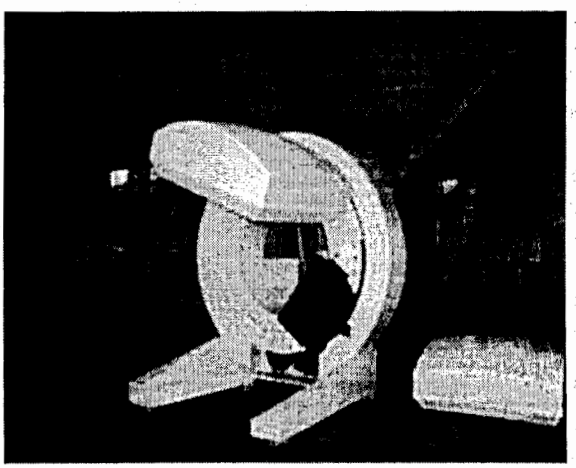

Figure1: The gantry with the detector units

In the digital detector unit, analog signals are transformed at the output of each photomultiplier and are further processed with a digital processor. The detector unit is equipped with a system of IR probes detecting objects within 5-10 m from the detector surface, thus allowing the implementation of the maximum resolution of the system in tomographic studies.

The detector units (up to two in number) are fixed to the gantry (see Fig. 1), which ensures their radial and angular movements by means of electric drives. The gantry is equipped with an electron microprocessor-based system providing both manual and computer control of detector positioning.

The current year we plan the engineering test of the gamma-tomograph prototype.

Construction of a positron-emission tomograph is a natural result of further works on diagnostics [2]. At present we have a team of highly skilled personnel involved in these works (NIIEFA, ITEP, CNIRRI). Provided support from ROSATOM, we consider it possible to have finished the designing of the main components of the tomograph by the end of 2005 and then start the engineering tests of the first domestic PET-center.

The radiotherapy system EFARAD [3] consists of: linear medical accelerators LUER–20M and SL75-5-MT, a radiotherapy topometric system TSR-100, a treatment planning system ScanPlan, an information system Inforad and a treatment verification system VeriRad.

The linear accelerator LUER-20M is intended for remote radiotherapy with photon beams and electrons with energies ranging from 5 to 20 MeV in static and arc modes. The accelerator allows one to perform complete course of treatment of the majority of oncological patients and may be used for medico-biological research. In July, 2004 the physical startup of the upgraded model of LUER-20M was realized in Yerevan. The machine meets international requirements MEC-601-1 and offers potentialities for stereotactic irradiation.

The linear electron accelerator SL75-5-MT is the basic therapy machine intended for radiotherapy with 6 MeV photon beams in static and arc modes. More than 50 similar machines have been designed and manufactured in NIIEFA and delivered to clinics in Russia.

The X-ray topometric system for radiotherapy TSR-100 is the basic means for preparation of treatment prescriptions. The system is intended for solution of biometrical problems of oncological patients and for verification of treatment plans. The system provides both projection images of a patient body (in the radiotherapy machine geometry with contouring radiation field) and transverse computer tomograms at specified levels. Thus the system combines both an X-ray simulator and a computer tomograph (CT). Conventional fluoro imager is replaced with a digital system for radiation registration equipped with a moving mechanism and collimators for fan-shaped X-ray beam scanning.

The treatment planning system ScanPlan provides planning of treatment with photon beams for any linear medical accelerator, though the main task is treatment planning for the SL75-5–MT accelerator.

The information system InfoRad contains computer-based workstations for doctors and radiology physicists, which are connected with the treatment system units, databases and archives. The system covers all the stages of radiotherapy process.

The EFARAD system is built by the module principle thus allowing flexible distribution of functions between the system hardware and upgrading the system by adding new modules. The system modules are integrated through standard interfaces and form a flexible automated information system intended for implementation of the closed cycle of radiotherapy process [4].

The prospects for further advancement of the radiotherapy system are discussed in detail in our report to be made on the conference.

Systems for Non-destructive Testing

Industrial systems for non-destructive inspection designed and constructed in NIIEFA are based on RF accelerators with electron energy ranging from 3 to 15 MeV. These systems are intended for radiographic inspection of defects in large-scale products with an equivalent steel thickness from 40 up to 600 mm. The systems are successfully used for non-destructive inspection of products of nuclear power plant industry, nuclear shipbuilding and in other fields.

Let's consider in brief one of the latest model of such accelerators with an electron energy up to 16 MeV at an X-ray dose rate up to 120 Gy/min (1 m from target). The general view of the irradiator is given below in Fig.2.

Figure 2: The UEL-15-D accelerator irradiator

The irradiator houses the accelerating structure, RF power supply system and pulse modulator. Nevertheless, the weight of the irradiator is no more than 1100 kg and its overall sizes are: 2040×880×920 mm^2, which is much less than those of foreign analogs. This can be attributed to its the rational layout, application of the KIU-111 low-voltage klystron (power – 6 MW, anode voltage-no more than 55 kV) and a 2 m long optimized biperiodical accelerating structure without focusing solenoids and

coils. The primary cone collimator forming the irradiation field is located at the accelerator inlet.

Nowadays, such innovative methods of non-destructive inspection as radioscopy and tomography are implemented.

In radioscopyy an object is scanned layer-by-layer with a fan-shaped X-ray beam. A line of scintillator detectors is used instead of X-ray film. The shadow image of defect is visualized on the monitor of the operator's workstation [5]. Compared to radiographic inspection, the radioscopic one offers lower operating costs and reduced time for data processing. The efficiency is several factors of ten higher, as the inspection is implemented practically in the real time mode. However, the radioscopic inspection is effective when testing objects with a thickness only no more than 350 mm (for steel).

When applied to radioscopy, a standard set of the linear accelerator equipment is supplemented with: a beam collimation system, detection system, system for positioning an object under inspection and operator's workstation with software.

The beam collimation system is intended for beam forming. It consists of three collimators: the primary collimator installed on the radiation source, the secondary collimator installed in front of an inspected object and a collimator placed in front of the detector line.

The positioning system servers to ensure linear travel of an inspected object perpendicular to the axis of the fan-shaped beam. To change the angle, the inspected object is rotated in the beam plane. The measuring element is the detector line of cadmium tungstate ($CdWO_4$) crystals installed behind the last collimator.

Special software serves for the data processing and visualization; it ensures preliminary processing of data and their digitization, data correction, image filtration and pseudo-colorization. The computer workstation allows the reconstruction of the object shadow image with a subsequent analysis of defects detected. Upon detecting a defect, an operator can localize and zoom up the fragment to have better opportunities for the defect sizing and spotting.

In the radioscopic systems developed in NIIEFA, the latest advances in the linear accelerators engineering, electronics and computer technology were applied, that made it possible to attain high spatial (about 1-2 mm) and density resolution (better than 1%) at an accelerator energy of 16 MeV.

Two-dimensional image obtained under radioscopic scanning can be easily interpreted when an inspected object is of simple internal structure. However, in some cases the structure of inspected object can be unambiguously identified only with computer- aided tomography.

Under tomographic inspection every object section is scanned under continuous or discrete rotation of object in the plane of the fan-shaped beam formed by the irradiator and beam collimation system. The data obtained as a result of angular scanning are written in file in the digital form and processed with methods of mathematical reconstruction. The application of the described procedure to a consequence of cross-sections allows one to obtain a complete image of the three-dimensional density distribution in an inspected object. The set of tomographic system equipment is similar to that of radioscopic system with some modifications made in the design of the positioning system and software.

Fig. 3 demonstrates introscopic and tomographic images of an inspected object.

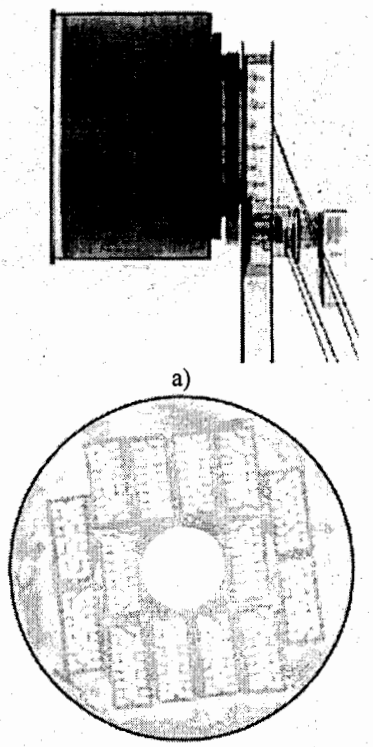

Figure 3: a) the introscopic image of inspected object, b) the tomographic reconstruction of the object.

EFASCAN System for Radioscopic Inspection of Large-scale Cargoes

As a result of increasing volume of world trade and increasing number and variety of terrorist acts assassinated all over the world there is an insistent need for effective inspection of all transported cargoes in the real time mode to detect weapons, ammunition and contraband goods. With this aim in view, an EFASCAN radioscopic inspection system has been developed in NIIEFA. It is intended for examination of vehicles and large-scale containers without their opening and is distinguished with high throughput [6].

Depending on the way of transportation (auto, sea, air), three versions of the system are suggested.

"EFASCAN" (see Fig. 4) allows the inspection of large-scale containers in a special radiation shielded hall. Radioscopic examination of objects is performed by means of the fan X-ray beam, which is generated by a

linear electron accelerator. During the scanning the transportation system moves the examined object across the X-ray beam with a constant speed of 0.4 m/s. Penetrated through the object radiation is registered by a detector line. Signals from the detectors are preliminary processed and transmitted to the workstations of the customs officers. The throughput of the system is 25 containers (2.5×2.5×12 m) per hour.

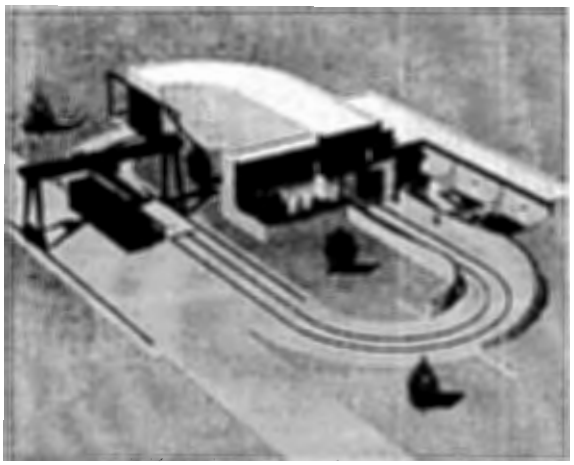

Figure 4: General view of the EFASCAN complex building

The basic (minimal) set of the equipment consists of: a linear electron accelerator, X-ray beam collimation system, detector line, data transfer system, data processing and visualization system, system for transportation of inspected objects, radiation, electrical and mechanical safety system, automated control system, cargo shipping documents input system and archiving system.

"EFASCAN" can be supplemented with the following options:

- Stereo viewing system of cargo content with an additional equipment such as second detector line, data transfer system, data processing and visualization system, two-slit X-ray collimation system, IR control polarization glasses and a special software. The system allows obtaining volume stereo image of cargo.
- System with two accelerators and double set of equipment, which allows X-ray images of the container in two projections – horizontal and vertical.
- System with dual energy of accelerator, which provides discrimination of groups of materials in the inspected object according to their average atomic number. Colored information on material of inspected cargo is visualized on the display of operator's workstation. The system facilitates the inspection routine of customs officers and detection of smuggled materials such as narcotic and explosive substances, non-ferrous and precious metals, etc.

In one of the modifications of the "EFASCAN-2" inspection system, the attending personnel is protected against ionizing radiation with local shields and due to remote control of the accelerator. Special crane is used for the transportation of the linac, detector line and X-ray beam collimation system.

It should be noted that with an available specialized vehicle, a mobile facility for inspection of cargoes on roads can be constructed. With this object in view, a small-size accelerator with local radiation shielding has been designed and manufactured in NIIEFA and is effectively used on customs inspection facilities HCV – MOBILE of the HEIMANN S.A. firm. Rational layout of the accelerator, module design of the radiation shielding made it possible to have such a compact irradiator 1480 kg in weight and 850×200×975 mm in size (see Fig.5). The energy of electrons can be chosen in the range from 1.9 to 4 MeV by changing the number of accelerating cells with the sizes of the irradiator kept unchanged.

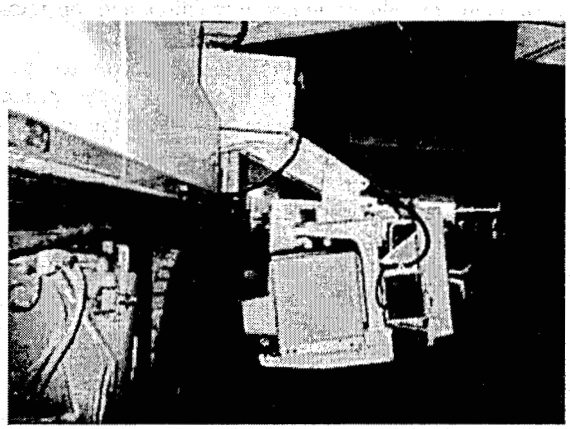

Figure 5: Linac for mobile inspection system.

"EFASCAN-3" is intended for the radioscopic examination of freight trains moving with a speed of 15 km/h maximum. A special detection system provides a spatial resolution up to 10mm and density resolution up to 1%. Protection against ionizing radiation is provided with local shields and due to remote control of the accelerator.

Main Advantages of the Above Systems:

- Continuous round-the-clock operation of customs checkpoint resulting in its higher throughput, efficiency and quality of inspection with low expenditures for its implementation.
- Obtaining most exhaustive real-time information on the object under inspection.
- High-speed data processing and high quality of images ensured by applied software.
- Opportunity to compare the actual contents of inspected containers with the cargo declared in the cargo manifest.
- Archiving the obtained data.
- Opportunity of scrupulous analysis of suspicious items with no reduction of the system throughput due to several available workstations.

System for Detection of Explosive, Fissionable and Narcotic Substances of Vegetable Origin

Nuclear methods are highly promising for detection of explosive, fissionable and narcotic substances and these are precisely nuclear methods, which may ensure further progress in this field.

The works on the development of a system intended for detection of explosive (ES) and fissionable (FS) substances are in progress in NIIEFA. The system is based on a compact linear RF accelerator of deuterium ions generating pulse flows of neutrons up to 10^{14} n/pulses by impinging a special target. The detection method is based on ES identification from nitrogen, oxygen and carbon atoms: their high concentrations unambiguously testify presence of explosive substances in an inspected object. Compared to other available means, this method offers an appreciably lower level of false alarms.

Nowadays, production facilities for manufacturing such systems are available, the accelerator and the interaction chamber have gone into production, the multi-detector system and electron apparatus used for generation and processing of signals from an inspected object have been manufactured, the major part of the software is available, and accelerating structures undergo tests. To test the detection system and the detection method itself, measurements were done with a beam of neutrons produced on a cyclotron. Analysis of the results has shown that radiation lines produced by constituent elements of ES can be identified. In practice, gamma-radiation background will be reduced due to the pulse operating mode of the accelerator and applied synchronous detector method. Considerable difficulties were experienced in manufacturing the accelerators with RFQ structures with an operating frequency of 433 MHz. However, after purchasing a modern precision versatile machine tool, a new process for electrodes' machining was developed, which allowed us to adhere to specified tolerances of 10 microns for dimensions defining the field symmetry and electrodes' modulation .We plan to carry out engineering tests of the system as early as next year.

CONCLUSIONS

The experience gained in the development and construction of electrophysical systems in NIIEFA allows us to draw some general conclusions concerning the trends for further progress of applied accelerators.

First, these accelerators, in themselves, are not in great demand both in Russia and abroad. To provide a final result of (diagnosis, treatment, customs document, processing or any ready product), the electrophysical systems call for an additional electrophysical equipment to be designed. In addition, creation of such systems usually involves contractors competent in corresponding fields of science and engineering sometimes, foreign partners. Besides, a designing firm should be granted the international quality certificate for production of corresponding electro-physical equipment, be entitled for training of operating personnel, have a possibility of remote diagnostics, warranty and after-warranty service of the equipment (i.e. should have service center).

I wish to draw your attention that in the present-day contracts and tenders, in addition to competitive performances of the equipment all the above-said requirements are stipulated.

Second, components of the electrophysical systems should be compatible in hardware and software, complete computer control should be provided and controls on the operator's panel should be minimum in number.

Third, the software of such systems is of prime importance, as it embodies the major part of intellectual labor (results of research, technological know-how and possible options).

In conclusion, I would like to express hope that accelerator-based electrophysical systems will become attractive in economic, financial and innovative aspects and will be widely applied not only to industry and medicine but also will come into use in everyday life.

REFERENCES

[1] M.F. Vorogushin, Yu.N. Gavrish, A.V. Sidorov, V.L. Novikov, G.G. Shimchuk, V.B. Sergienko, D.A. Ovsyannikov, "Designing of the prototype of the two-detector gamma-tomograph", Abstracts of the Conference "Topical Issues of Nuclear Medicine and Radio-pharmaceutics", Dubna (June 20-26, 2004), Dubna, p. 275.

[2] G.G. Shimchuk et al, "Potentialities and Outlooks of PET-centers in Russia, "Proceedings of the Xth Meeting on Applied Accelerators", St.Petersburg, 2001. pp. 197-200.

[3] M.F. Vorogushin et al, "Computer-aided System for Radiotherapy", The XVII th Meeting on Accelerators. Protvino, 2000, v.2, pp. 366-369.

[4] S.V. Kanaev, M.F. Vorogushin, V.A. Shyshov, "Characteristics of Domestic System for Radiotherapy of Oncological Patients", Voprosy Onkologii, St.Petersburg, 2003, v.49, №5, pp. 668-675.

[5] Yu.N. Gavrish et al, "Comprehensive System for Non-destructive testing", Proceedings of the XVIIth Meeting on Accelerators, Protvino, 2000, v.2, pp. 317-322.

[6] M.F. Vorogushin et al, System for Customs Inspection of Vehicles and Large-scale Containers "EFASCAN". VANT, series "Electrophysical Apparatus", St.Petersburg, 2002, №1 (27), pp. 42-45.

STATUS OF THE COOLER SYNCHROTRON COSY-JUELICH AND FUTURE PLANS

J. Dietrich*, U. Bechstedt, R. Eichhorn, R. Gebel, K. Henn, V. Kamerdzhiev, A. Lehrach, B. Lorentz, R. Maier, D. Prasuhn, H. Schneider, R. Stassen, H. Stockhorst, R. Tölle,
Forschungszentrum Juelich, 52425 Juelich, Germany

Abstract

The cooler synchrotron COSY delivers unpolarized and polarized protons and deuterons in the momentum range 300 MeV/c up to 3.70 GeV/c. Electron cooling at injection momentum and stochastic cooling covering the range from 1.5 GeV/c up to maximum momentum are available to prepare high precision beams for internal as well as external experiments in hadron physics. The beam is fed to external experiments by a fast kicker extraction or by stochastic extraction.
In particular results of recent runs with the beam stabilizing transverse feedback system for intense electron cooled beams are reported. Future plans are briefly discussed.

INTRODUCTION

The accelerator facility [1,2] consists of the injector cyclotron JULIC, the synchrotron and storage ring COSY with 184 m circumference and experimental areas. Unpolarized and polarized protons and deuterons are accelerated in the momentum range from 300 to 3650 MeV/c. The floor plan of COSY with its 4 internal and 3 external experimental areas is shown in figure 1.

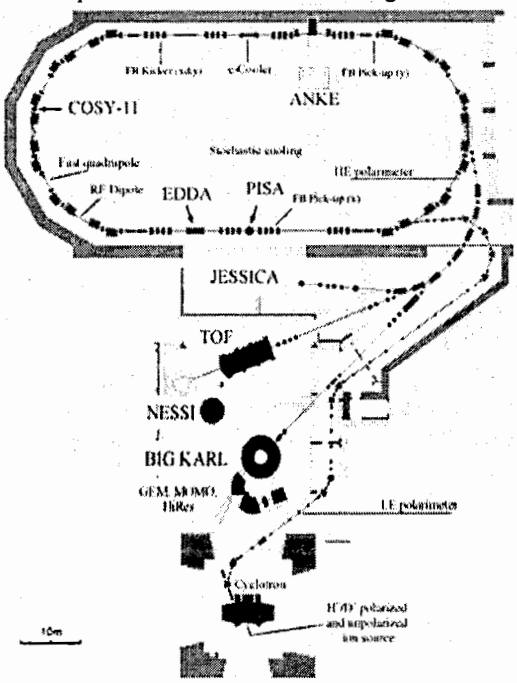

Figure 1: The COSY floorplan

The main topic of research is the production and interaction of strange mesons close to production threshold. Increasing the phase space density by electron cooling at injection momentum and conservation of beam emittance during experiments on the circulating beam (internal) at high momenta by use of the stochastic cooling system are the two outstanding features of COSY.

BEAM TIME STATISTICS

COSY has improved its running over the 11 years of operation from 3500 h per year in 1993 up to 7500 h in 2003. The reliability of COSY increased from 80 % in the first year of operation to more than 90 % in the last years. Approximately 2/3 of the year is dedicated to user operation. Figure 2 shows the beam time distribution during the year 2003.

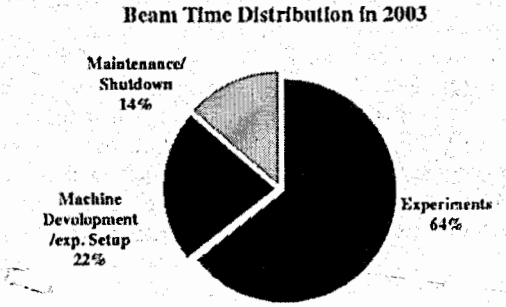

Figure 2: Beam time distribution

In the first years of COSY operation, only unpolarized protons were requested by the experiments. This has changed over the years, as the demand for polarized proton and deuteron beams increased. Unpolarized deuterons were available first for the MOMO collaboration in the beginning of 2002. Polarized deuterons with different combinations of vector and tensor polarization were successfully delivered to the experiments in 2003 (Figure 3).

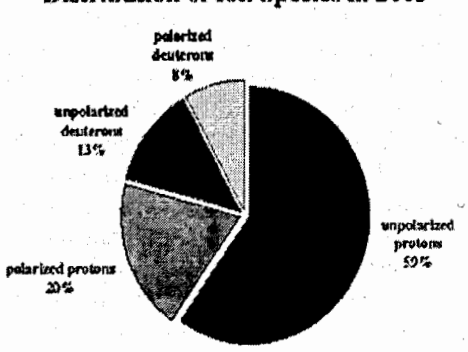

Figure 3: Beam time distribution among the ion species

*j.dietrich@fz-juelich.de

Table 1 shows a summary of the different operation modes and ion species with the achieved particle intensities after acceleration.

Table 1: Particle intensity of the accelerated beam for the different ion species and operation modes

Unpolarized Protons	Single injection	$1.4*10^{11}$
	Single injection with electron cooling	$1.5*10^{10}$
	Multiple injection with electron cooling and stacking	$5.0*10^{10}$
Polarized Protons	Single injection	$1*10^{10}$
	Single injection with electron cooling	$5.0*10^{9}$
	Multiple injection with electron cooling and stacking	$1.2*10^{10}$
Unpolarized Deuterons	Single injection	$1.3*10^{11}$
	Single injection with electron cooling	$4*10^{10}$
Polarized Deuterons	Single injection	$6*10^{9}$

BEAM FEEDBACK AND STACKING

The intensity of the electron cooled coasting ion beam at COSY is limited by two different particle loss mechanisms [3]. The interplay of the electric field of the electron beam and ions with large betatron amplitudes passing the cooler section outside the electron beam is assumed to be responsible for incoherent losses directly after injection. Particle losses after several seconds of cooling are due to coherent transverse beam oscillations. These oscillations are caused both by the increase of the space charge impedance and the weak Landau damping due to the small momentum spread of the cooled beam [4]. Fig. 4 shows the beam current signal indicating incoherent losses directly after injection and coherent losses after 20 s together with beam position monitor (BPM) Δ-signals indicating horizontal and vertical oscillations.

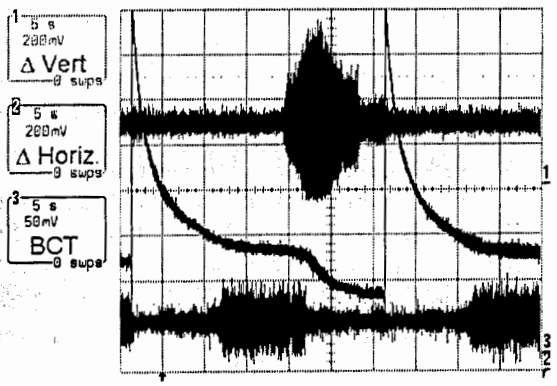

Figure 4: Beam behaviour during electron cooling. The beam current transformer (BCT) signal (black) is plotted together with horizontal (red) und vertical (blue) BPM Δ-signals. Time scale is 5 s/div

The dominating particle loss is due to the vertical oscillation because of the larger amplitude and the smaller aperture of the vacuum chamber.

A transverse feedback (FB) system, also called damper, makes it possible to damp coherent beam oscillations without any change of the machine optics [5]. BPM Δ-signals in the frequency domain (Fig. 5) and the beam current signal (Fig. 6) illustrate the performance of the FB system in the vertical plane.

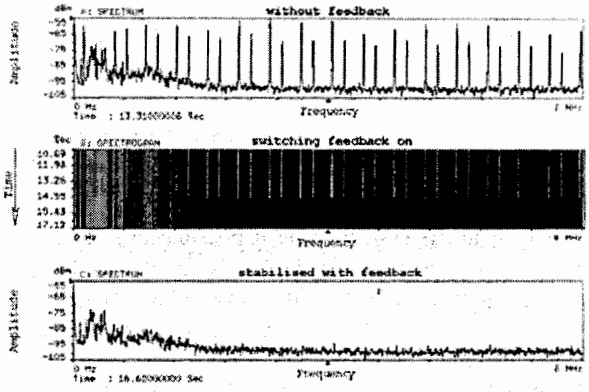

Figure 5: Fast Fourier transform of the vertical BPM Δ-signal of the electron cooled coasting proton beam at injection energy without FB (spectrum A), switching vertical FB on (spectrogram B), FB is on (spectrum C)

Without FB, betatron sidebands corresponding to the vertical coherent beam oscillation are observed. Switching the FB on makes them disappear.

Another very useful application of the FB system is stacking [2] the electron cooled ion beam by repeated injections (Fig. 7) to increase the intensity. In the case of stacking the beam of a single injection is cooled by the electron cooling system for two seconds. Then the closed orbit of the stored beam is again moved close to the stripper foil without loosing the cooled stored beam, and a new injection takes place, adding intensity to the stored beam. This procedure can be repeated many times to increase the total intensity of the stored beam while the electron cooler operates continuously.

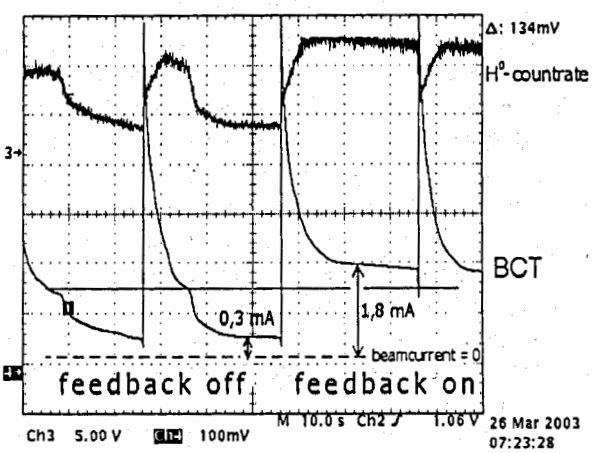

Figure 6: BCT and H^0-countrate signals without FB and with FB switched on. Time scale is 10 s/div

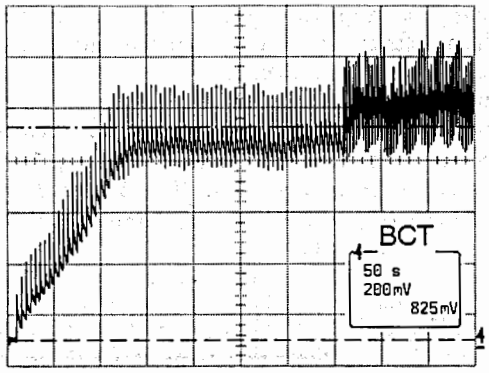

Figure 7: BCT signal during stacking of the cooled proton beam with active vertical FB. Time scale is 50 s/div. Intensity scale is 200 mV/div (2 mA beam current)

The vertical FB system made it possible to stabilise the cooled proton beam at a level of $2*10^{10}$ particles (1.8 mA) after a single injection. With the stacking technique a maximum of $1.2*10^{11}$ cooled protons (9.2 mA) at injection energy.

In September 2004 the horizontal FB system was successfully commissioned.

The intensity of single injected uncooled polarized beams in COSY is limited to approximately $1*10^{10}$ particles, because of the lower intensity of the polarized beam available at injection. However, due to the short beam lifetimes at injection energy and the long cooling time (several seconds), the intensity of the beam is reduced by approximately one order of magnitude. To increase this intensity, stacking injection is applied. By use of the vertical FB it was possible to reduce the particle losses and increase the intensity of the stacked beam to $1.2*10^{10}$ stored polarized protons. In particular for the TRIC experiment 15 injections with 4 s. intervals are stacked using electron cooling (I_e=170mA) and vertical FB giving $8*10^9$ polarized protons in flat top at 1.692 GeV/c. The flat top time is 1 hour.

FUTURE PLANS

The electron cooling at COSY (electron energy 25-100 keV) corresponds to proton energies up to 184 MeV. Electron cooling at electron energies of about 2 MeV [6] is considered as a necessary intermediate step towards the electron cooler, foreseen for the High Energy Storage Ring (HESR) of the GSI Darmstadt future accelerator project. Thus it will play a central role in conjunction with the involvement of the Forschungszentrum Juelich, Institute of Nuclear Research in designing and building the HESR. It will also be a good use for fast compensation of beam heating by high-density internal targets at COSY.

Further improvements are also planned for the experimental facilities, e.g.:

ANKE: installation of spectator detectors and polarized target (atomic beam source plus storage cell

TOF: implementation of a silicon microstrip telescope, a straw tube tracker in vacuum and frozen spin polarized target

WASA: transfer of the WASA detector from CELCIUS (Uppsala, Sweden) to COSY [7].

For the electron cooler and WASA detector installation additional funding is needed.

SUMMARY

COSY is a unique accelerator in the medium energy range for polarized and unpolarized beams of protons and deuterons. It delivers beam to users for over 5400 hours per year with a high reliability of more than 90 %. During 2003 the availability of polarized deuteron beams with different combinations of vector and tensor polarization for experiments at the COSY accelerator facility was added. A transverse feedback system is very useful when fighting coherent beam oscillation. Since it does not affect the tune it can be turned on and off without any changes in the machine optics. Installing the vertical and horizontal dampers at COSY gave significant intensity increase at single injection and the possibility of stacking electron-cooled beams. Future plans are the design of a 2 MeV electron cooler and installation of the WASA detector in COSY.

ACKNOWLEDGEMENTS

We appreciate the helpful discussions on electron cooling and beam stability with H.J. Stein, I.N. Meshkov, V.V. Parkhomchuk.

REFERENCES

[1] R. Maier, Cooler Synchrotron COSY – performance and perspectives, NIM A 390 (1997) 1-8.

[2] H. Stockhorst et al., Progress and Developments at The Cooler Synchrotron COSY", Proceedings of the 8th European Particle Accelerator Conference (EPAC 02).

[3] H.J. Stein et al., Intensity Limits of Electron-Cooled Ion Beams at COSY, IKP Annual Report 2002.

[4] V. Kamerdzhiev et al., Instability phenomena of electron-cooled ion beams at COSY, Nucl. Instr. Methods, in press.

[5] V. Kamerdzhiev et al., Transverse Feedback System for the Cooler Synchrotron COSY-Jülich – First Results, Proc. DIPAC-2003.

[6] V.V.Parkhomchuk, private communication.

[7] J. Greiff, Investigation of Inelastic Reactions in Deuteron Proton Collisions Between Td=437 and 559 MeV Using the PROMICE/WASA Detector at CELSIUS, PhD thesis, University of Hamburg, 1999.

THE "SALO" PROJECT

Yu.M. Arkatov, A.V. Glamazdin, A.N. Dovbnya, I.S. Guk,
S.G. Kononenko, F.A. Peev, A.S. Tarasenko
National Science Center "Kharkov Institute of Physics and Technology",
1 Akademicheskaya St., Kharkov, 61108, Ukraine,
M. van der Wiel, J.I. Botman Technische Universiteit Eindhoven, Den Dolech 2, P.O. Box 513,
5600 MB Eindhoven, The Netherlands

Abstract

The NSC KIPT (Ukraine) and the Technische Universiteit Eindhoven (The Netherlands) are now considering the possibility of creating the electron accelerator that would meet the present-day requirements of the physical experiment. The recirculator circuit with the use of a superconducting accelerating structure TESLA is found to hold the most promise.

Technological decisions and circuit designs have been chosen to create the machine with an energy up to 730 MeV and with a continuous beam for investigations into high energy physics, nuclear physics, neutron physics and free-electron laser (FEL) physics.

INTRODUCTION

The Kharkov electron linacs LU-2000 and LU-300, built in the sixties of the last century, have become hopelessly obsolete, both morally and physically. The attempt to create a stretcher at the accelerator LU-2000 also appeared unsuccessful. The nuclear power engineering demands in Ukraine for scientific investigations and a rapid decrease in the number of specialists in the area of nuclear physics and engineering generate a need for creating a new accelerating installation that would meet the current requirements of the physical experiment. As it became clear from the analysis of physical programs on nuclear physics and devices used for the investigations [1-4], the electron accelerator must provide a continuous polarized electron beam of energy higher than 50 MeV. At present, the most promising accelerating structure for this accelerator seems to be a superconducting continuous-beam accelerating section developed for the linear collider TESLA. With the use of an RF-gun photo- injector, this structure may also provide short electron bunches needed for FELs and the neutron source.

THE CHOICE OF THE ACCELERATOR SCHEME

In the early eighties the majority of 100 ... 2000 MeV electron linacs built before exhausted their potentials for the use in nuclear physics experiments because of the small ratio of pulse length to the interpulse time. The second life of the accelerators was expected to be given due to the use of storage rings-beam stretchers, owing to which it was expected to extend the filling factor up to 50 ... 80%. About 15 projects of the facilities were proposed. By 2002, only 6 projects were realized:

1. Pulse Stretcher Ring EROS (Electron Ring of Saskatchewan),
2. Amsterdam Pulse Stretcher (APS), NIKHEF,
3. MAX I, MAX-lab, Lund,
4. SHR, MIT-Bates Linear Accelerator Center,
5. Electron accelerator ELSA, Bonn,
6. KSR, Kyoto University.

For the last decade there have no new stretcher designs, and the idea is dying together with physical destruction of old accelerators. By the present time the EROS and APS facilities have been shut down and disassembled; the nuclear-physical studies are performed only at three installations: MAX I, SHR, ELSA. The parameters of ejected beams in the stretchers are worse than in continuous microtrons and recirculators, therefore all nuclear-physical programs of the closed facilities were taken up to the accelerators of Jlab and MAMI.

The most part of nuclear-physical investigations with electron beams is conducted at present at continuous-beam facilities: S-DALINAC (TH Darmstadt), MAMI (Mainz U), and CEBAF (Jlab) [1-4]. The progress in the development of superconducting structures has put forward the possibility of creating superconducting linear accelerators with energy from 1 to 2 GeV that would operate in the continuous mode. With these accelerators as the basis it will be possible to develop higher-energy accelerators using the idea of multiple pass of the beam through the accelerator.

THE ACCELERATING STRUCTURE

At the moment it is the superconducting accelerating structure TESLA, devised at DESY, that has the parameters most suitable for electron acceleration. Developed are the processes for mass production of sections, cryomodules, and also, a few methods for the treatment of section surfaces that provide altogether the accelerating gradient up to 35 MV/m at a continuous mode of operation [5]. At really operating facilities that incorporate several sections, a 1 mA current was obtained in the continuous mode of operation [6] at an accelerating gradient of 10 MV/m. The performance characteristics of sections are time-stable and do not deteriorate the operating parameters provided that all service requirements are met. Several types of cryomodules were designed and manufactured for different numbers of sections. [4].

In all accelerator designs proposed, a 20 MV/m accelerating gradient was chosen as the one that can provide a rather high acceleration rate at moderate

expenditures for cooling the continuously operating sections [4]. At this gradient the refrigerator power, counting on one section, does not exceed 26 W at a temperature of 1.8 K.

High-frequency (1300 MHz) amplifiers with an average power up to 30 kW have been designed and are really in operation at continuous-beam facilities.

THE ELECTRON INJECTORS

The main lines of applicability of the accelerator under design are nuclear-physical investigations, intense neutron beam production and use, creation of FELs and their use for physical studies. To cope with the tasks, it is necessary to have several injectors at the accelerator.

To perform many nuclear and physical investigations at energies higher than 50 MeV, polarized electron beams are needed. Here, the polarized electron sources of the MAMI microtron and the Thomas Jefferson National Accelerator Facility [7, 8] present the greatest interest as prototypes, because the micro- and macrostructure of the beams from these accelerators are close to the ones expected at the SALO facility. These sources provide quasi-continuous electron beams with a current up to 100 μA, polarization of ~ 80-90% and a continuous running period of the injector equal to a few hundreds of hours.

For the injectors of neutron sources and FEL, of importance are the requirements of obtaining the highest possible values of average current and the current in the bunch. The photoinjectors with a RF gun most fully meet these requirements [4], because this design makes it possible to accelerate the highest charge in the bunch. For the facility under development, the superconducting RF gun-based injector being developed for the ELBE accelerator can be taken as a prototype [9]. The gun uses 3 + ½ cavities of the accelerating structure TESLA at a frequency of 1300 MHz. The charge in the bunch is up to 1 nC, the average current is up to 1 mA.

THE RECIRCULATOR WITH A SUPERCONDUCTING ACCELERATING STRUCTURE FOR AN ENERGY OF 400 TO 750 MEV

First of all, we discuss the restrictions on the overall dimensions of the accelerator, following from the possibility of placing it in the existing rooms of the linear accelerator LU-2000 (see Fig. 1).

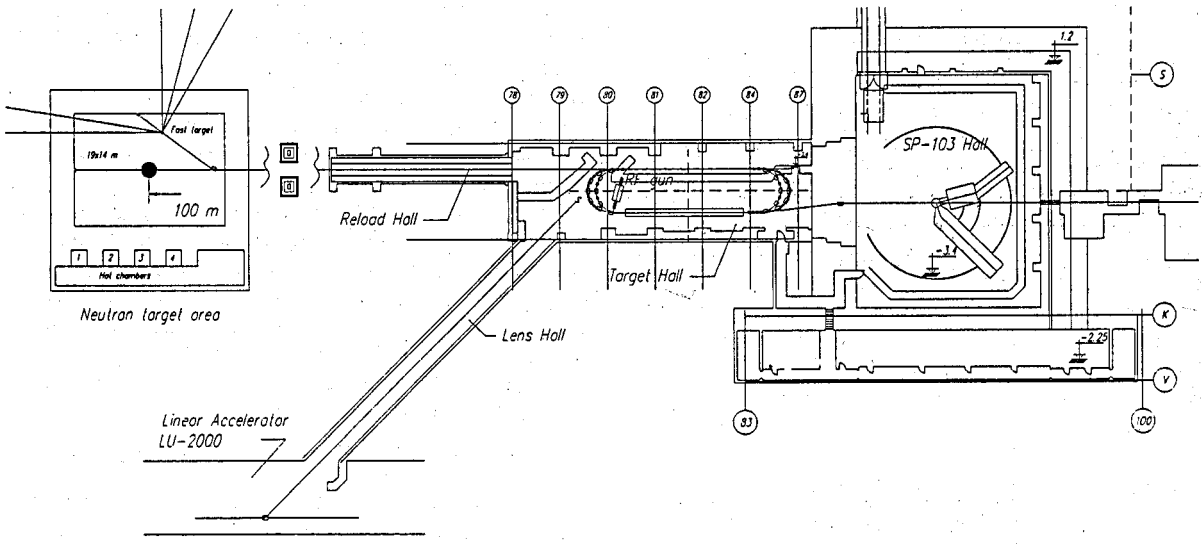

Fig.: 1

The target hall appears to be the most suitable place to install the recirculator. This is due to the fact that the target hall is adjacent to the hall SP-103 accommodating the magnetic spectrometer, and also to Building 46 that can be used to place the accelerator complex control. The hall SP-103 can be used for both accommodating new spectrometers and the experiments with FEL radiation. The reload hall, via which the equipment was admitted to the target hall, may also accommodate the equipment designed for experiments with the electron beam and the FEL radiation. Across this hall, the electron beam will be transported to the neutron source. Along the lens corridor, the beam may be guided to the LU-2000 bunker and the pre-existing hall of direct exit. So, the location of the recirculator in the target hall permits not only the use of the pre-existing experimental halls, but also the construction of some new rooms. The floor area that may accommodate the recirculator elements is equal to 3739m^2.

The elaboration of the recirculator design is performed by the NSC KIPT and the Technische Universiteit Eindhoven (The Netherlands) on the basis of the Agreement about joint creation of the accelerator at the NSC KIPT that would meet the present-day requirements of the physical experiment.

For realization of the project, in 2003, in the framework of the Agreement, the Technische Universiteit Eindhoven (The Netherlands) transferred 10 dipole magnets and 32 quadrupole magnets of the electron storage ring EUTERPE to the NSC KIPT.

Twelve sections placed in a standard 15.927 m long cryostat, designed for the TESLA collider, were chosen as an accelerating system. The accelerating gradient is expected to be 20 MeV/m. The first turn of beam is accomplished by means of 10 magnets of the storage ring EUTERPE (B1) (see Fig. 2), the second turn is realized with the use of other-type 10 magnets (B2). Electrons of 9.5 MeV energy are injected into the recirculator magnet with its yoke turned outside. With this arrangement of the gun in the recirculator, the highest beam energy will be obtained in the SP-103 hall. The spacing between the straight gaps of the recirculator is equal to 5.45 m; the gap length is 19 m. The beam focusing will call for 20 quadrupoles. The second straight gap may be used to accommodate the undulator for the FEL.

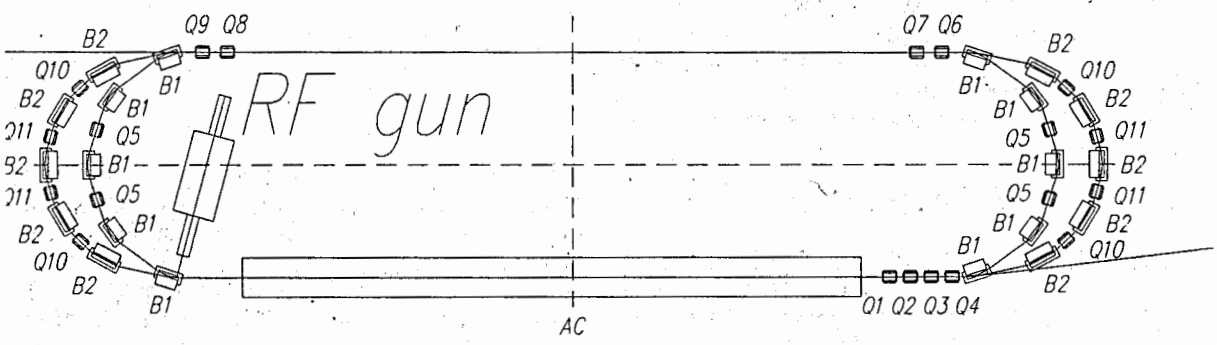

Fig.: 2

The injection magnet (see Fig. 2) bends the beam from the injector, that acquires a 240 MeV gain in the accelerating structure and may be used in the SP-103 hall. With five magnets switched on the beam may be directed to the reload hall and further, to the neutron target. With additional 5 magnets of the first ring in the "on" condition the beam will pass through the accelerating structure for the second time, and being of 490 MeV energy may be used in the SP-103 hall. As the first five magnets of the second ring are switched on, the beam may be used in the reload hall, in the neutron target hall; and when the other two magnets of this ring are switched on, the beam may be directed to the LU-2000 bunker. A full actuation of all the magnets of the second ring makes it possible to produce a 730 MeV electron beam in the SP-103 hall. The target beam current will not exceed 100 μA.

At neutron-source operating conditions, the energy gain at the accelerating structure is expected to be 120 MeV, the current on the uranium or tungsten target is to be 1 mA.

REFERENCES

[1] V.B. Ganenko, O.G. Konovalov, A.Yu. Korchin, N.I. Maslov, N.G. Shevchenko, Perspective directions of experimental research on fundamental physics at intermediate energies on the proposed 730 MeV electron accelerator NSC KIPT // *Problems of Atomic Science and Technology. Series: Nuclear Physics Investigations.* 2004. № 5(44), p. 166-169.

[2] *OPPORTUNITIES IN NUCLEAR SCIENCE. A Long Range Plan for the Next Decade.* The DOE/NSF Nuclear Science Advisory Committee, U.S. Department of Energy Office of Science Division of Nuclear Physics, National Science Foundation Division of Physics Nuclear Science Section, April 2002.

[3] *NUPECC LONG RANGE PLAN 2004: PERSPECTIVES FOR NUCLEAR PHYSICS RESEARCH IN EUROPE IN THE COMING DECADE AND BEYOND,* edited by: Muhsin Harakeh, Daniel Guerreau, Walter Henning, Mark Huyse, Helmut Leeb, Karsten Riisager, Gerard van der Steenhoven and Gabriele-Elisabeth Korner. NuPECC REPORT, April 2004.

[4] Yu.M. Arkatov, A.V. Glamazdin. I.S. Guk, A.N. Dovbnya, S.G. Kononenko, M. van der Wiel, J.I.M.Botman, F.A. Peev, A.S. Tarasenko. *BASELINE ACCELERATOR FACILITY AT NSC-KIPT FOR NUCLEAR AND HIGH-ENERGY PHYSICS RESEARCH. "SALO" PROJECT.* National Science Center – Kharkiv Institute of Physics & Technology, Kharkiv, 2004, 94 p.

[5] Lutz Lilje .High gradients in TESLA nine-cell cavities. // *TESLA collaborating Board Meeting.* Frascati, 28 May 2003.

[6] P. Michel , A. Buchner, P.Evtushenko, F. Gabriel, U. Lehnert, J. Teichert and J.Voigl ander for the ELBE-crew FZ Rossendorf, Strahlungsquelle ELBE, PF 510119, D-01314 Dresden, Germany, Comissioning Of The Elbe Superconducting Electron Linac *//Proceedings of EPAC 2002, Paris, France/* p. 817-819.

[7] Ch. Nachtigall, E. Reichert, M. Schemies, M. Steigerwald, K. Aulenbacher, H. Euteneuer, D. v. Harrach, P. Hartmann, J. Hoffmann, P. Jennewein, K.-H. Kaiser, H. J.Kreidel, M. Leberig, J.Schuler, C. Zalto The new polarized beam injection at MAMI *//Proceedings of the EPAC 98/* p.1430-1432.

[8] M. Baylac et.al. *Jefferson Lab polarized electron source.* SRF Conference. September 2002. 31 p.

[9] Jochen Teichert, Hartmut Buettig, Pavel Evtushenko, Dietmar Janssen, W.-D. Lehmann, Ulf Lehnert, Peter Michel, Christof Schneider, Juergen Stephan (FZR, Dresden), Vladimir Volkov (BINP SB RAS, Novosibirsk), Ingo Will (MBI, Berlin), A Superconducting Photo-Injector with 3+1/2- Cell Cavity for the ELBE Linac, *//Proceedings of the EPAC 2004/* p. .

LASER COOLING IN ELECTRON STORAGE RING AND ITS LIMITS

A.N. Lebedev
P.N.Lebedev Physical Institute, Moscow, Russia

Abstract

The evolution of synchrotron and betatron emittances of an electron beam under action of laser irradiation and consequent emission of hard quanta is analyzed. Dependencies of the cooling rate on structure functions at the irradiation point as well as on the parameters of the electron and laser beams are calculated and optimized. The invariance of the sum of the decrements is proved.

The work is fulfilled within the frames of NATO grant SfP-977982.

INTRODUCTION

The possibility of generation of monochromatic X-ray radiation by backward scattering of laser light at a relativistic electron beam attracts now special attention [1, 2]. The frequency transformation easily follows from simple kinematic relations and has an order of magnitude of $4\gamma^2$, where γ is Lorentz factor. Besides, the scattered X-rays are well directed (angle $\sim 1/\gamma$)what is typical for radiation from high energy electrons. A weak point of the method is a rather small cross-section which imposes serious requirements upon the laser power and the beam density.

It is rather obvious that electron beams circulating in a storage ring are preferable from this point of view if their life-time is large enough. The latter depends on many factors including transverse spreading of the beam inherent in the method and caused by the recoil of emitted hard quanta. This effect is well known for cyclic accelerators in connection with quantum fluctuations of synchrotron radiation. However, in our case a quantum is essentially harder and requirements to the beam transverse size are more stressed.

Similarly, one could count on radiation cooling also inherent in the scattering process. Really, a radiation quantum should be re-emitted practically along the instantaneous velocity of a relativistic electron which gets both longitudinal and transverse recoil momentum. The first is restored by the RF compensating system while the second produces radiation "friction" exactly in the same way as in synchrotrons. Although one can not expect really strong damping for existing parameters the effect has to be considered because the spectral and angular distribution of the scattered light differs from that in synchrotrons and depends on parameters of the laser beam.

LASER COOLING

We neglect below intrinsic damping due to synchrotron radiation and consider electrons performing independent synchrotron and betatron oscillations:

$$y = x + R\psi u; \tag{1}$$

$$x = \sqrt{\frac{\varepsilon}{\pi}}\beta^{1/2}\cos\int\frac{ds}{\beta}; \tag{2}$$

$$x' = \sqrt{\frac{\varepsilon}{\pi}}\beta^{-1/2}\left(\frac{\beta'}{2}\cos\int\frac{ds}{\beta} - \sin\int\frac{ds}{\beta}\right);$$

$$u = \sqrt{\frac{\epsilon}{\pi}}\sqrt{\frac{\Omega}{q\alpha}}\cos\int\Omega ds; \tag{3}$$

$$u' = -\sqrt{\frac{\epsilon}{\pi}}\sqrt{\frac{q\alpha}{\Omega}}\sin\int\Omega ds. \tag{4}$$

Here u is a relative energy deviation from the equilibrium value, β and ψ are periodic structure functions of the magnetic system, R is the mean radius of the equilibrium orbit, primes denote derivatives with respect to the equilibrium orbit arc s, q is an RF field harmonic number, $\alpha = \overline{\psi}$, Ω is a synchrotron oscillations frequency in rotational frequency units. The values ε and ϵ have the meaning of area enclosed by phase trajectory ellipsis in phase planes (x, x') and (u, u') correspondingly being integrals of motion. For bounding phase trajectories they are identified as transverse and longitudinal emittances. Being expressed via phase plane coordinates they are equal to

$$\frac{\varepsilon}{\pi} = \frac{x^2}{\beta} + \frac{1}{\beta}\left[\frac{x\beta'}{2} - \beta x'\right]^2; \tag{5}$$

$$\frac{\epsilon}{\pi} = \frac{q\alpha}{\Omega}u^2 + \frac{\Omega}{q\alpha}u'^2. \tag{6}$$

Meeting a laser photon at the light and electron beams crossing point the electron energy is instantaneously changed by the value Δu keeping the coordinates y and u' and the instantaneous velocity y' constant (see Fig.1).The latter means that the scattered photon is emitted perfectly along the electron trajectory. With the same precision one can neglect the energy change when a relatively soft laser photon is absorbed. As a result, the integrals ε and ϵ experience instantaneous changes:

$$\frac{\Delta\varepsilon}{2\pi R\Delta u} = x\left[-\frac{\psi}{\beta} + \beta'\beta^{1/2}\left(\frac{\psi}{\beta^{1/2}}\right)'\right] - \tag{7}$$

$$-\beta^{3/2}x'\left(\frac{\psi}{\beta^{1/2}}\right)' + \ldots;$$

$$\frac{\Delta\epsilon}{2\pi R\Delta u} = \frac{q\alpha}{\Omega}u + \ldots. \tag{8}$$

Here and below the structure functions and their derivatives are taken at the crossing point. A destination of the second order changes will be considered later.

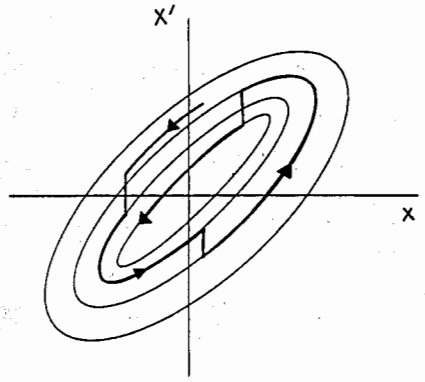

Figure 1:

To find the average variation rate $d\varepsilon/ds$ and $d\epsilon/ds$ the expressions above are to be multiplied by the scattering probability $P(\Delta u, y, y', u, u')$ and averaged over all betatron and synchrotron phases. To do this we present the probability as an expansion

$$P(\Delta u, y, y', u, u') = \tag{9}$$
$$= P_0 + \frac{\partial P}{\partial y} y + \frac{\partial P}{\partial y'} y' + \frac{\partial P}{\partial u} u + \frac{\partial P}{\partial u'} u' .$$

The first term here is the probability of "ideal" collision with the equilibrium electron, the second and the third ones describe coordinate and angular discrepancies between the electron and light beam axis. The last term correspond to a possible influence of lack of synchronization between electron and light pulses.

Note that after averaging over phases denoted below by the angular brackets all terms of the first order with respect to y, y', u, u' vanish. Besides, it follows from (1) that:

$$\begin{aligned}
&\langle xy \rangle = \frac{\varepsilon}{2\pi}\beta; \quad \langle xy' \rangle = \frac{\varepsilon}{4\pi}\beta'; \\
&\langle xu \rangle = \langle xu' \rangle = 0; \quad \langle x'y \rangle = \frac{\varepsilon}{4\pi}\beta' \\
&\langle x'y' \rangle = \frac{\varepsilon}{2\pi\beta}\left(\beta'^2/4 + 1\right); \\
&\langle x'u \rangle = \langle x'u' \rangle = \langle uu' \rangle = 0; \\
&\langle u^2 \rangle = \frac{\epsilon}{2\pi}\frac{\Omega}{q\alpha}; \quad \langle u'^2 \rangle = \frac{\epsilon}{2\pi}\frac{q\alpha}{\Omega}.
\end{aligned} \tag{10}$$

So, we get:

$$\begin{aligned}
&\left\langle \frac{\Delta\varepsilon}{\varepsilon} \right\rangle = \Delta u \left[-\psi \frac{\partial P}{\partial y} - \psi' \frac{\partial P}{\partial y'} \right] R; \\
&\left\langle \frac{\Delta\epsilon}{\epsilon} \right\rangle = \Delta u \left[R\psi \frac{\partial P}{\partial y} + R\psi' \frac{\partial P}{\partial y'} + \frac{\partial P}{\partial u} \right].
\end{aligned} \tag{11}$$

Besides re-emission process the transverse emittance is influenced by the RF field necessary for radiation losses compensation. We shall suppose it being concentrated within a narrow accelerating gap normal to the equilibrium orbit. A particle gets there an instantaneous increase in energy, keeping y and u' constant. There is a simultaneous change of y' because the accelerating field does not change the transverse momentum $p_{mathrm y}$. For this reason the change of the emittance has to be calculated under condition $p_y = \text{const}$, or[1].

$$\Delta y' = \Delta \frac{p_y}{p} = -\frac{p_y}{p} u = -y'u, \tag{12}$$

as far as in the ultrarelativistic case the relative changes of energy and of total momentum are equal to each other. Moreover, the probability of the gain is now identically equal to unity because the energy income does not depend on the possible scattering at previous turns.

It easy to see that after averaging over phases the condition (12) gives an additional change of the emittance

$$\Delta\varepsilon = -\varepsilon u; \quad \Delta\epsilon = 0 \tag{13}$$

which does not depend on structure functions at the point of compensation.

Noting that $-P\Delta u$ and Δu are equal to the relative energy W emitted per one turn we get the increments of betatron and synchrotron oscillations damping :

$$\Gamma_b = -R\psi \frac{\partial W}{\partial y} - R\psi' \frac{\partial W}{\partial y'} + W; \tag{14}$$

$$\Gamma_s = R\psi \frac{\partial W}{\partial y} + R\psi' \frac{\partial W}{\partial y'} + \frac{\partial W}{\partial u}. \tag{15}$$

They have much common with the usual radiation damping decrements but contain the local values of the structure functions. In particular the theorem about the decrements sum [3] looks as

$$\Gamma_b + \Gamma_s = \frac{\partial W}{\partial u} + W. \tag{16}$$

It says that the coordinate and angular discrepancies of laser and electron beams do non influence the total phase volume and yield a decrement re-distribution only. By the way, the term proportional to the coordinate shift between the beams vanishes unless the beams have a zero crossing angle.

Bearing in mind that the intensity of radiation of a relativistic particle is proportional to the square of its energy the relation (16) can be rewritten as

$$\Gamma_b + \Gamma_s = 3W. \tag{17}$$

The laser cooling as opposed to synchrotron radiation one depends on the laser power and thus on the final output of hard quanta. Even in certain ambitious projects [2] the damping time can not be less than a second. This hardly might provide a serious limitation of the emittance growth due to quantum fluctuations discussed below.

[1] We do not consider here the influence of the magnetic component of the RF field which creates no additional damping [3]

EXCITATION BY RECOIL MOMENTUM FLUCTUATIONS

A quantum nature of radiation is described by the next terms of expansion of ε and ϵ over powers of Δu. A single emission act gives

$$\Delta_2\varepsilon = \pi R^2 (\Delta u)^2 \left[\frac{\psi^2}{\beta} + \beta^2\left(\frac{\psi}{\beta^{1/2}}\right)'^2\right]; \quad (18)$$

$$\Delta_2\epsilon = \pi R \frac{q\alpha}{\Omega} (\Delta u)^2 . \quad (19)$$

In the limit of $\hbar \to 0$ the value

$$\langle (\Delta u)^2 P_0 \rangle = E_q W$$

where E_q is a relative energy of the emitted quantum defined as

$$E_q = \langle (\Delta u)^2 P_0 \rangle / \langle \Delta u P_0 \rangle .$$

So, in average, the scattering process results in the emittances increase rate:

$$\frac{d\varepsilon}{ds} = \pi R^2 E_q W \left[\frac{\psi^2}{\beta} + \beta^2\left(\frac{\psi}{\beta^{1/2}}\right)'^2\right]; \quad (20)$$

$$\frac{d\epsilon}{ds} = \pi R \frac{q\alpha}{\Omega} E_q W .$$

This rate has to be compared with damping due to laser cooling. Note that both are proportional to the laser power so that the final steady-state emittance has an universal value of order of

$$\varepsilon_{st} \approx \frac{1}{\Gamma_b}\frac{d\varepsilon}{ds} \approx \pi R^2 E_q \left[\frac{\psi^2}{\beta} + \beta^2\left(\frac{\psi}{\beta^{1/2}}\right)'^2\right] .$$

This value determines, of course, whether the stored electrons can be exploited for a long time or they would be burning down and require continual reinforcement.

SCATTERING CROSS SECTION AND PHOTON ENERGY

To use the relations obtained above one has to know the the cross section of the process as a function of the incident photon angle. The differential cross section for a solid angle do is [4]:

$$\frac{d\sigma}{do} = 2r_0^2 \frac{(\Delta u)^2}{\kappa_1^2} \times \quad (21)$$

$$\times \left[4\left(\frac{1}{\kappa_1} + \frac{1}{\kappa_2}\right)^2 - 4\left(\frac{1}{\kappa_1} + \frac{1}{\kappa_2}\right) - \left(\frac{\kappa_1}{\kappa_2} + \frac{\kappa_2}{\kappa_1}\right)\right]$$

where

$$\kappa_1 = -2(\Delta u)_i \gamma (1 - \beta\cos\theta_i); \quad (22)$$

$$\kappa_2 = 2(\Delta u)\gamma(1 - \beta\cos\theta) . \quad (23)$$

Index i here and below marks values related to an incident photon, θ is an angle between the direction of the photon and the particle velocity. The energies of an incident and scattered photons are related by:

$$(\Delta u) = (\Delta u)_i \frac{1 - \beta\cos\theta_i}{1 - \beta\cos\theta + (\Delta u)_i (1 - \cos\mu)} \quad (24)$$

where μ is an angle between their directions:

$$\cos\mu = \sin\theta \sin\theta_i \cos\nu - \cos\theta\cos\theta_i \quad (25)$$

and ν is a polar angle in do.

For small angles θ the value $1 - \beta\cos\theta$ reaches its minimum of the order of $1/2\gamma^2$ then increases sharply starting from angles $\approx \gamma^{-1}$. So, for all angles of interest

$$1 - \beta\cos\theta \gg (\Delta u)_i$$

if the particle energy $\gamma \ll mc^2/\hbar\omega_i$. This condition means neglect of quantum Compton effect and is well fulfilled for all parameters of interest.

Following the standard procedure we get after some arithmetic in the relativistic limit, i.e. for $\cos\theta_i$ differing markedly ($> \gamma^{-2}$) from unity:

$$\frac{W}{W_i} = \frac{8\pi}{3}\frac{r_0^2}{BS}\gamma^2 (1 - \cos\theta_i) \quad (26)$$

where S is the average cross section of the interaction region, $B > 1$ is a bunching factor and r_0 is the electron classical radius.

To complete the picture note that in the same limit the averaged frequency multiplication factor is:

$$\left\langle \frac{\omega}{\omega_i} \right\rangle = \frac{7}{5}\gamma^2 (1 - \cos\theta_i) . \quad (27)$$

It is lesser than the ideal value $4\gamma^2$ even for head-to-head collisions because of averaging over emission angles. Note that the relations (26) and (27) are not valid for collinear beams.

ON OPTIMIZATION OF THE STRUCTURE FUNCTIONS

It is easy to see that to make the emittance growth smaller[2] the value of

$$U = \frac{\psi^2}{\beta} + \beta^2\left(\frac{\psi}{\beta^{1/2}}\right)'^2 \quad (28)$$

[2] Sometimes this is a square of transverse deviation what should be minimized.

should be as small as possible while the mutual geometry of the electron and light beams can influence the decrements redistribution only (here and below β is again a structure function).

Note that the structure functions ψ and β are not independent as far as $\psi(s)$ is a periodic solution of

$$\psi'' + g(s)\psi = \frac{K(s)}{R}, \tag{29}$$

while the amplitude function β satisfies the nonlinear equation

$$\left(\beta^{1/2}\right)'' + g(s)\beta^{1/2} = \beta^{-3/2}. \tag{30}$$

with the same focussing function $g(s)$. Here $K(s)$ is the equilibrium orbit curvature.

Multiplying (29) by $\beta^{1/2}$ and (30) by ψ gives the general equation relating the structure functions

$$\beta\frac{\mathrm{d}}{\mathrm{d}s}\beta\frac{\mathrm{d}}{\mathrm{d}s}\left(\frac{\psi}{\beta^{1/2}}\right) + \left(\frac{\psi}{\beta^{1/2}}\right) = \frac{K}{R}\beta^{3/2}. \tag{31}$$

Using this relation and differentiating U with respect to s to find an extremum we have:

$$U' = \left[\frac{\psi^2}{\beta} + \beta^2\left(\frac{\psi}{\beta^{1/2}}\right)'^2\right]' = 2\frac{K}{R}\beta^{3/2}\left(\frac{\psi}{\beta^{1/2}}\right)'. \tag{32}$$

Thus, U reaches its extremal values at the same points where $\psi/\beta^{1/2}$ does while

$$U_{\mathrm{ext}} = \left(\frac{\psi^2}{\beta}\right)_{\mathrm{ext}}. \tag{33}$$

Within a straight section U is a non-zero constant which can be expressed in terms of the positive β function. Really, considering $\phi = \int \mathrm{d}s/\beta$ as an independent variable in (32) we obtain

$$\left[\frac{\mathrm{d}^2}{\mathrm{d}\phi^2} + 1\right]\left(\frac{\psi}{\beta^{1/2}}\right) = \frac{K}{R}\beta^{3/2} \tag{34}$$

with the periodicity conditions in the interval $0 < \phi < 2\pi\nu$ where $\nu = (2\pi)^{-1}\int_0^{2\pi R}\mathrm{d}/\beta$ is the betatron oscillation frequency. The solution is straightforward:

$$\frac{\psi}{\beta^{1/2}} = \int_0^{\phi}\frac{K}{R}\beta^{3/2}\sin(\phi-\phi')\,\mathrm{d}\phi' + \tag{35}$$
$$+\frac{1}{2\sin\pi\nu}\int_0^{2\pi\nu}\frac{K}{R}\beta^{3/2}\sin(\pi\nu+\phi-\phi')\,\mathrm{d}\phi'.$$

At a point of an extremum where $\left(\psi/\beta^{3/2}\right)' = 0$ the function U reaches the value

$$U_{\mathrm{ext}} = \frac{1}{4\sin^2\pi\nu}\left[\left(\int_0^{2\pi\nu}\frac{K}{R}\beta^{3/2}\cos\phi'\mathrm{d}\phi'\right)^2\right.$$
$$\left.+\left(\int_0^{2\pi\nu}\frac{K}{R}\beta^{3/2}\sin\phi'\mathrm{d}\phi'\right)^2\right]. \tag{36}$$

So, one can say that the excitation of oscillations always takes place. To minimize it a defocusing (?) lense could be helpful at the crossing point as well as negative curvature portions of the equilibrium orbit with large values of β function.

REFERENCES

[1] F.Arutyunian, V. Tumanian. Phys. Lett. **11** (1963) 176; R. Milburn. Phys. Rev. Lett. **10** (1963)75

[2] A.Agafonov et al. Problems of Atomic Science and Technology. Series: Nuclear Physics Investigations **1**(2001)126

[3] A.Kolomensky and A.Lebedev. Theory of Cyclic Accelerators, North Holland (1965)

[4] A. Akhiezer and V. Berestetsky. Quantum Electrodynamics (in Russian). Fizmatgiz, Moscow (1949)

INTENSIVE ION BEAM IN STORAGE RINGS WITH ELECTRON COOLING

Yu.Korotaev, I.Meshkov, A.Sidorin, E.Syresin, JINR, Dubna, Russia
J. Dietrich, V.Kamerdjiev, R.Maier, D.Prasuhn, H.J.Stein, H.Stockhorst, FZJ, Juelich, Germany
K.Noda, S.Sibuya, T.Uesugi, NIRS, Chiba, Japan

Abstract

Results of experimental studies of the electron cooling of a proton beam at COSY (Juelich, Germany) and an ion beam at HIMAC (Chiba, Japan) are presented. Intensity of the ion beam is limited by two general effects: particle loss directly after the injection and development of instability in a deep cooled ion beam. Methods of the instability suppression, which allow increasing the cooled beam intensity, are described.

INTRODUCTION

Electron cooling method is widely used to increase an ion beam density in the six dimensional phase space. To increase intensity of the stored beam the stacking- cooling procedure is applied: injected beam is cooled to small dimensions and thereafter a new injection can be performed into free part of the ring acceptance. Such a procedure is repeated to saturation of the stored beam current. At high phase space density one of the general limitations of the ion beam intensity is related to development of coherent instabilities of the stored beam. Different types of instabilities developing at a high beam phase density were observed at a few coolers [1]. Specific instability, which appears directly at electron cooling application, was firstly observed in CELSIUS storage ring [2]. This instability leading to decrease of the ion beam life-time in the presence of an electron beam was named "electron heating".

Both types of instabilities were observed at COSY since beginning of the electron cooling system operation. Coherent instability of the stored ion beam limits the beam intensity at HIMAC storage ring. Results of the instability investigations performed at COSY and HIMAC during last years are presented in this report in comparison with previous results from CELSIUS and LEAR. At COSY the experiments were done with coasting proton beam at injection energy (45 MeV), at HIMAC - on coasting beam of Ar^{18+} at energy of 6 MeV/u. Aspecial attention is paid to study of an influence of the electron beam neutralization on stability of the circulating ion beam.

"ELECTRON HEATING"

The initial particle losses are resulted from strong diffusion process which power is proportional to the electron beam current. To investigate the diffusion at most clear conditions the ion beam lifetime can be measured at detuned electron beam energy. In this case the electron cooling does not work, but the electron beam noise acts on the injected beam and so called "electron heating" processes can play a role also. An example of results of such measurements at COSY is presented in the Fig. 1, where the electron energy is detuned by 2 keV from the value required for cooling. The proton beam lifetime increases with decrease of the proton beam intensity (Fig. 2) and after about 10 sec reaches saturation at relatively long value.

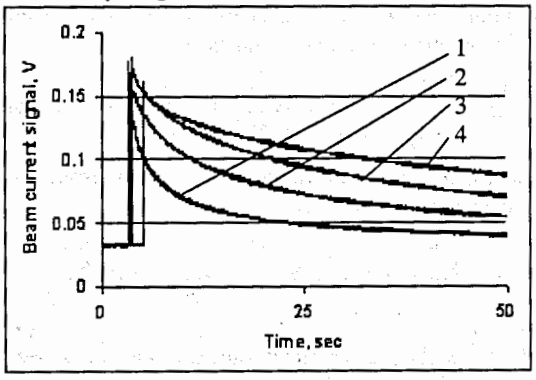

Fig. 1: Proton beam current as a function of time at electron beam current of 243 (1), 95 (2), 45 (3) and 0 (4) mA.

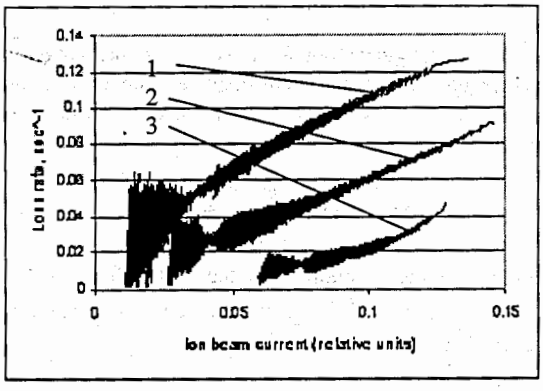

Fig. 2: Rate of the proton losses versus the beam intensity. Electron current is 243 (1), 45 (2) and 0 (3) mA.

Decrease of the beam intensity is related mainly to a loss of the particles with amplitude of betatron oscillations larger than electron beam radius. Nonlinearity of the electron beam self-fields can be a reason of the loss [2]. Other explanation proposed in [3] is based on assumption, that the interaction of the proton and electron beam leads to the proton beam coherent oscillations and electric field of these oscillations generate the proton beam heating.

At COSY the proton beam life-time in presence of the electron beam decreases by about 10 times, at CELSIUS

this effect is even more pronounced – the proton beam at injection (which practically coincides with injection energy at COSY) decreases by up to 100 times in presence of intensive electron beam. At HIMAC the ion beam life-time is not affected by the electron beam, but there the ion beam radius at injection is less than electron beam one.

COHERENT INSTABILITY

Single Injection

After fast losses caused by the "electron heating" and some period of the beam cooling new particle loss can appear due to coherent instability. After injection at COSY the initial losses take place during first 5 sec of the cooling process (Fig. 3, lower curve). The cooling process is accompanied by H^0 production in the cooling section (upper curve in the Fig. 3) and H^0 count rate increases during initial particle loss. It reflects the fact that the lost particles have an amplitude of betatron oscillations larger than electron beam radius. The H^0 count rate saturates at approximately the same moment as the proton beam intensity stabilizes.

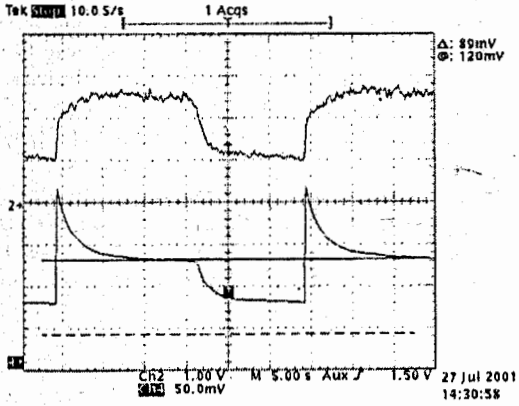

Fig. 3: Proton beam intensity at COSY during repeated injection at low frequency.

Coherent oscillations of the circulating beam starte after about 7 seconds of the cooling but initially do not lead to the particle loss. In the case presented in the Fig. 3 initially the dipole oscillations appeared in the longitudinal and horizontal plane. These oscillations were registered in the spectrum of the beam Schottky noise, or directly from pick-up electrodes using oscilloscope. After some period of time the horizontal oscillations were transformed to the vertical ones. The coherent oscillations of the beam in vertical plane lead to fast particle losses due to smaller value of the vertical acceptance.

Cooling - Stacking

The instability of the intensive proton beam in the cooling-stacking mode was investigated in details at COSY [4]. The instability nature is the same as in the case of single injection - coherent oscillations of the stored ion beam: initially in the longitudinal and horizontal degree of freedom and, after some time, the oscillations "jump" into the vertical plane. Coherent instability during stacking leads to random variations of the beam intensity near saturation and limits the stored beam intensity. More probably explanation of the instability origin is the plasma oscillations of the ion beam in accordance with the theory developed in [3]. The coherent oscillations appear when the ion beam density increase to the level corresponding to more than one plasma oscillation of the ions during passage of the electron beam. The transformation of horizontal coherent oscillations into the vertical ones leading to particle losses was observed also at HIMAC as well.

Instability Suppression

The instabilities of cooled ion beam can be avoided by preservation of "overcooling" of the beam core. For instance at CELSIUS and later at COSY an additional external heating of the beam in longitudinal and transverse degrees of freedom and/or misalignment of the electron beam were tested for instability suppression. However, both of these methods stabilize the stored beam but do not give a substantial increase of its intensity. The external heating leads to higher value of the particle loss after injection due to decrease of dynamic aperture of the ring. The misalignment of the electron beam leads to non-equilibrium distribution in the transverse degree of freedom and, in principle, can provoke a chromatic instability. The experience of the CELSIUS cooling system operation demonstrated that more effective way to suppress the stored beam instability is artificial increase of the electron beam energy spread. This was done by connecting the electrically insulated inner structure in the drift tube to a hi-fi amplifier, and modulating the voltage at this structure. For instance, at 115 keV electron energy at CELSIUS it was demonstrated that most effective is square-wave modulation at amplitude of 50 V [5].

Formation in the electron gun the hollow electron beam is another and, as one can expect, more effective way to avoid overcooling the ion beam core and related instabilities. The results of experimental investigations of the electron beam profile in such a gun were presented in [6].

The instability threshold depends not only on the beam current and on the magnitude of the transverse machine impedance but also on the particle momentum spread. Therefore to avoid beam losses the chromaticity should be negative below transition. Stabilization of the proton beam by adjustment of the chromaticity accomplished with sextupoles was demonstrated at COSY [7].

Fig. 4 shows two cycles of the COSY beam. The injected proton beam (current of 2 mA) with 293.8 MeV/c (45 MeV) is electron cooled for 10 s and then is accelerated within 1.8 s to the flat top momentum of 2085 MeV/c. In the first cycle a strong vertical oscillation occurs leading to beam loss immediately after injection. In this case the tunes and chromaticities measured after 8 s were equal to $Q_x = 3.587$, $Q_y = 3.696$ and $\xi_x = -2.8$,

$\xi_y = 0.3$, respectively. In the second cycle the sextupole family located in the arc section of the ring was powered only after injection until acceleration started with −1.7 % to shift the vertical chromaticity ξ_y from +0.3 to −0.6 within 100 ms. By this measure the coherent vertical betatron oscillations at injection could be significantly suppressed and intensity of the accelerated beam was increased by two times.

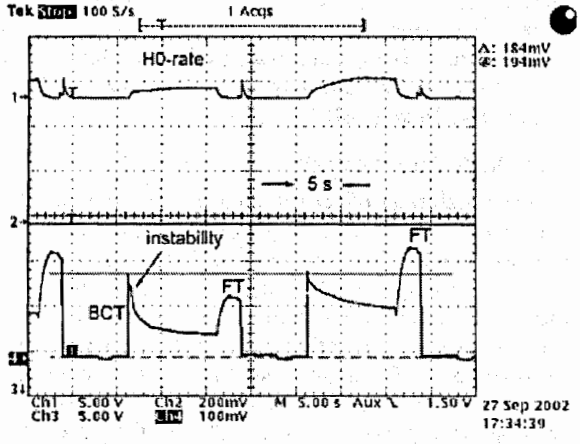

Fig. 4: In the first cycle, without sextupole, a strong beam loss after injection due to a coherent vertical betatron oscillations (instability) is visible in the beam current signal (BCT). This beam loss is compensated by the sextupole family in the next cycle. The flat top (FT) intensity is doubled. The horizontal line in the lower trace points at the same number of injected protons in both cycles. (100 mV BCT signal corresponds to 1 mA proton current).

Results of a feed back system application to increase stored beam intensity was demonstrated, for instance, at LEAR [1]. There strong transverse instabilities occurred once the intensity exceeds a few 10^8 protons. A large number of modes was observed at all energies accessible with electron cooling (5.3 - 50 MeV). Therefore, a feedback system of the bandwidth of 0.1 - 70 MHz was implemented, to stabilise the first 100 or so dipole modes. It was then possible to store up to about 3×10^9 protons with the small emittances given by the equilibrium between intrabeam scattering and cooling in the energy range accessible. Higher intensities, up to 8×10^{10} protons, could be cooled to the intra beam scattering limit, when the stochastic cooling system of a reduced gain with a bandwidth up to 500 MHz was used as additional dipole damper.

At COSY the vertical feed back system was designed and implemented after investigations of the particle loss nature. Its bandwidth up to 70 MHz was chosen to suppress all the exiting modes. The system application made it possible to stabilize the cooled proton beam at a level of 2×10^{10} particles (1,8 mA) after a single injection. With the stacking technique a maximum of $1{,}2\times10^{11}$ cooled protons (9,2 mA) at injection energy were stored without instability, which is about two times higher than without a feed back system application [8].

ION CLOUD IN AN ELECTRON COOLING SYSTEM

The ions of residual gas are trapped in the electron beam in transverse direction by the electron beam electric field. When the vacuum chamber radius is varied along the cooling system from cathode to collector the condition of the ion trapping in longitudinal direction can be also met. The trapped ions partially compensate the electron beam electric field and this effect leads to so called "natural neutralization" of the electron beam. The level of the natural neutralization in COSY is measured by two independent methods and is about 37%, that is in good agreement with estimations based on geometry dimensions of the vacuun chamber [9]. In HIMAC level of the natural neutralization is about 15%.

Thus in the cooling section the circulating ion beam interacts with the primary electron beam, secondary electrons and different species of neutralizing ions, which can lead to various types of multi-stream instabilities [10]. The stability of antiproton beam at HESR ring of FAIR project (GSI) in presence of neutralizing ions was descussed in [11] where was shown that even a few percent of the neutralization level can lead to sufficient decrease of the instability threshold. Influence of the neutralizing ions on the circulating beam stability was experimentally investigated at HIMAC [12] and later at COSY.

The ions trapped in the electron beam oscillate in the longitudinal magnetic field of the cooler solenoid and electric field of the electron beam with frequency determined by the following formula

$$\omega = \sqrt{\omega_i^2(1-\eta_{neutr}) + \omega_B^2/4} \pm \omega_B/2, \qquad (1)$$

where $\omega_B = \dfrac{ZeB}{Am_p}$ is the cyclotron frequency of the ion at mass of Am_p and charge Ze in the magnetic field B, $\omega_i^2 = \dfrac{Ze^2 n_e}{2Am_p}$ is the ion plasma frequency in the electron beam of the density of n_e. To control the neutralization level and to clear the electron beam from one of the ion spesies one can use resonant excitation of the ion oscillations with transverse sinusoidal electric field. This field is applied to pair of electrodes, so called "shaker electrodes", wich are, for instance, position pick-ups in the cooling section. At shaker frequency equal to the ion oscillation frequency the ions leave very fast the electron beam and neutralization level is changed. That leads to a change of potential at the electron beam axis and, as result, to a change of the revolution frequency of the ions circulating in the ring. This change of the revolution frequency can be compensated by change of the electron gun cathode potential. Dependensies of the cathode potential at constant ion beam revolution frequency on the shaker frequency measured at HIMAC and COSY are presented in the Fig. 5, 6.

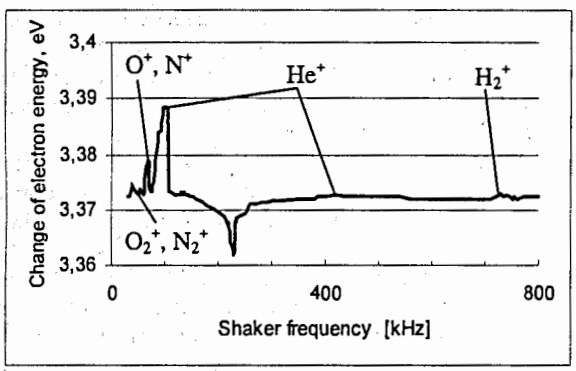

Fig. 5: Spectrum of resonance shaker frequencies measured at HIMAC cooler.

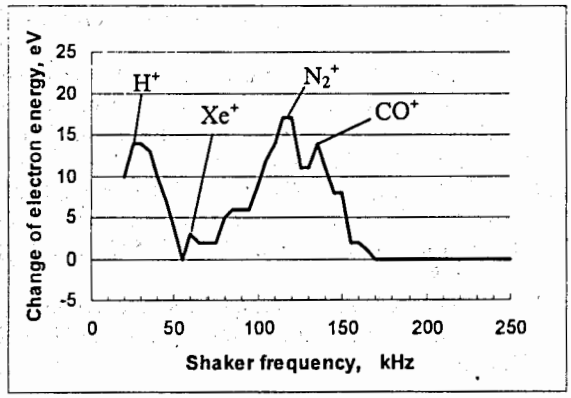

Fig. 6: Spectrum of resonance shaker frequencies measured at COSY cooler.

The measurement were performed at different shaker voltage, which was varied in the range from 10 to 60 V. Width of the resonant peaks increases with increase of the voltage (Fig. 7). The peak shape is typical for nonlinear resonance and at a high value of the shaker voltage a hysteresis behavior appears. At increase of the shaker frequency the neutralization level decreases monotonically, but at some frequency it jumps to initial value. At decrease of the shaker frequency the opposite jump of neutralization level takes place at smaller value of the frequency.

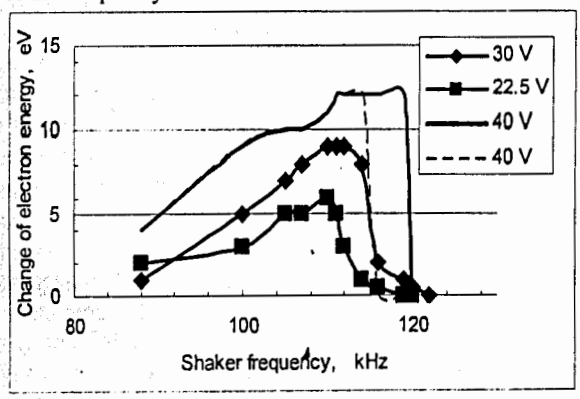

Fig. 7: Shape of the resonant peak at 90 – 120 kHz as function of the shaker voltage amplitude. At 40 V there is a hysteresis effect – solid line corresponds to an increase of the shaker frequency, dashed line – to a decrease.

In the experiments at HIMAC the clearing of the electron beam from the residual gas ions led to increase of the stored beam intensity after stacking by about 2 times. Simultaneously the Schottky noise power of the circulating beam was of sufficiently less level [12].

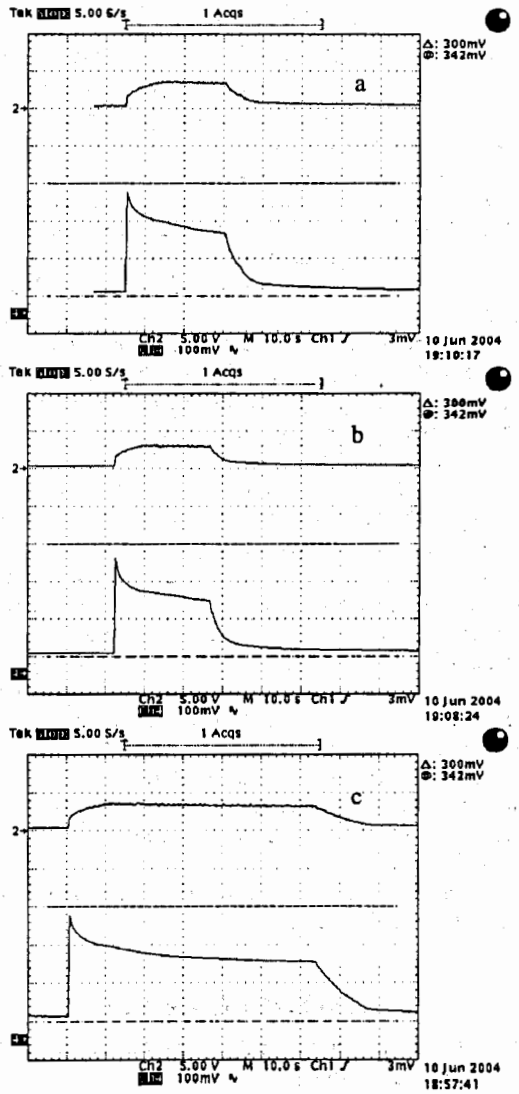

Fig. 8: Ion current versus time: a) shaker is off, b) non resonant excitation, c) excitation on resonant frequency of 114 kHz.

Influence of the neutralization on the proton beam stability at COSY is well illustrated in the Fig. 8. Without shaker or at nonresonant shaker frequency a coherent instability leading to fast particle losses appears after approximately 25 s (Fig. 8 a, b). At clearing the electron beam from one specie of the ions (the frequency of 114 kHz, which corresponds to molecular nitrogen ions) the instability develops after about 70 s and the ion loss rate at instability decreases by about 3 times (Fig. 8 c). This indicates that the threshold ion beam phase space density increases and instability increment decreases. However, in

the cooling-stacking process the maximum beam intensity is slightly affected by the shaker in the case of monochromatic excitation. It means that at high proton beam intensity the beam stability can be determined by interaction with the ion cloud consisting of other species.

CONCLUSIONS

The experimental studies of stacking process at COSY and HIMAC cooler-synchrotrons have shown the limitation of the ion beam intensity due to three phenomena related each to other:

1) fast losses directly after injection,
2) slow losses in the cooled proton beam caused by a coherent instability with transformation of horizontal oscillations into vertical ones,
3) trapping of residual gas ions in the cooling electron beam.

The fast initial losses are supposed to be a result of an influence of the electron beam field nonlinearity. Another explanation is related to plasma oscillations in the ion and electron beams, which lead to noise of big amplitude reducing the ion lifetime.

The second stage of the loss takes place when coherent oscillations appear in the cooled ion beam. The transformation of horizontal coherent oscillations into the vertical ones leads to particle losses due to smaller value of the vertical acceptance. One of the more effective ways for coherent instability suppression is a feedback system application.

Comprehensive explanation of these effects was not done yet and they have to be studied in more details. Last results of the experiments at both rings – COSY and HIMAC demonstrated importance of the electron beam neutralized state control especially at cooling of intense beams. At low ion beam intensity neutralization of the electron beam can decrease the cooling time, at high intensity the ion cloud in the cooling section can provoke instability of the cooled beam.

AKNOWLEGMENTS

This work is supported by RFBR grant #02-02-16911 and INTAS grant #03-54-55-84.

REFERENCES

[1] J.Bosser et al., Stability of cooled beams, NIM A 441 (2000), pp. 1-8.

[2] D.Reistad et al., Measurements of electron cooling and «electron heating» at CELSIUS, Workshop on Beam Cooling, Montreux, 1993, CERN 94-3, pp. 183 – 187.

[3] V.Parkhomchuk, D.Pestrikov, Coherent instabilities at electron cooling, Workshop on Beam Cooling, Montreux, 1993, CERN 94-3, pp. 327 – 329.

[4] V. Kamerdzhiev et al., Instability phenomena of electron-cooled ion beams at COSY, NIM A 532 (2004), pp. 285-290.

[5] L.Hermansson, D.Reistad, Electron cooling at CELSIUS, NIM A 441 (2000), pp. 140-144.

[6] A. V. Bubley, V. M. Panasyuk, V. V. Parkhomchuk and V. B. Reva, Measuring a hollow electron beam profile, NIM A 532 (2004), pp. 413 - 415.

[7] H. Stockhorst, H.J. Stein, D. Prasuhn and R. Maier Stabilization of an Electron Cooled Proton Beam at Injection with Sextupoles, IKP annual report, Juelich, 2002.

[8] V. Kamerdzhiev, J. Dietrich, I.N. Meshkov, I. Mohos, A.O. Sidorin, H.J. Stein, Application of Transverse Feedback for Electron Cooled Ion Beams at COSY, IKP annual report, Juelich, 2003.

[9] A. Sidorin, I.N. Meshkov, H.J. Stein, H. Stockhorst Natural Neutralization in the Electron Beam of the COSY Electron Cooler, IKP annual report, Juelich, 2001

[10] A.V.Burov, Secondary particle instability in storage rings with electron cooling, in Proceedings of Workshope on Beam Cooling and Related Topics, Montreux, 1993, CERN 94-3, pp. 230 – 234.

[11] P. Zenkevich, A. Dolinskii and I. Hofmann, Dipole instability of a circulating beam due to the ion cloud in an electron cooling system, NIM A 532 (2004), pp. 454 – 458.

[12] E.Syresin, K.Noda, T.Uesugi, I.Meshkov, S.Shibuya, Ion lifetime at cooling stacking injection in HIMAC, HIMAC-087, May 2004.

NUMERICAL SIMULATION OF PARTICLE DYNAMICS IN STORAGE RINGS USING BETACOOL CODE

I. Meshkov, A. Sidorin, A. Smirnov, E. Syresin, G. Trubnikov, JINR, Dubna, Russia
P. Zenkevich, ITEP, Moscow, Russia

Abstract

Numerical simulation of particle dynamics in storage rings is one of key issues in accelerator physics. Now a lot of programs are developed for the simulation of charged particle dynamics. The main goal of BETACOOL code [1] is simulation of beam parameters in presence of electron cooling together with other physical effects which effect on circulating beam: intrabeam scattering, internal target, beam-beam effect, scattering on residual gas, etc. This code is being developed since 1996 [2] and is used in different science centres which have electron cooling system under operation or are developing the new project of these systems.

This work is supported by RFBR grant #02-02-16911 and INTAS grant #03-54-5584.

INTRODUCTION

An electron cooling method is widely used for ion beam parameter control in storage rings. Presently there are more than 20 storage rings in operation and under construction, which are equipped with electron cooling devices. The BETACOOL program developed for simulation of electron cooling process is actively used in several research centers: FZJ, GSI (Germany), RIKEN, NIRS (Japan), BNL (USA), JINR, ITEP (Russia) [3-8]. The BETACOOL is programmed with object oriented method using C++ language. Interface part for Windows operation system is developed on the basis of BOLIDE system (Builder Object Library & Interface Development Environment) [1], which is dedicated to fast elaboration of the physics and mathematics applications.

General goal of the BETACOOL program is to simulate long term processes (in comparison with the ion revolution period) leading to variation of the ion distribution function in 6 dimensional phase space. The ion beam motion inside the ring is supposed to be stable and is treated in linear approximation.

Structure of the program permits to simulate ion distribution function evolution using a few independent numerical algorithms. Each algorithm simulates the ion beam dynamics at the same input beam and ring parameters and uses in simulations the same set of effects acting on the beam distribution function.

This report discusses last version of the BETACOOL program, which includes three algorithms for beam dynamics simulation and takes into account the following processes: electron cooling, intrabeam scattering, ion scattering on residual gas atoms, interaction of the ion beam with internal target and some others.

BASE ALGORITHMS

Three basic algorithms for simulations of the ion distribution function evolution are realized in the program now:

- RMS (root mean square) dynamics simulation,
- Simulation of distribution function evolution using Monte-Carlo method (Model Beam algorithm),
- Multi particle tracking based on Molecular Dynamics technique.

The physical model used in RMS dynamics simulation is based on the following general assumptions:

1) the ion beam has Gaussian distribution over all degrees of freedom, and is not changed during the process.

2) algorithm for analysis of the problem is considered as a solution of the equations for RMS values of the beam phase space volumes of three degrees of freedom.

3) maxima of all the distribution functions coincide with equilibrium orbit.

The evolution of the ion beam parameters during its motion inside the storage ring is described by the following system of four differential equations:

$$\begin{cases} \dot{N} = N\sum_j \dfrac{1}{\tau_{life,j}}, \\ \dot{\varepsilon}_h = \varepsilon_h \sum_j \dfrac{1}{\tau_{h,j}}, \\ \dot{\varepsilon}_v = \varepsilon_v \sum_j \dfrac{1}{\tau_{v,j}}, \\ \dot{\varepsilon}_{lon} = \varepsilon_{lon} \sum_j \dfrac{1}{\tau_{lon,j}}, \end{cases} \qquad (1)$$

where N is the particle number, ε_h, ε_v, ε_{lon} are root mean square values of horizontal, vertical and longitudinal beam emittance correspondingly. Characteristic times are functions of all three emittances and particle number and have positive sign for a heating process and negative for cooling one. The negative sign of the lifetime corresponds to the particle loss and the sign of the lifetime can be positive in the presence of particle injection, when particle number increases. Index j in Eq.(1) is the number of process involved into calculations. The algorithm structure is designed in such a way that allows including any process into calculation, which can be described by cooling or heating rates. Numerical solution of the system (1) is performed using Euler method with automatic step variation. Result of the simulation is the emittance and particle number time dependencies. The ion ring optic

structure is necessary only for intrabeam scattering (IBS) simulation. The IBS growth rates are calculated in accordance with one of analytical models using ring lattice functions imported from output file of the MAD program.

Step of the system (1) integration over time is determined by characteristic times of investigated effects and calculation speed can be very fast. However, in some cases the basic physical model can not provide realistic simulation mainly due to basic assumption about Gaussian shape of the ion distribution function. This assumption is more or less realistic in an equilibrium state of the ion beam when the equilibrium is determined by many processes of stochastic nature. If the equilibrium does not exist due to fast particle loss or at initial stage of the beam cooling the ion distribution function can be far from Gaussian. The same situation takes place in an experiment with internal targets which dimensions are not coinciding to the ion beam dimensions. The ionization energy losses of the ion beam in the target can not be correctly calculated in the frame of this model also.

Investigation of the ion beam dynamics at arbitrary shape of the distribution function is performed using multi particle simulation in the frame of Model Beam algorithm. In this algorithm the ion beam is presented by array of modeling particles. The heating and cooling processes involved into simulations lead to change of the particle momentum components and particle number, what is calculated in accordance with step of dynamics simulation over time. Each effect is located in some position of the ring characterizing by the ring lattice functions. Transformation of the beam inside the ring is provided using linear matrix at random phase advance between the effect locations. Results of the simulations can be presented both as the beam profile evolution in time or as time dependencies of the beam emittance and particle number.

The real ion ring optic structure is necessary only for IBS diffusion power calculation only. The change of the particle momentum due to IBS is calculated on the basis of one of the analytical models as in the case of RMS dynamics simulation.

For simulation of the IBS process through Coulomb interaction between ions the Tracking algorithm is used. One of the goals of this algorithm development is to simulate a formation of crystalline state of the ion beam. In the crystalline state of the ion beam the IBS process can not be treated in the frames of analytical models, which are based on assumption of Gaussian shape of the ion distribution function. To speed up the calculations in the tracking algorithm the IBS simulation are performed using Molecular Dynamics technique presuming periodical ion distribution in the longitudinal direction. Therefore, this algorithm can be used for coasting beam only.

In the frame of the tracking algorithm the particle motion equations are integrated in the real optic structure of the ring. The ring structure is imported from input MAD file. Each cooling or heating effect involved into calculations together with IBS is located in some optic element. Calculation of the particle co-ordinates variation due to action of an effect is provided using the effect MAP. The effect position in the ring is described in input MAD file using special marks.

Structure of basic objects of the BETACOOL namely - the models of the ion ring and the ion beam, are developed in such a way, that allows realizing all three algorithms at the same input parameters. The heating and cooling effects are realized on the basis of common standard and at the same parameters can be used in each algorithm.

STRUCTURE OF EFFECTS

In the present version of the program the ion beam dynamics can be simulated taking into account one or a several effects from the following list (Figure 1):

1. Electron cooling,
2. Scattering on residual gas,
3. Interaction with internal target,
4. Collisions with encounter beam in the collider mode of the ring operation,
5. Particle losses at cooling section, collision point, acceptance, etc.,
6. Intrabeam scattering,
7. Additional External heating of the ion beam (by artificial noise source, for instance).

Algorithms for beam-beam effect, stochastic and laser cooling are under development now.

The effect structure permits to uniformly use each effect in all basic algorithms. For this purpose each effect is presented by three models: transformation map, kick of the ion momentum, characteristic time calculation.

The effect used as a transformation map is associated with some optic element of the ring and its position is marked in input file. The map transforms the particle co-ordinates from the entrance to the exit of the element and calculates particle loss probability.

On the basis of transformation map in each effect the procedures for calculation of the particle momentum kick and for characteristic time calculation are developed. Calculation of the momentum kick is used in Model Beam algorithm, characteristic times are necessary for RMS dynamics simulation.

The most develop effects are electron cooling and intrabeam scattering which includes a lot of physical models and different numerical algorithms.

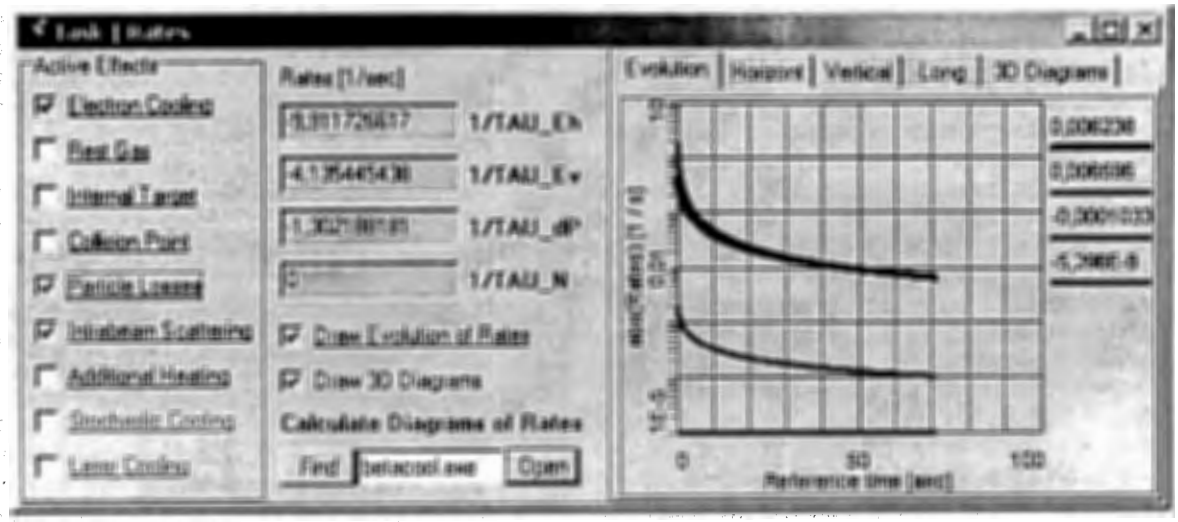

Figure 1: Form for the control of active effects and visualisation of growth rate evolution

ELECTRON COOLING

Structure of the effects can be illustrated on example of electron cooler model.

Usually an action of electron cooling on the ion dynamics inside a storage ring is described using a few standard simplifications:

1. Angular deviation of the longitudinal magnetic field line is substantially less than the ion beam angular spread.
2. Ion transverse displacement inside the cooling section is substantially less than electron beam radius.
3. Ion beam temperature is substantially larger than electron one and ion diffusion in the electron beam can be neglected.
4. Electron beam has a round shape of cross-section and uniform density distribution in the radial direction.

Under these assumptions and using asymptotic of the analytical friction force presentation the formulae for characteristic times of emittance and momentum spread decrease at electron cooling were obtained [9]. In the first version of the BETACOOL program electron cooling was simulated in accordance with this model [2]. This model is also used in a few program dedicated to electron cooling simulation. However this model can not cover all possible versions of the electron cooling system design.

In the last time modifications of the usual configuration of the electron cooling system were proposed. To avoid instability of the ion beam related with extremely large density of the cooled beam it was proposed to use so called "hollow" electron beam – the beam at small density in the central part. Extension of the electron cooling method in the region of electron energy of a few MeV related with an RF acceleration of the electrons. In this case one can expect Gaussian distribution of the electrons in radial plane and, if the electron bunch is shorter than the ion one, in longitudinal direction also. Calculation of the cooling times in this case requires modification both the electron beam model and the base physical model.

Other expected peculiarity of the medium energy cooling system is a big length of the cooling section – up to about 20 - 50 m. To obtain very high accuracy of the magnetic field is difficult technical task and cost of the cooling system will strongly depend on the required level of the accuracy. Therefore, before design of the cooling section solenoid, one needs to investigate influence of the magnetic field line curvature on the cooling process. All the effects can be taken into account by numerical solution of the ion motion equations in the cooling section.

To solve all the problems related with the cooling process simulation a hierarchy of objects was developed in the frame of the BETACOOL program. Structure of the electron cooler presentation permits to extract procedures of different levels and to include them into calculation of the cooling process in other programs. The cooling simulation is based on a friction force calculation in the particle rest frame. The friction force can be calculated in accordance with one of the analytical models from a library or using results of numerical calculations imported from external file. The next layer of the simulation is related with a cooler representation as a map, transforming particle coordinates from entrance to the exit of the cooling section and calculating the ion loss probability due to recombination with electrons. Calculation of the cooler map is based on a model of electron beam that provide transformation of the ion velocity to the frame related with the electron beam and takes into account real geometry of the cooler. Now in the BETACOOL three models of electron beam are available for simulations: uniform cylinder, Gaussian cylinder and Gaussian bunch. Model of the hollow beam will be realized in nearest future. The cooler model takes into account variation of the magnetic field in the cooling section. For this aim the co-ordinates of the electron beam trajectory inside cooling section is input from additional

file and the ion motion equations are solved numerically inside the cooler.

The map of the cooler can be used directly in the frame of the Molecular Dynamics algorithm, or in other tracking procedures. On the basis of the map one can calculate kick of the ion momentum after crossing the cooling section that is necessary for simulation of the ion distribution evolution in the frame of the Model Beam algorithm. The map of the cooler is used also for the cooling rate calculation that is necessary for RMS dynamics simulation. The cooling rate calculation can be performed using two model of the ion beam – the cooling rates for "RMS particle", or cooling rates for the ion beam with Gaussian distribution in all degrees of freedom.

INTRABEAM SCATTERING

Intrabeam scattering (IBS) in the ion beam causes two processes: relaxation of the beam to thermal equilibrium between degrees of freedom and diffusion growth of 6D phase volume of the beam due to variation of lattice parameters along ring circumference.

All usually used numerical algorithms of IBS growth rate calculation are based on the model of the collisions proposed by A. Piwinski.

Three models for IBS calculation – Piwinski, Martini (extended Piwinski) and Jie Wei models are realized in new version of BETACOOL program for Gaussian distribution of ions over velocity. The Martini model does not require additional assumptions for calculation of the beam emittance growth times. Piwinski model can be deduced from Martini model neglecting a variation of dispersion and beta function along the ring orbit (uniform optics). In the model proposed by Jie Wei characteristic times of emittance variation are calculated for real lattice parameters of the ring under a few additional assumptions, which correspond to storage rings at ion energy over the transition energy (for instance RHIC, BNL).

Simulation of the intrabeam scattering (IBS) process is based on calculation of the particle momentum variation due to coulomb interactions with other particles of the beam. In the BETACOOL the particle momentum variation can be calculated using analytical expressions for diffusion coefficients or, for coasting ion beam, using Molecular Dynamics (MD) technique. On the basis of both approaches each optic element of the ring is presented as a map for IBS process.

The map of the IBS process based on direct calculation of the ion coulomb interaction can be combined with the transformation map of optic element calculated from external focusing fields. In such a form the IBS process is simulated in the frame of tracking algorithm based on MD technique. This algorithm uses as input parameters the particle array presenting the ion beam and characteristics of external focusing fields.

The map of IBS process based on analytical theory calculates the growth rates for three degrees of freedom by numerical evaluation of integrals over ion distribution function assuming that the distribution function has Gaussian shape. The values of the growth rates are used for calculation of the individual particle momentum variation. The calculation of the growth rates requires as input parameters the RMS beam emittance and lattice functions of the ring in given optic element.

In the frame of RMS dynamics simulation the growth rates calculated in each optic element are averaged over the ring circumference. This procedure requires as input parameters the RMS beam emittances and description of the ring optic structure. The ring optic structure can be presented in both variants: as a specification of the optic elements or as dependencies of the lattice functions on the longitudinal co-ordinate along the ring circumference. In the first case the program initially provides tracking of Twiss parameters along the ring and transforms the ring model to the form of the lattice functions.

In the frame of a few models for the IBS growth rates calculation one needs mean parameters of the ring only. In this case detail description of the ring optic structure is not necessary and the IBS process can not be presented by a transformation map. Such models of the IBS can be used only in Model Beam algorithm and RMS dynamics simulation.

ORDERED BEAM SIMULATION

The idea of crystalline beam has received a large interest by now. The achievement of very low temperature in the beam rest frame opens new possibilities in accelerator physics. The increase of the luminosity in the collider and in experiments with targets is a very important asset for investigation of rare radioactive isotopes. The ordered state of circulating ion beams was observed at several storage rings [10].

The simulation of 1D crystalline beam with BETACOOL code was done [11]. The sudden reduction of momentum spread in the ESR experiment is described with this code. The simulation shows good agreement with the experimental results and also with IBS theory.

For the achievement of ordered ion beams with a large number of particles and with a realistic cooling force a special strategy of the cooling process can be elaborated. The longitudinal component of IBS heating has the break-up where heating rates have very small value in comparison with the theoretical prediction. If the initial parameters of ion beams can be chosen near the break-up that the ordered state for a large number of particle $N = 10^5$ can be achieved for real cooling system with electron beam current I_{ecool} = 5 A (Figure 2). During cooling process we may apply additional heating in the transverse direction, for example, heating by an RF-kicker. Initially, the momentum spread continues decrease and emittance will increase. When the beam parameters have to satisfy the condition $T_\perp >> T_\parallel$ we can switch off the additional heating and the ion beam will continue to cool down to the ordered state. The experimental verification of the new strategy for the achievement of an ordered ion beam

with large density can open new possibilities in the accelerator physics.

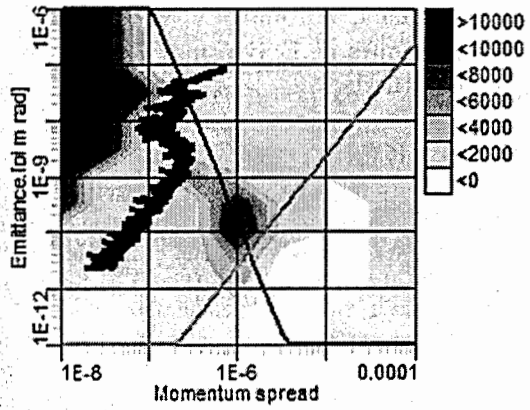

Figure 2: Numerical simulation for TARN-II with using of Molecular Dynamics technique. Black solid line – criterion of ordered state [10], grey solid line – equilibrium between transverse and longitudinal temperatures, grey islands – heating growth rates from IBS, points – particle dynamics with electron cooling

SOFTWARE STRUCTURE

The BETACOOL program is a part of software developed for electron cooling simulation. The software is divided in two independent parts: physical code, which is written using only standard C++ syntax and interface part, which is an executable program working under Windows environment. Connection between two parts of the program is provided using three types of the files: input, output and files used for control of the calculation process. Such a structure on the one hand allows to use the program on PC, to control the calculation process and analyze results during simulations. From the other hand the physical part of the program can be compiled for UNIX operation system and used for calculations independently on interface. The interface part in this case can be used for preparation of the input file and result visualization after completion of the calculations. All input and output files are in the text format and can be edited without interface program. The parameters in the input file are divided by groups in accordance with the structure of BETACOOL objects.

The interface part of the software consists of executable file Bolide.exe, *.dfm files containing information about BETACOOL exterior and input files for post processing of the calculated data. Development of the BETACOOL exterior is possible without recompilation of the Bolide.exe file. The interface part provides also service in work with the file structure on the disc.

The physical part of the software consists of the executable file Betacool.exe compiled for Windows or UNIX operation system and files of input parameters. For intrabeam scattering calculation one needs to use file of lattice parameters, for instance, MAD file. Additional input files are used for electron cooling simulation at friction force calculated by other program and for input of magnetic field errors in the cooling section.

The source code of the physical part of the software consists of tree relatively separated parts:

- interface part, which supports the format of input and output files common with the BOLIDE system,
- library of base numerical algorithms including description of dimensional variables, templates of the program self counters, procedures for matrix algebra, algorithms of numerical solution of differential equations,
- physical codes describing objects of the program and procedures with them.

Structure of the BETACOOL program exterior corresponds to the structure of general objects in the source code and correspondingly to the structure of input file.

REFERENCES

[1] http://lepta.jinr.ru/bolide.htm

[2] A. Lavrentev, I.Meshkov "The computation of electron cooling process in a storage ring", preprint JINR E9-96-347, 1996.

[3] I.Meshkov, A.Sidorin, A.Smirnov, E.Syresin, T.Tanabe, T.Katayama, "Computer simulation of ECOOL and IBS process in ACR and DSR using BETACOOL program", preprint RIKEN-AF-AC-21, 2000.

[4] N.Alekseev, V.Bykovsky, D.Koshkarev, Y.Korotaev, I.Meshkov, et al, "Project of TWAC Electron Cooler", Physica Scripta, Vol. T104, 160–163, 2003.

[5] V.Mikhailov, A.Butenko, I.Issinsky, I.Meshkov, et al, "Progress in the Nuclotron Booster Design", proc. of EPAC 2002, Paris.

[6] I.Meshkov, R.Maier et al, "Electron cooling application for luminosity preservation in an experiment with internal targets at COSY", Dubna 2001, Jul-4031.

[7] E.Syresin, A.Smirnov, A.Noda, K.Noda, T.Shirai, H.Fadil, "S-LSR low ion energy mode", preprint NIRS HIMAC-086, 2004.

[8] http://www.ual.bnl.gov

[9] I.Meshkov, "Electron cooling: Status and Perspectives", Phys. Part. Nucl., 25, (6), 1994, 631.

[10] I.Meshkov, A.Sidorin, A.Smirnov, E.Syresin, T.Katayama, "Ordered State of Ion Beams", preprint RIKEN-AF-AC-40, 2002.

[11] I.Meshkov, A.Sidorin, A.Smirnov, E.Syresin, T.Katayama, H.Tsitsui, D.Mohl, "Simulation Study of Ordered Ion Beams", preprint RIKEN-AF-AC-42, 2003.

THE LEPTA COMMISSIONING

E.Boltushkin, V.Bykovsky, A.Ivanov, A.Kobets, Y.Korotaev, V.Lohmatov, V.Malakhov, I.Meshkov, V.Pavlov, R.Pivin, I.Seleznev, A.Sidorin, A.Smirnov, E.Syresin, G.Trubnikov
S.Yakovenko, JINR, Dubna, Russia

Abstract

The project of Low Energy Particle Toroidal Accumulator (LEPTA) is dedicated to construction of a positron storage ring with electron cooling of positrons circulating in the ring. Such a peculiarity of LEPTA enables it automatically to be a generator of positronium (Ps) atoms, which appear in recombination of positrons with cooling electrons inside the cooling section of the ring. The project has a few goals:

- Dynamics in the modified betatron
- Electron cooling with circulating beam
- Electron cooling of positrons
- Positronium generation in flight
- Positronium physics
- Feasibility of antihydrogen generation in flight

All key elements of the ring: kicker, electron beam injection system, helical quadrupole, septum magnet are tested and expected design parameters were achieved for those elements. LEPTA construction has been completed and circulating electron beam has been achieved.

This work is supported by RFBR grant #02-02-16911 and INTAS grant #03-54-5584.

INTRODUCTION

The Low Energy Particle Toroidal Accumulator (LEPTA) is proposed for the electron cooling of positrons and generation of antihydrogen and positronium in flight [1÷5]. The LEPTA facility (Fig.1) includes small positron storage ring with circumference of 17.2 m equipped with electron cooling system and positron injector consisting of a low energy positron source based on β^+ -active sodium isotope and penning-type trap for preliminary storing of positrons. The energy of positron beam circulating in the ring is planned to be at 10 keV, the value of focusing magnetic field is equal to 400 G.

The peculiarity of the LEPTA ring is the longitudinal focusing magnetic field for both circulating positron beam and cooling electron beam. The longitudinal magnetic field provides the positron magnetisation and, as a consequence, long lifetime of the circulating positrons. However, to form closed orbit of circulating beam one needs to use additional helical quadrupole coil. In the presence of longitudinal magnetic field the beam superposition and separation requires especial design of injection complex.

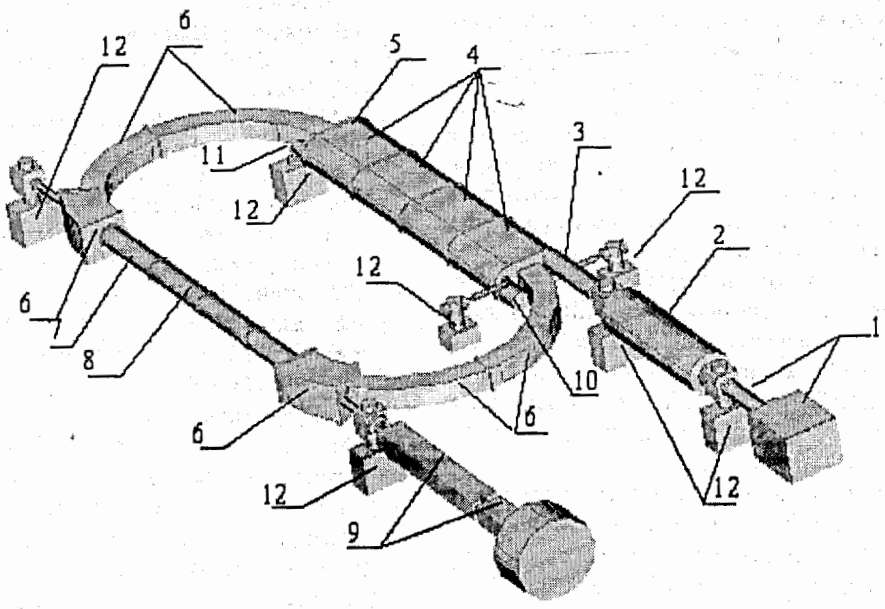

Figure 1: Design of the LEPTA. 1 – positron source, 2 – positron trap, 3 – positron transfer section, 4 – septum solenoids, 5 – kicker (inside septum solenoid), 6 – toroidal solenoids, 7 – solenoid and helical quadrupole inside it, 8 – electron cooling section, straight solenoid, 9 – experimental channel, 10 – electron gun, 11 – collector of the electrons, 12 – vacuum pumps

PARTICLE DYNAMICS IN LEPTA RING

To form a closed orbit of circulating positron beam, the centrifugal drift of the positrons is compensated by applying a bending magnetic field in the toroidal sections of the ring. The long-term stability of the positron beam is provided by additional helical coil, which forms a quadrupole magnetic field, similar to the "stellarator" one. This coil consists of two pairs of spiral conductors with opposite current direction and is placed inside one of the straight solenoids around the vacuum chamber. Required gradient of the quadrupole field was calculated using especially developed computer code BETATRON [6].

Both beams – circulating positron and single-turn electron ones – are magnetized and the problems of the beams injection, superposition and separation are complicated enough in this case. These problems are solved by the following way.

At the first stage of the ring working cycle the electron gun is switched off. The positron beam from injector is directed into the septum coil and moves in horizontal direction to the equilibrium orbit. After that, it is displaced in vertical direction by the field of special electric kicker, which is placed in the septum solenoid next to the septum. At the exit of the kicker the positron beam has to reach the equilibrium orbit. Applying of bending magnetic field of the corresponding value compensates centrifugal drift of the positrons inside the toroidal sections. The field of the septum coils does not act on the particle, which moves along the equilibrium orbit due to the septum design. When the positron beam fills the total ring circumference, the kicker is switched off and electron gun of the cooling system is switched on. The electron beam after traveling through the septum coil is placed below the median plane of the ring. Inside the first toroidal section electrons drift up in the longitudinal toroidal field and the bending one, which compensates the drift of the positrons. Total displacement of the electrons in vertical direction is equal to:

$$\Delta = \pi(\rho_p + \rho_e), \qquad (1)$$

where ρ_p, ρ_e are the positron and electron Larmor radii. Inside the cooling section both beams travel together (in the same direction), and both beams are overlapped. Inside the second toroidal section the electrons drift up again and to the left in the septum coil and come to the collector.

General problems, which have to be experimentally investigated before starting experiments with positronium generation, are the following:

- beam parameter distortion during injection,
- beam parameter distortion after crossing the helical quadrupole,
- superposition and separation of two magnetized beams – circulating positron and single-pass electron ones,
- stability of the circulating beam,
- dependence of the circulating beam lifetime on vacuum conditions,
- variation of the circulating beam temperature due to transverse-longitudinal relaxation,
- beam parameter distortion after crossing the resonance of the fast mode of betatron oscillation.

TUNING OF THE RING KEY ELEMENTS USING PULSED ELECTRON BEAM

Tests of the injection complex and helical quadrupole were performed before the ring assembling. Other experiments will be done with circulating electron beam during the ring commissioning.

The helical quadrupole has to provide the beam rotation as a whole around its axis. The rotation angle is proportional to square of the quadrupole field gradient. The distortion of the angular spread of the beam after crossing the helical quadrupole is minimized by adiabatic variation of the quadrupole field gradient at the entrance and at the exit of the coil. The designed and constructed helical quadrupole coil has in each cross-section the geometry of "Panofsky lens" which provides a maximum linearity of the field (Fig.2). The gradient variation at the entrance and exit of the coil is provided by corresponding variation of the number of winding turns. A correct calculation of the particle dynamics in the coil is practically impossible due to difficulties in measurements of the fringe fields.

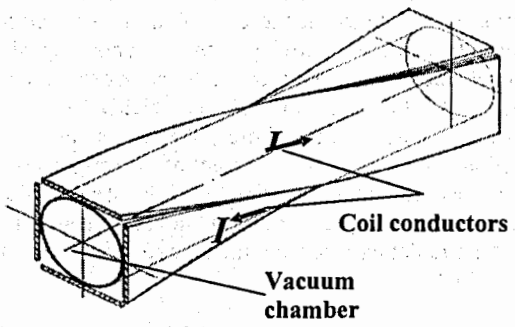

Figure 2: Scheme of the helical quadrupole

Test of the helical quadrupole was performed using two electron beams operated in the pulsed mode at pulse duration of 10 – 30 μs. Both beams were cut from a beam of diameter of about 13 mm at crossing a diaphragm with two small holes. Diameter of the holes was 1.5 mm and distance between the holes was 10 mm. One of the beams was aligned to the axis of the quadrupole using correction coils. Relative displacement of the second beam was measured as a function of the quadrupole winding current. Beam position at the exit of the system was observed with a luminescent screen. At the first stage of the experiment the dependence of the beam rotation angle on the winding current was measured (fig.3). The dependence is in a good agreement with theoretical estimation for any value of the beam radial position. It is equal to:

$$\varphi = k\frac{G^2}{B^2}s, \qquad (2)$$

where φ is beam rotation angle, G is magnetic field gradient, which is proportional to the helical quadrupole current, B is longitudinal magnetic field, s is the

quadrupole length, k is numerical coefficient defined by geometry of the quadrupole.

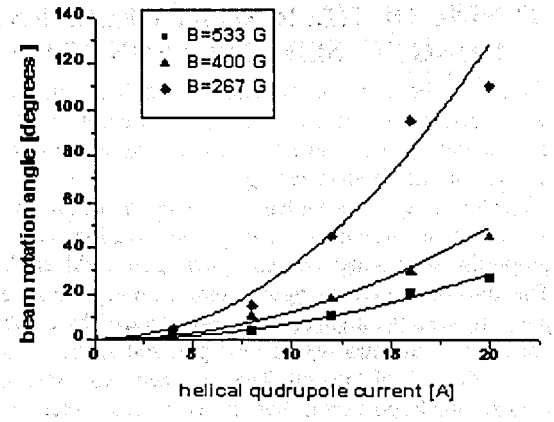

Figure 3: Dependence of the beam rotation angle on the helical quadrupole current at different longitudinal magnetic fields

The injection complex, which included septum coils and vacuum chamber of the kicker which were placed inside septum solenoid, was tested with electron beam from the electron gun installed at the exit of the kicker. Electron beam in this case was moving in the direction opposite to nominal one. First it was crossing the kicker, then the septum. At this test instead the kicker were used correction coils, which shifted the beam in vertical direction. At the same fixed current of the septum coil the beam was consequently directed into three different channels of the septum: positron injection channel, the tube for circulating beam and the tube for cooling electron beam (fig.4).

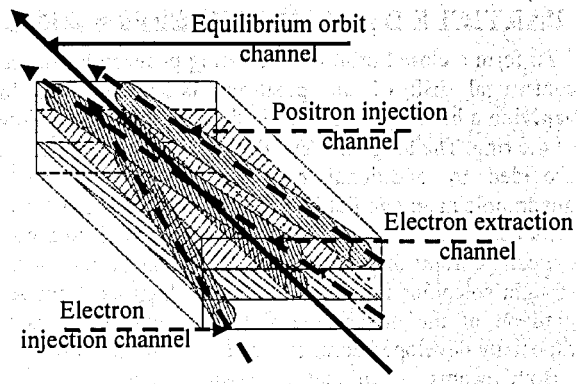

Figure 4: Septum scheme

At the exits of those channels the electron beam was observed with luminescent screens. Results of this test show a good capability of the scheme for superposition and separation of magnetized beams.

The injection complex was installed in the ring after the tuning and the ring assembling was completed. The electron gun was installed at its nominal position (fig. 1). The electron beam orbit of the cooling system was traced.

TUNING OF THE RING

When kicker was installed at the LEPTA the ring assembling was completed and tuning of the closed orbit was started. PU stations and segment diaphragms for diagnostics of the circulating beam were used (Fig. 5). Vertical and horizontal corrector coils placed before septum entrance allow the beam to pass the septum.

The optimal septum magnetic field was defined during the first test. Segment diaphragms placed at the kicker entrance allow more accurate septum tuning. Voltage of the kicker was optimized in accordance with necessary displacement (6 cm) of the beam up to the equilibrium orbit. This displacement was checked with segment diaphragms, which are placed at the exit of the kicker.

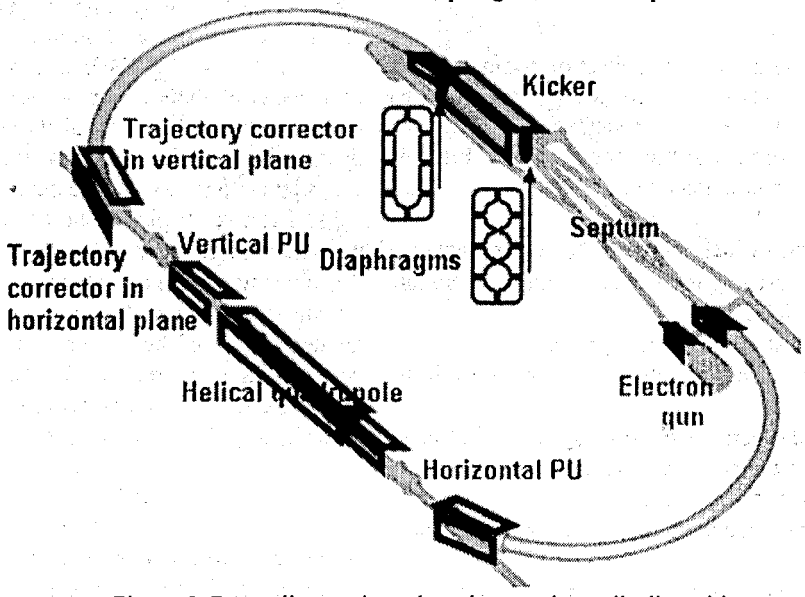

Figure 5: Beam diagnostic tools and correction coils disposition

Corrector coils, which are located at the entrance and at the exit of the first toroidal section, allow beam to pass the straight section. The beam was observed with two PU stations (Fig. 6), which are installed in the straight section. Each station consists of two plates formed from a cylinder cut along axis.

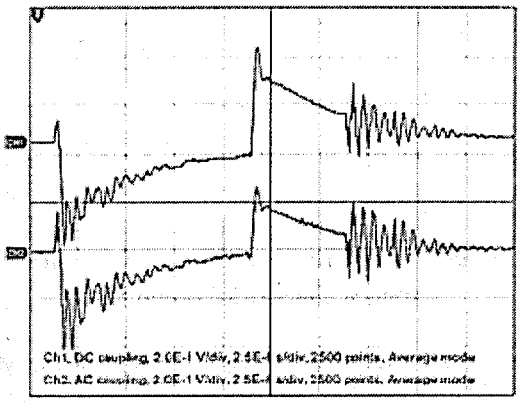

Figure 6: Signals from vertical PU station. Time scale: 2,5 μs/div. Top curve is signal from top plate of the PU station and bottom curve – from bottom plate

Duration of the signal from PU was about 10 μs (Fig. 6), but length of injected beam was about 15 μs (Fig. 7).

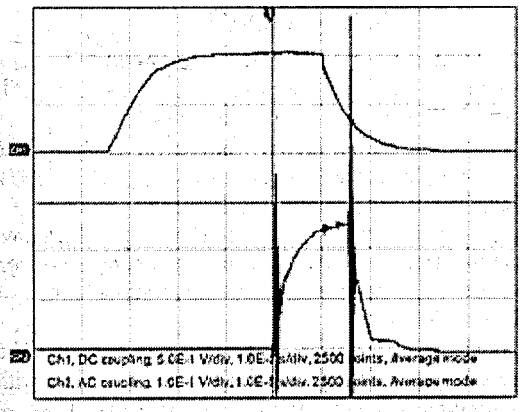

Figure 7: Time dependence of kicker signal (top curve) and pulse of injected electron beam (bottom curve). Time scale: 10 μs/div

The kicker has been turned on before injection of the electron beam, and has been turned off when electron beam fills the whole equilibrium orbit. Electron beam was observed with PU at the moment only when the kicker is switched on. On the next step beam was passed through the second toroidal section using corrector coils at the entrance and exit of second toroidal section. Position of electron beam was controlled with segment diaphragm placed at the exit of central channel of the septum.
Circulating electron beam was observed also with PU after back edge of the kicker pulse (fig.8). Only a few

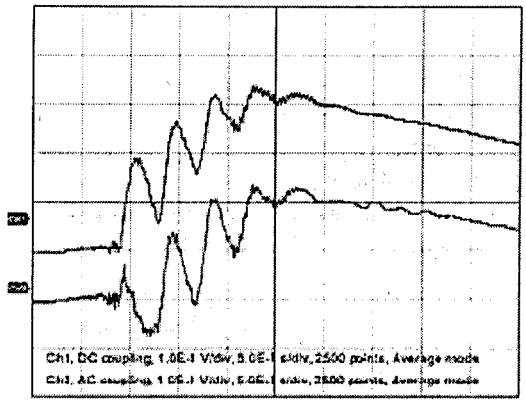

Figure 8: A few first turns of the beam in the ring. Signals from vertical PU station

turns exist without the helical quadrupole filed. The helical quadrupole allows achieving the stable motion in the ring. The back edge of the kicker pulse is about 30 ns, the revolution time is about 300 ns. As result when kicker is turned off the circulating beam does not fill the whole equilibrium orbit and circulating beam can be observed with PU (fig.9).

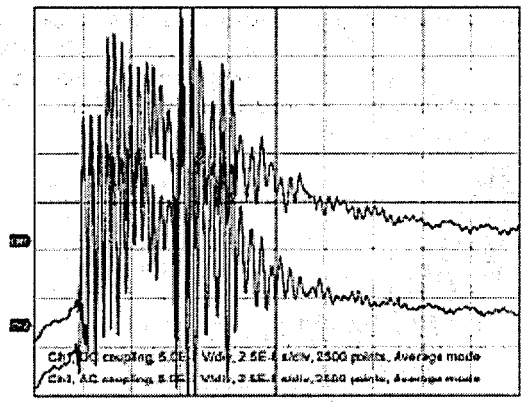

Figure 9: Circulating beam. Signals from vertical PU station

Some noise exists at the moment when electron gun turns off. To avoid this problem the signal from circulating beam was transformed to computer (fig.10, black curve). Then the closed orbit was broken using corrector coil, which is placed at the end of the straight section, i.e. the electron beam makes one turn only, and PU signal from injected beam was not changed. The signal from the injected electron beam was transformed to computer also (fig.10, top (red) curve). On the next step the signal from circulating beam (fig.9) was subtracted by the signal from injected beam (fig.6). As result the clear useful signal of the circulating beam was obtained (fig.10, bottom (green) curve).

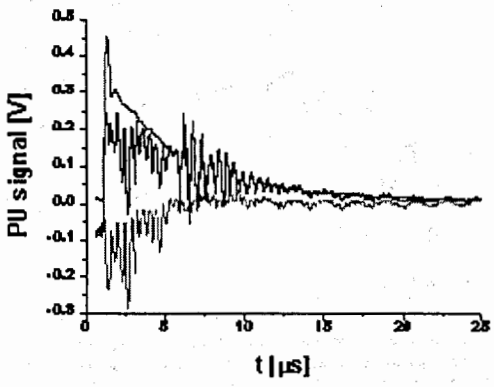

Figure 10: The digital signals from vertical PU

In accordance to the calibration of PU stations the circulating beam current in the first turn was about 60 mA. The injected beam current was about 120 mA. Circulating beam is observed during 10 μs that corresponds to 20 turns. Then the amplitude of the PU signal continuously decreases. It means the beam becomes coasting or disappears. However the small amplitude of PU signal with slow frequency during 200 μs was observed (fig.11). Sometimes this signal was modulated with the revolution frequency. The slow frequency corresponds to a rotation of the beam as a whole around the axis and is produced by the field of the helical quadrupole.

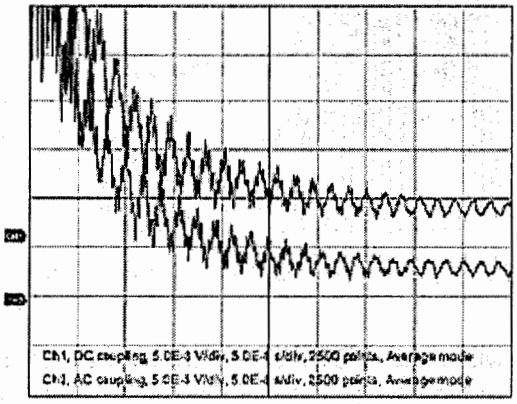

Figure 11: Slow mode of oscillation. Signals from vertical PU station

The measurement this slow betatron tune dependence on the helical quadrupole current was done (fig.12). The slow betatron tune is equal to

$$Q = \frac{f_{slow}}{f_{revolution}} \qquad (3)$$

The signals of slow frequency from different plates of PU station have the opposite phase (fig.11) that confirms the rotation of the beam as a whole. Approximation of the experimental dependence of the rotation angle on the quadrupole current with parabolic curve shows that the ring has additional focusing by nonlinear magnetic field of the bending coils in toroidal section or the space charge of the electron beam influences on beam dynamics. Both effects or one of them make the beam rotation in the direction opposite to the helical quadrupole one.

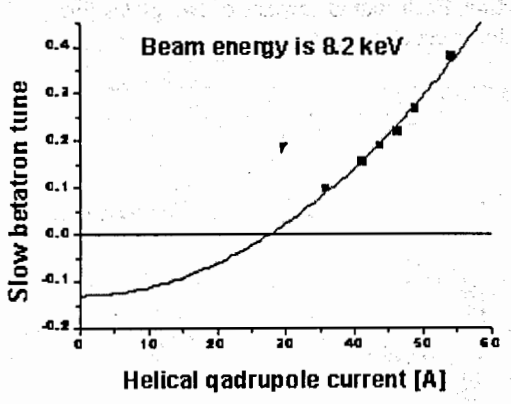

Figure 12. The dependence of the slow betatron tune on the helical quadrupole current

SUMMARY

New storage ring LEPTA was assembled at JINR. First experiments with the pulsed electron beam show the validity of the injection scheme. The circulation of the electron beam was observed for a few hundreds turns.

REFERENCES

[1] I.N. Meshkov, A.N. Skrinsky, Antihydrogen beam generation using storage ring, NIM A 379 (1996) 41, preprint JINR E9-95-130, Dubna, 1995.

[2] I.N.Meshkov, A.O.Sidorin, Conceptual design of the low energy positron storage ring, NIM A 391 (1997), 216 – 220.

[3] Yu.V.Korotaev, I.N.Meshkov, S.V.Mironov, A.O.Sidorin, E. Syresin, The low energy positron storage ring for positronium generation, Proc. of EPAC 1998, p. 853

[4] I.Meshkov, A.Sidorin, A.Smirnov, E.Syresin The particle dynamics in the low energy storage rings with longitudinal magnetic field, Proc. of EPAC 1998, p. 1067.

[5] V.Antropov, E.Boltushkin, V.Bykovsky, et al. Particle dynamics in the Low Energy Positron Toroidal Accumulator, first experiments and results, Proc. of EPAC 2004.

[6] I.Meshkov, A.Sidorin, A.Smirnov, E.Syresin, G.Trubnikov, The computer simulation of the particle dynamics in the storage ring with strong coupling of transverses modes, Proc. of EPAC 2000.

IFEL PROJECT WITH HIGH ACCELERATING GRADIENT

G.A. Baranov, M.F. Vorogushin, A.A. Kuchinski, Yu.A. Svistunov, P.V. Tomashevich
FSUE "D.V. Efremov Scientific Research Institute of Electrophysical Apparatus",
St. Petersburg, Russia
A.A. Varfolomeev, S.V. Tolmachev, T.V. Yarovoi
RCL, Russian Research Center "Kurchatov Institute", Moscow, Russia

Abstract

Project of an IFEL experimental installation with powerful TW CO_2 laser is proposed by the Russian Research Center "Kurchatov Institute" and the D.V. Efremov Scientific Research Institute (NIIEFA) These institutes have experience in design and manufacturing of different devices having connection with IFEL, such as S-band electron linacs, a high-brightness pre-accelerated RF photo injector, powerful CO_2 lasers and high quality strong field undulators. It is supposed to achieve local gradients near 1 GV/m and average accelerating gradients up to 100 MV/m.

INTRODUCTION

Inverse Free Electron Laser schemes for particle accelerate were proposed as accelerators for many years. Now when SSC project is closed creation of the IFEL turns out especially important. This scheme is probability more perspective for reliable acceleration than Laser Wake Field Accelerator or Laser Beat Wave Accelerators. The Inverse Free Electron Laser is actually, a very efficient scheme for microbunching and phase-locking electrons at the optical scales. Up to now, only modest energy gain has been achieved mostly because of the limitations of the peak radiation power available. Most of worked out acceleration schemes are based on using powerful CO_2 lasers. Modern TW picosecond lasers can provide radiation intensity up to $10^{18} \div 10^{19}$ W/cm^2 at the focus. This is correspond to electric field strength 60 GV/cm. Physical processes in the laser accelerators are complex enough and need further study. Although USSR in 60÷80^{-th} had leadership in theoretical investigations, now most of essential experimental works are producing in USA. Russia is evidently backward in this research sphere.

This project supposes IFEL developing with special undulator without plasma. Estimations showed that here one can obtain significant accelerating gradients of dense electron bunches in contrast to Plasma Beat Wave Accelerator. With help of proposed IFEL it can be obtained greater energies and significant greater electron capture into acceleration. Realization of the project means developing and manufacturing the following devices:

- CO_2-master oscillator of picosecond range;
- superatmospheric CO_2-amplifier with 100 cm^2 aperture;
- high-current photo-injector of 1 MeV electron energy;
- rf linac with working frequency 2856 MHz and output electron energy 15-20 MeV;
- non-adiabatic tapering of the undulator.

Up to now best result on laser acceleration had been achieved in the collaboration of the "Kurchatov Institute" and UCLA. Electron beam was accelerated by laser beam from 15 to 35 MV. Intensity of CO_2-laser beam was 400 GW. There is possibility to improve this result if CO_2-laser installation produces subpicosecond pulses with high intensity (up to 1 TW), good synchronization of laser and electron pulses will be provided and special optical channels will provide efficient transportation and focusing of laser beam used acceleration. It is supposed to create special laser driver to obtain strong focusing laser beams (Rayleigh range is a few cm) in single pulse mode and IFEL module which are fed by two laser beams of single driver.

PREACCELERATION SCHEME

The IFEL require an electron accelerator capable of delivering pulse train of electron bunches of high charge density. A high electron quality beam needed a high peak current (~100 A) and low transverse beam emittance (<10π mm·mrad).

A photoinjector is a laser-switched photoemissive source located in an rf accelerator cell. By placing the photoemitter in high-gradient rf cavity, the space-charge effects due high electron densities can be substantially reduced. A laser-switched electron source gives control over all aspects of the electron distribution: peak current, spatial and temporal distribution. This type of source has also a large flexibility in interpulse spacing; the interpulse spacing can range from picosecond pulse separation to a single pulse. Provisional acceleration's scheme, including photoinjector and linac, is given on fig. 1 (left part of drawing). Photoinjector can produce micropulse length of 2 picosecond and gun voltage of 1 MV. The alpha magnet is a momentum filter and is able to limit the electron energy spread to less than 0.5 %. Simultaneously it increases peak current up to 10 times. The electron source is LaB_6 cathode. Using of the laser allows to limit the emission to the correct rf phase. In this mode LaB_6 was operated just below its normal emission temperature, and laser is used to pulse cathode. It is possible to obtain electron beam with peak current 70-80 A and emittance about (4-5)π mm·mrad. Accelerating structure has working frequency 2856 MHz. The same frequency has gun cavity. Accelerating structure is

combined and includes parts with standing wave and travelling wave. Main parameters of electron beam are given in table 1.

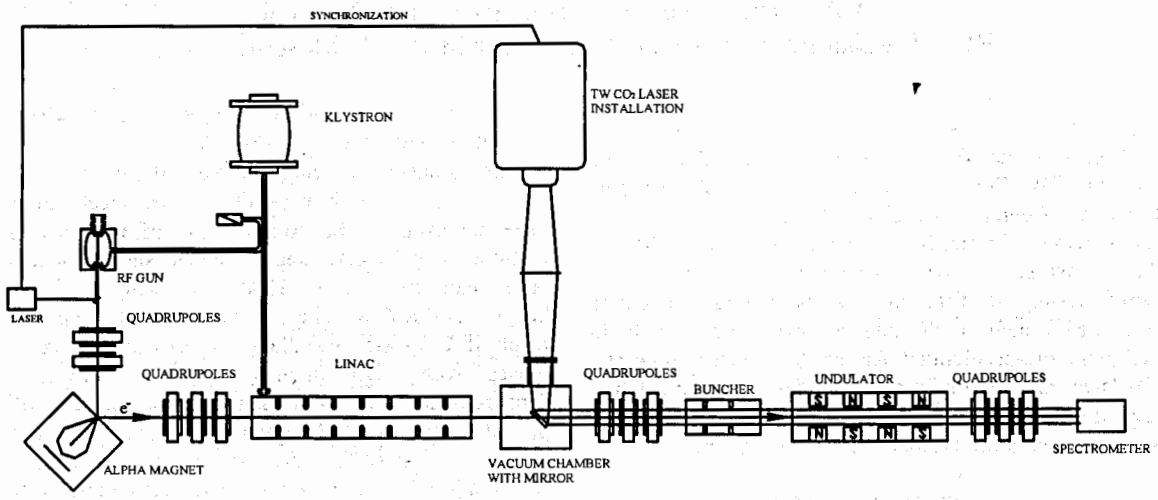

Figure 1: Schematic layout of the IFEL facility

Table 1: Main characteristics of preliminary rf acceleraton

Input beam energy, MV	1
Output beam energy, MV	15
Output bunch length, ps	> 2
Emittanc, mm·mrad	5
Electron bunch charge, nC	0.1

LASER ACCLERATOR SCHEME

Principle scheme of designed IFEL is given on fig.1. Powerful TW laser worked out in the Efremov Institute [1] must provide required electromagnetic field for accelerating of 15 MV electrons after additional bunching. At the last time in several scientific centers master oscillators of picosecond diapason with wave length near 10 μm had created (in partly at BNL in USA and Moscow State University). Because contemporary forming and compression systems of 10 μm range subnanosecond laser pulses have limitation of output generator energy about 10^{-5} J, it is appeared problem of pulsed amplification up to 10^5-10^6 times. Effective solving of this task may be prove with help large-aperture superatmospheric amplifiers only. Here main problem is to provide stable volumetric discharge of laser pumping in high pressure and big interelectrode gaps. Experimental researches fulfilled in the Efremov Institute indicate that required amplification may be obtained under following conditions:

- working mode with tightened front of voltage;
- preionization of a gas mixture (in our case CO_2:N_2:He) by soft Roentgen rays;
- using of intermediate small-inductive storage unit precisely matched with load.

At present working out of modern CO_2-amplifier is completed in the Efremov Institute. Main parameters of amplifier and IFEL's laser system are given in table 2 and table 3.

Table 2: Main parameters of amplifier

Working volume, cm^3	(5-10)x10x10
Interelectrode distance, cm^3	5-10
Pressure of gas mixture, atm	5-10
Quantity of molecular gases, %	≥ 15
Specific energy contribution, J/l·atm	≥ 100
Coefficient of small signal amplification, cm^{-1}	≥ 0.02

Table 3: Main parameters of IFEL's laser system

Laser power, TW	0.8-1
Wave length, μm	10.6
Laser waist size, μm	350
Raleigh range, cm	>3.6

Undulator of designed IFEL may be fulfilled as analog of undulator which was built by Coherent Radiation Laboratory of Kurchatov Institute for IFEL

experiment at the Neptun Laboratory. Undulator initial period was 1.5 cm and period at exit 5 cm. It corresponds to electron output energy 55 MeV. Another option is possible when electrons are accelerated preliminary up to 20-25 MeV in rf linac. Then necessity of creation a new undulator is appeared. As accelerating structure in this case may be used the modified structure of LUER-20M linac.

CONCLUSION

Scientific Production Division of Linac and Cyclotrones and Laser Technologies Division of the Efremov Institute have significant experience on designing, manufacturing and exploitation of linacs, their injection systems, powerful lasers of different types. Specialists of RRC Kurchatov Institute have the same experience on designing, manufacturing and exploitation undulators and deep knowledge in IFEL research area. Now it is possible taking into account results of UCLA experiment to optimize laser beam parameters and obtain higher gain of electron energy than in other projects. It is clear that serious difficulties will appear during solving of synchronization problem of laser beams and electron bunches and diagnostic system creation.

REFERENCES

[1]. G.A. Baranov et al., "CO_2-amplifier of high pressure for forming of TW picosecond laser pulses", Thesis 18 International Conference "Influence of intensive energy flows on substance", 2003, p.21 (in Russian)

[2]. A.A. Varfolomeev et al., An undulator with non-adiabatic tapering for the IFEL project. NIM, in Physics Res. A483(2002), 377-382.

ON VIOLATION OF THE ROBINSON'S DAMPING CRITERION AND ENHANCED COOLING OF PARTICLE BEAMS IN STORAGE RINGS

E.G. Bessonov*, Lebedev Physical Institute RAS, Moscow, Russia

Abstract

Limits of applicability of the Robinson's damping criterion and the problem of enhanced cooling of particle beams in storage rings beyond the criterion are discussed.

INTRODUCTION

Losses of energy by particles in external fields caused by friction forces lead to a decrease of the six-dimensional phase space (emittance) occupied by particle beams in storage rings and damping of a particle transverse and longitudinal oscillations. There is a correlation of damping decrements determined by Robinson's damping criterion [1]-[5]. This criterion limits the rate of particle cooling in storage rings. Below, we would like to pay attention on violation of this criterion in schemes of selective interaction of particles with targets. Schemes of enhanced cooling of ion, electron and muon beams are discussed. We start by reviewing Robinson's damping criterion.

LIMITS OF APPLICABILITY OF THE ROBINSON'S DAMPING CRITERION

The motion of a particle in storage rings is described by its deviations from the ideal orbit in transverse radial x, vertical y directions and a by deviation $\varphi = \psi - \psi_s$ of the particle phase from the synchronous one in a curvilinear coordinate system (x, y, φ). In a linear approximation deviations (x,y,φ) are described by linear, differential equations. We can introduce a six-dimensional coordinate vector $\vec{u}$ with components $(x, x', y, y', \varphi, \Delta\varepsilon)$ and write the equations in the form of a system of six linear, differential equations, where $x' = \partial x/\partial s$; $y' = \partial y/\partial s$; s, the longitudinal coordinate of a particle along the ideal (reference) orbit; $\Delta\varepsilon = \varepsilon - \varepsilon_s$, the deviation of the particle energy from synchronous one. In the matrix presentation:

$$\frac{d\vec{u}(s)}{ds} = Q(s)\vec{u}(s), \qquad (1)$$

where $Q(s) = ||q_{ji}(s)||$ is a six-order matrix with components $q_{ji}(s)$ (j,i = 1...6). The Eq. (1) has six linear independent solutions $\vec{u_j}(s)$ with components $u_{ji}(s)$ ($u_{j1} = x_j$, $u_{j2} = x'_j$, $u_{j3} = y_j$,... $u_{j6} = \Delta\varepsilon_j$,). The solution of the Eq. (1) has the form $\vec{u}(s) = M(s) \cdot \vec{u}(0)$, where $M(s) = ||m_{ij}(s)||$ is a transfer matrix, $\vec{u}(0)$ the initial vector. Six linear independent solutions $\vec{u_j}(s)$ compose the matrix $U(s) = ||u_{ji}(s)||$. The Wronskian of this matrix, $W(s) = |U(s)| = |Q(s)| \cdot |U(0)|$, represents the six-dimensional volume of the polyhedron in the phase space occupied by the beam. The values $dW(s)/ds = SpQ \cdot W(s)$, $W(s) = W(0) \cdot \exp(\int SpQ \cdot ds) \simeq W(0) \cdot \exp(< SpQ > \cdot s)$, where $SpQ = \sum_{j=1}^{6} q_{jj}$, $W(0)$ is the initial Wronskian, sign <> denotes averaging. This is the Jacobean formula [2], [6]. On the other hand, $u_{ji}(s) \sim \exp(\alpha_i \cdot s)$ and the rate of change of the 6-dimensional volume of the polyhedron $\sim \exp[2 \sum \alpha_i s]$, where $\alpha_i = \alpha_x, \alpha_y, \alpha_\varepsilon$ are fractional averaged damping decrements. Therefore

$$\alpha_{6D} = 2\sum_{i=1}^{3} \alpha_i = < SpQ > . \qquad (2)$$

SpQ is determined by the diagonal elements of the matrix $||q_{ji}(s)||$. In the transverse plane, the particle momentum loss does not lead to a change of the direction of the momentum and position of the particle ($q_{11} = q_{33} = q_{55} = 0$). Acceleration of the particle changes the direction of the momentum on the value $|\Delta\vec{p}|/|\vec{p}| = \overline{P} \cdot s/c \cdot \varepsilon_s$. It leads to matrix elements $q_{22} = q_{44} = -\overline{P}/c \cdot \varepsilon_s$, where $\overline{P}$ is the average rate of particle energy loss; ε, the particle energy; subscript s refers to the reference orbit; c, the velocity of light. The rate of change of the particle energy is $\partial\varepsilon/\partial t = -(\partial\overline{P}/\partial\varepsilon)|_s \cdot \Delta\varepsilon + (\partial P_{rf}/\partial\psi)|_s \cdot \varphi$ and matrix element $q_{66} = -(\partial\overline{P}/c \cdot \partial\varepsilon)|_s$. Substitution of diagonal matrix elements to (2) leads to generalized Robinson damping criterion [3], [4]:

$$\sum \alpha_i = \frac{1}{2}\alpha_{6D} = -\frac{1}{c}\frac{\overline{P_s}}{\varepsilon_s} - \frac{1}{2c}\frac{\partial\overline{P}}{\partial\varepsilon}|_s. \qquad (3)$$

The proof of the Robinson's damping criterion was reduced to application mathematical Jacobean formula. Non-diagonal matrix components responsible for the beam dynamics of particles in a lattice was not used. Two diagonal components responsible for damping in the transverse plane are determined by the average power of the particle energy loss and one diagonal component responsible for damping in the longitudinal plane is determined by the partial derivative of the power energy loss. The value α_{6D} in (2), (3) determine the rate of damping of the 6-dimensional phase space volume (emittance) occupied by the beam (cooling). Coefficients α_i and α_{6D} can be both positive and negative [2], [3].

If there is no coupling between radial x and vertical y planes in a storage ring, the same calculations can be performed separately for vertical and longitudinal damping coefficients:

$$\alpha_y = -\frac{1}{2c}\frac{\overline{P_s}}{\varepsilon_s}, \qquad \alpha_\varepsilon = -\frac{1}{2c}\frac{d\overline{P}}{d\varepsilon}|_s. \qquad (4)$$

The radial decrement follows from Eq. (3):

* bessonov@x4u.lebedev.ru

$$\alpha_x = -\frac{1}{2c}\left[\frac{\overline{P}_s}{\varepsilon_s} + \frac{\partial \overline{P}}{\partial \varepsilon}|_s - \frac{d\overline{P}}{d\varepsilon}|_s\right]. \quad (5)$$

Damping times $\tau_{i,min} = -1/c\alpha_{i,max}$ are limited by Robinson's damping criterion (3) by the value

$$\tau_{i,min} = \frac{\varepsilon_s}{J_{i,max}\overline{P}_s}. \quad (6)$$

where $J_{i,max}$ is determined by the dependence $\overline{P}(\varepsilon)$ if all decrements are greater or equal zero. The value $J_{i,max} = 2$ if synchrotron radiation (SR) or backward Compton scattering are used ($\overline{P} \sim \varepsilon^2$) [7]. In the case of radiative ion cooling (backward Rayleigh scattering, $\overline{P} \sim D/(1+D)$, $D \sim \varepsilon$): $J_{i,max} = (3+2D)/2(1+D)$, where D is the saturation parameter [8]. For ionization muon cooling $(\partial\overline{P}/\partial\varepsilon)|_s$ is rapidly decreasing with the energy for $\varepsilon_\mu < 0.3$ GeV, but is slightly increasing for $\varepsilon_\mu < 0.3$ GeV ($J_{i,max} \sim 1$) [9]. The partial derivative $(\partial\overline{P}/\partial\varepsilon)|_s$ can be very high only in the case of laser cooling of ion beams by homogeneous broadband laser beam with rapidly increasing linear dependant spectral intensity in the frequency range corresponding to the ion energy spread $\sigma_{\varepsilon,0}$. In this case $\overline{P} \simeq \overline{P}_s(\varepsilon - \varepsilon_s + \sigma_{\varepsilon,0})/\sigma_{\varepsilon,0}$ $(0 < \varepsilon - \varepsilon_s < 2\sigma_{\varepsilon,0})$, $(\partial\overline{P}/\partial\varepsilon)|_s = \overline{P}_s/\sigma_{\varepsilon,0} \gg \overline{P}_s/\varepsilon_s$, $J_{i,max} \simeq \varepsilon_s/2\sigma_{\varepsilon,0}$,

$$\tau_{i,min} = \frac{2\sigma_{\varepsilon,0}}{\overline{P}_s}. \quad (7)$$

Next conditions were used to prove the Robinson's damping criterion: 1) cooling in the radio frequency (RF) bucket, 2) linear dependence $\overline{P}(\Delta\varepsilon)$, 3) stationary process. Violation of these conditions can lead to the violation of the criterion, the concept of decrement, non-exponential damping and fast cooling.

ENHANCED COOLING OF PARTICLE BEAMS IN STORAGE RINGS BEYOND THE ROBINSON'S DAMPING CRITERION.

Below three examples demonstrate fast laser cooling of ion beams beyond the Robinson's damping criterion. Internal ion selectivity and Rayleigh scattering are used.

1) Monochromatic laser beam target with scanning frequency is used when the RF system of the storage ring is switched off (RF buckets, linear dependence $\overline{P}(\Delta\varepsilon)$ and stationary conditions are absent) [10]. Ions interact with the counter-propagating laser beam at resonance energy, decrease their energy in the process of the laser frequency scanning until all of them reach the minimum energy of ions in the beam. At this frequency the laser beam is switched off. The higher the energy of ions, the earlier they start interacting with the laser beam, the longer the time of interaction. Ions of minimum energy do not interact with the laser beam at all. Cooling is available.

2) Ion and broadband laser beams interact in a straight section of a storage ring. The laser beam is homogeneous in limits of the ion-laser beam interaction region (IR) and has sharp frequency edges. The frequency band of the laser beam is sufficient for all ions to interact with the laser beam. The RF system of the storage ring is switched off (violations of conditions 1, 2). The minimum initial energy of ions corresponds to interaction with laser beam photons of high-frequency edge. Ions decrease their energy until all of them reach the minimum energy of ions in the beam. Cooling is available.

In these examples the energy spread of the ion beam is decreased by a linear (non-exponential) law to a small value limited by quantum processes of Rayleigh scattering. The damping time is determined by (7). Both non-exponential and exponential damping times determined by (7) are $\varepsilon/4\sigma_{\varepsilon,0} \sim 10^2 \div 10^3$ times shorter than damping time for radiative ion cooling if scattered powers are the same[1]. These methods work only longitudinally and can use both a dispersion and dispersion-free laser-ion IR. To cool the beam in the transverse plane the emittance exchange through a synchro-betatron resonance [11] or dispersion coupling by a wedge-shaped or by a moving broadband laser target [12], [13] can be used.

3) Ion and broadband laser beams interact in a straight section of a storage ring. The laser beam is homogeneous in limits of the ion beam and has sharp frequency edges. The RF system of the storage ring is switched on. The synchronous energy of ions corresponds to interaction with photons of high-frequency edge of the laser beam. The spectral intensity of the laser beam is linearly decreased from a maximum at the low-frequency edge to zero at the high-frequency edge. The power of the scattered radiation depends on the ion energy according to the law: $\overline{P} =< P_{max} > [(\varepsilon - \varepsilon_s)/\sigma_{\varepsilon,0}]$ at $\varepsilon_s < \varepsilon < \varepsilon_s + \sigma_{\varepsilon,0}$ and $\overline{P} = 0$ at $\varepsilon < \varepsilon_s$, where $\overline{P}_{max} = \overline{P}(\varepsilon - \varepsilon_s = \sigma_{\varepsilon,0})$. A discontinuity in the rate of energy loss was introduced: ions with an energy more than the synchronous energy interact with the laser beam and ions with less energy do not.

In this case, a synchronous ion does not lose energy. There is no friction and damping of synchrotron oscillations at the energy $\varepsilon < \varepsilon_s$ and there is damping at the energy $\varepsilon > \varepsilon_s$. The minimum damping time will be determined by (7) if we accept $\overline{P}_s = \overline{P}_{max}/2$.

Below a scheme for the emittance exchange and for three-dimensional cooling of muon beams is considered.

4). An homogeneous flat material target moves in the proper region of a storage ring to the position of a closed orbit of muons having a minimum energy, stop at this position and is extracted from the region for a short time $\Delta t \ll T_s$, where T_s is the revolution period of the muon. The RF system is switched off. A straight section with low-beta and high-dispersion function is used for efficient selection of closed orbits by the target. The higher the energy of muons, the earlier they start interaction with the target, the longer the time of interaction. Ions of minimum energy and

[1] Exponential damping leads to decrease of the beam dimension $e \simeq 2.7$ times for one damping time while non-exponential damping leads to much greater decrease and much faster cooling.

zero amplitude of betatron oscillation do not interact with the target at all (external selectivity of interaction).

In this method the energy spread is decreased by a non-exponential law to a value limited by a jump processes of the energy loss in the target and the initial spread of betatron oscillations. However friction and external selectivity of interaction of a moving target with a particle beam do not lead to cooling of the beam. In this case particles are deepened in the target to the depth larger then their amplitudes of betatron oscillations for many turns, interact with the target at the deviations from the closed orbit x_{b0} of one sign and that is why receive the unwanted increase of amplitudes of betatron oscillations simultaneously with the decrease of the energy spread. This statement follow from the change of the amplitude of betatron oscillations

$$\delta A = -(x_{\beta 0}/A)\delta x_\eta \qquad (8)$$

which is valid in the approximation $|\delta x_\eta| \ll |x_{\beta 0}| < \sigma_{x,0}$, where δx_η is the jump of the closed orbit; A, $\sigma_{x,0}$, the amplitude and betatron beam size [12], [13][2].

If the tune of muons $\nu_x \simeq m + 1/2$, the relative velocity

$$k_2 = \frac{|v_{T_2}|}{|\dot{x}_{\eta\, in}|} > 2 + \frac{\sigma_{x,0}}{|\delta x_\eta|}, \qquad (9)$$

particles are deepened in the target to the depth larger then their amplitudes of betatron oscillations for one turn, interact with the target at deviations from their closed orbits of alternate signs and receive the unwanted increase of amplitudes of betatron oscillations only one time. Here $\dot{x}_{\eta\, in} = \delta x_\eta / T_s$, m is a whole number. Muons having zero initial amplitudes of betatron oscillations obtain amplitudes $A = |\delta x_\eta|$ after the first crossing the target and lose them after the second one (at this moment their position is displaced at a distance $2|\delta x_\eta|$ to a new position of their closed orbit). The initial phase space area occupied by muon beam in the transverse plane will be splitted by 2 composite parts consisting of many regions. Central muons in one part of these regions will be at rest (even crossing the target) and central muons in the regions of the other part will oscillate with the amplitude $|\delta x_\eta|$ (odd crossing the target). This scheme leads only to an emittance exchange.

We can use a sequence of even number of flat moving targets N_T. Targets have to locate in sequence at a distance determined by a 180° phase advance for the lattice segment. Thicknesses of targets is N_T times less than in case of one target in the ring considered above. In this case the jump of closed orbits at the exit of the target and the corresponding degree of excitation of amplitudes of betatron oscillations will be 2 times less then for one target with N_T times larger thickness [13]. This scheme leads to emittance exchange as well.

[2]This interaction is similar to interaction of ions and monochromatic laser beams with scanning frequency (see above). However, in the last case laser beams overlap being cooled ion beams, interaction occur at the deviations from their closed orbits of different signs and that is why dos not lead to excitation of betatron oscillations.

If one wedge-shaped moving target is used, its thickness is decreased in the direction of the target velocity, the velocity of the target is greater then $\dot{x}_{\eta,in}$ at the position of the closed orbit of the particle, the target overlap the muon beam the emittance exchange for motionless target and cooling for moving target will occur. In this case the rate of compression of the ion beam in the longitudinal plane depends on the slope of the target but the rate of anti-damping in the transverce plane depends both on the slope and the velocity of the target. Muon can cross the target at positive (in the direction opposite to target velocity) and negative deviations from its closed orbit at different moments of time, thickness of the target at this pair moments and the position of closed orbit can be constant and the amplitude of muon betatron oscillations will not be changed.

CONCLUSION

In this paper we pointed out limits of applicability of the Robinson's damping criterion. New schemes of three-dimensional enhanced cooling of ion beams beyond the criterion where developed. Using external selectivity for emittance exchange and cooling was discussed.

Author thanks A.M.Sessler and Robert Palmer for useful discussion and acknowledges the support of this work by the RFBR under Grant No 02-02-16209.

REFERENCES

[1] K.W.Robinson, Report CEA (1956) (not published); Phys. Rev., 1958, v.111, No 2, p.373.

[2] A.A.Kolomensky and A.N.Lebedev, CERN Symposium 1, 447, Geneva (1956); Nuovo Cim. Suppl., v.7, 43 (1958); Theory of Cyclic Accelerators. North Holland Publ., C^0, 1966.

[3] A.A.Kolomensky, Atomnaya energiya, v.19, p.534, (1965).

[4] H.Wiedemann, Particle Accelerator Physics I and II (Springer-Verlag, New York, 1993).

[5] H.Bruck, Accelerateurs Circulaires de Particules, Institut National des Sciences at Techniques Nuclearies Saclay, Press Universitaires de France, 1966.

[6] V.I.Smirnov, Kurs vyschei matematiki, vol.3, part 2, p.438, GITTL, Moscow, 1951.

[7] Zh. Huang, R.D.Ruth, Phys. Rev. Lett., v.80, No 5, 1998, p. 976.

[8] E.G.Bessonov and Kwang-Je Kim, Preprint LBL-37458 UC-414, 1995; Phys. Rev. Lett., 1996, vol.76, p.431.

[9] D.Neuffer, Particle accelerators, V.14, p.75, 1983.

[10] J.S.Hangst, J.S.Nielsen, O.Poulsen, P.Shi, J.P.Shiffer, Phys. Rev. Lett., v.74, No 22, p.4432 (1995).

[11] H.Okamoto, A.M.Sessler, and D.Möhl, Phys. Rev. Lett. 72, 3977 (1994).

[12] E.G.Bessonov, Proc. 18th Int. Conf.on High Energy Accelerators, HEACC 2001, March 26-30, 2001, Tsukuba, Japan, http://conference.kek.jp/heacc2001/ ProceedingsHP.html (P2new11); physics/0203036.

[13] E.G.Bessonov, physics/0404142.

LINAC4, A NEW H⁻ LINEAR INJECTOR AT CERN

R.Garoby, K.Hanke, A.Lombardi, C.Rossi, M.Vretenar, CERN, Geneva, Switzerland
F. Gerigk, RAL, Chilton, UK

Abstract

Linac2, the present injector of the CERN PS Booster, limits the performance of the proton accelerator complex because of its low output energy (50 MeV). To remove this bottleneck, a higher energy linac is proposed (called "Linac4") which will double the brightness and the intensity of the beam delivered by the PSB and ensure the "ultimate" beam is available for LHC. Linac4 will deliver H⁻ ions at a kinetic energy of 160 MeV. It is designed to be usable as the front-end of a future multi-GeV multi-MW linear accelerator, the "Superconducting Proton Linac" (SPL). R&D for Linac4 is now actively taking place with the support of the European Union through the Joint Research Activity HIPPI ("High Intensity Pulsed Proton Injectors"), and of three ISTC projects involving three major Russian laboratories (BINP, IHEP and ITEP) and two nuclear centres (VNIIEF and VNIITF). The design of this new accelerator and the on-going developments are described.

INTRODUCTION

The beginning of LHC operation, expected in 2007, will mark the start of a crucial phase for its chain of injectors. They will have to provide reliably the nominal beam to the collider and, at the same time, to satisfy demanding users, like the neutrino experiment CNGS and the radioactive ion community of ISOLDE. For this reason a study group has worked during 2003 and part of 2004 to identify possible scenarios for improving the performance of the "low" energy injector chain [1]. The replacement of the present PS Booster (PSB) proton injector, the Linac2, has been clearly identified as a very effective way to increase the performance of the PSB and of the whole accelerator complex. The switch to an H⁻ linac associated with charge-exchange injection into the PSB, and the upgrade of the injection energy from 50 MeV to 160 MeV will double the brightness of the proton beam for the LHC and the intensity available from the PSB for other users. This new injector, called Linac4 [2], is being designed at the same time as the front end of a more ambitious accelerator, the SPL, a 4 MW 2.2 GeV linac that would upgrade the CERN hadron injector system to the requirements of the next class of experiments in the field of neutrino and radioactive ion physics and could contribute to push the LHC beam beyond its ultimate intensity.

LINAC4 DESIGN PARAMETERS

The goal of Linac4 is the doubling of the bunch population in the PSB, so that a single PSB batch will be sufficient for the PS to deliver the required beams for LHC and CNGS. The fundamental parameter to be considered is the incoherent space charge tune shift at PSB injection as a function of beam energy, which scales like $1/\beta\gamma^2$. In order to gain a factor two on the beam intensity, the injection energy has to be increased from 50 to 160 MeV.

While the average beam intensity in Linac4 is modest when feeding the PSB, with 30 mA peak current and 0.1% duty cycle, the SPL operation is much more demanding and requires 13 mA with 14% duty cycle. The RF structures and the beam dynamics have been designed to comply with both requirements. In order to obtain the longitudinal time structure required by the CERN scheme for a Neutrino Factory, a high performance chopper line is needed at 3 MeV.

Beam parameters are summarized in Table 1 for the two foreseen uses of Linac4.

Table 1: Linac4 parameters.

	PSB	SPL	
Beam Energy	160		MeV
Maximum repetition rate	2	50	Hz
Source current	50	30	mA
RFQ current	40	21	mA
Chopper beam-on factor	75	62	%
Current after chopper	30	13	mA
Pulse length (max.)	0.5	2.8	ms
Average current	15	1820	μA
Max. beam duty cycle	0.1	14	%
Transv. norm. emitt. (rms)	0.33	0.33	π mm mrad
Long. emittance (rms)	0.47	0.47	π deg MeV

ACCELERATOR LAYOUT AND BEAM DYNAMICS

The beam dynamics of Linac4 has been designed according to the challenging SPL operating mode [3]. With such a high beam power and the need to provide hands-on-maintenance, a severe control of the beam quality all along the accelerator is required; halo formation has to be avoided and losses must be kept at a minimum level in order to avoid material activation. For this reason, the evolution of the longitudinal and transverse phase advance has been kept as smooth as possible. The possibility of resonant emittance exchange has been prevented by keeping the phase advance ratio $0.5 < k_l/kt < 0.8$ all along the accelerator. The bore aperture is made larger than 7 to 8 times the r.m.s. beam size all along the machine.

Chopper line

The most serious exception to the above mentioned rules is represented by the chopper section, at 3 MeV. Fig. 1 shows the beam envelopes along the chopper line.

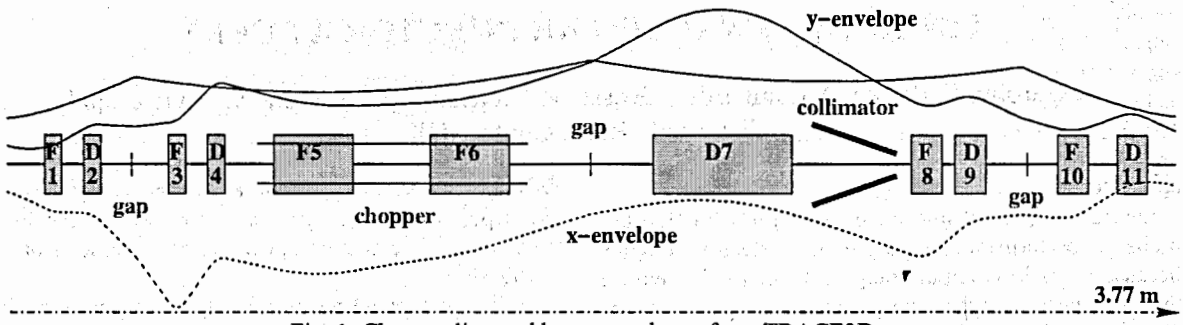

Fig. 1: Chopper line and beam envelopes from TRACE3D

The change in the transverse phase advance period is clearly visible. In fact the periodicity of the FODO lattice could not be kept because of the mechanical constraint of installing a 1 m long chopping structure.

The beam halo originating from this part of the accelerator will be removed by movable scrapers and by the collimation aperture of the dump for the chopped beam.

This chopping line is specified for the needs of the SPL as a proton driver for a Neutrino Factory, where the beam is accumulated in an accumulator ring with an RF frequency of 44 MHz. A 2 cm transverse separation is required between the transmitted and the chopped beam at the cone-shaped beam dump that is located 1 m downstream from the last chopping cavity. This is achieved by means of a 1 m long chopper structure where the beam experiences a 800 V effective voltage transverse kick. Beam deviation is amplified by the two quadrupoles F5 and F6 and reaches 7 mrad at the chopper exit; a 90° phase advance between the chopper and the beam dump then provides the required separation. Two FODO cells by each side of the chopper section perform the transverse matching between the RFQ and the DTL, mastering the transition through the slow phase advance chopper section (20 $\beta\lambda$). Simulations show that effective matching to the DTL can be obtained on a very wide range of beam currents, from 20 mA to 60 mA. Three nose-cone equipped pillbox cavities perform the longitudinal matching along the chopper line. 98% of the main beam is transmitted through the line and the chopped beam is eliminated to better than 0.02%.

Acceleration from 3 MeV to 160 MeV

A schematic layout of Linac4 is shown in Fig. 2, and the transition energies between the different RF structures are indicated.

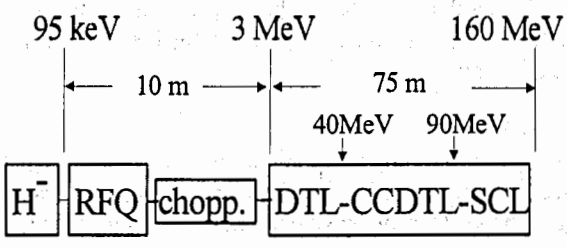

Fig. 2: The Linac4 schematic layout

The DTL Alvarez is the standard choice for accelerating particles with a β range lying between 0.05 and 0.4. The transition energy from the RFQ to the DTL Alvarez has been decided on the basis of a compromise between the need to avoid any irradiation of the chopper line and the adoption of a reasonable DTL drift tube size , which can house the quadrupole of required strength. In this respect the choice of a FOFODODO lattice in the DTL permits to obtain the same phase advance per unit length of the FODO lattice using a quadrupole with a factor $\sqrt{2}$ less gradient. In the Linac4 this choice for the DTL structure becomes favourable with respect to the RFQ already at 3 MeV, giving an effective shunt impedance per unit length which is almost twice as much that of the RFQ, allowing for a lower longitudinal phase advance and a much larger bore aperture. While the DTL could work with acceptable efficiency up to about 100 MeV, a mechanically simpler and more efficient RF structure has been introduced in this design from 40 MeV, the CCDTL.

Fig. 3 shows a comparison between DTL and CCDTL in terms of effective shunt impedance as a function of the beam energy.

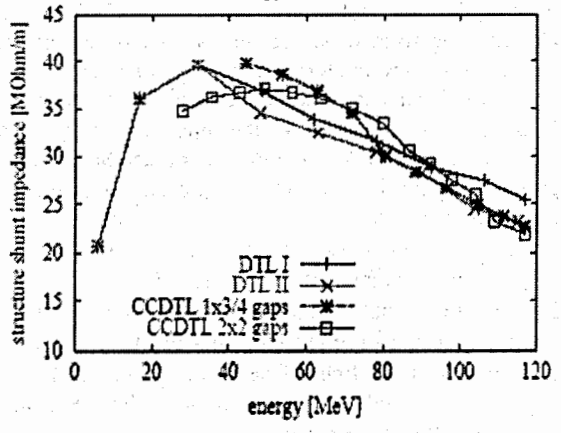

Fig. 3: Effective shunt impedance for DTL and CCDTL structures.

The idea of using compact DTL resonators, resonantly coupled to each other, was first tested at Los Alamos, where the potentiality of taking the quadrupoles out of the vacuum was fully understood. The shunt impedances per unit length of DTL and

CCDTL are comparable, the simpler mechanical construction and the easier accessibility to the quadrupoles have led us to give preference to the CCDTL in the segment between 40 MeV and 90 MeV.

Each CCDTL tank consists of three gaps. The intra-tank distance is kept constant in order to standardize the coupling cells and the $3\beta\lambda/2$ spacing between gaps of adjacent tanks, to allow sufficient place for quadrupoles, is obtained by changing the drift tube length on the end walls. The focusing period along the CCDTL is $7\beta\lambda$.

In the CCDTL the FODO lattice can be re-established, thanks to the increased length of the focussing period. The beam quality is preserved at the transition between the DTL and the CCDTL by slightly changing the synchronous phase and by allowing the beam to expand with the adoption of larger bore aperture quadrupoles (14 mm).

The final section of Linac4 (90 MeV to 160 MeV) is is built as a Side Coupled Linac (SCL), operating at 704.4 MHz. This choice maximizes the effective shunt impedance, as shown in Fig. 4.

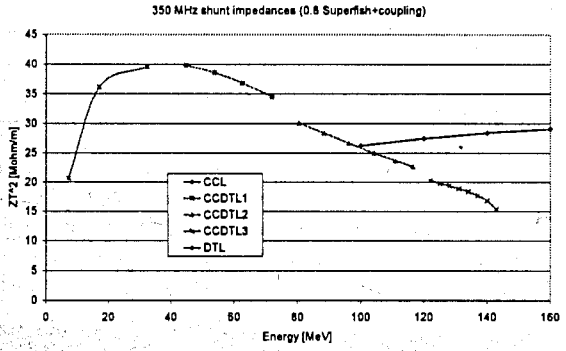

Fig. 4: Shunt impedances for different kinds of accelerating structure.

The accelerating and coupling cells are constant inside each tank, because of the limited variation of the particle velocity. The tank length results from the periodicity of $16\beta\lambda$ of the FODO lattice, which corresponds to a good compromise between RF efficiency and effective beam focusing.

The synchronous phase is ramped at the frequency transition in order to compress the bunch in the longitudinal phase space and to optimize the matching.

A ratio of about 0.7 is kept between longitudinal and transverse phase advance, thus requiring a gradient of 17 T/m from the permanent magnet quadrupoles.

Tanks are grouped by 4 and fed by a single 4 MW klystron. The coupling between tanks is done by means of $3\beta\lambda/2$ bridge couplers.

End to end simulations have been performed, assuming a 6-D waterbag beam distribution from the ion source, with 4% energy spread. The PATH code has been used and it has been cross-checked with IMPACT. Some discrepancies remain between the two simulations and the analysis is going on. The responsibility for the 73% of transverse emittance growth is mainly shared among the LEBT (33%) and the RFQ (14.4%) and a fundamental role will be played by the beam distribution at the output of the ion source output. The reduction to 2% of the effective energy spread at the source output (mainly due to beam divergence) could drastically reduce the transverse emittance growth at the end of Linac4. Therefore, testing the low energy part of Linac4 is very important for the whole project. An additional unexpected increase of longitudinal emittance within the DTL is presently under study. Table 2 summarizes the results of beam dynamics calculations over a population of 50000 particles.

[1] average value of emittance.

RF ACCELERATING STRUCTURES

As shown in Fig. 2, different kinds of accelerating structure are used in the Linac4. The main characteristics of the different accelerating sections are listed in Table 3.

Table 3: Linac4 main parameters.

Section	Output energy (MeV)	No. of cavities (tanks)	RF Freq. (MHz)	Peak RF power (MW)	No. of klystr.	Length (m)
LEBT	0.095	-	-	-	-	2
RFQ	3	1	352.2	0.9	1	6
Chopper	3	3	352.2	0.1	-	3.7
DTL	40	3	352.2	4.8	5	16.7
CCDTL	90	27	352.2	5.6	6	30.1
SCL	160	20	704.4	13.8	5	27.8
Totals		54	-	25.2	17	86.3

Table 2: Emittance growth, transmission and energy per section from PATH (50000 particles)

section	freq. [MHz]	length [m]	W_{out} [MeV]	$\varepsilon_{rms,t}$ [1)] [π mm mrad]	$\varepsilon_{rms,l}$ [π mm mrad]	$\Delta\varepsilon_{rms,t}$ [1)] [%]	$\Delta\varepsilon_{rms,l}$ [%]	transm. [%]
LEBT		1.27	0.095	0.188	-	33	-	100
RFQ	352.2	5.96	3	0.25	-	14.4	-	98.9
CHOPPER	352.2	3.77	3	0.286	0.5	4.9	0.6	91
DTL	352.2	16.71	40	0.3	0.5	5.0	0.0	99.9
CCDTL	352.2	30.54	90	0.315	0.58	3.8	1.2	100
SCL	704.4	27.78	160	0.327	0.59	-0.6	0.2	100
TOTAL		86.03	160	0.325	0.59	73	18	89.9

The IPHI RFQ

The 95 keV beam extracted from the ECR ion source is matched by the LEBT to an RFQ that has been designed by CEA Saclay and IN2P3 and is presently under construction. This IPHI ("Injecteur de Protons de Haute Intensite") RFQ is 6 m long. It is able to operate in CW mode with 100 mA beam current and accelerates the beam from 95 keV to 3 MeV. An agreement between CERN and the IPHI collaboration has led to a change of the original RFQ parameters [4] in order to adapt them to the requirements of the Linac4 and SPL and in particular to optimize the operation of the beam chopper line. A very detailed description of the IPHI RFQ has been presented at EPAC04 [5].

The DTL

The DTL section of Linac4 is made up of 3 tanks of the Alvarez type. The first tank is fed by one 1 MW klystron of the LEP kind, while two klystrons feed each of the following two tanks.

Transverse focusing is provided by Permanent Magnet Quadrupoles in the first tank, while Electromagnetic Quadrupoles are used in the second and third tanks.

A detailed list of parameters is shown in Table 4.

Table 4: Summary of Linac4 DTL parameters

DTL		**units**
Input Energy	3	MeV
Output Energy	40	MeV
RF Frequency	352.2	MHz
Number of tanks	3	
Aperture radius	10	mm
Gradient	3	MV/m
Lattice	FFDD	
Max. surface field	1.1	Kilpatrick
Length	16.7	m
Real estate gradient	2.21	MeV/m
Number of quads	111	

The first tank is being presently designed in the frame of an ISTC (International Science and Technology Centre - Moscow) supported project involving two Russian scientific centres, ITEP (Moscow) and VNIIEF (Sarov). It will be submitted to high power RF at CERN at the end of 2006.

CEA and IN2P3 give additional contribution to this section of the Linac4 by developing the high power coupler for the DTL tanks within the EU funded Joint Research Activity (JRA) HIPPI.

The CCDTL

The CCDTL section of Linac4 (40 MeV to 90 MeV) is composed of 27 small DTL tanks, with 3 accelerating gaps each, that are grouped into 6 modules. Each module, about 5 m long, is fed by one 352.2 MHz klystron and the tanks within the module are resonantly coupled to each other by means of coupling cells.

The RF operating mode is $\pi/2$ between tanks and coupling cells, which assures a satisfactory mode separation and stability for the whole resonant module.

Also in the case of the CCDTL, ISTC is supporting the activity of BINP (Novosibirsk) and VNIIEF (Sarov) in order to develop a high-power prototype of two complete tanks that will be tested at CERN in 2006. The main parameters concerning the CCDTL section are listed in Tab. 5.

Table 5: Summary of Linac4 CCDTL parameters.

CCDTL		**units**
Input Energy	40	MeV
Output Energy	90	MeV
RF Frequency	352.2	MHz
Number of tanks	27	
Gradient	3	MV/m
Lattice	FD	
Max. surface field	1.3	Kilp.
Aperture radius	14 - 16	mm
Synchronous phase	-25	deg
Length	30.1	m
Real estate gradient	1.7	MeV/m
Number of quads	28	

A first prototype of two half-tanks is under construction at CERN and will be tested at high power in 2005. The purpose is to check the accuracy of the computations and to measure the thermal load at the coupling irises [6]. Fig 6 shows the CAD model of the CERN prototype.

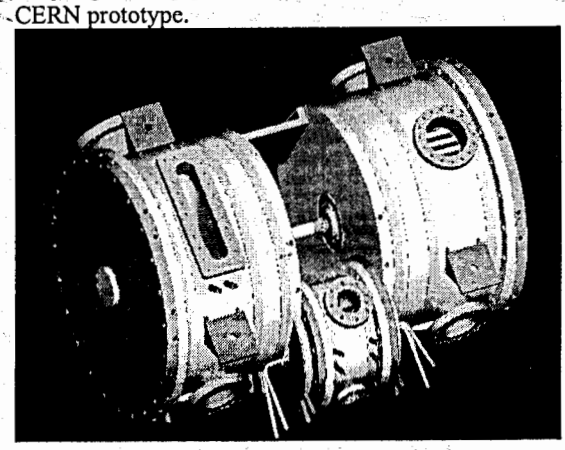

Fig 6: Assembled CCDTL prototype.

The SCL

The loss of efficiency of the CCDTL above ~90 MeV, as shown in Fig. 4, has lead to the choice of a $\pi/2$-mode Coupled Cavity Linac (CCL). The doubling of the RF frequency to 704.4 MHz in this section further contributes to the increase of efficiency. Among the possible choices, the Side Coupled Linac (SCL) has been adopted because of easy machining, tunability,

intrinsic stability and because of the large experience with this type of structures. In Table 6 the SCL main parameters are listed.

Table 6: Summary of Linac4 SCL parameters.

SCL		units
Input Energy	90	MeV
Output Energy	161.3	MeV
Length	27.8	m
RF Frequency	704.4	MHz
No. cells/tank	11	
No. tanks	20	
No. tanks/klystron	4	
Structure RF power	11.7	MW
Beam RF power	2.1	MW
Total RF power	13.8	MW
Total RF power (SPL)	12.6	MW
Max. power/klystron	2.8	MW
No. of klystrons	5	
Shunt Impedance	24.5-30.4	MΩ/m
Q-value	14-17	x 10^3
Gradient	4	MV/m
Synchr. phase	-25	deg
Peak electric field	0.76-0.81	Kilpatrick
Aperture radius	16	mm
Focusing	FD	
Quad. gradient	17.5	T/m
Transv. phase advance	23-20	deg/m
Long. phase advance	17-13	deg/m

IN2P3 and CEA (France) also contribute to the SCL within their participation to the HIPPI JRA. The ISTC funds the realization at BINP-Novosibirsk of a 2-cell full-copper technological model.

Further Options under Study

As a possible alternative to the Alvarez DTL, IHEP (Protvino) and VNIIEF (Sarov) are developing an RFQ-DTL structure at 352 MHz, with the support of the ISTC. This structure should benefit from a high shunt impedance, but also represents a technological challenge at that frequency. A full scale prototype is being designed and constructed. It will be tested at high power without beam.

Within the JRA HIPPI, superconducting alternatives to the SCL are being investigated. Two alternative schemes are under consideration, one adopting 704.4 MHz elliptical cavities and the other based on 4-gap spoke cavities operated at 352.2 MHz.

INTEGRATED SCHEDULE

The Linac4 project is now considered as a very useful step for the upgrade of the LHC injector chain. With the purpose of testing the technological issues and checking the beam dynamics at low energy, a test place is being realized at CERN in order to characterize the beam at 3 MeV, at the chopper line exit. This first section of Linac4 has been called SPL Front End. It will give valuable information about the halo formation mechanism and the validity of the chopping technique adopted. A tentative schedule for the realization of Linac4 and of the SPL is shown in Fig. 7, integrated with the planning for the construction of the 3 MeV Test Place.

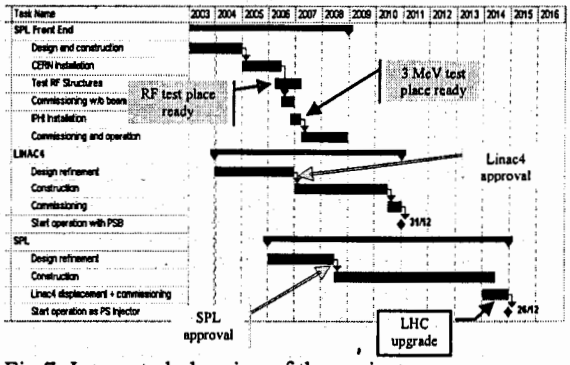

Fig.7: Integrated planning of the project.

ACKNOWLEDGMENTS

We acknowledge the support of the European Community-Research Infrastructure Activity under the FP6 "Structuring the European Research Area" programme (CARE, contract number RII3-CT-2003-506395) and the valuable collaboration of the CERN Groups involved. As mentioned in the main text, the ISTC supported projects # 2875, 2888 and 2889 are important contributions which accelerate the developments for Linac4 and the SPL.

REFERENCES

[1] M. Benedikt, K. Cornelis, R. Garoby, E. Métral, F. Ruggiero, M. Vretenar, "Report of the High Intensity Protons Working Group", CERN-AB-2004-022.

[2] R. Garoby, K. Hanke, A. Lombardi, C. Rossi, M. Vretenar, "Design of Linac4, a New Injector for the CERN Booster", Linac 2004, Lucerne, August 2004.

[3] F. Gerigk, E. Benedico, A. Lombardi, E. Sargsyan, M. Vretenar, "Beam Dynamics for a New 160 MeV H^- Linac at CERN (Linac4)", Linac 2004, Lucerne, August 2004.

[4] P-Y. Beauvais, "Status Report on The Saclay High-Intensity proton Injector Project (IPHI)", EPAC 2000, Vienna, June 2000.

[5] P.-Y. Beauvais, "Recent Evolutions in the Design of the French High Intensity Proton Injector (IPHI)", EPAC04, Lucerne, July 2004, Switzerland.

[6] M. Vretenar, Y. Cuvet, J. Genest, C. Vollinger, F. Gerigk, "Development of a 352 MHz Cell-Coupled Drift Tube Linac Prototype", Linac 2004, Lucerne, August 2004.

EXPERIMENTS WITH CARBON IONS ACCUMULATION IN THE ITEP-TWAC STORAGE RING

N.N. Alexeev, G.N. Akimov, P.N. Alekseev, V.N.Balanutsa, A.M.Bertjaev, S.V. Gaponenko, Ju.M. Gorjachev, A.S. Juravlev, V.P. Zavodov, P.R. Zenkevich, A.V. Kirillov, D.G. Koshkarev, A.D. Milijachenko, G.A. Nikitin, V.I. Nikolaev, B.S.Okorokov, V.G. Samsonov, D.V. Sosnin, B.Ju. Sharkov, A.V. Shumshurov, V.A. Shchegolev. ITEP, Moscow, Russia

Abstract

The ITEP-TWAC Facility is in two years of experiments with accumulation of fully stripped carbon ions of near relativistic energy (200-400 MeV/amu) by using the charge exchange injection technique. First stacking of the beam has been obtained in the storage ring U-10 in 2002. Adjustment of the multiple injection conditions, the magnetic field correction, and diminishing of disturbing influence of the relevant equipment components to the coasting beam let to gain an injected beam intensity by factor of fifty to reach the level of $2 \cdot 10^{10}$ stacked particles. Current results of activities for the accumulation process optimisation are presented.

INTRODUCTION

The upgrading of ITEP's accelerator complex with the aim of creating a heavy-ion accelerator-accumulator ITEP-TWAC on the base of U-10 proton synchrotron was started in 1997 [1]. In modifying the proton synchrotron into a heavy-ion accumulator, the existing proton-beam acceleration technology was retained, and an opportunity to accelerate ions in the U-10 up to relativistic energies was also provided. The basic project parameters of the complex are presented in Table 1.

Table 1: Project parameters of the ITEP-TWAC Facility

Operation mode	Beam parameters	
Proton Accelerator	Energy, GeV	10
	Intensity, c^{-1}	10^{11}
Ion accelerator	Accelerated ions	to U
	Energy, GeV/amu	2-4
	Intensity, n/c	10^{11}
Ion accumulator	Accumuletad ions	to Zn
	Particle energy, MeV/amu	to 700
	Beam energy, kJ	100
	Beam power, TW	1

The first stage of the reconstruction is completed with the result that the technological scheme of the new facility is fully created to do experiments with carbon beam accumulation using charge exchange injection technique. During the reconstruction, a 4 MeV/amu ion linear injector I-3 was built [2], an ion booster synchrotron UK was started up [3] and a multiple injection of ions from the UK into the accumulator ring, converted from the U-10 proton synchrotron, was realized [4-8]. The adjustment work had resulted in stacking of the carbon nuclei in the U-10 ring at an energy of 200 MeV/amu, as well as their acceleration in the U-10 up to an energy of 4 GeV/amu [8]. The intensity of the stacked carbon nuclei beam reaches presently 2×10^{10} particles, with the factor of 50 for the injected beam intensity increase. The stacked beam is compressed in the longitudinal direction and extracted into a transport channel to be used in experiments.

MULTIPLE INJECTION LAYOUT

The ion accumulation procedure is based on the charge-exchange injection with using a fast bump system for minimising the stacked beam perturbation over penetrating through the stripping foil material. Schematic layout of the beam trajectory at injection and the injection elements are shown in Fig.1.

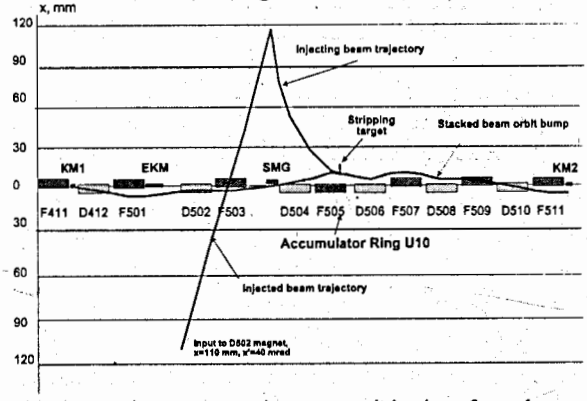

Fig.1: The ion beam trajectory at injection from booster synchrotron UK to accumulator ring U-10.

The septum magnet SMG with magnetic length of 0.8 m is placed outside of the U10 ring between magnets F503 and D504. This magnet is used not only for the beam injection but for extraction too. The SMG steers the injected beam to the centre of the stripping foil of the 10x20 mm size, which is placed in the vacuum chamber of the F505 with displacement of 20 mm from the ring equilibrium orbit. The fast bump system matching of both injected and circulating beams includes three kicker magnets installed in the short straight sections after of the magnets F411, F511 and F711. The first kicker magnet gives the kick of ~3 mrad deflecting the stacked beam to the stripping foil at a moment of the injected beam passing through the transfer line. The two beams becoming one after passing through the stripping foil are set to the ring orbit downwards by the kicker magnets in straight sections of F511 and F711. The foil material is mylar with the thickness of 1.5 mg/cm^2.

INJECTION EFFICIECY

There are many factors to be responsible for the charge exchange injection effectiveness. Some of them are raised from the beam interaction with the stripping foil material; others are depended on vacuum and beam stability conditions in accumulator ring. Parameters of the stacking beam are listed in Table 2. The calculated values of the beam interaction with the stripping target parameters are presented in Table 3. As can be seen from this table, the

Table 2: Parameters of the stacking beam

Type of ions	$C^{4+}=>C^{6+}$
Energy, MeV/amu	200
Momentum spread, %	±0.04
Emittance, π mm·mrad	~5
Beam intensity, ppc	$\sim 5\cdot10^{8}$

beam loss factor is less than 10^{-4}, so it can be neglected. The momentum spread increase may be essential, but in our case it can be not taken into account because of the beam stacking with accelerating voltage of ~1 kV that matched with momentum spread of the injected beam.

Table 3: Parameters of beam interaction with the target

x_t, mg/cm^2	1.5
σ_i, barn	2
$\overline{\delta x'^2}$, (rad)^2	10^{-8}
$\overline{\delta p/p}$	$5\cdot10^{-5}$
$\overline{\delta\varepsilon}$, π mm·mrad	0.15
$\overline{\delta Q_x}$	$4\cdot10^{-4}$
$\overline{\delta Q_z}$	$1\cdot10^{-3}$

Emittance increase by the multiple coulomb scattering is the main factor of beam loss at interaction with the stripping foil. The beam lifetime for parameters from table 3 is estimated by the value of $\sim 20\cdot A_{x,z}$ [s].

The beam lifetime in the real machine depends not only on the particles interaction with the target but on the vacuum and beam stability conditions in accumulator ring too. Summarizing the beam disturbing factors listed in Tables 4-5 we got the estimated beam lifetime as $\sim 25\cdot A_{x,z}$.

Table 4: Beam interaction with residual gas parameters

P, Torr	10^{-8}
x_t, mg/cm^{2}s	0.2
$\overline{\delta x'^2}$, (rad)^2/s	$1.5\cdot10^{-9}$
$\overline{\delta p/p}$, s^{-1}	$7\cdot10^{-6}$
$\overline{\delta\varepsilon}$, π mm·mrad/s	0.02
$\overline{\delta Q_x}$	$4\cdot10^{-5}$
$\overline{\delta Q_z}$	$1.5\cdot10^{-4}$

As can be seen from the working diagram of the U-10 ring shown on Fig.2, there is two accessible regions of beam stability between betatron stopbands of third, forth and fifth orders. The stable spot of the beam tune shift

Table 5: Parameters of U-10 magnet imperfections

Pulsed magnetic fields of beam transfer line UK/U-10	$\delta r<10^{-3}$, $\delta Q<10^{-3}$
Difference of the fast bump kicker magnets wave forms	$\overline{\delta\varepsilon}\sim10^{-2}$ π mm·mrad
Imperfection from UK magnetic cycle	$\delta B/B<10^{-4}$, $\delta Q<10^{-3}$
The orbit distortion from the fast bump	$\delta A_x\sim10$-20 π mm·mrad
Ripples of power supplies of main magnet and correction circuits	$\delta B/B\sim1.5\cdot10^{-5}$, $\delta Q\sim3\cdot10^{-4}$

$\Delta Q_x x \Delta Q_z=(2x8)\cdot10^{-3}$ occupied by the injected beam is small enough and should be changed by moving the working point to the free space of top-right square.

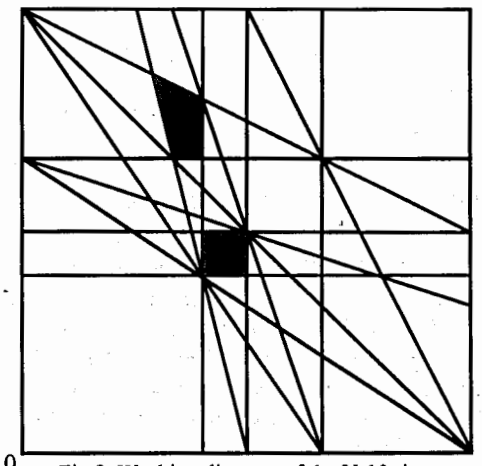

Fig.2: Working diagram of the U-10 ring.

EXPRIMENTAL RESULTS

First beam accumulation was obtained in March 2002. Subsequent improvement of the charge exchange injection technique and the quality of accumulator ring let us to rise beam stacking stability. The beam transfer from booster synchrotron UK to the accumulator ring U-10 is shown on Fig. 3. It's seen that only six bunches from tens in the UK ring are transfered to accumulator ring due to the small

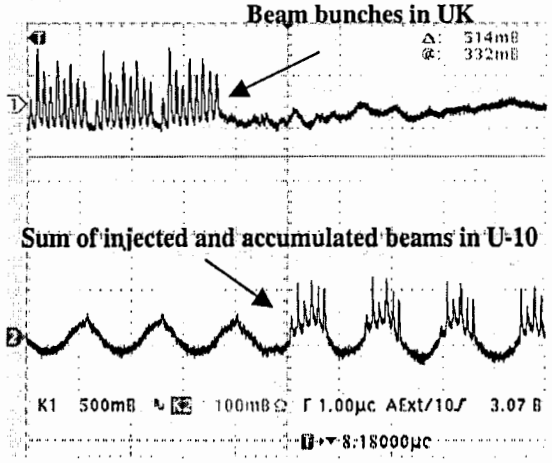

Fig.3: Beam transfer from UK to U-10.

width of fast bump pulse that is shorter than revolution time of the beam. This discrepancy should be eliminated by longitudinal compression of the beam before ejection. We had successfully tested methodic of beam compression on the raising magnetic field in the UK ring but didn't got injection efficiency increase because of the beam momentum spread and tune shift extension. We

hope to get positive result after improving the tune shift correction system and changing the working point.

The stabilized process of the beam accumulation is shown on oscillograms of Fig.4-6. It' seen linear increase of the stacked beam intensity during more that thirty injection cycles. This is result of successive stabilization a

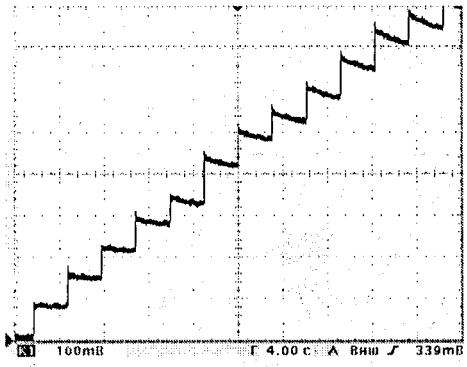

Fig.4: The start of beam stacking in U-10.

whole lot of elements on the way from laser ion source to stripping foil. Reduction of the intensity growth rate coursed by growing loss of stacked particles leads to the saturation of the stacked beam intensity. As can be seen from Fig. 6, the level of saturated intensity is more than 50 times of injected one.

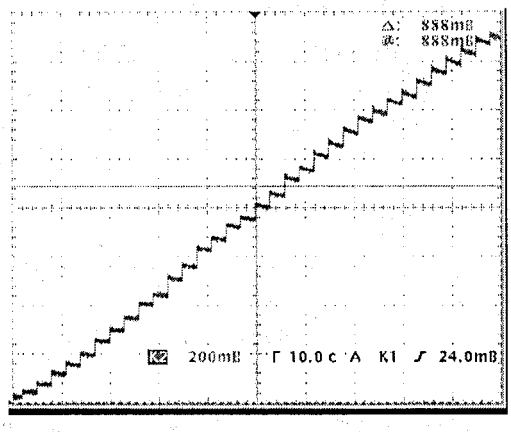

Fig.5: The linear increase of stacked beam intensity during more than 30 injection cycles($1V/10^{10}$).

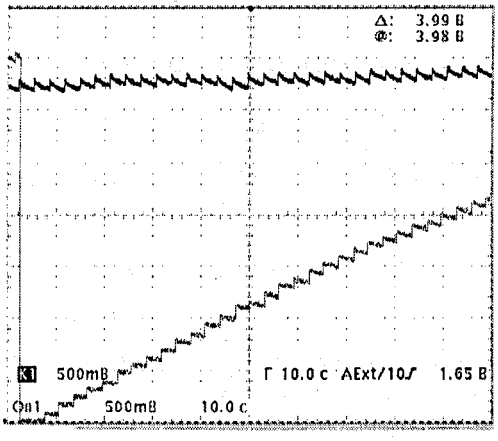

Fig.6: Saturation of the stacked beam intensity on the level of $2 \cdot 10^{10}$ particles.

Analysis of a different factors contribution to the beam loss rate can be done measuring the beam lifetime at the fast bump to be on and off. Results of these measurements at some preliminary state of machine and vacuum in the accumulator ring of $\sim 10^{-8}$ Torr are shown on Fig. 7. Using equality $\tau_o = 25 \cdot A_{x,z}$, we get estimation of the accumulator ring dynamic acceptance as $A_{x,z} \sim 10\ \pi$ mm·mrad. Designating δA as acceptance reduction from the orbit

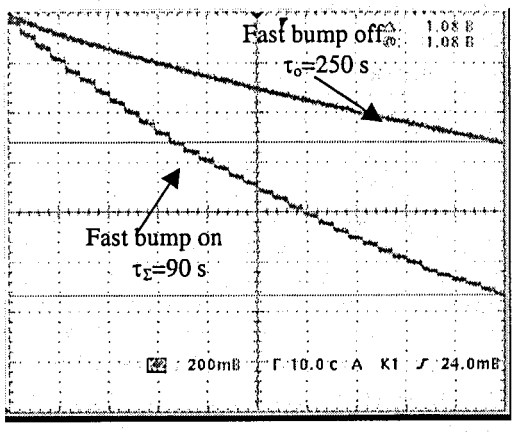

Fig.7: The stacked beam loss time.

displacement by the fast bump at injection, and considering equality $(\tau_o \tau_\Sigma)/(\tau_o - \tau_\Sigma) = 20\ (A_{x,z} - \delta A)$, it estimates $\delta A \sim 3\ \pi$ mm·mrad. For the intensity growth shown on Fig.5-6, the beam lifetime is $\tau_\Sigma = 150$ s that was reached by reducing the value of δA.

CONCLUSION

1. Experiments with carbon ions accumulation in the U-10 ring demonstrated the progress in the accumulated beam intensity that is fifty times the intensity of injected beam.

2. Further advance in intensity is expected from improvement of vacuum in the ring, decrease the stripping foil thickness and elimination of difference in the waveforms of the fast bump kickers.

3. The accumulator acceptance and momentum spread of accumulated beam are limited now through irregular setting of working point because of the settling problem of the tune shift correction limit.

REFERENCES

[1] D.G.Koshkarev et al., "ITEP Accelerator Facility Upgrade", XV Workshop on Charged Accelerator, Protvino, v.2 (1996) p.319.

[2] N.N.Alexeev, et al., "Beam dynamics in matching channel of ITEP-TWAC Heavy Ion Injector I-3" - In Proc. EPAC -2000, p.1283-1285.

[3] N.N.Alexeev, et al., "Acceleration of C^{4+} ions in Booster Synchrotron UK at ITEP".XVII Workshop on Charged Accelerator, Protvino, , v.2 (2000) p.231.

[4] N.N.Alexeev, et al.,"Non-Liouvillian accumulation of carbon nucleons in the ITEP TWAC Facility"

[5] P.Zenkevich, et al., "Strategy of intense ion beam accumulation by use of charge exchange injection". Nucl. Instr. Meth. in Rhys. Res., A464 (2001) 616.

[6] Alexeev N.N., et al. "Status of the Terawatt Accumulator-Accelerator project" Laser and Particle Beams 20 (2002) 385-391.

[7] N.N.Alexeen, et al. "Commissioning of Storage Ring TWAC", Atomic Energy,v.93, n.6 (2002) 474-479.

[8] N.N.Alexeev, et al. "Accumulator-Accelerator ITEP-TWAC". Particle and Nuclei, Letters. 2004. No 3(120), 78-87

SLOW EXTRACTION SYSTEM FROM IHEP ACCELERATOR U-70 STATUS AND DEVELOPMENT

Yu.S. Fedotov, A.G. Afonin, Yu.G. Karshev, V.V. Lapin, A.V. Maximov, A.V. Minchenko, I.I. Sulygin, V.I. Terekhov, E.F. Trojanov, IHEP, Protvino, RF

Abstract

Slow extraction system of the accelerated proton beam from U-70 is used for physical experiments with the counting principles with the spill duration of 1-2 seconds on the flat-top magnetic field at energy 50-70 GeV. The slow extraction system commissioning took place in 1979. Initial efficiency of an extraction did not exceed 83-85%. Inclusion in extraction system an electrostatic deflector with the wire septum of 0.1 mm thickness has allowed to simplify the scheme of an extraction which began to contain only two septum-magnets in 24-th and 26-th straight sections. Extraction efficiency was 85-87% that was insufficiently for an extraction of intensity more $1 \cdot 10^{13}$ ppp. Modernization of the system of the resonant extraction with inclusion in structure of the accelerator two additional quadrupole lenses has allowed to increase structural β-function in the location of electrostatic septum to reduce losses on it and on the first septum-magnet three times and reach extraction efficiency 95±2%. For suppression of modulations of intensity of an extracted beam the method of phase displacement on RF-separatrices of 200 MHz is used. Effective time (duty factor) of an extraction reaches thus 95%.

HISTORY

Historically the slow extraction system was created after the fast extraction system start. The direction of the extracted beam was set in view of a direction of channels of fast extracted protons and secondary particles in an experimental hall [1]. The slow extraction system is based on the resonant growth of radial betatron amplitudes with the help of a nonlinear third order resonance $3Q_r = 29$. This resonance possesses a number of advantages in comparison with other resonances and the working point on a diagram of betatron frequencies lays near $Q_{res} = 9\frac{2}{3}$. The resonant harmonic of square-law nonlinearity is created by two pairs of sextupole lenses. In each pair lenses have a different sign and located oppositely on a ring of the accelerator so they raise all odd harmonics of square-law nonlinearity and do not create the constant component (that influence on chromaticity). Two pairs are located from each other under a corner 90°, and with their help it is possible to adjust of resonant harmonic phase on 360°. Sextupole lenses located in straight sections (SS): 12; 42; 72; 102 (see Fig. 1).

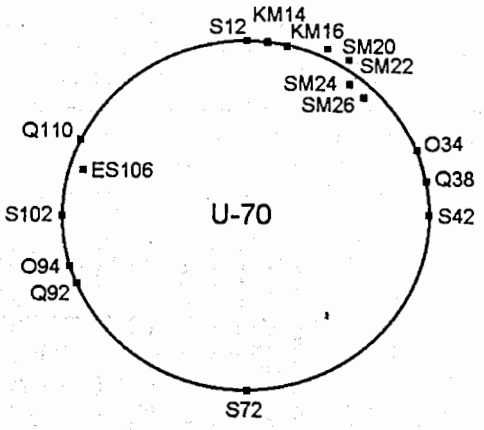

Figure 1: The arrangement of extraction system elements on the ring of accelerator U-70: S – sextupole lens, Q – quadrupole lens, O – octupole lens, KM – fast kicker-magnet, SM – septum-magnet, ES – electrostatic septum

In order to change the radial betatron tune at approaching on a working resonance at extraction the quadrupole lens located in 38-th straight section used. Perturbed by the radial resonance the beam firstly got to the bend-magnet SM18 (see Fig. 2) having septum with effective thickness of 0.7 mm.

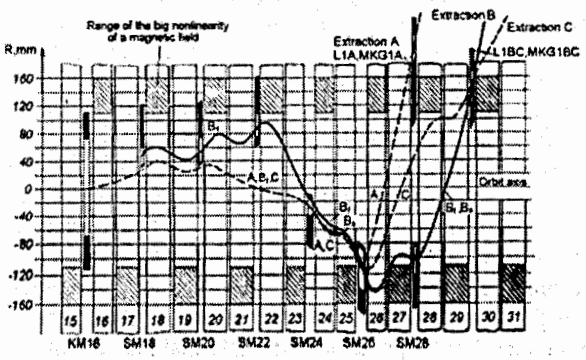

Figure 2: The initial scheme of beam trajectories of fast and slow extraction

Further the beam was transferred on the chain through magnets SM20, SM22 and SM28. Last magnet directed proton beam to 30-th straight section. Slow extraction efficiency did not exceed 83—85% in so complex multistage scheme. In order to increase extraction efficiency electrostatic septum (ES106) with thickness of 0.1 mm (about 0.15 mm effective thickness at 3 m long)

and working strength of the electric field 70 kV/sm have been established in SS106. At such parameters of the septum deflection of the beam did not exceed 0.3 mrad. The angular width of a beam on input of the deflector at extraction of the beam with emittance 2 mm·mrad makes also 0.3 mrad. Therefore clear split of extracted and circulating beam at input in SM18 practically was not. Extraction efficiency with electrostatic septum has reached 85—87% that was insufficiently for an extraction of the high intensity. In connection with change of the program of physical experiments configuration of the experimental hall and channels of transportation of particles [3] has been changed. The scheme of a fast extraction of a proton beam has been changed and essentially simplified (see Fig. 3). It became three-stage.

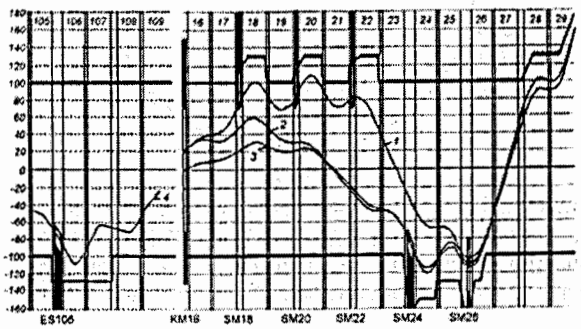

Figure 3: The modern scheme of fast and slow extraction

At modernization of the fast extraction scheme has undergone changes and configuration of the scheme of a slow extraction. The arrangement of the first deflecting septum-magnet after electrostatic septum coincides with an arrangement of septum-magnet SM24 of the fast extraction system. Thus, there came to uniform configuration the extraction systems including three elements of the slow extraction (ES106; SM24; SM26) and three elements of the fast extraction (KM16; SM24; SM26). The full quantity of elements in the extraction scheme began to be only four, and two of them are the common for fast and slow extraction. Increase of the efficiency of the slow extraction have not taken place, as parameters of the beam thus have not changed. In accordance with requirements of experimental complex using slowly extracted beam, extraction of the intensity more then $1 \cdot 10^{13}$ ppp demand the essential increase of the extraction efficiency. Efficiency of the slow extraction in our scheme is defined by losses of the extracted beam on the first two elements: electrostatic septum ES106 and septum-magnet SM24. Additional losses can arise due to limitation of the extraction devices apertures, especially vertical. At excitation of the working resonance of slow extraction $3Q_r = 29$ the parasitic coupling resonance of the third order $2Q_z + Q_r = 29$ is simultaneously raised. At growth of radial amplitude in the working resonance vertical amplitude grows due to a coupling resonance. Losses on first septum are defined by effective thickness of wires of 0.15 mm and increase of the effective thickness seen by the beam along the length $l_{ES} = 3$ m due to angular width $\Delta r'_{106} = 0.3$ mrad in the extracted beam near ES106 $\Delta r = \Delta r' \cdot l_{ES}$. Losses on the septum-magnet are defined by size of clearance between the extracted and circulating beams, arising due to deflection of the extrected beam in ES106. The angular beam width in outgoing separatrices on the first extracted device is defined by emittance and volume of the structural β – function $\Delta r'_{106} = \frac{\pi}{\sqrt{3\pi\sqrt{3}}} \frac{r\sqrt{\varepsilon_r}}{\sqrt{\beta_{r106}}}$. From here one can see in order to reduce of the angular beam width on first septum it is necessary to increase β – function.

MODERNIZATION OF THE SLOW EXTRACTION SYSTEM

To change volume of the structural β – function it is possible by introduction quadrupole lenses into magnetic structure of the accelerator with the force $k = \frac{G_q l_q}{B_0 R_0}$, where G_q – gradient of the magnetic field, l_q – his length, $B_0 R_0$ – beam rigidity:

$$\beta = \beta_0 - \beta_0^2 \sin(2\Delta\psi)\frac{k}{2} + \beta_0^3 \sin^2(\Delta\psi)\frac{k^2}{4},$$

$\Delta\psi$ - phase advance from quadrupole up to the point of supervision. For localization of the disturbance it is necessary to use at least two quadrupole lenses with the phase advance between them equal to odd number π. Additional quadrupole lenses on the accelerator U-70 ring have been established in SS92 and SS110. Force of lenses is chosen so that it was possible to increase $\sqrt{\beta_{r106}}$ up to 1.5 times. Thus the angular width in the beam decreases up to 0.2 mrad, and we have visible spatial clearance between extracted and circulating beams on the septum-magnet SM24. Deflected in ES106 beam passed through quadrupole lens in SS110 receives additional spatial displacement of

$\Delta r_{24} = -m_{12(106-110)} m_{12(110-24)} k_{110} \Delta r'_{ES} = -4.3$ mm,

where $m_{12(106-110)} = 23$ m, $m_{12(110-24)} = 25$ m – transfer matrix element from SS106 up to SS110 and from SS110 up to SS24 accordingly. The common deflection of the beam in SS24 makes about 6 mm.

On Fig. 4-5 results of the numerical simulation of the resonant process in the old and modernized slow extraction system are shown.

On Fig. 5 the angular clearance between the circulating beam (to the right of coordinate of –65 mm) and the beam deflected in ES106 is seen. On Fig. 6-7 the radial movement phase plane in SS24 is shown.

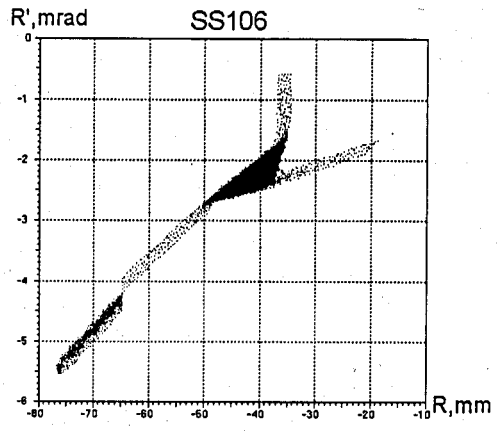

Figure 4: The phase plane of radial movement in SS106 in not modernized slow extraction system

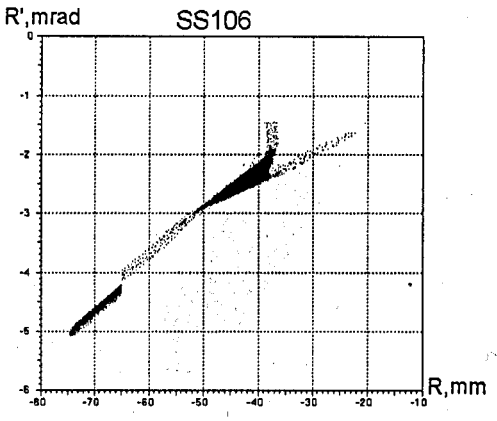

Figure 5: The phase plane of radial movement in SS106 in the modernized slow extraction system

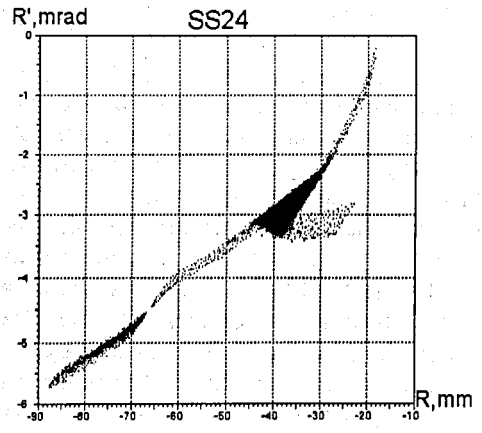

Figure 6: The phase plane of radial movement in SS24 in not modernized slow extraction system

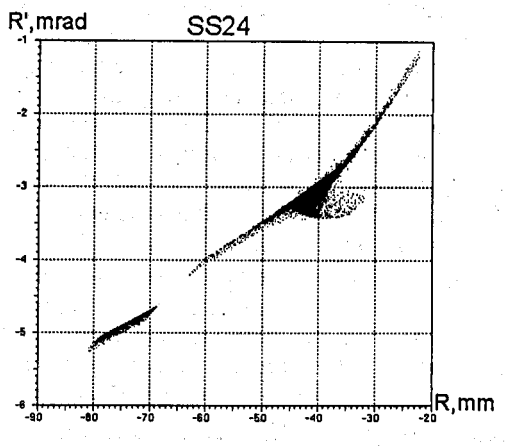

Figure 7: The phase plane of radial movement in SS24 in the modernized slow extraction system

On Fig. 7 the clearance about 6 mm between circulating and extracted beams is seen that coincide with an analytical estimation. It's enough for locating of current strip of the bend-magnet SM24 having effective thickness of 2.4 mm. The numerical estimation of losses on both magnets makes about 5%. Therefore the expected efficiency estimation of the extraction should be not less than 95%.

EXPERIMENTAL RESULTS AFTER MODERNIZATION

The increase of the structural β-function demands the increase of the resonant harmonic force of parabolic nonlinearity of a working resonance. It leads to growth of the coupling resonance harmonic and its stronger influence on vertical movement. For reduction of the coupling resonance influence it is necessary to move from a line $2Q_z + Q_r = 29$ as it is possible further. The working diagram of betatron frequencies of U-70 is shown on Fig. 8.

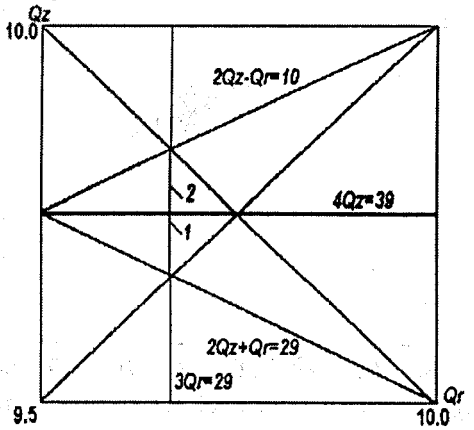

Figure 8: Working diagram of betatron frequencies and course of a working point at moving on the resonance in old (1) and the modified (2) system

The line 1 shows a course of a working point at moving on the resonance at slow extraction before modernization. The working point of betatron frequencies on the diagram is established by gradient correction system. The current limit in this system does not exceed 100 A. With such current at energy 70 GeV a working point approaches close to a line of the resonance $4Q_z = 39$. At start of the modified system of the slow extraction the high particles losses took place and efficiency of an extraction have been found out did not exceed 50% instead of expected 95%. Researches of behavior of the beam near to a working point have shown, that losses of the beam are caused by a resonance $4Q_z = 39$, normally exited by cubic nonlinearity of accelerator magnetic field. With sextupole lenses only, far from a line of working resonance $3Q_x = 29$, it is lost about 80% intensity on a line $4Q_z = 39$. Frequency shift from this line approximately on 0.02 provided beam conservation with sextupole lenses switching on. Explanation of such beam behavior it is possible only by resonance $4Q_z = 39$ influence with parabolic nonlinearity in the second approximation of the theory of averaging. The system of the working resonance excitation of the parabolic nonlinearity with the help of four powerful sextupole lenses is the strong source of some resonances if to take into account the second approximation. It excites all odd harmonics of parabolic nonlinearity, therefore a resonance $4Q_z = 39$ is a reason of the beam losses. Numerical simulations of the amplitude growth in our system near to a line $4Q_z = 39$ have shown correctness of this point of view. On Fig. 9 the phase plane of vertical motion is shown at initial frequency $Q_z = 9.745$. Obvious display of the fourth order resonance is visible.

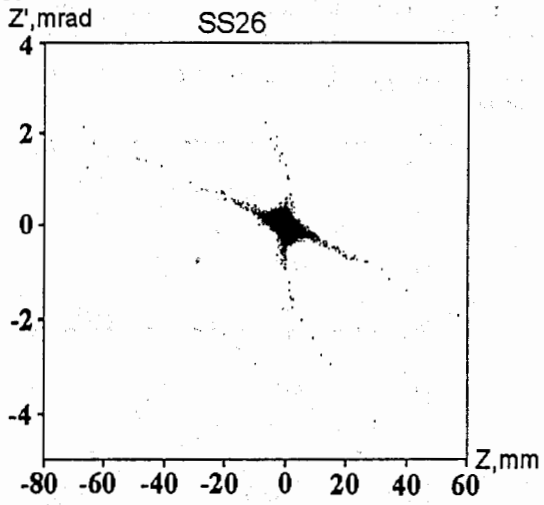

Figure 9: Phase plane of the vertical motion near resonance $4Q_z = 39$

To set a working point at the slow extraction above line $4Q_z = 39$ one have reduced energy of the accelerator up to 64 GeV (field B_0 from 12 up to 11 kGs). It has enabled to reach initial position of a working point of the slow extraction at $Q_z = 9.78$ (a line 2 on Fig. 8). On Fig. 10 the phase plane of the vertical motion in SS26 is shown. One can see the absence of the fourth order resonance. In SS26 the vertical size of the ejected beam has the maximum volume. Because of the influence of the coupling resonance the vertical size makes ±10 mm at initial ±7 mm. The vertical magnet aperture is equal 25 mm and sufficient freedom for accommodation of a beam is not present. The vertical closed orbit distortions can reach volume of 7-10 mm. Therefore at slow extraction it is necessary to adjust ejected beam position in the bend-magnet SM26 aperture with the high accuracy by the vertical correction system. At performance of all requirements on adjustment of the slow extraction system and careful setting of ejected beam on the extraction trajectory the extraction efficiency 95%±2 is reached with the intensity $1.5 \cdot 10^{13}$ ppp.

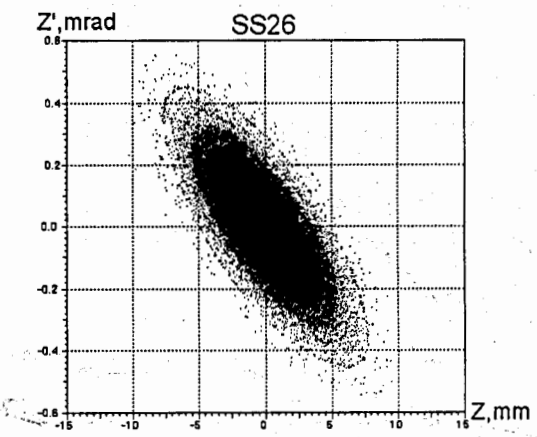

Figure 10: Phase plane of vertical motion of ejected beam in SS26 with initial $Q_z = 9.78$

At extraction intensity more than $5 \cdot 10^{12}$ ppp due to beam coupling with RF stations and other elements of the vacuum chamber of the accelerator the beam instabilities arise in longitudinal motion with the frequencies of the ~5 MHz, witch leads to modulations of ejected intensity. It decreases efficiency of experimental physical set on 30-40%. For suppression of these effects after switching off 6 MHz RF system the 200 MHz RF station is switched on. The frequency modulation of 200 MHz with frequency deviation of ±500 Hz in a range of 1000-1500 Hz changes the beam density distribution in a phase plane of longitudinal motion, doing it more flat. This procedure eliminates instability rising on high frequencies and improves quality of slow ejected beam [3].

For suppression of the ejected beam intensity modulation on low frequencies the method of phase displacement with use of accelerating station on the frequency of 200 MHz is also used. For additional suppression of modulations the low-inductance quadrupole lens included in a beam intensity feedback

system [4]. It allows to receive a quality of a slow extracted beam with duration more than 1 sec with duty-factor of the extraction ~95% (see Fig. 11).

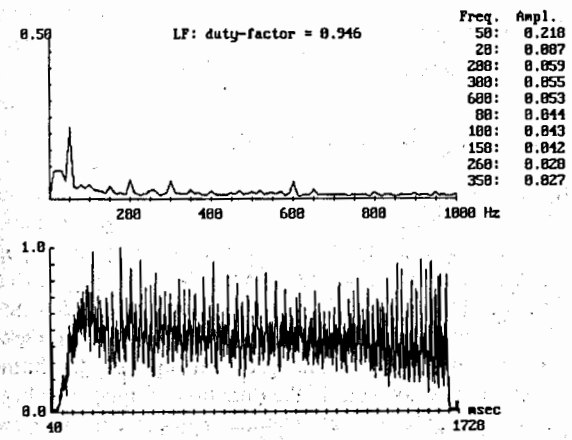

Figure 11: Spectrum and spill of slow ejected beam in last runs

Difficulties of adjustment of system of the slow extraction, defined by lacks of the vertical correction systems of the beam orbit demand the increase of the vertical aperture of SM26 up to 30-35 mm. Thus the efficiency of the extraction up to 97% can be achieved.

REFERENCES

[1] K.P.Myznikov, V.M.Tatarenko, J.S.Fedotov, "Performance of systems of a slow and fast extraction of protons of accelerator IHEP on energy 70 GeV", IHEP RAS 70-79, Serpukhov, 1970, 34 pages, (in Russian).

[2] A.G. Afonin, V.I. Dianov, A.V. Maximov, "Optimization of the scheme of a slow extraction of a proton beam from U-70", IHEP 92-121, Protvino, 1992, (in Russian).

[3] B.A. Kalinin, V.G. Kudryavtsev, A.J. Malovitsky, K.P. Myznikov, I.I. Sulygin, "Research and suppression of a self-grouping of a beam at a slow extraction of particles from U-70", The report at the given conference.

[4] V.V. Lapin, D.V. Korobov, O.V. Zjatkov, V.A. Jaichkov, "The first stage of modernization of a feedback on intensity of the extracted beam in slow resonance extraction from proton synchrotron IHEP on 70 GeV", The report at the given conference.

LEBEDEV PHYSICAL INSTITUTE RACETRACK MICROTRON UPGRADE

V.G.Kurakin, V.M.Alekseev, V.P.Busygin, A.V.Koltsov,
Lebedev Physical Institute, Moscow, Russia
P.V.Kurakin
Keldysh Institute of Applied Mathematics, Moscow, Russia

Abstract

Lebedev Physical Institute racetrack microtron is in use since the mid of eightieth of the last century. Currently it serves as free electron laser driver at the Lebedev Physical Institute Radiation Complex. Flexibility of the design and high pulse intensity of accelerated beam are the features of this machine. The experience that had been acquired during long period of accelerator use has brought us to decision to upgrade the machine in order to bring it to modest level of operation with precise beam parameters and prepare it for new tasks as well. New configuration assembling will be combined with non steady beam dynamics exploration. The latter assumes also high current instabilities study, first of all beam intensity auto modulation. The project includes two stages. The final one assumes electron beam energy increase up to the level of 50 MeV, and this requires three additional orbits assembling. We plan to replace existing monitoring and control system with modern computer based system, and together with accelerator exploration this will comprise the first step of the accelerator upgrade. The whole project is scheduled to be completed in three years.

INTRODUCTION

Lebedev Physical Institutive Racetrack Microtron was developed as new injector for the Lebedev Institute electron synchrotron to the maximum energy 1.3 GeV [1]. It was assumed that new machine would replace old injector based on classical microtron. Higher energy of injected beam seemed to be reliable measure to improve synchrotron performance in the sense of higher beam intensity and beam stability. Racetrack had been commissioned in the mid of eightieth with the unexampled beam parameters for such class of accelerators [2]. Intensities achieved - 0.25 A at the energy 30 MeV as well as 0.3 A at the energy 24 MeV – are more typical for RF linear accelerators rather then for microtrons, while energy spread less than 1% was inherent to microtron. The maximum energy achieved was limited by accelerator orbits had been mounted, while the maximum beam current was limited by beam instability. Plans of electron synchrotron use had been changed to racetrack commissioning moment. The main accent had been moved to the physics on extracted electron beam with tagged photons method and synchrotron configuration with old injector seemed to be quite adequate for this new task. At the same time racetrack parameters appeared to be quit suitable in order to use the machine as a free electron laser driver [3]. Racetrack team had been oriented to the radiation complex development on the bases of existing high current racetrack, and scientific appropriate program had been declared soon [4]. Far infrared free electron laser (FEL) commissioning was the main result of this program [5]. One of the items of the program supposed the further racetrack development in the direction of improving beam parameters as well as accelerator upgrade. This item was frozen for decay due to limited recourses available. Followed are some considerations as well as details concerning this program realization.

CURRENT RACETRACK CONFIGURATION

Lebedev Physical Institute High Current Racetrack is a key component of the Radiation Complex and serves as the electron beam driver for far infrared FEL. The remarkable feature of the complex is that racetrack can be used in any of two quite independent modes. First, it may provide electron beam for FEL, and active part only, namely linear accelerator is used for this purpose. Second, racetrack itself might be used as stand alone accelerator for other electron beam based program.

The racetrack consists of pare of 180 degrees bending electromagnets with uniform magnetic field and the RF linear accelerator being located between these. Synchronism of electrons motion relative RF field in the linac is realized by increase of any new turn circulation time by integer number of RF period that is equal two in our accelerator. RF liner accelerator is formed by the main accelerating structure on the basis of disk loaded waveguide and additional RF resonator at the entrance of the main structure. Electron beam from low voltage electron gun is guided on the axis of the RF linac by means of two magnet 90 degrees inflector that provides almost transparent beam passage from subsequent racetrack orbits. Electron beam being accelerated in linac then is rotated in bending magnet through 180 degrees and moves in beam pipe (return path) to the next bending magnet. This magnet rotates beam through 180 degrees again, thus directing electrons on the accelerating section axis. Here the electron beam crosses inflector and enters the linear accelerator again, thus increasing its energy any additional passage in linac. Beam focusing is provided by electromagnetic quadruple doublets that are installed on return paths at the bending magnets edges and at accelerating trajectory path. The focusing of the electron beam that passes through RF linac is performed by

electromagnetic solenoid. Correcting coils are consist of two pares windings that induce magnetic field in transverse direction relative beam motion. These are installed at the bending magnets edges allowing independent control of transverse motion that is quite necessary to compensate magnetic field errors as well as control errors. Luminescent screens as well as induction monitors and Faraday caps are used to control accelerated beam intensity and its position. RF power for RF field in linac excitation is provided by RF amplifier on the basis of klystron with output up to 25 MW. The power is delivered to the main accelerating structure and resonator through power divider that divides the input power in proportion 9 to 1. The main racetrack parameters are collected in table 1.

Table 1: Main racetrack parameters

Orbit number	1	2	3	4	5
Beam energy (MeV)	6	12	18	24	30
Pulse current (A)	0.5	0.4	0.28	0.23	0.2
RF pulse duration	9 μs				
Current pulse duration	5-6 μs				
Energy spread (%)	1.5-0.7				
Hor. emittance (mm)	7 mm*mrad				
Vert. emittance	3 mm*mrad				
Bunch phase length	20-36 degrees				
Max. klystron output	25 MW				
RF wavelength	16.5 cm				
Repetition rate	0.1-5 Hz				

RACETRACK PERFORMANCE – BEAM DYNAMICS AND INSTABILITY

High racetrack intensity imposes definite features on racetrack performance. First of all one has to adjust accelerator systems and parameters at the injection intensity close to maximum value. At low beam intensity synchronism is achieved at low input RF and as a result at low RF field at the entrance of the main accelerator structure. This results in accelerator full admittance quite different from optimal value (design parameters). The second, operator has continually adjust many parameters with any new beam passage through accelerating structure, because any new beam loading results in disturbance of injection conditions and this leads in turn in change of full beam admittance. Thus, many accelerator parameters have to be controlled and adjusted, at list three of them being crucial. These are RF field amplitude in main RF structure, RF Field in resonator and phase shift between these two.

The second feature of our machine is high beam dynamics sensitivity to the main parameters changing. This is due to the fact that regime with $\Delta q=2$ is used as well as due to injection schema. This high accelerator sensitivity to the main parameters results to the end to beam intensity instability [2], that manifests itself as intensity auto modulation (Fig. 1). Linear theory of the phenomena can be found in [3], hear we restrict ourselves by qualitative explanation.

Fig. 2 illustrates schematically (energy, phase) a dependence of racetrack acceptance in phase space energy-phase on accelerating voltage U_Σ applied to accelerating gap as well as a dependence of injected beam admittance location on injection parameters – injection energy U_{inj} and injected beam average phase φ_{inj}. The overlapped area corresponds to the electrons that will be captured and accelerated to the end point.

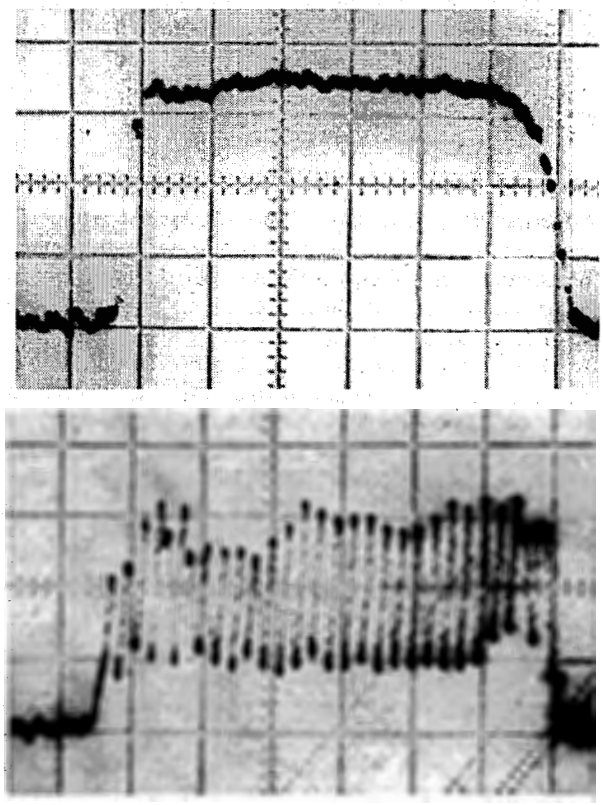

Fig. 1: Stable (upper oscillogram) and unstable modes of racetrack operation. Scales: vertical - 65 mA/div, horizontal - 1 μs/div.

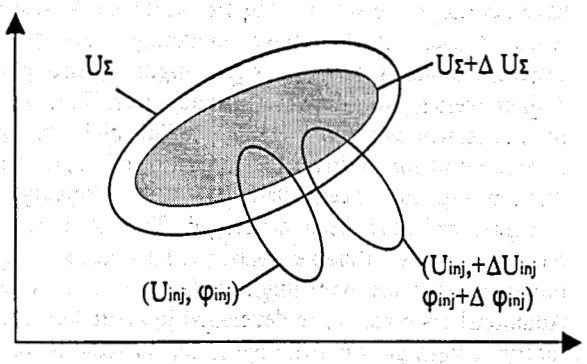

Fig. 2: A dependence racetrack acceptance (dark region) and injected beam emittance on accelerating voltage and injection parameters

These dependences result in the appearance of the feedback in the system beam intensity – accelerating voltage due to the fact that the whole accelerating voltage amplitude is the vector sum of the voltage induced by RF generator and the voltage due to beam radiation (beam loading). Depending on the operation point location on the volt-ampere characteristic this feedback may be positive or negative and stable acceleration is realized at the operating point with positive beam differential conductivity. But negative in static sense feedback may be converted into positive at the definite frequencies due to finite response time of the electron beam and accelerating voltage. This in turn may result in the instability predicted [6,7] and experimentally observed [2].

PLANS FOR RACETRACK UPGRADE

During long period of accelerator use our racetrack appeared to be reliable installation with stable accelerated beam parameters. Many accelerator parameters have been improved during this time interval but still there are remaining things among accelerator systems to be replaced with modern ones. Among the numerous motivations for accelerator upgrade the main one might be considered as fundamental. Up to now our racetrack remains the leader in pulse intensity among the microtone machine class and we foresee the possibility to increase this parameter simultaneously improving performance stability. It had been experimentally observed that the highest beam intensity takes place at the injection parameters corresponding to all orbits locations being shifted away from linac axis. The machine had been simulated with injection parameters corresponding to experimentally found and new flanges had been manufactured with appropriate orbits location. This new layout might result in better beam stability and higher intensity. On the other hand this is the way to mount additional three orbits as it was planed at the accelerator designing stage and to increase final microtron energy up to 50 MeV.

To do this next steps are foreseen. First of all existing microtron monitoring and control system has to be replaced with new computer based one. Up to now we have developed the set of computer controlled devices in CAMAC standard for new monitoring and control system. Among these pulse signal digitizer, analog-to-digit converter, timer, waveform synthesizer. This has to be supplement with computer controlled high stability tunable oscillator to drive RF amplifier, and appropriate development has been started already. Appropriate computer code has been developed. This code allows building up any desirable measurement console at the program run time, one might find out details in [8]. Additional code has to be developed in order to control racetrack adjustment in real time scale. We expect that all this makes it possible to reach much more deep dynamics understanding than ever before.

CONCLUSION

Several steps are foreseen to realize plans for racetrack upgrade. New accelerator configuration has been completed. This configuration differs from the old one by return paths replacement by some distance from linac axis. As we expect, this will result in less beam losses during acceleration as well as better intensity stability. This follows from microtron simulation and intensity auto modulation theory. New monitoring and control devices in CAMAC standard have been developed that will be used in new computer monitoring and control system. New computer controlled high stability RF oscillator is under development now. All this will be helpful in racetrack tuning and beam dynamics study. Equipment for additional three orbits will be manufactured meanwhile and these will be assembled. Racetrack tuning with all 8 orbits mounted is considered as final step of the accelerator upgrade.

REFERENCES

[1] V.I.Alekseev, K.A.Belovinsev, V.A.Boiko, R.M.Voronkov, A.I.Karev and V.G.Kurakin, Racetrack microtron as an injector for synchrotron Pakhra, Zh. Tekh. Fiz. 46 (1976), pp 2558-2562, in Russian.

[2] K.A.Belovinsev, A.I.Karev and V.G.Kurakin. The Lebedev Physical Institute Racetrack Microtron. Nuclear Instruments and Methods in Physics Research, A261(1987), pp38-38.

[3] V.G.Kurakin. High Current Racetrack Microtron as a Free Electron Laser Driver. Nuclear Instrument and Metods in Physics Research, A341(1994), pp 407-411.

[4] K.A.Belovinsev, A.I.Bukin, E.G.Gaskevich, A.I.Karev, A.V.Koltsov, V.A.Kuznetsov, V.G.Kurakin and S.V.Sidorov. Radiation complex on the basis of a racetrack microtron. Nuclear Instruments and Methods in Physics Research, A341(1994) ABS 45-AAS 46.

[5] V.G.Kurakin, A.V.Agafonov, A.I.Bukin, A.V.Koltsov, A.N.Lebedev. Far Infrared FEL Commissioning at Lebedev Physical Institute, in Proceedings of the Seventh European Particle Accelerator Confernce, Vienna, Austria, 26-30 June 2000, pp 749-751.

[6] A.I.Karev and V.G.Kurakin. Auto-oscillation mechanism of beam destruction in a racetrack microtron, Lebedev Physical Institute preprint, No. 174(1978) 15 pp., in Russian.

[7] K.A.Belovintsev, A.I.Karev, V.G.Kurakin. Computer investigation of racetrack microtron. Trudi FIAN 135 (1983), pp. 146-147, in Russian.

[8] V.G.Kurakin, A.V.Koltsov, P.V.Kurakin. FlexUsI – Intrface Builder for Computer Based Accelerator Monitoring and Contol System. These Proceedings.

STATUS OF THE NOVOSIBIRSK HIGH POWER FREE ELECTRON LASER

V.P. Bolotin, D.A. Kayran, B.A. Knyazev, E.I. Kolobanov, V.V. Kotenkov, V.V. Kubarev, G.N. Kulipanov, A.N. Matveenko, L.E. Medvedev, S.V. Miginsky, L.A. Mironenko, A.D. Oreshkov, V.K. Ovchar, V.M. Popik, T.V. Salikova, S.S. Serednyakov, A.N. Skrinsky, O.A. Shevchenko, M.A. Scheglov, N.A. Vinokurov*, N.S. Zaigraeva
Budker Institute of Nuclear Physics SB RAS, Novosibirsk, Russia

Abstract

The first stage of Novosibirsk high power free electron laser (FEL) was commissioned in 2003. It is based on normal conducting CW energy recovery linac. Now the FEL provides electromagnetic radiation in the wavelength range 120 - 180 micron. The average power is 200 W. The measured linewidth is 0.3%, which is close to the Fourier-transform limit. The assembly of user beamline is in progress. Plans of future developments are discussed.

INTRODUCTION

A new source of terahertz radiation was commissioned recently in Novosibirsk [1]. It is CW FEL based on an accelerator–recuperator, or an energy recovery linac (ERL). It differs from the earlier ERL-based FELs [2, 3] in the low frequency non-superconducting RF cavities and longer wavelength operation range. The terahertz FEL is the first stage of a bigger installation, which will be built in three years and will provide shorter wavelengths and higher power. The facility will be available for users in 2004.

ACCELERATOR-RECUPERATOR

Full-scale Novosibirsk free electron laser is to be based on the four-orbit 50 MeV electron accelerator-recuperator (see Fig. 1).

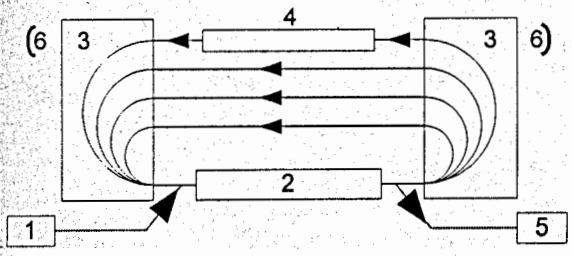

Fig. 1: Scheme of the accelerator-recuperator based FEL. 1 - injector, 2 - accelerating RF structure, 3 - 180-degree bends, 4 – undulator, 5 – beam dump, 6 – mirrors of optical resonator.

It is to generate radiation in the range from 3 micrometer to 0.2 mm [4, 5]. The first stage of the machine contains a full-scale RF system, but has only one orbit. Layout of the accelerator–recuperator is shown in Fig. 2. The 2 MeV electron beam from an injector passes through the accelerating structure, acquiring 12 MeV energy, and comes to the FEL, installed in the straight section. After interaction with radiation in the FEL the beam passes once more through the accelerating structure, returning the power, and comes to the beam dump at the injection energy. Main parameters of the accelerator are listed in Table 1.

Table 1: Accelerator parameters (first stage)

RF frequency, MHz	180
Number of RF cavities	16
Amplitude of accelerating voltage at one cavity, MV	0.7
Injection energy, MeV	2
Final electron energy, MeV	11
Maximum bunch repetition rate, MHz	22.5
Maximum average current, mA	20
Beam emitance, mm·mrad	2
Final electron energy spread, FWHM, %	0.2
Final electron bunch length, ns	0.1
Final peak electron current, A	10

The FEL is installed in a long straight section of a single-orbit accelerator-recuperator. It consists of two undulators, a magnetic buncher, two mirrors of the optical resonator, and an outcoupling system. Both electromagnetic planar undulators are identical. The length of each undulator is 4 m, period is 120 mm, the gap is 80 mm, and deflection parameter K is up to 1.2.

Both laser resonator mirrors are identical, spherical, 15 m curvature radius, made of gold plated copper, and water-cooled. In the center of each mirror there is a hole. It serves for mirror alignment (using He-Ne laser beam) and output of small amount of radiation. The forward mirror has the hole with the diameter 3.5 mm, and the rear one - with the diameter 8 mm.

RADIATION STUDY

For FEL operation we used both undulators. Beam average current was typically 8 mA at repetition rate 5.6 MHz, which is the round-trip frequency of the optical resonator and 32-th subharmonics of the RF frequency $f \approx 180$ MHz. Instead of fine tuning of the optical resonator length we tuned the RF frequency. The tuning curve is shown in Fig. 3.

The radiation wavelengths was tuned in the range 120 – 180 micrometers depending on the undulator field amplitude. The shortest wavelength is limited by the gain decrease at a low undulator field, and the longest one – by the optical resonator diffraction loss increase. The minimum relative linewidth (FWHM), measured with Fabri-Perot etalon, was near $3 \cdot 10^{-3}$. The loss of the optical resonator was measured with a fast Schottky diode detector [6]. Switching off the electron beam, we

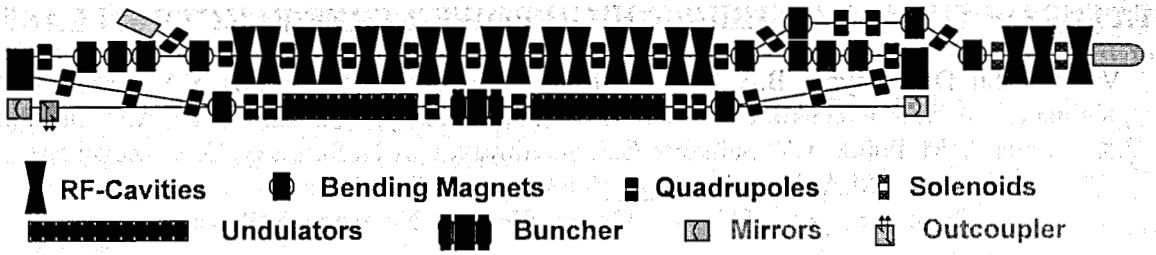

Fig. 2: Scheme of the first stage of the Novosibirsk high power FEL

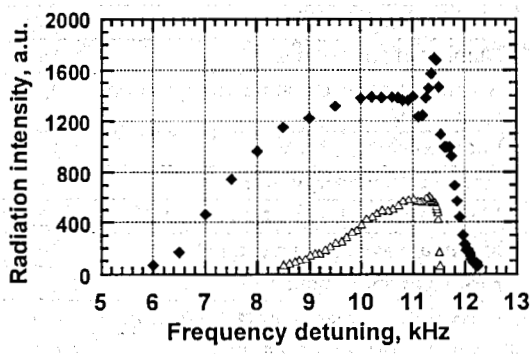

Fig. 3: Laser intensity vs. RF frequency detuning f-180400 kHz (diamonds at repetition rate 5.6 MHz, triangles at repetition rate 2.8 MHz)

measured the power decay time. The typical round-trip loss values were from 5% to 8%. The typical radiation parameters are listed in Table 2.

Table 2: The radiation parameters

Wavelength, mm	0.12...0.18
Minimum relative linewidth, FWHM	0.003
Pulse length, FWHM, ns	0.05
Peak power, MW	0.6
Repetition rate, MHz	5.6
Average power, kW	0.2

OPTICAL BEAMLINE AND FIRST EXPERIMENTS

To transmit the radiation from the rear mirror hole to user stations, the beamline from the accelerator hall to the user hall was built. Now the beamline is filled by nitrogen. It is separated from the accelerator vacuum by the diamond window, and from the air by the polyethylene window.

To demonstrate the capabilities of our terahertz source we tested the PMMA ablation (see Fig. 4) and CW discharge in the atmosphere-pressure argon (see Fig. 5). The beamline extension with places for five stations and first experimental station will be ready by the end of this year.

ACKNOWLEDGEMENTS

The work was supported by the integration grant 174/03 of the Siberian Branch of Russian Academy of Science.

Fig. 4: The conic hole in the PMMA cube, done with the terahertz radiation ablation. One division is 5 mm.

Fig. 5: The CW discharge in the focus of the parabolic mirror.

REFERENCES

[1] E. A. Antokhin, R. R. Akberdin, V. S. Arbuzov et al., Preprint BINP 2003-53, Novosibirsk, 2003.
[2] G.R. Neil et al. Phys. Rev. Lett. 84 (2000), p. 662.
[3] E.J. Minehara. NIM A, V. 483, p. 8, 2002.
[4] N.G. Gavrilov et al. IEEE J. Quantum Electron., QE-27, p. 2626, 1991.
[5] V.P.Bolotin et al. Proc. of FEL-2000, Durham, USA, p. II-37 (2000).
[6] V.V. Kubarev, G.M. Kazakevich, Y.V. Jeong, B.C. Lee. NIM A, V. 507, p. 523, 2003

*vinokurov@inp.nsk.su

THE TRANSFORMATION OF THE TESLA TEST FACILITY INTO THE VUV FEL USER FACILITY AT DESY

A. Gamp, Deutsches Elektronensynchrotron DESY, D22670, Hamburg
for the TESLA Collaboration*

Abstract

After the end of the very successful operation of the TESLA Test Facility in November 2002, the modification of TTF into a VUV FEL user facility took place during the years 2003 and 2004. The injector complex was completely modified. By the beginning of this year 5 cryomodules were installed and the vacuum system was closed. For bunch length measurements there is a special S-band structure driven by a SLAC 5045 Klystron and an Electro-Optical-Sampling Experiment. Six undulator modules of 30 m total length have also been installed.

Until May 2004 the five cryogenic modules and their rf power input couplers were conditioned up to full rf power. In one cavity of the first module an accelerating gradient of 35 MV/m with beam could be demonstrated. The last module (No.5) can be reliably operated at an average gradient of 25 MV/m.

So far, beam has been sent only through the first module and through the first bunch compressor. First emittance measurements show values around 3 πmm mrad.

In the second half of this year completion of installation of technical components like power supplies, beam diagnostic elements etc. took place prior to full commissioning of the entire machine which started in the beginning of September.

INTRODUCTION

In 1993 the TESLA Test Facility was set up at DESY with the goal to demonstrate the feasibility of an e^+e^- Linear Collider based on superconducting L-Band cavities operated at the accelerating gradient 25 MV/m [1]. Only one year later efforts to extend it to a SASE FEL (Self Amplified Spontaneous Emission Free-Electron Laser) facility with initial operation in the 100 nm wavelength range started [2]. During this so- called TTF phase I production methods for superconducting 9-cell cavities operating at gradients above 25 MV/m and for the assembly of cryogenic accelerating modules of 12 metres length were successfully established. There are eight 9-cell cavities in a cryogenic module. Stable operation with beam at average gradients close to 23 MV/m in one cryogenic module has been demonstrated. With two cryomodules beam currents of several nC were accelerated up to 270 MeV. In February 2000 first lasing was achieved [3]. By the end of the TTF I operation saturation of the SASE gain was obtained in the entire FEL wavelength range of 80 – 120 nm [4].

The necessary conditions which had to be fulfilled in order to obtain these results were the acceleration of electron bunches with high peak current and low emittance and the high field quality in the undulator magnets [5]. Under these circumstances there was interaction between the photons and the electron bunches during the entire passage through the undulator which led to microbunching and finally gain saturation.

Since 1997 until November 2002, where TTF I operation ended, 15000 hrs. of beam time were accumulated. During the last two years about 50% of the time was allocated to FEL operation including a large percentage of scientific user time.

After the end of TTF I its transformation into the VUV FEL user facility began immediately. To reach saturation at the minimum design wave length of 6.4 nm the energy of the electron bunches must be increased to 1 GeV and the magnetic length of the undulators has to be doubled to six undulator segments with a total length of almost 30 m. Besides a new injector, an additional bunch compressor and 5 cryogenic modules, which have been installed so far, ultimately the installation of a third harmonic rf system, a seeding monochromator and an additional cryogenic module are planned .

The design beam parameters are:

Energy	1 GeV
Max. bunch charge	4 nC
Min. bunch spacing	110 ns
Bunch length	150 fs
Peak current	2500 A
Max. number of bunches per macrobunch	7200
Max. rep. rate of macrobunches	10 Hz
Normalized emittance at the undulator entrance	2 π mm mrad
Energy spread	2 MeV
Longitudinal emittance	40 keV mm
Beam size in the undulator	65 μm
Min. wave length of FEL radiation	6 nm

* TESLA Collaboration: **Armenia:** CANDLE, Yerevan Physics Institute, **P.R. China:** IHEP Academia Sinica, Tsinghua Univ., Beijing Univ. **Finland:** Inst. of Physics Helsinki, **France:** CEA/DSM Saclay, IN2P3 Orsay, IPN Orsay, **Germany:** Max-Born-Inst. Berlin, BESSY Berlin, HMI Berlin, DESY Hamburg and Zeuthen, GH Wuppertal, Univ. Hamburg, Univ. Frankfurt, GKSS Geesthacht, FZ Karlsruhe, TU Darmstadt, TU Berlin, TU Dresden, RWTH Aachen, Univ. Rostock, **Italy:** INFN Frascati, Legnaro, Milano, INFN and Univ. Roma II, Sincrotrone Trieste, **Poland:** Polish Acad. of Sciences, Inst. of Physics, Univ. Warsaw, INP Cracow, Univ. of Mining & Metallurgy, Cracow, Polish Atomic Energy Agency, Soltan Inst. for Nuclear Studies, **Russia:** IHEP Protvino, INP Novosibirsk, INR Troitsk, MePhI Moscow, JINR Dubna, ITEP Moscow, **Spain:** Ciemat, **Switzerland:** PSI Villigen, **United Kingdom:** CCLRC-Daresbury and Rutherford, Royal Holloway Univ. London, Queen Mary Univ. London, Univ. College London, Univ. of Oxford, **USA:** Argonne National Lab., Cornell Univ., Fermilab, Thomas Jefferson Lab., MIT, UCLA.

In the following a description of the VUV FEL user facility and a discussion of performance and status of the major components will be given.

THE VUV FEL USER FACILITY

An overview of the VUV FEL is shown in fig. 1. The injector consists of a Cs_2Te photocathode which is mounted on the back plane of a 1.5-cell 1.3 GHz copper cavity with a peak accelerating field of 40 MV/m [6]. This cavity can be reliably operated up to the full pulse length of 800 μs. In contrast to the gun used in TTF I, the newly installed one has a cylindrically symmetric rf power input coupler to avoid asymmetric fields which cause transverse emittance growth.

The rms length of the bunches leaving the first cryomodule is about 2 mm. In the subsequent first bunch compressor they are compressed to about .4 mm rms.

Peak currents of the compressed bunches of 1 – 1.5 kA have been measured.

In the next two cryomodules the beam is accelerated to 450 MeV. The measured average gradients of the cavity voltage in these two modules are 19 MV/m and 20 MV/m respectively. In the second bunch compressor the rms bunch length is reduced to 50 μm [10] and the expected peak current in the electron bunches is 2.5 kA. From extensive start to end simulations the expected output power level of the SASE FEL radiation is near or above the 5 GW level for these beam parameters.

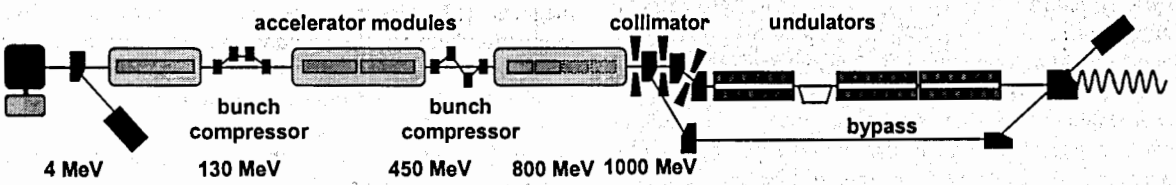

Figure 1: Overview over the VUV FEL. Five cryogenic modules have been installed so far. A sixth module will be installed by 2006. In the remaining space for a possible seventh module presently a transversely deflecting S-band structure has been installed for bunch length measurement.

The cathode is illuminated by UV laser pulses [7]. The gun was set up and optimized at the Photoinjector Test Facility PITZ at DESY Zeuthen. The best values for transverse emittance obtained at PITZ were close to 1.5 π mm mrad [8]. The electrons are accelerated in the 1.5 cell cavity of the gun to about 4 MeV and are injected into the first cryogenic module which is located only 2 metres downstream. In routine operation the first 4 superconducting 9-cell cavities in this module will be operated at the average gradient of 12 MV/m, the gradient in the remaining four cavities will be 20 MV/m. There is one cavity in this module which has demonstrated successful operation at 35 MV/m with beam. This cavity has been electropolished . Due to the acceleration of the electrons to 130 MeV in this module a strong suppression of the Coulomb forces in the space charge dominated low energy beam transport area is achieved.

Behind the first cryomodule the installation of an additional rf system operating at the third harmonic frequency 3.9 GHz is foreseen in the year 2006. It has been shown [9] that one can effectively enhance the bunched peak current by such an rf system which corrects the nonlinear distortions of the longitudinal phase space arising from the rather long bunch length of 10-20 ps full width. The pulse length is necessary to achieve low emittance.

From the three additional cryomodules which will ultimately be located behind the second bunch compressor two modules have been installed so far. Both have demonstrated an average accelerating voltage gradient of 25 MV/m for the full flat top pulse length of 800 μs and 500 μs filling time. Acceleration up to 800 MeV is possible with these 5 modules. The sixth module will be entirely equipped with electropolished cavities which are expected to run up to 35 MV/m. Installation in the tunnel is planned for the year 2006.

Presently, in the location foreseen for a possible 7th module, a transverse deflecting S-band structure of 3.66 m length has been installed for bunch length measurements [11]. Both, the structure and its SLAC 5045 driving klystron are a contribution from SLAC. The cavity has been conditioned to the specified 20 MW input power pulses of 1μs length at 1 Hz repetition rate.

Between the last cryogenic module and the undulator section there is a collimator system [12] to protect the permanent NdFeB undulator magnets which are sensitive to radiation damage. There is transverse collimation to cut off particles from the beam halo and energy collimation to suppress particles resulting from dark current. The minimum value of the aperture radius is 2 mm. Within the considered range of energy deviations from -50% to +25% only particles with $|\Delta E/E_0| < 3\%$ will be transmitted through the collimator and enter the undulator section. The collimator efficiency defined as the ratio of energy deposit in the undulator due to particle loss to the energy in the beam is 10^{-6}.

The new undulator section [13] for the VUV FEL is made up of the same magnets as for TTF I. Compared to TTF I there are now 6 sections with the total length of 30 m. The integrated combined function focusing system has been replaced by an electromagnetic doublet structure.

At a later stage the so-called seeding option will be built. It will provide a fully coherent beam with narrow bandwidth. It requires the installation of three more undulators with a total length of 15 m.

For protection of the undulator magnets from radiation damage during commissioning, temporary tests and beam optimization procedures the entire section can be bypassed by a simple beam transport line which has been installed in parallel.

BEAM DIAGNOSTICS AND PROTECTION SYSTEMS

A necessary condition for the SASE process to occur is the spatial overlap of the low-emittance-high-peak-current electron beam with the photon beam over the entire 30 m length of the undulator with a precision of some 10 □m. To achieve this goal, a very large and sophisticated amount of diagnostic elements in the VUV FEL for electron beam diagnostics, machine protection and photon beam diagnostics [14] is needed.

The electron beam diagnostic system has to measure beam position, charge and losses with single bunch resolution. Most methods for bunch length measurement are not suitable for single bunch resolution, but rely on many bunches. The standard stripline BPMs are located inside the quadrupole magnets. For each BPM, the position of the electrical centre with respect to the magnetic centre of the quadrupole was determined individually on a measurement bench with a precision of 10 □m. Dark current from the gun will be measured with reentrant cavity monitors of about 500 nA sensitivity which are located in the injector and in the collimator section.

The ends of the undulator section and the diagnostic sections between the modules are equipped with button monitors and wire scanners.

In the flat wide parts of the dispersive sections of the bunch compressors there are arrays of 4 button monitors.

For beam size measurements we have about 25 OTR screens and 8 wire scanners. The obtained resolution is better than 20 μm for OTRs and 2 μm for the wire scanners.

The individual bunch charge in the range of .5 – 5 nC is measured by fast toroids with a time constant below 110 ns and an accuracy of better than $5x10^{-3}$. These signals are also used to measure the transmission for a fast (3□s) protection system. Other machine protection signals are derived from fast beam loss measurements with scintillators or aluminum cathode electron multipliers. The distribution of radiation-dose along the linac and the undulators is obtained from the measurement of the transmission attenuation of optical fibres on an hourly basis, and from TLD crystals on a weekly basis.

The beam phase can be measured with $.2^0$ precision by mixing down the 1.3 GHz signal component from impedance matched ring electrodes to the base band.

For bunch length measurement several methods are under consideration in addition to the afore mentioned S-band structure which acts like a streak camera with an expected resolution of about 100 fs. Similar resolution is expected from Electro-Optical sampling where the changes of the optical properties of a crystal under the influence of the electromagnetic field of the bunches are probed by an ultrashort laser pulse [15]. Autocorrelation measurements of far infrared transition radiation (FIR) in an interferometer are also used for bunch length determination. Qualitative optimisation of bunch compression is done by maximizing the output of a simple pyro detector. It is proportional to the coherent FIR emitted by the bunches.

SASE diagnostics and optimisation is done with the help of SASE photons scattered from a gold wire and amplified in a multi channel plate detector. The dynamic range is about 10^7 due to calibrations at different voltage settings. In addition the radiation pulse energy and the photon beam position can be measured with a newly developed detector which is based on the photoionisation of a rare gas at low density. It has also a very large dynamic range.

THE RF SYSTEM

The high power 1.3 GHz rf system consists of four Klystrons manufactured by Thales (formerly Thomson). The normal conducting photoinjector cavity and the first cryomodule are each fed by a TH 2104C 5 MW tube. The following two cryomodules are connected to one TH 1801 Multi-beam-klystron (MBK) which was developed by Thales for the TESLA Project. The MBK prototype has delivered the specified 10 MW output power at an efficiency near 65% already in the year 2000. Since then two more MBKs were delivered to DESY. However, the tubes had to be returned because of gun arcing problems. After investigation and modification improved MBKs are expected to be delivered to DESY by the end of this year.

In the meantime there are two other manufacturers, CPI and Toshiba, who are building independently designed MBKs. The prototypes should also be delivered to DESY during this year. Unlike the Thales tubes, where all cavities operate in the fundamental TM 010 mode, there are cavities operating in higher modes (TM 020) in the tubes by the other manufacturers.

In principle the rf power needed for operation of the last three cryomodules at 25 MV/m can be provided by one additional MBK. For operation at much higher gradient – up to 35 MV/m seem realistic for module 6 – another klystron would be available.

The modulators must generate HV pulses up to 120 kV and 140 A. The max. pulse length is 1.57 ms and the max. rep. Rate is 10 Hz. The voltage droop in the flat top is below 1%. The three bouncer type modulators with a 1:12 step-up rate pulse transformer which were designed and built by FNAL are still in use at DESY. In the meantime 8 more modulators based on the same principle have been designed and built by joint efforts of DESY and German industry. The leakage inductance of the new pulse transformers has been significantly reduced. Its value is

now below 200 μH which is almost half the value of the first transformers. Accordingly the pulse rise time to the 98% level decreased from almost 400 μs to below 200 μs. The increased efficiency (65%) of the MBK as compared to the single beam 5 MW klystron (45%) plus a few per cent gain in efficiency resulting from the smaller pulse rise time would lead to a significant reduction of operation cost for the TESLA Linear Collider where the average wall plug power for the rf supply is close to 75 MW.

A detailed description of the high power rf system is given in [16].

During several years of operation a very powerful digital low level rf system (LLRF) has demonstrated reliable beam operation with rf phase and amplitude stability of 0.5^0 and 0.5% respectively [17].

The vector sum of the rf signals of up to 32 cavities is calculated by a DSP. Deviations of the vector sum from the nominal signal are corrected in a vector modulator at the low rf power level at the klystron drive.

CAVITIES AND AUXILIARIES

The performance of the superconducting 9-cell cavities has continuously improved since 1994, where the first of the three production series' started [18]. By the year 2001 the average accelerating gradient has increased from values below 20 MV/m to above 25 MV/m at Q-values $>10^{10}$ as is shown in fig. 2. At the same time the spread in performance was reduced by the factor 3. The main reasons for this success can be attributed to improved welding techniques and stricter Niobium quality control.

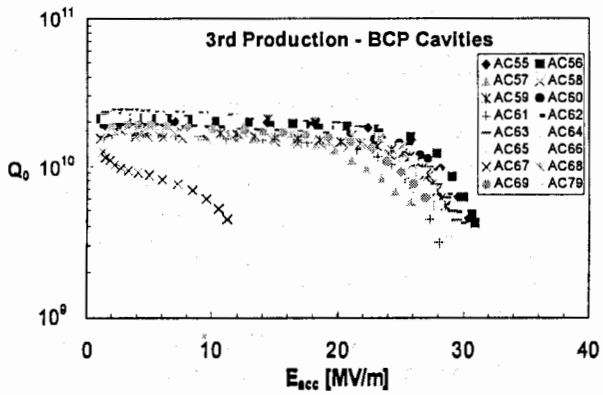

Figure 2: Accelerating gradient vs. unloaded quality factor for several 9 cell cavities from the last production series which have undergone standard Buffered Chemical Polishing treatment. Values well above 25 MV/m at $Q_0 > 10^{10}$ have been obtained routinely. The untypical performance of cavity AC 67 is due to a He-leak which became apparent only during the test.

During the last years a further amelioration of cavity performance has been achieved by the KEK-DESY collaboration on electropolishing. After several single cell cavities had reached gradients in excess of 35 MV/m, there are now also several electropolished 9 cell cavities which have been operated at gradients above 35 MV/m [19]. An example is shown in fig. 3.

There are no signs of degradation neither in the cavities nor in the power input couplers. One cavity in the first cryomodule has reached 35 MV/m with beam.

Detuning of the cavities due to Lorentz forces during the pulse becomes an important issue at these gradients. At 35 MV/m it amounts to 1.2 kHz, i.e. four loaded bandwidths. The possibility of active compensation of the Lorentz force detuning during the macropulse of 1.3 ms length by a mechanical tuner based on piezo-electric elements has been demonstrated. The cavities in the cryogenic module 6 will be equipped with these elements.

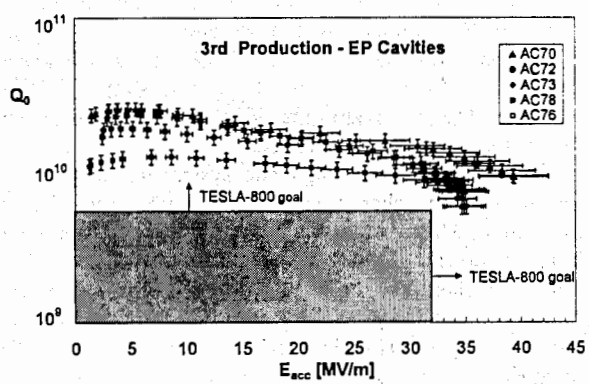

Figure 3: Accelerating gradient vs. unloaded quality factor for several 9 cell cavities from the last production series. These cavities have been electropolished. The results which lie well above 35 MV/m at $Q_0 > 10^{10}$ surpass the requirement for the 800 GeV version of the TESLA linear collider.

The rf power input couplers have also been improved in several iterations. The very robust and reliable couplers from the last version have been tested at full pulse length (1.3 ms) and 10 Hz repetition rate with cavities up to 35 MV/m and up to 1 MW for traveling wave operation at 2 Hz operation on the test stand. Over 60 couplers of this type have been built so far.

SUMMARY

During 10 years of combined effort within the international TESLA collaboration convincing evidence for the feasibility of a Linear Collider based on superconducting technology was given. Cavity production- and module assembly techniques have resulted in the production of complete cryogenic modules which are providing an average accelerating gradient up to 25 MV/m. Even 40 MV/m have been reached in tests of electropolished 9-cell cavities. At least 35 MV/m seem also realistic as an average gradient for the next module.

Besides the wide field of developments directly related to the cavities (welding techniques, material science,

chemistry, coupler development, extensive field calculations and measurements) sophisticated digital low level rf techniques which guarantee high field stability in the presence of beam loading and lorentz forces and microphonics, high efficiency Multibeamklystrons, long pulse high voltage modulators, beam diagnostics techniques, optical laser systems and many other things needed to be developed.

As a result a beam of very high quality could be accelerated in the TESLA Test Facility. It was used to drive a SASE FEL. Saturation at wavelengths around 100 nm was obtained and first scientific user experiments have taken place. TTF is now being transformed into a VUV FEL user facility. We hope for first lasing in the optimal wavelength range around 30 nm by the end of this year and for saturation in the beginning of 2005.

The ultimate goal is reliable user operation in the wavelength range from 100 to 6 nm.

Finally we would like to mention that the International Technical recommendation Panel (ITRP) which had the charge to recommend a Linear Collider Technology – the choice was between the cold L-band TESLA Technology and the warm X-band JLC-X/NLC Technology – had published its recommendation in favour of the cold Technology a few weeks ago on August 20th. Amongst the reasons for this recommendation the planned construction of the superconducting XFEL free electron laser, which is based on the technology described in this paper and which will test many aspects of the linac, as well as arguments related to the reduced power consumption of superconducting cavities and to the comparatively low rf frequency were quoted.

REFERENCES

[1] Proposal for a TESLA Test Facility, DESY TESLA-93-01 (1992)

[2] A VUV Free-Electron Laser at the TESLA Test Facilty, CDR, DESY TESLA-FEL-95-03 (1995)

[3] J. Andruszkov et. al., Phys. Rev. Lett. 85 3825 (2000)

[4] V. Ayvazyan et. al., Nucl. Instr. Meth. A 507 368 (2003)

[5] J. Pflueger Nucl. Instr. Meth. A 445 366 (2000)

[6] S. Schreiber et al., Proc. of "The physics and applications of high brightness electron beams", Chia Laguna, Sardinia, (2002), ed J. Rosenzweig, G. Travish, L. Serafini, World Scientific, Singapore, ISBN 981-238-726-9.

[7] S. Schreiber et al., Nucl. Instr. Meth. A 445 427 (2000)

[8] K. Abrahamy et al., Proceedings of the EPAC2004, (2004)

[9] K. Flöttman et al., DESY TESLA-FEL-01-06 (2001)

[10] T. Limberg et al., Proceedings of the EPAC2002 811 (2002)

[11] R. Akre et al., SLAC-PUB-9241 (2002)

[12] V. Balandin et al., DESY TESLA-2003-17 (2003)

[13] J. Pflüger et al., in Proceedings of the FEL 2002 held at Argonne (2002) and DESY TESLA-FEL 2002-06 56 (2002)

[14] J. Feldhaus and D. Nölle in proceedings of the EPAC 2004 (2004)

[15] M. Hüning in Proceedings of the DIPAC 2001 56 (2001)

[16] S. Choroba in High Energy and High Power RF, Proceedings of the 6th Workshop on High Energy Density and High Power RF, Berkeley Springs, West Virginia, 22-26 June 2003, AIP Conference Proceedings, Vol. 691, P. 1-14

[17] S.N.Simrock in Proceedings of the 2004 Linac Conference, Luebeck Germany (2004)

[18] A. Gamp in proceedings of the XVII National Accelerator Conference in Protvino, Russia (2000)

[19] L.Lilje et al. Nucl. Instr. Meth. A 524 1 (2004)

OPERATION AND PLANS ON THE ACCELERATOR COMPLEX IN KURCHATOV CENTER OF SYNCHROTRON RADIATION

V.Korchuganov (BINP, Novosibirsk; RRC Kurchatov Institute, Moscow), M.Blokhov, M.Kovalchuk, Yu.Krylov, V.Kvardakov, L.Moseiko, N.Moseiko, V.Novikov, S.Zheludeva, D.Odintsov, V.Rezvov, V.Ushkov, A.Valentinov, A.Vernov, L.Yudin, Yu.Yupinov (RRC Kurchatov Institute, Moscow)

Abstract

Kurchatov Synchrotron Radiation Source began the work as a first dedicated synchrotron radiation facility in Russia in 1999. The accelerator complex includes 80 MeV linac accelerator as an injector and two storage rings: 450 MeV SIBERIA-1 and 2.5 GeV SIBERIA-2, which are used for the experiments in the range of SR from VUV up to hard X-ray. Large progress was achieved in increasing SIBERIA-2 stored current during last year. The SR dose is rising fast and the lifetime is also grown. The report describes the current work and the plans on the accelerator facilities development.

INTRODUCTION

At present, the Kurchatov SR source operates close to the design parameters. Table 1 presents the main features of the acting optical structure of the storage rings Siberia-1 and Siberia-2.

Table 1: Main parameters of Siberia-1 and Siberia-2 rings

Parameter	**Siberia-2**	**Siberia-1**
Energy	2.5 GeV	0.45 GeV
Circumference	124.13 m	8.68 m
Optical structure	Modified DBA	FODO
Superperiods	6	1
Bet. tunes: ν_x, ν_y	7.772; 6.692	0.793; 0.895
Mom.compaction	0.0104	1.64
Damping *x ,y, s, ms*	3.04; 3.17; 1.49	7.15; 7.15; 3.57
Hor. emittance	78-98 nm-rad	880 nm-rad
RF harmonic	75	1
Energy spread	0.000953	0.00034
Dipole field: B_y	1.7 T	1.5 T
ID space	2x3m($\eta = 0$) 5x3.2m($\eta \neq 0$)	-
Bunch length: σ_s (without IDs)	1.84 cm	30 cm
SR pulse duration	0.14 ns FWHM	2.35 ns FWHM
SR pulse spacing	5.5-414 ns	28.9 ns
Current	100-150 mA (multibunch)	100-300 mA (single bunch)
Life time (100 mA, coupling 1%), hrs	10-14 (multibunch)	1.5 (single bunch)

WORK WITH ELECTRON BEAM

Electron storage

As rule the work on Siberia-2 SR goes in the multi-bunch regime with a current of 100-120 mA by filling of 1/2 to 1/3 of the ring (25 to 37 bunches).

The synchrotron oscillations collective modes appear after injection of first four or five bunches. Nevertheless we have realized that it is possible to store the electrons in all 75 bunches without specially made empty gap widely used to prevent ion trapping (see Fig.1a).

The energy ramping of the electrons with current in many bunches exceeding 150 mA is characterized by both big synchrotron motion in coherent modes and losses of the beam part. The losses depend on the number of bunches and modulate the particles numbers in bunches correspondingly with the synchrotron mode number (see Fig.1b).

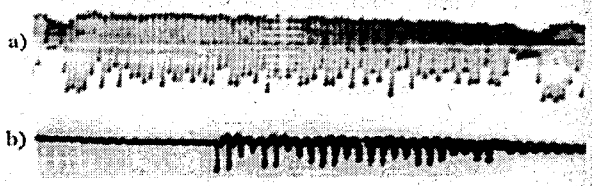

Figure 1a: The typical picture of the filling at the injection. Figure1b: The modulation due to collective mode instability losses during an energy ramping.

In single bunch mode the storage is accompanied by the bunch lengthening and microwave instability leading to the increasing of energy spread. In result the enlargement of the bunch was stopping the storage near 72 mA due to the losses of the particles as a consequence of the energy acceptance limitation. The maximum single bunch current accelerated up to 2.5 GeV was about 30-35 mA and was again limited by the coherent synchrotron oscillations, which are strong when ramping the energy within 0.45-1 GeV.

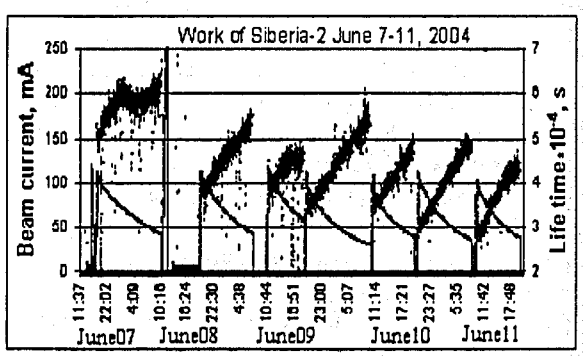

Figure 2: Work of Siberia-2 in June 7-11, 2004

During routine operation on SR experiments the electron storage and acceleration regimes are reproduced

in a stable way. Figure 2 shows the dependence of the beam current and the lifetime versus the time at 2.5 GeV during the runs in June 07-11, 2004. Now the maximum currents achieved are: 300 mA (450 MeV) for Siberia-1 in a single bunch mode; 270 mA (450 MeV) and 150 mA (2.5 GeV) for Siberia-2 in multibunch mode.

Vacuum

During last year the vacuum system of Siberia-2 was opened twice. In May 27, 2003, aluminium vacuum chamber in one of the BMs was replaced on new one in order to remove a vertical cutting of the SR beam. Next opening was made in February 2004 in order to change the vacuum insulator of the inflector. In both cases the vacuum chamber was degassed with an SR beam during two week without warming it up.

With the increasing of the electron current the serious problem became. It was so called "hot" points arisen inside Siberia-2 vacuum tube due to SR parasite hit, which damaged the vacuum and the lifetime. Five such "hot" points with the sizes about 1-2 mm^2 were found and three of them were removed. As a result the vacuum condition was sharply improved and the lifetime was increased in a factor 2. After the spray of the titanium films in the magneto-discharge pumps around the ring the lifetime has exceeded 14 hours at 100 mA in the beginning of the week. But some degradation of the lifetime is observed to the end of the week run, perhaps due to both the gas loading from the working photon SR beam lines and some titanium films saturation (see Fig.2).

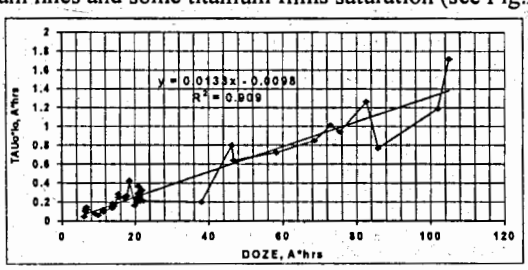

Figure 3: Dependence of the beam current and the lifetime product on the collected doze at 2.5 GeV

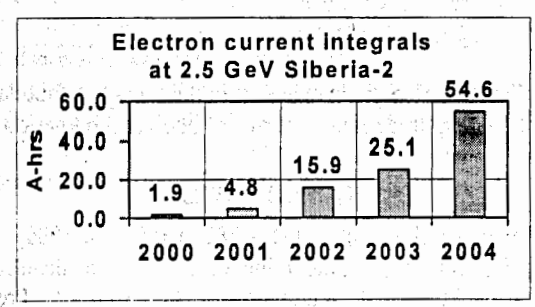

Figure 4: Annual dozes at Siberia-2

Till now the lifetime is generally defined by the SR stimulated gas desorption. In fact Fig. 3 represents near linear behaviour of the product of an electron beam current and a life time versus total SR doze collected by the vacuum chamber from the beginning of work. Intensity of works with SR increased in 2004. As a result a total integral of current overcame 100 A*h on June 8, 2004 and the doze of one half of 2004 is more than summarized doze of the 2000-2003 years (see Fig.4).

COD CORRECTION AT SIBERIA-2

Electron closed orbit distortion (COD) is measured by 24 pick-up stations with 10 micron accuracy at SIBERIA-2 storage ring. Correction system allows to achieve standard values of COD (at azimuths of BPMs) which are close to σ_z = 0.2 mm and σ_x = 0.7 mm. To find COD at the 72 quadrupole lenses azimuths we also use the method of their gradient changes with the correction coils existing on quadrupole lenses poles. From this method the transversal relative distances between neighboring BPMs and quadrupole lenses centers are found and taken into account to improve COD control.

PHOTON BEAMS STABILIZATION

The photon beams of Siberia-2 move vertically due to the temperature change of the magnets and supports with a time constant ~ 20 hrs. Total vertical displacement during 5-days operation at 2.5 GeV was reaching 2-3 mm at a distance 15-20 m. Oppositely the elements and the photon beams are coming back into initial positions after 2-days operation break. Now the feed-back system was made on two SR beam lines to correct SR beam position. It includes luminescent screens, TV-cameras, computer code with a space resolution of 2-3 mkm and the control of 3 magnetic correctors, which create the local electron orbit distortion in vertical plane. The turned-on feed-back demonstrates that SR beam drift is damped with a precision of ± 4-5 mkm during long time runs (see Fig.5).

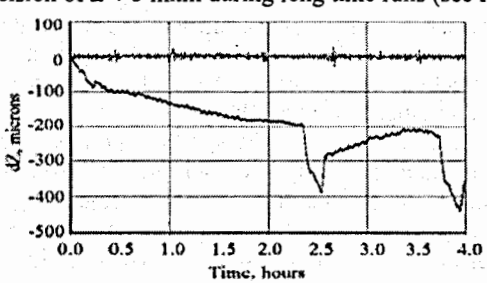

Figure 5: SR beam vertical position at X-ray station with feed-back system turned-on and turned-off

SR BEAMS

The Siberia-2 SR extraction scheme is the same for each of the superperiods [2]. There are 39 SR extraction channels in total. Those include: 24 channels with SR from the bending magnets with the characteristic wavelength λ_c = 1.75 Å and horizontal angles ± 5 mrad; 10 SR channels with λ_c = (0.25-0.4) Å from the two SCMP wigglers; 5 channels from multipole low field wigglers.

The works of SR stations at Siberia-2 are now performed with SR from the bending magnets over the

photon energy range of 4 to 40 keV and with (10^{13}-10^{11}) phot/s/0.1%BW fluxes. Usually 7-8 12-hour shifts are scheduled each week for work with the SR beams. Figures 6, 7 shows diagrams of user time during last years dated on June 2004.

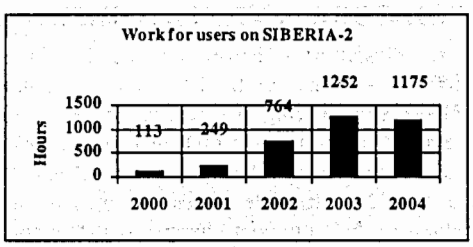

Figure 6: Siberia-2 as SR Source

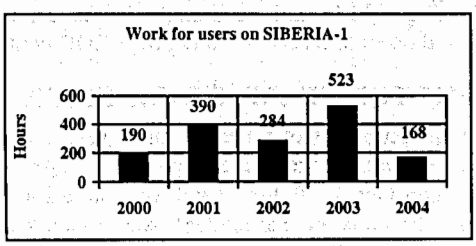

Figure 7: Siberia-1 as SR source

EXPERIMENTAL STATIONS

Nine experimental stations are in operation at the X-ray experimental hall of Siberia-2 [3], which are dedicated for: protein crystallography, precise X-ray optics, X-ray crystallography and material science, medical and industrial diagnostics, LIGA, EXAFS, small angle scattering, time-resolved small-angle diffraction, X-ray luminescence. Three experimental stations are in operation at the VUV experimental hall of Siberia-1 for: photoelectron spectroscopy, VUV luminescence and optical investigations of solids.

The main directions of the scientific program include the structure diagnostics of an atomic level space resolution of organic and inorganic objects; protein crystallography and biotechnology, nanotechnology and nanodiagnostics; material science, X-ray optics, new methods for medical diagnostics, industrial nondestructive control; deep X-ray lithography et cetera.

PLANS ON SIBERIA-2

The main task of future efforts is to increase intensity and lifetime of SR beams in Siberia-2 as well as to decrease the electron beams emittances as a result of work with new magnetic optics of the ring in order to augment SR brightness [2].

Optics with 66 nm-rad Horizontal Emittance

This optics keeps DBA structure. But it has a changed betatron frequencies: ν_x=7.85 ν_y=3.79. The natural chromaticities stay relatively small: ζ_x=–15.4, ζ_y=–11.7, the calculated dynamical apertures are as such as –20 mm < DA_x < 29 mm, -24 mm < DA_y < 24 mm. The structure "66nm-rad"do not require a special modification of the "iron".

Optics with a 18 nm-rad Horizontal Emittance

The case of non-zero dispersion in all sections of Siberia-2, a structure with 18 nm-rad horizontal emittance at 2.5 GeV seems to be quite achievable at the present variability of parameters of magnetic elements. It has the betatron tunes ν_x=9.708, ν_y=5.623, the chromaticities ζ_x=–21.4, ζ_y=–19.7 and the DAs -19 mm < Δx < 25mm, –12mm < Δy < 12 mm. Such optics makes it possible to obtain a diffraction-limited radiation in vertical plane with rather shot wavelength of λ_{fund}=6Å at E=1.33 GeV. But the "18 nm-rad" structure implies a modernization of the injection system and an optimization of the sextupole magnets positions on the Siberia-2 ring.

Installation of Wigglers

Activity in the protein crystallography and in material science is linked with an installation of the multipole superconducting wiggler. Now we begin to make 7.5 T wiggler with the 19 poles, the space period of 164 mm, photon flux up to (10^{14}-10^{12}) phot./s/0.1%BW and photon energies up to 200 keV.

Booster Synchrotron for Siberia-2

The 80-2500 MeV synchrotron (Figure 8a) will support 1 Hz top up energy injection of the electrons in Siberia-2, the work with small DAs in new Siberia-2 optics, periodical injection and constant intensity of SR ("infinite" lifetime), stability of photon beams. Booster has a 12-fold symmetry DBA optics (Figure 8b) with ε_x=52 nm-rad, a circumference of 110.9 m.

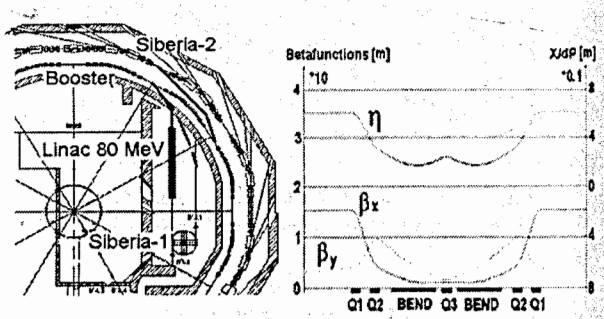

Figure 8: Booster installation in the tunnel of Siberia-2 and the amplitude functions of one booster superperiod

REFERENCES

[1] V.V.Anashin et al., NIM, A282, p.369-374,(1989).

[2] S.T.Belyaev, V.N.Korchuganov, M.V.Kovalchuk et al., "Status of Kurchatov SR Source", Proc. RUPAC2002, Obninsk, Russia .

[3] M.V.Kovalchuk, V.V.Kvardakov et al., "Kurchatov Synchrotron Radiation Center", The 5-th Asian SR Forum, March 16-17 2004, Japan, Ext. Abstract, p. 77-80.

INVERSE FEL HIGH ENERGY GAIN ACCELERATION SCHEMES OPTIMIZED FOR DIFFERENT ELECTRON BEAM ENERGY RANGES

A.A. Varfolomeev#, S.V. Tolmachev, A. Varfolomeev Jr., T.V. Yarovoi
RRC "Kurchatov Institute", Moscow 123182, Russia

Abstract

Vacuum laser acceleration schemes IFEL are investigated in diffraction dominated version. CO_2 laser of TW power is regarded as the IFEL driver.

INTRODUCTION

Up to present time many proof-of-principle experiments on laser acceleration were made and time of laser accelerator models construction is coming. In this report we discuss mainly the pure vacuum acceleration paying more attention to the physics than to technology. Further physics study is necessary since common opinion is not yet elaborated which type of the laser or the plasma acceleration schemes can really be the most efficient in providing high acceleration rates of high brightness particle beams. Our review consists of three parts which include recent experimental data on the vacuum acceleration, projects on developing next stage IFEL experiments in strong laser fields and some new concepts of the vacuum acceleration respectively.

RESULTS ON VACUUM ACCELERATION

We will consider far field acceleration in vacuum and namely Inverse Free Electron Lasers (IFELs). The acceleration process is described by the same as in the FEL physics well known equations. A relatively great total energy gain in the IFEL case makes the whole problem more complicate including the electron beam dynamics evolution, providing stability in the nonlinear interaction processes, the radiation losses as well as some technological aspects as the beam focusing, the undulator tapering for the interaction synchronism providing and etc. First detailed theoretical analyses of this problem for the high energy electrons were given in the papers [1,2]. The IFELs with a focused laser beam demand a more correct approach with using simulations. Interesting experimental results on IFELs have been obtained update [3-8]. All of them are actually proof-of-principles ones.

The achieved acceleration rates (≤70 MeV/m) and the total energy gains (≤20 MeV) are less impressive than the acceleration gradients (>100 GeV/m) demonstrated in some Laser-induced Wake Field Accelerators (LWFA) or Plasma Wake Field Accelerators (PWFA). However, this acceleration was demonstrated on small path lengths (~1 mm) and the obtained beams had large energy spread (up to 100%) with small number accelerated particles [9].

For increasing acceleration rates the following reserves should be taken into account: laser beam with longer wavelengths is more efficient for the IFELs; laser pulse power can practically be raised up to TW and higher levels (not only by increasing total pulse energy but by shortening the pulse length as well); focused laser beam provides very high fields at the focus which can be used for acceleration. Some of these reserves were used in the work [8] where a record rate (70 MeV/m) has been obtained. All these aspects as well as analysis given below show that the diffraction dominated IFEL scheme is the most perspective for electron acceleration by laser fields up to 1 ÷ 10 GeV.

PROTOTYPE OF THE FIRST MODULE OF HIGH RATE IFEL

The original version of the UCLA-Kurchatov Institute project [10,11] can be regarded as a prototype of diffraction dominated IFEL. Schematic layout of the IFEL performance is shown in Fig. 1. The 14 MeV electron beam from a photoinjector+booster linac system enter the undulator. A CO_2 laser beam in Gaussian mode is focused by a lens with focal distance of 2.6 m to a tight spot of a few hundreds microns. Basic parameters of the IFEL device are given in Table 1. Very specific undulator construction was constructed with strong tapering and small magnetic field tolerances [12]. Both the magnetic fields and the undulator periods have been tapered to provide synchronism of the laser beam interaction with a captured electron bunch along the entire undulator length. Non-adiabatic approach and numerical 3D simulations were made. Fig. 2 shows the undulator magnetic field profiles and simulated electron energies. Characteristics of the output electron beam are presented in Table 2.

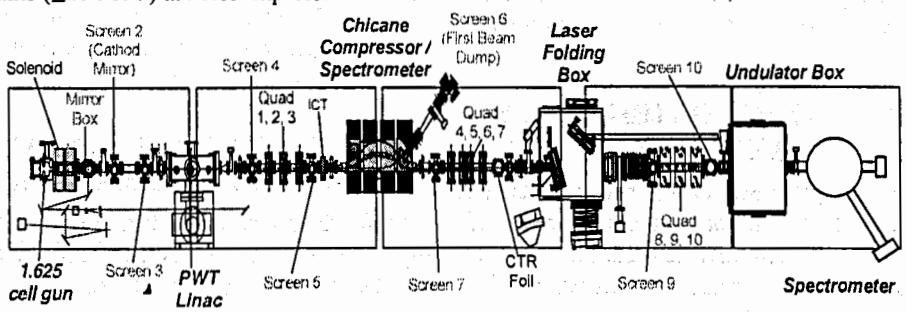

Figure 1. Schematic layout of the IFEL device for the experiment.

Table 1: Basic parameters of the IFEL device.

Laser beam parameters:	
Wave length λ	10.6 μm
Power range	0.4 – 0.8 TW
Pulse length	240 ps
Rayleigh length z_R	3.6 cm
Waist at the focus w_0	0.35 mm
Initial electron beam parameters:	
Initial energy	14 Mev
Energy spread	0.5%
Emittance ε_n	10 mm×mrad
Charge	300 pC
Pulse length	6 ps – 3 ps
Rms radius at the focus	0.15 mm
Undulator parameters:	
Total undulator length	524.5 mm
Undulator period at the entrance $\lambda_w(0)$	15.16 mm
Undulator period at the exit $\lambda_w(z_{max})$	52.1 mm
Initial field strength	0.115 T
Field strength at the exit	0.626 T
Number of periods	17.5

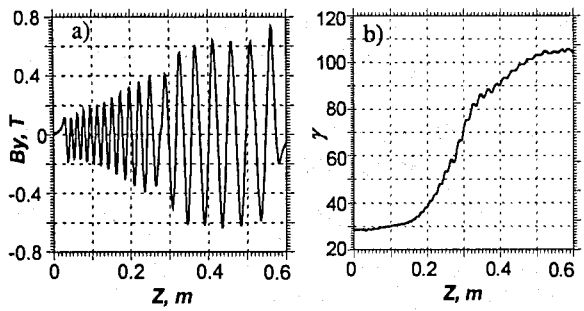

Figure 2: Magnetic fields (a) and accelerated electron energy along the undulator depth (b).

Table 2: Output electron beam parameters from the IFEL.

Energy	55 MeV
Microbunch length	3 fs
Peak current	3 kA
Transverse emittance	10 mm×mrad
Trapped fraction	>20%

Very important issues: the predicted gain of the accelerated particles is twice larger than in the experiment [8]; b) large accelerating gradient is possible (up to ~100 MeV/m); c) appreciable fraction of the primary microbunches is captured for the laser acceleration (tens %%).

THE SECOND STAGE OF HIGH RATE IFEL

The second stage Project means design and construction of an additional IFEL module for further acceleration of electron beam after exit from the first IFEL module (Fig. 3). This cascade of two diffraction dominated IFEL modules driven by the same CO_2 high power laser should

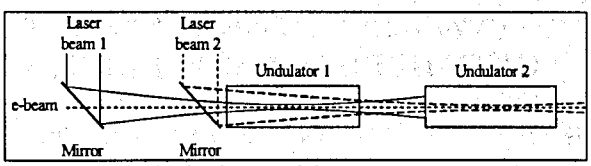

Figure 3: Principal scheme of the two IFEL beam lines.

provide total electron beam acceleration up to 85 MeV [13].

Simulations were made simultaneously for both IFEL acceleration sections so electron beam parameters obtained by simulations at the exit of the first section were used as primary beam parameters for the second IFEL section. Short intersection gap was assumed to be a drift space. The undulator parameters are given in Table 3 and magnetic field profiles are shown in Fig. 4. Simulation results are given in Fig. 5.

Table 3: Parameters of the second IFEL stage undulator.

Period range	4.2 – 5.4 cm
Gap	1.2 cm
Field amplitude range	0.76 – 0.86 T
Total length	63.2 cm
Number of periods	13

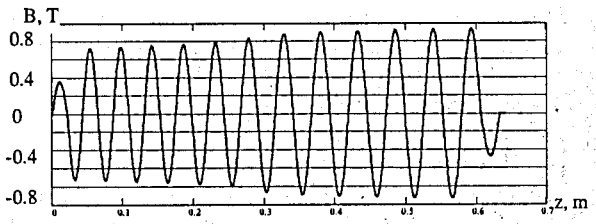

Figure 4: Magnetic field profile along the second IFEL undulator axis.

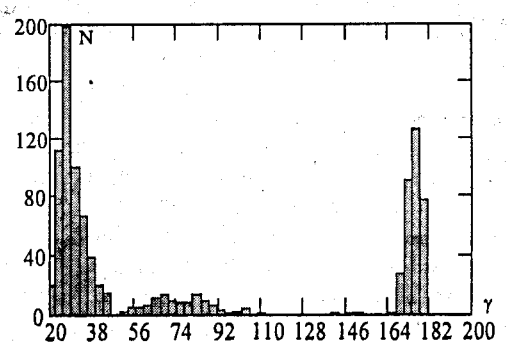

Figure 5: Energy distribution of electrons at the exit of the second IFEL undulator section.

Up to 95% of electrons entering the second undulator can be captured for acceleration and accelerated up to 90 MeV, total capture ratio of the initial beam is 31%.

FREE SPACE ACCELERATION BY GAUSSIAN MODE LASER FIELD

Principal scheme of the free space accelerator is given by Fig. 6. No undulator is using and the laser beam and the electron beam are not collinear. Two mirrors inserted

into resonator turn the Gaussian beam and terminate the laser field interaction with electrons. Small holes in the

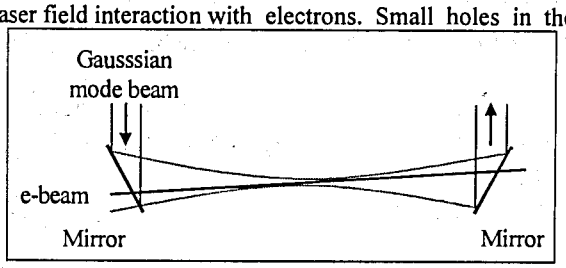

Figure 6: Schematic of the noncollinear interaction with Gaussian mode CO_2 laser beam.

mirrors made for the electron beam propagation are not harmful for the Gaussian mode especially if these holes are out of the first Fresnel zone.

The interaction is proportional to the electric field projection component on the electron beam trajectory E_α, where α is the noncollinearity angle the Guoy phase shift increase the electron slippage. Some compensation of the phase slippage follows from the term noncollinearity [15]. At some α_{opt} slippage variation over z near laser focus becomes more smooth.

The accelerating field profiles of the Gaussian mode are given in Fig. 7. For γ>600 the energy exchange is positive in a wide region of the electron beam trajectory and namely in the ranges $-6z_R$ - $+6z_R$. The profiles are practically not dependent on the laser power P and on γ as well (since the used angle α_{opt} does not depend on γ.).

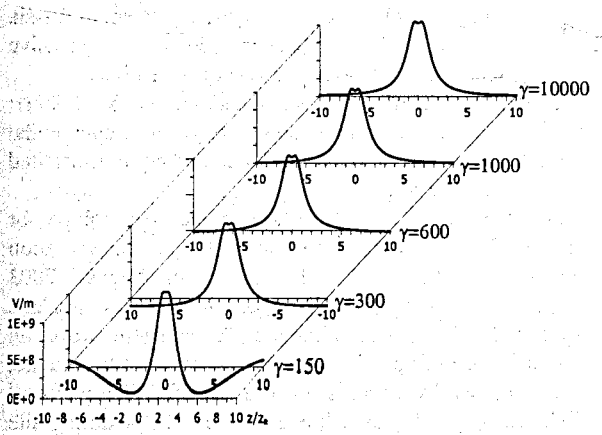

Figure 7: Accelerating field profiles E_α for z_R=3 cm, $\alpha = 1/2\sqrt{\lambda_s/2z_R}$, $\varphi_0=\pi/2$, λ=10.6 μm, P=10^{13} W.

The acceleration gradients not dependent on the electron energy are given by $dE_{el}/dz\,(MeV/m) = 9.2\left[\sqrt{P(W)}/z_R\,(m)\right]$, where P(W) is the laser power in W.

One of the important problem concerning realization of this free space laser acceleration is focusing of the accelerated beam with conservation of a high precision alignment of the electron beam. Fortunately for the beams with not small γ the transverse field in the xz plane acting on an elrectron propagating along the noncollinar trajectory is $F_{tr} = eE_x\,(1-\alpha^2\gamma^2)/2\gamma^2$. It is seen that this field provides selffocusing of the electron to the trajectory defined by the slope angle $\alpha = 1/\gamma$. Dynamical phase stability required for the acceleration in the multistage system can be provided as well see for details [15].

CONCLUSION

Short pulses of Gaussian CO_2 laser beam of high power (0.5 – 1.0 TW) can provide 100 – 1000 MeV/m acceleration rate in wide energy range of electrons.

REFERENCES

[1]. E.D. Courant, C. Pellegrini, W. Zakowicz, Phys. Rev. A32, №5, 2813-2823 (1985)

[2]. A.A. Varfolomeev, Yu.Yu. Lachin. Sov. Phys. Tech. Phys. 31, No 11, 1273-1278 (1986)

[3]. I. Wernick, T.C. Marshall, Phys. Rev. A 46, 3566-3568 (1992)

[4]. A. Van Steenbergen, J. Gallardo, et. al., Phys. Rev. Let. 77, 2690-2693 (1996)

[5]. Y. Liu, X.-J. Wang, D.B. Cline, et. al., Phys. Rev. Let. 80, 4418-4421 (1998).

[6]. W.D. Kimura, L.P. Campbell, C.E. Dilley, et. al., Phys. Rev. Spec. Top. AB 4, 101301-1-101301-12 (2001); Phys. Rev. Lett. 86, 4041 (2001).

[7]. L.P. Campbell, C.E. Dilley, S.C. Gottshalk, et. al. Proceedings of the PAC2003, p.p. 1909-1911.

[8]. P. Musumeci, S. Tochitsky, S. Boucher, et. al. Proc. of the 26-th Int. FEL Conf., Aug. 29 – Sept. 3, 2004, Trieste, Italy.

[9]. P. Sprangle, Ch. Joshi, Final Report on the Advanced Acceleration Technique, Proceedings of Snowmass 2001, Working Group, T8.

[10]. P. Musumeci, C. Pellegrini, et. al., Proceedings of the PAC2001, p.p. 4008-4010.

[11]. A.A. Varfolomeev, S.V. Tolmachev, et. al., Nucl. Instr. And Meth. A483, 377-382 (2002).

[12]. S.V. Tolmachev, A.A. Varfolomeev, et. al. Proceedings of the 26-th International Free Electron Laser Conference, Aug. 29 – Sept. 3, 2004, Trieste, Italy.

[13]. A.A. Varfolomeev, S.V. Tolmachev, et. al. Int. Report CRL-01-04, RRC KI 2004, Moscow.

[14]. A.A. Varfolomeev, A.H. Hairetdinov, Proceeding of 4 EPAC, p.p. 799-801.

[15]. A.A. Varfolomeev, A.H. Hairetdinov, AIP Conference Proceedings 279, Ed. J.S. Wurtele, AIP, New York, (1993), p.p. 319-320.

[16]. A.A. Varfolomeev. Joint Advanced Accelerator and Beam Dynamics Workshop, July 1 – 6, 2002, Chia Laguna, Sardinia, Italy.

HIGH MAGNETIC FIELD SUPERCONDUCTING MAGNETS FABRICATED IN BUDKER INP FOR SR GENERATION

K.V. Zolotarev*, A.M. Batrakov, S.V. Khruschev, G.N. Kulipanov, V.H. Lev, N.A. Mezentsev, E.G. Miginsky, V.A. Shkaruba, V.M. Syrovatin, V.M. Tsukanov, V.K. Zjurba, Budker INP, Novosibirsk, Russia
D. Kraemer, BESSY, Berlin, Germany

Abstract

BESSY operates a 3-rd generation synchrotron light source in VUV to XUV region at Berlin-Adlershof. The main radiation sources in storage ring are special magnetic elements as undulators and wigglers. 3 superconducting shifters and one multipole superconducting wiggler are operating giving enhanced photon flux for 10-25 keV X-ray region. As the superconducting elements presently are located in straight sections, BESSY intends to exchange 4 of conventional room-temperature bending magnets by superconducting ones.

The report contains brief description of 9 Tesla superbend prototype as a candidate for replacing of conventional magnets of BESSY-2, which was designed, fabricated and tested at Budker INP and was commissioned at BESSY in June 2004 .

Main parameters of 9 Tesla superconducting bending magnet prototype as well as testing results are presented.

INTRODUCTION

It is well known the synchrotron radiation spectrum is defined by both on electron energy in the storage ring and magnetic field strength in irradiation point. In order to move the spectrum in the short wavelength region superconducting wigglers and shifters with high magnetic a field are installing into straight sections of storage rings. But as a rule, straight sections are already occupied by such insertion devices as undulators while main workstations of 3 generation storage rings use radiation from traditional bending magnets. For storage rings with energy up to 2 GeV the spectrum from bending magnet is limited to energy of photons up to 25 keV and it strongly limits opportunities of realization of experiments. Besides for superconducting insertion devices like shifters and multipole wigglers there is a problem of the 'second source' which may limit to spatial and energy resolutions in experiments if it is required.

Moreover, because the bending angle in Superbend magnet is big enough, the radiation from Superbend can be easily spited on a few beamlines and can be used for few experiments simultaneously. So it is a real way to increase a total efficiency of synchrotron radiation centre.

Also, the distance between radiation point and first X-ray optic element can be reduced for Superbend beamline in comparison with insertion device.

From this point of view Superbend is free of these problems and it is rather cheap approach allowing considerably to expand an opportunity of experiments of already existing and expensive experimental stations, having expanded spectrum in a hard X-ray region part.

Main disadvantage of the Superbend in comparison with superconducting high field insertion devices that it is a basic element of the storage ring and all its systems should be not less reliable in comparison with traditional magnetic elements in the storage ring.

The idea of creation of superconducting bending magnet with a high field for replacement of traditional warm magnet in already existing SR sources was aroused in Budker INP since 1989 [1-2] In 1992 prototype of superconducting bending magnet with working field of 6 Tesla was fabricated and successfully tested in Budker INP. There was a decision to create a batch production of such bending magnets for creation of family of compact SR sources consisting of superconducting and traditional bending magnets. Disorder of a financial system in Russia at that time unfortunately had brought in the corrective amendments and these plans could not be realized.

Break in this direction was made in USA in 2001: several superconducting bending magnets (Superbends) with a field above 5 Tesla [3,4] were made and installed on ALS storage ring.

Starting from 2001 9 Tesla Superbend prototype for BESSY-2 was started to fabricate in collaboration between Budker INP and BESSY. In August, 2003 Superbend was successfully tested in own cryostat and field 9.37 Tesla was obtained. After some work on minimization of heat in-leak into own cryostat the magnet was successfully commissioned at BESSY. The maximal field value 9.6 T was achieved in June 2004 during site acceptance testes at BESSY.

MAGNET SYSTEM

The SB magnet system is dipole consisting of two superconducting coils assembled above and below the vacuum chamber. The main parameters of the SB magnet are given in Table 1.

*Zolotarev@inp.nsk.su

Table 1: The main parameters of the SB magnet.

Vertical aperture, mm Horizontal aperture, mm	30 75
Pole gap, mm	46
Operating magnetic field, Tesla Maximum magnetic field, Tesla	3.3 - 8.5 9.38
Coil material	Nb_3Sn, NbTi
Edge angle, degree	1.3
Current in coil for 8.5 Tesla, A	264
Ramping time 0-7 Tesla, min Ramping time 0-9 Tesla, min	<5 <15
Eff. magnetic length along beam, m	0.1777
Bending angle, degree	11.25
Bending radius, m	0.905
Stored energy for 8.5 Tesla, kJ	180
Cold mass, kg	1300

The SB magnet coil consists of five sections. The first and second sections are winded from Nb3Sn wire. The third section is winded from NbTi wire. The fours section is winded from NbTi wire and used for correction. The coil main parameters are given in Table 2.

Table 2: The coil main parameters.

Coil Sections	Wire Type	Number of layers (turns in the layer)	Total Turns
1	Nb_3Sn (80%), d=1.24mm	10 (77, 76)	765
2	Nb_3Sn (50%), d=1.24mm	10 (77, 76)	765
3	Nb-Ti, d=0.92 mm	18 (105, 104)	1881
4 corrector	Nb-Ti, d=0.92 mm	4 (105, 104)	418
5 bandage	Stainless steel, d=1 mm	4 (95, 94)	378

Special bandaging system is used to prevent winding wire motion under pondermotive forces action. The bandaging system consists of bandaging section of the coil and stainless steel ring with 150 bolts. This bolts press on the bandaging section via four special form stainless steel plates. The sketch and photo of SB magnet coils with bandaging system are given in Figure 1, 2.

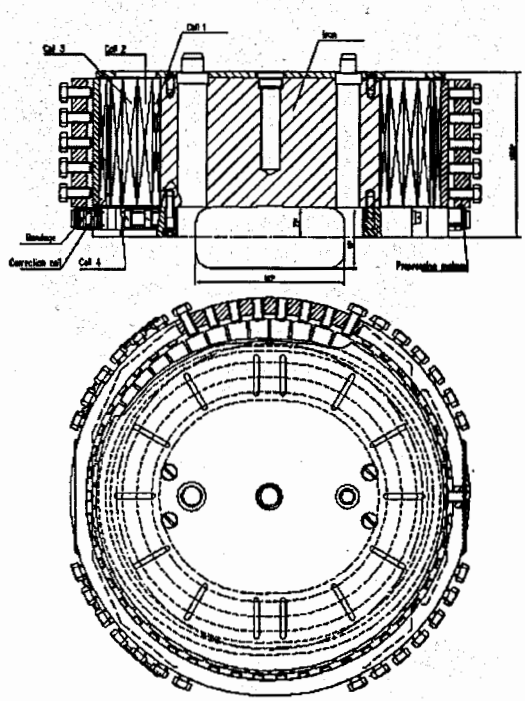

Figure 1: Sketch of assembled coil.

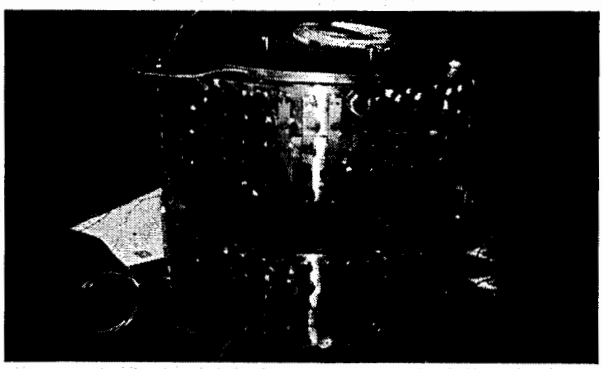

Figure 2: Photo of assembled pole.

The ARMCO iron yoke is used to return the magnetic flux and to support the coils. The photo of the assembled superconducting bending magnet is given in Figure 3.

MEASUREMENT RESULTS

For checking of parameters of magnetic field of superconducting bending prototype magnet for BESSY II the number of magnetic measurement experiments were performed during August 19-22, 2003 and were repeated during commissioning of magnet in June 2004.

These measurements were performed for next values of magnetic fields: 3.3, 6.3, 7.0 and 8.47 T.

For testing of quality of magnetic fields a special carriage was fabricated. 5 Hall probes were mounted on the thin ceramic plate with step 8 mm. Plate can be inserted in the carriage on few positions with different altitudes (z coordinates). Carriage is pulled though the vacuum chamber by step motors and permits to measure value of vertical component of magnetic field in some points along beam trajectory and in the some vicinity of it (±16 mm in the transversal horizontal direction).

Repeating such measurements on the different vertical coordinates, it's possible obtain 3d map of magnetic field distribution around electron trajectory. The measurement were performed for 450 points along beam trajectory (with 1 mm step), and for 6 positions of Hall probes plate in measurements carriage (also with 1 mm step in vertical direction). Every measurement includes acquisition of 5 Hall probes witch are placed in transverse direction with 8 mm distance. The results of this profiling for different values of maximal magnetic fields are presented on the Figure 5.

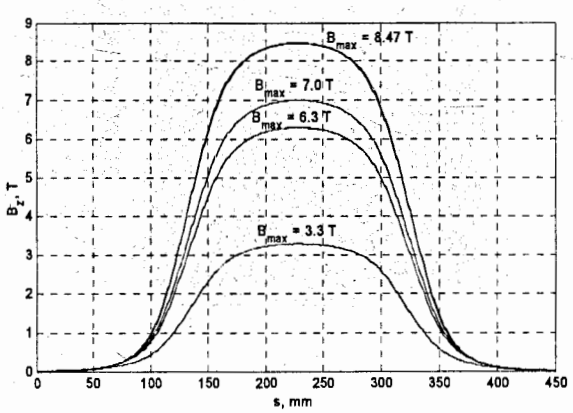

Figure 5: The longitudinal profiles of magnetic field over

The field distribution in different planes in the magnet center is presented on Figure 6.

These data are quite enough to make analysis of nonuniformity of field and for estimation of multipole contributions. The results of multipole expansion of above mentioned data are presented on the Table 3.

Table 3: Multipole component in the center of magnet for working field value 8.5 T.

Multipole of order n	Skew component value	Normal component value
Dipole n=1, T	0	8.5584
Quadrupole n=2, T/m	0.47125	0.02383
Sextupole n=3, T/m^2	2.7034	-22.62
Octupole n=4, T/m^3	235.41	222.54

REFERENCES

[1] L.G.Morgunov, "Development of compact storage rings at Siberia-SM", Synchrotron Radiation News, Nov./Dec. 1990.

[2] G.N.Kulipanov, N.A.Mezentsev, L.G.Morgunov, V.V.Sadjaev, V.A.Shkaruba, S.V.Sukhanov, P.D.Vobly , " Development of supercunducting compact storage rings for technical purposes in the USSR" Proceedings of the 4th International Conference Synchrotron Radiation Instrumentation, 15-19 July 1991, Chester, UK, p.731-736

[3] D. Robin et al "Superbend project at the Advanced Light Source", Proceedings of the 2001 Particle Accelerator Conference, Chicago

[4] J. Zbasnik, et al., "ALS Superbend Magnet System", Proceedings of the 2000 Applied Superconductivity Conference, Norfolk, VA, September 2000.

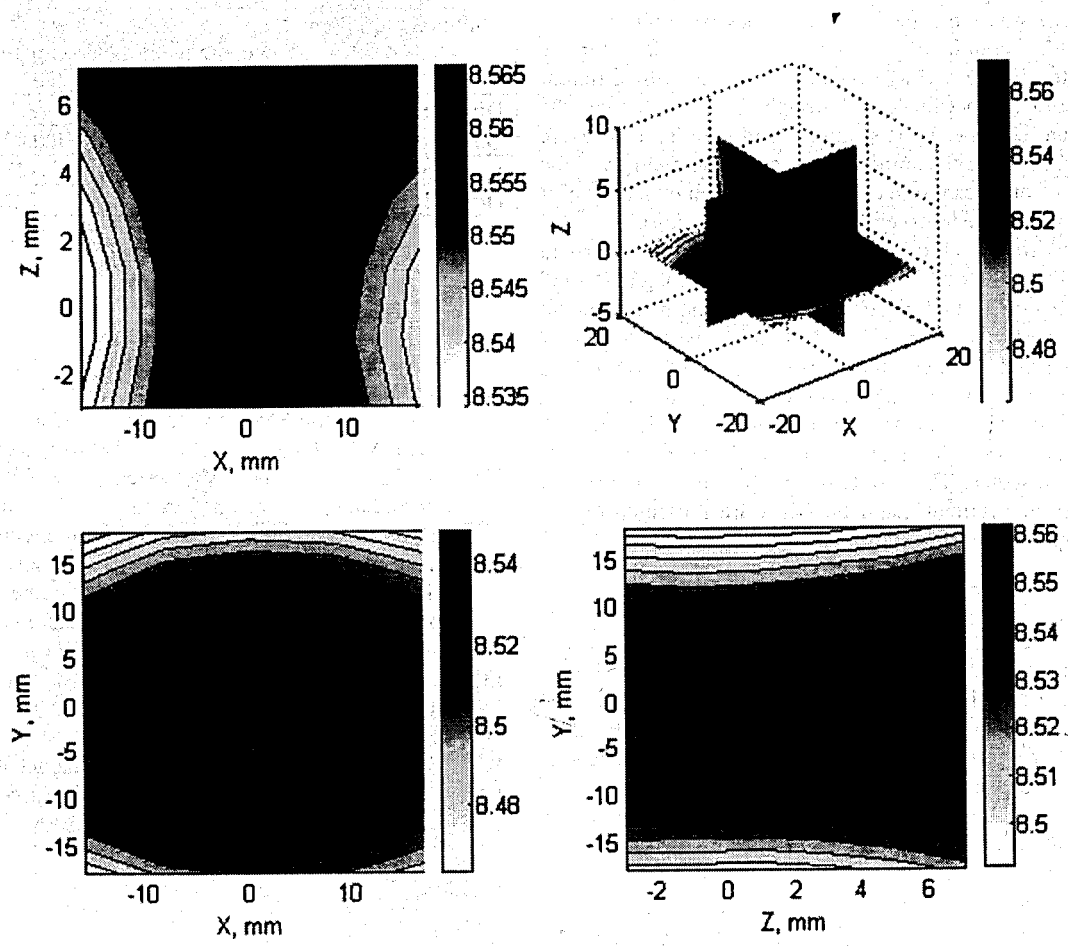

Figure 6: Ddistributions of magnetic field in the center of magnet for working field value 8.5 T.

STATUS OF THE WORK ON THE BASE DIRECTIONS OF THE «RF SUPERCONDUCTIVITY FOR ACCELERATORS» PROGRAM AT THE FEDERATE PROBLEM LAB AT IHEP

L. Sevryukova *, N. Ivanov **,
*Federate Problem Lab at IHEP, Protvino, Moscow Region, Russia, ** RUSATOM, Moscow

Abstract

In this report result of the study of electrophysical phenomena on the superconducting cavity surface, including plasma, bifurcation, hysteresis, emission and diffusion phenomena are considered. Science intensive recourse –saving technologies of superconducting cavities are being studied on the base of these phenomena. The superconducting cavities are made of Nb and Nb film, alloy film or HTC ceramics, which cover the working surface of the weldless copper shells using ion-plasma technologies (axial and planar magnetron sputtering).

Quality monitoring (optical, emission, electrochemical and high frequency) of the working surface condition of superconducting cavities is developed under the realization of new technologies.

The brief review of the experimental equipment is used as training base for individual students, post-graduate students and research staff in the field of technologies that use superconductivity phenomenon and ionic-plasma, electrochemical and high-vacuum technologies as well.

For realization of the joint project of accelerator SVAAP (Superconducting Vertical Accelerator for Applied Purpose) on the energy 15-20 MeV the specified science intensive technologies are used in collaboration with MEPHI.

Special attention has been given to the RF superconducting cavity, its geometry, mechanical stresses, HOM and technology.

Results of study of the technology developed in the Federate Problem Lab for Technology and Study SC Cavities at the Institute for High Energy Physics look promising.

STUDY OF THE ELECTROPHYSICAL PHENOMENA

We study and use next electrophysical phenomena in superconducting cavity technology [1]:

1. Electrical Instability Phenomenon in the systems with the negative differential resistance. It is found under certain conditions of the typical electrical instability during the anodic dissolution process for Nb and Cu. It is determined of the common electrical instability features in semiconductors (film Nb_2O_5) and in electrochemical systems [2] .We found bifurcation phenomena and current oscillations, described by strange attractor.

2. We have studied the hysteresis phenomena in electrochemical system and we are found of the good correlation of the hysteresis loop area and crystallographic orientation of the working surface of superconducting materials [2].

3. We have studied the possibility to clean the working surface of the superconducting cavities to the depth, which is more, than of RF field penetration. New cleaning method from Ta impurity has been proposed [3].
It is based on the well-known method of electric transfer, in particular, on its special case of the deep cleaning by means of electric transfer of an impurity through oxide barrier, and a layer of purified metal is kept behind the oxide barrier [4].

4. We have studied the volt - current characteristics and the dissolution process rate of the Nb surface lower or Nb films under superposition of alternating voltage with frequency 100-1000 Hz and we have found frequencies, corresponding to the electrochemical polishing, the impurity removing and the electrical deposition of the very clean Nb [5].

5. One of the ways of solving the problem of the accelerating fields increasing is to suppress the field emission effects. This work is devoted to study the oxide films influence on the Nb surface, specially created to decrease the field emission [6]. The theoretical modeling of oxide cover influence on the Q-factor of TESLA-shape superconducting cavity at frequency 3 GHz and the cover thickness at accelerating fields of 10 MV/m, 15 MV/m and 20 MV/m well correlates with experimental dependence of emission dark currents, measured under of DC field.
The combination of the technological parameters of anode oxidation is different in each case of application and is determined as a result of multifactor optimization.
Investigation of Nb – Nb_2O_5 system in wide temperature range is of certain interest because 300 K provides a metal – semiconductor system, 70 K provides a metal – dielectric system and 4.2 K provides a SC metal - dielectric system, i.e. oxide barrier changes it's nature, too.

6. Study of the thermomagnetic phenomena. Theoretical calculations of the reliable operation of SC cavity on the base of Nb/Cu have been discussed in detail in [7].

7. Study of the plasma phenomena. The peculiarities of magnetron sputtering of the superconducting materials and copper as an accompanying material is being studied. The current – voltage characteristics and curves

of magnetron discharge ignition in planar and axial geometry are studied in our lab [8].

The geometry of electrode system and the working gas pressure are optimised. We are studying now the peculiarities of magnetron sputtering of the superconducting materials on copper shells of the different magnetron sputtering methods: axial, planar and complex axial and planar. Depending on kind of superconducting material (Nb, allow H2B, High Tc} and the frequency band we use different set-up and equipment.

METHODS OF THE TECHNOLOGICAL CONTROL

It is necessary to underline a special role of the study and technological control methods. We use the next methods:

- It is noteworthy that at manufacturing copper shells

of the superconducting cavities on the base of Nb/Cu,
we need to control quality namely of the first layers at the galvanoplastic copper laying, which then become a working surface at superconducting Nb laying by magnetron sputtering method.. For these purposes we use the acoustic emission as a method of the technological control [9]

- Control of the field emission properties of the Cu and

Nb working surface films [10].

- Control of the secondary emission properties and

Auger spectroscopy [11].

- Control of the working surface state by means of

SIMS method.

DEVELOPMENT OF THE TECHNOLOGIES ON THE BASE OF OUR RESEARCHES

Electrochemical Polishing

Electrochemical polishing with current oscillation "pocket", described by strange attractor.
The technological process of Electro polishing has been developed from a very interesting phenomenon – excitation of low frequency current oscillation by constant voltage.
Practically, we have the possibility to conduct this process on the three level with metal removal that varies in thickness (Fig. 1)

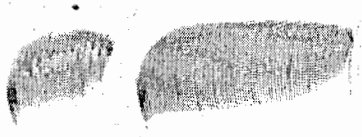

Fig.1: Pocket oscillation under Nb electrochemical polishing

Small pockets correspond to 0.1 micron of metal removal per pocket and long ones – to 0.01 micron of metal removal per pocket [2]

Electrochemical Cleaning

Electrochemical cleaning technology of the Niobium working surface from Ta. Fig. 2 shows the effect of cleaning the working surface of Nb from Ta impurity.

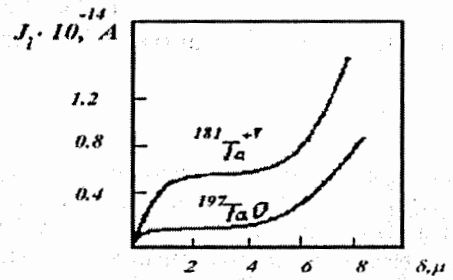

Fig. 2: Effect of cleaning the Nb surface

We see that in this case the Ta impurity in the surface Nb layer is distributed almost uniformly at the depth of 5 μм whereas in deeper layers an exponential growth is observed at the depth of 6.5μм followed by flattop

All results presented here point out at the existence of the Nb purification effects from Ta through the oxide layer [8].

Galvanoplastic Technology

A copper layer is formed electrochemically on a rotating Al mandrel taking the form of cathode, that later will be the working surface of the copper shell of SC cavity. Unfortunately an intricate configuration of cavity results in different distances between the anode and the cathode and therefore in different thickness of copper shell walls. We have solved this problem by means of the optimization of all parameters of the technological process and of development the special setup for it. On Fig. 3 you can see setups to realize this technology .

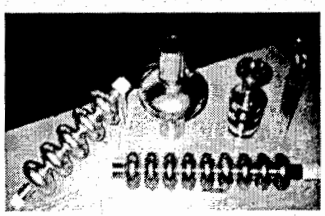

Fig. 3: The copper shells manufactured in the Lab

Buffer Layer Technology

Besides of Nb, high T_c material on the YBaCuO base is perspective for high accelerating field problem. On the seminars on future prospects for high energy physics and the RF Superconductivity Workshops the question about the opportunity to obtain accelerating field of order to 400 MV/m with the use of the YBaCuO film was discussed long ago. We have a lot of difficulties with this question now. To deposit a film of required quality at the working of copper shell it is necessary to solve the problem to guarantee the YBaCuO film stability with 3 –10 μк thickness. The problem is to conjugate crystallographic structure of YBaCuO and copper.

According to that the conjugation possibility increases if Cu lattice parameters start increasing and approach to the lattice parameters of YBaCuO. There are many opinions of different firms on buffer layers between copper and YBaCuO. Using them different buffer layers have been tested, and the best preliminary results have been got for buffer layer from solid solution of Al-Cu.

Magnetron Sputtering Technology

We felt it necessary to manufacture the accelerating SHF cavities of different geometry for frequencies of 2.45 GHz, 3 GHz and 1.3 GHz and also the SC cavities for stabilising SHF generators by the SC cavities with 9GHz frequency; we decided to develop and use two set-ups: for axial magnetron spattering, for planar magnetron spattering [8] and set-up for complex magnetron sputtering [9]

THE SVAAP PROJECT

The results of the study of the technology and SC cavities were for the first time used in the linear accelerator project for the electron accelerator at the energy of 15-20 MeV with the RF structures on the base of Nb/Cu [10]

CONCLUSION

1. Complex study of the electrophysical phenomena on the superconducting material working surface (Nb films, alloy H2B films and YBaCuO films) has permitted us to develop the high scientific technologies.
2. The high scientific technologies are protected by the patent and Author's Certificates.
3. The complex of the experimental and technological equipment for manufacturing, treatment, technological control and study of the superconducting materials and cavities has been developed, that is the base for scientific researcher, the students and post graduate students.
4. The high scientific technologies have been used in the project of the SVAAP on the energy 15 –20 MeV (Superconducting Vertical Accelerator for Applied Purposes).

It is noteworthy that the works are being conducted with the support of the Russian Fond Fundamental Research Grand № 03-02-17030, Grant 04.06.23 of The Ministry of Russian Federation for Atomic Energy and Ministry of Russian Federation for Education at the "Scientific – Innovation Collaboration" Program and Russian President grant MK –1304.2004.8.

ACKNOWLEDGEMENTS

The authors of report thank O. Patarakin, Yu. Orlov, V. Kiselev for interest to this work and financial support.

REFERENCES

[1] V. Gadetski, L. Sevryukova. Use of the Electrophysical Phenomena in SC Cavity Technology. In: Proc. of the XIV Workshop on Charge Particle Accelerators. Dubna, Russia, 1994, v.1, p. 158-160.

[2] V. Efremov, L. Sevryukova, M. Hein. Improved Method for Electrochemical Polishing of Nb SC Cavities. 5-th Workshop of RF Superconductivity, SRF-1991, DESY, Germany, 1991, v.1, p.433-456.

[3] A. Korotkov, S. Pesterev, L. Sevryukova. Feasibilities of the Methods of Anode Oxipolishing and Anodization in Technology of the SC Cavities. 6-th Workshop of RF Superconductivity, 1993, CEBAF, Newport News, USA, 1993, v.2, p.809-837.

[4] O. Matveeva, L.M. Sevryukova. The Influence of Oxide Barrier on the Removing of Ta from Nb. Proc. of the 16-th INVSTA Workshop on Outgasing of Materials: the Kinetics and Thermodynamics. Graftavallen, Sweden, April 1997, 32 p.

[5] L. Sevryukova, S. Obraztsov. Method of the Electro-chemical Polishing for Niobium. Author's Certificate № 797274, 1978 (BI № 2, 1981, p. 255)

[6] V. Efremov, S. Pesterev, L.M. Sevryukova. Field Emission Properties on Nb with Thin Oxide Films. Proc. of the 5-th European Vacuum Conference . Salamanca, Spain, 1996, N 553, A V 4 Po002.

[7] O.M. Mamaev, L.M. Sevryukova, N.A. Ivanov. Study of the Thermomagnetic Instability for SC structure of SVAAP Accelerator on the base of Nb/Cu. 10-th Workshop of RF Superconductivity, SRF-2001, Tsukuba, Japan, Sept. 2001, p. 574-577.

[8] L. Sevryukova. Status on RF Superconductivity at the Institute for High Energy Physics. - SRF-2001, Tsukuba, Japan, Sept. 2001. p. 39 - 43.

[9] O. Matveeva, L. Sevryukova. Acoustic Emission at the Manufacturing and Treatment of the SC Cavities. IHEP Preprint № 90-70, 1990, Protvino Moscow Region, 8 c.

[10] M. Pesterev, L M. Sevryukova. Study and Development of the Methods for Suppression of the Emission Effects on the Superconducting Cavities. In: Proc. of the Conference «Vacuum Science and Technique». Sudak, Ukraine, 2003, v.2, c. 325-332.

[11] M.P. Chernov, V.A. Kiselev, L.M. Sevryukova, I.A. Zvonarev. First Experimental Results for High Tc Magnetron Sputtering on the Working Surface RF Accelerating Cavities. Proc. of the 7-th Workshop on RF Superconductivity, 1995, Gif sur Yvette, France, 1995, v.2, p. 503-508 .

[12] L.M. Sevryukova, V.I. Suzdalev, D.L. Filippov. Method of Manufacturing of the SC Cavity. Patent RU 2231235 C2, 20.06.2004.

STATUS OF SUPERCONDUCTING RADIOFREQUENCY SEPARATOR CRYOGENIC SYSTEM

A. Ageyev, A. Bakay, E. Kashtanov, S. Kozub, M. Muraviev, A. Orlov, P. Pimenov, K. Polkovnikov, P. Slabodchikov, V. Sytnik, S. Zintchenko, IHEP, Protvino, Russia

Abstract

The OKA experimental complex proposing to use the technique of RF beam separation to produce a Kaon beam is under construction at IHEP. Two deflecting superconducting niobium cavities operating at 1.8 K are the basic elements of the separator. To provide cooling at this temperature commercially available 500 W, 4.5 K helium refrigerator is used to cool liquid helium bath of the satellite refrigerator. The last one is actually a big warm up heat exchanger with flow imbalance and very low pressure drop. Vacuum group consists of two stages of roots blowers and one stage of rotary slide valve pumps. Pump stages are separated by intermediate gas coolers. The schematic, thermodynamics, design capacity and current construction status of the cryogenic system are presented.

INTRODUCTION

In January, 1998, two cryostats with niobium superconducting deflectors were transported from CERN to IHEP to be used as the basic elements of the radiofrequency separator for production of separated K-mesons [1]. Working temperature of deflectors is 1.8 K and an estimated total heat load at this temperature level is about 250 W. Taking into account high cost of a cryogenic system of this capacity it was decided to take all appropriate measures to reduce the price of the system. Main solutions in this direction were:

- to use cryogenic and vacuum equipment produced in Russia
- to refuse construction of new buildings and to place cryogenic system equipment in the already existing buildings situated close to the separator location
- to use already existing equipment for helium storage, purification and compression in spite of there is rather big distance (~ 1 km) from this equipment to the helium refrigerator.

A special cryogenic test facility was built up at IHEP for inspection tests of the cryostats with deflectors [2]. At this facility cryostats were initially cooled down to 80 K and vacuum leak tested. Then they were tested at 4.2 K, this time cavities were RF powered. Adding the vacuum pumping group to the test facility allowed to perform tests at lower temperatures. For example, it is possible to keep cavity at 1.8 K as long as 2 weeks. Recently cavity is stably cooled at 1.6 K. Experience gained during development, construction and operation of this test facility was very useful in the work on the separator cryogenic system development.

GENERAL SYSTEM DESCRIPTION

Cryogenic system simplified flowchart is shown in Fig. 1a.

The superconducting cavities are cooled by a satellite refrigerator which consists of the large vacuum heat exchanger HEX1, liquid helium bath and of two small heat exchangers HEX2 located close to the each cryostat with deflector. The word "satellite" is used here to stress that such a refrigerator having no gas expanders can not produce cold at the liquid helium temperature level without external source of cold. Typically another refrigerator equipped with turbines works as an external source of cold. In our case commercially available helium refrigerator of KGU-500 type provides this external cooling. It cools liquid helium bath at about 4.5 K. Temperatures below 4.5 K (down to 1.8 K) are reached by pumping helium vapor. A system of vacuum pumps ("pumping machine") is used to pump helium gas. Cold of the helium vapor is recuperated in the heat exchangers of the satellite refrigerator.

Thermodynamic cycle of the satellite refrigerator is shown schematically in Fig. 1b.

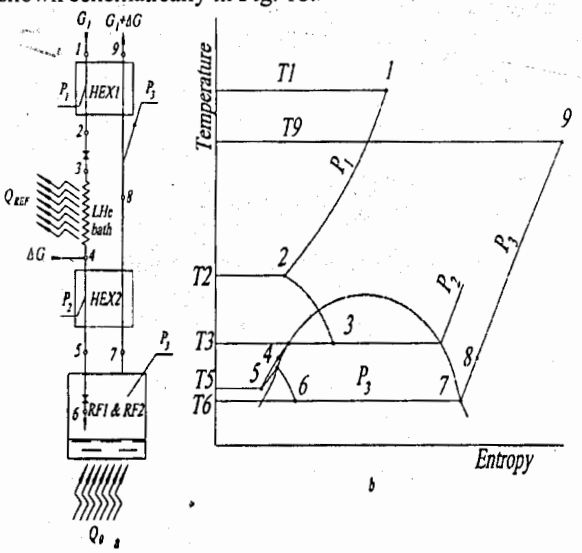

Fig. 1: Separator cryogenic system flowchart (a) and thermodynamic cycle (b).

System Operation

After compressors pressurized helium gas flow is divided in two parts. One part at pressure of 28 bar is used in helium refrigerator KGU-500 where helium is liquefied into the dewar. Another part with mass flow rate G_1 goes to the inlet of the heat exchanger HEX1. After passing all heat exchangers of the refrigerator KGU-500 and heat exchanger coil of the liquid helium storage vessel helium flow at about 25 bar and 4.5 K is fed along a short cryogenic transfer line to the expansion valves in the liquid helium bath. One J-T valve is opened enough to keep the level of liquid helium in the bath. Mass flow rate through another J-T valve is ΔG, that is flow imbalance of the heat exchanger HEX1. This flow imbalance improves the efficiency of the HEX1. Helium vapor from the liquid helium bath and from the storage dewar returns to the heat exchangers of the refrigerator.

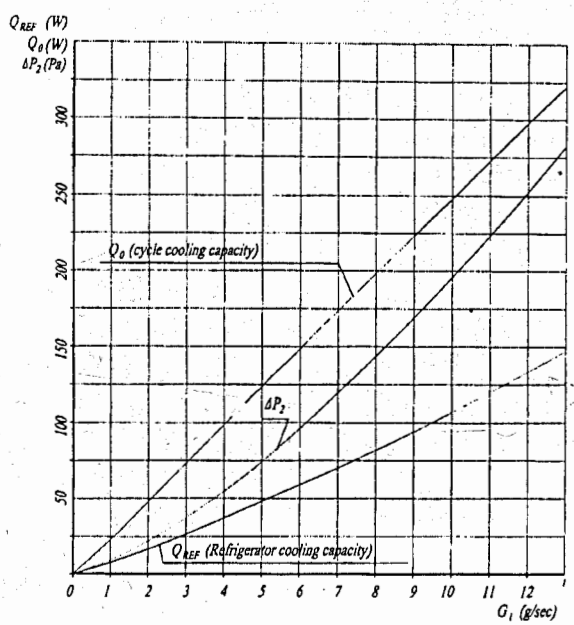

Fig. 2: Cooling capacity of the system and low pressure flow pressure drop.

There are two coiled heat exchangers in the liquid helium bath: main and auxiliary. Pressure in the bath is about 1.05 bar, and pressure of helium flows in these heat exchanges should be somewhat higher to have subcooled liquid at theirs exits and at the inlets into the low temperature heat exchangers HEX2 located near the cryostats with deflectors.

High pressure flow of the satellite refrigerator is cooled by low pressure helium gas in the large vacuum heat exchanger HEX1. After expansion in J-T valve in the liquid helium bath and after cooling in the main heat exchanger of the bath this flow G_1 is mixed with imbalance flow ΔG. Along a cryogenic transfer line this mixed flow comes to the distribution box from which it is distributed to the low temperature heat exchangers HEX2 of the cryostats RF1 and RF2. In these heat exchangers, incorporated into the transfer line, liquid helium flow is cooled down to the final expansion temperature. After expansion in the J-T valves, located in the cryostats RF1 and RF2, liquid and vapor separate. Superfluid liquid replenishes the helium vessels of cryostats. Vapor, after passing through the low temperature heat exchangers, cryogenic transfer line and large vacuum heat exchanger, has temperature close to the room temperature. An electric heater at the exit from the large vacuum heat exchanger heats up helium gas to the ambient air dew point. Then gas is pressurized by pumping machine and returns to the gasholders. Low pressure flow from the KGU-500 refrigerator returns to the same gasholders, but through the separate pipe line. Gasholders are connected with suction of the main compressors, so at this point cooling cycle is closed.

System Cooling Capacity Estimation

To determine most suitable operation parameters a computer model of the cryogenic system was developed. It includes the verificatory calculations of the counterflow heat exchangers HEX1 and HEX2 and calculations of the thermodynamic cycle. Subroutines for calculating thermophysical properties of helium were used in this computer simulation.

The heat transfer surface areas and characteristic dimensions of the channels of the heat exchangers sections were determined taking into account the real geometry of the pipes tightly wrapped with a spiral wire.

The heat transfer surfaces of the both upper and lower sections of the heat exchanger HEX1 as well as the heat transfer surface of the heat exchanger HEX2 have been divided into 500 portions to reach the required accuracy of the flows inlet and outlet temperatures calculation. In the used iteration algorithm an absolute accuracy of temperature calculation for the single portion of a heat transfer surface was about 10^{-8} K. Calculation accuracy for the inlet and outlet flows temperatures of the heat exchanger as a whole was about 10^{-4} K. Relative inaccuracy of the heat balance calculations was 4% at the most.

Satellite refrigerator (or cycle) cooling capacity Q_0, required cooling capacity of the KGU-500 refrigerator Q_{REF} and total low pressure flow pressure drop ΔP_2 were considered as the main parameters. These parameters calculation results versus satellite refrigerator high pressure flow mass flow rate G_1 are presented in Fig. 2 for the relative flow imbalance $\Delta G/G_1$ of 10%, cooling temperature 1.8 K and 14 bar helium pressure at the inlet into the satellite refrigerator. These results show that the developed cryogenic system has a considerable margin concerning KGU-500 refrigerator available cooling capacity. Total low pressure flow pressure drop is within the specified limits.

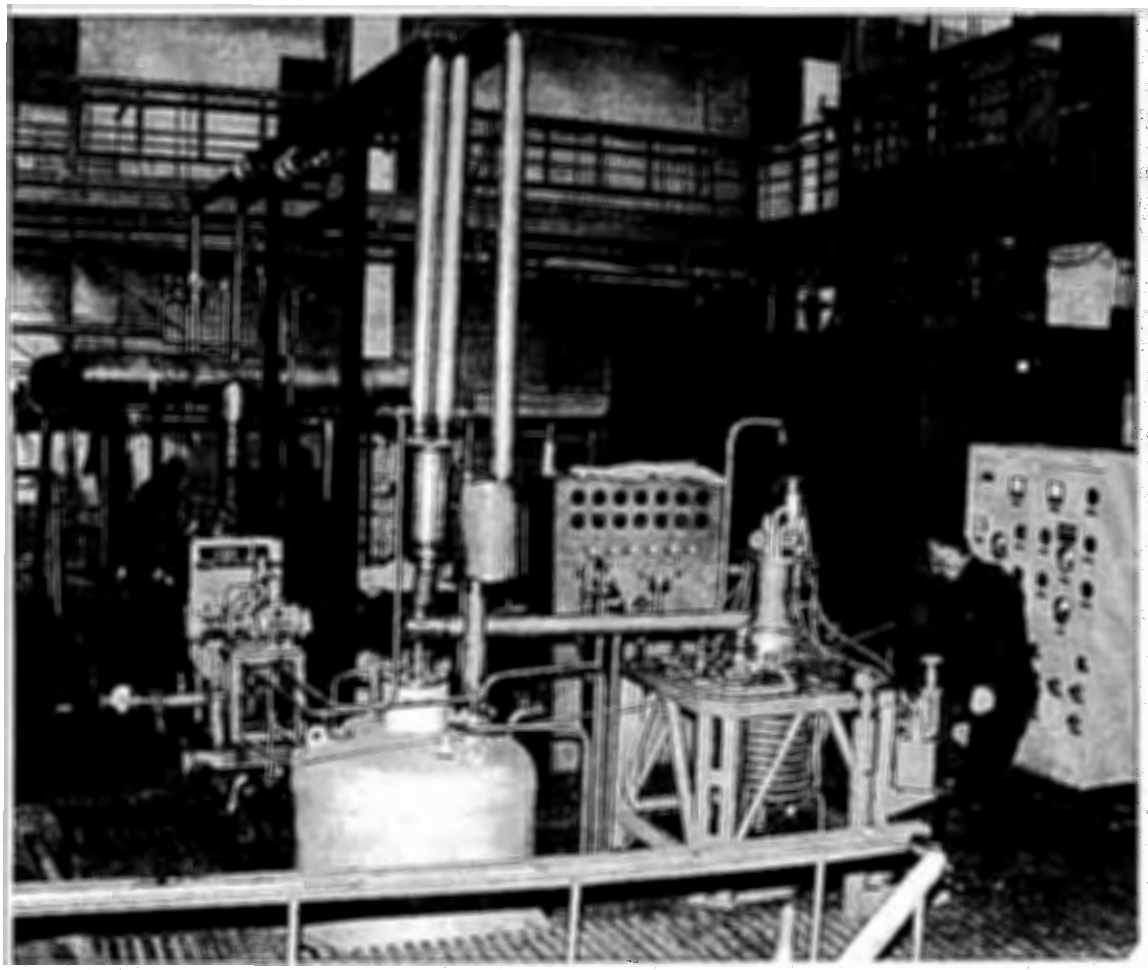

Fig. 3: Helium refrigerator, large vacuum heat exchanger and liquid helium bath (last two in the background) during erection.

STATUS OF WORK

To date main subsystems projects are developed, many of them already manufactured or purchased. Installation work is in progress, tests and commissioning of subsystems being prepared with an aim of gradual integration of them into a complete system.

Helium refrigerator of the KGU-500/4,5-140 type (500 W at 4.5 K or 140 l/hr of liquid helium) was delivered by "NPO Geliymash", JSC. Work on the refrigerator piping is close to finish (Fig. 3). Upgrading of the helium storage, compressing and purification systems are in progress. Commissioning tests of refrigerator are planned to be performed in November this year. At the same time liquid helium bath cryostat will be tested.

Large vacuum heat exchanger is very similar to the heat exchanger delivered to DESY by IHEP [3]. Heat exchanger is manufactured, installed and connected by pipe lines with other cryogenic equipment according the project.

Sections of the helium cryogenic transfer line about 100 m in total length were manufactured by "Cryogenmash", JSC, according IHEP technical specifications and delivered to IHEP. Small heat exchangers HEX2 were manufactured by IHEP, delivered to "Cryogenmash" and built into the appropriate transfer line sections. An agreement with "Cryogenmash" on transfer line mounting and testing is under preparation.

REFERENCES

[1] "Superconducting Separator Emerges from Sleep", CERN Courier, v.38, No.3, April 1998, p.12.

[2] Bakay A.I. et al., "Cryogenic 1,8 K Test Facility for Cryostats with Superconducting Cavities of RF-Separator", RUPAC-2002, Obninsk, October 2002, p. 445.

[3] E. Kashtanov et al, "Large Low Pressure Heat Exchanger for the TTF Cryogenic System", ICEC18, Mumbai, February 2000, p.315.

HIGH-FREQUENCY POWER GENERATORS FOR ACCELERATORS

Edward P. Goryunov, Alexander M. Dolgov, Saveliy M.Zhytomirsky,
Eugenie B. Isserlin, Olga E. Kildisheva, V.I. Levashov, A.O.Levashov,
M.I. Lyutov, Vitaly V. Maslov, A.A. Petrov, Eugenie A. Petrov,
Vladimir G. Rautian, Vladimir I. Sukhikh.

"TIRA" Joint-Stock Company has created a number of power high-frequency generators, as well as pulse modulators for physical units.

The most typical devices of them are briefly described in this paper.

Fig.1: HF generator Georgit-2. 25kW, 38MHz.

"TIRA" Joint-Stock Company founded in 1994 on the basis of the subdivision of Russian Institute for Power Radiobuilding and of the plant "Priboy" (former "Komintern" Amalgamation), during 10 years of its existence, has developed the pulse modulators and high-frequency generators to orders of diverse research centers from several countries all over the world. They represent a particular line and may be applied in diverse units irrespective of initial destination.

The paper [1] is dedicated to developments of pulse modulators.

The most part of HF generator developments is shown in Table 1.

The generators are typically constructed on the basis of multistage amplifier circuit with crystal-controlled driving oscillator or synthesizer. The power is amplified up to 100 W level by means of transistor amplifier provided with inputs for smooth control of power level between 100% and 20%, pulse keying at duty cycle from 1 up to 100 and high-speed circuit blanking (few tens μs). The latter is used for protection of accelerator tank and oscillator itself against emergencies in them and also is applied at tank burn-in. Further, the power is amplified by means of tube stages.

The tube amplifier up to 30 kW is a two-stage device based on triodes constructed as common-grid circuit with direct coupling between stages via π-circuit. The anodes of both stages are powered from one rectifier having a half-voltage mid-point for the first stage. The three-tube circuit is used to provide a greater power, if necessary.

The "right-hand" characteristic tubes are preferred because the separate bias source is not needed for them. All the developments are based on power oscillating tubes produced by "Svetlana" Joint-Stock Company. Thereby, the preference is given to those tube types (e.g. 3 CW 30000 A7, 3 CW 5000 A7) that may be also supplied by other western companies: CPI, Richardson et al. to provide a guaranteed delivery in any country.

There is no a direct western counterpart for the most powerful national tetrode ГУ-101А only.

The one-tube self-excited oscillator circuit with tube control grid power modulation is used where the oscillator is intended for laser ignition and a high frequency stability is not required.

Anode voltage sources are diode rectifiers provided with crowbar, if necessary, for tube protection. Thereby, the ac power-line voltage is turned off by means of controllable circuit-breaker in time period less than 6 ms. Therefore, the thyristor regulators are not typically used. The anode voltage stepped increase is provided through power starting resistors that are then short-circuited by contactor.

In 5 kW self-excited oscillator, the controllable anode-voltage source with no-transformer input with intermediate frequency conversion fulfils the functions of output high-frequency power regulator and stabilizer.

Table 1:

№	Name	Year	Destination	Physical distribution	Country-Customer	Technical data			
						P_{out}, kW	f, MHz	P_p, MW	E_p, kV
1.	Ameritsy-1	1994	Modulator for UHF generator	Yale University Linac	USA	–	–	65	22
2.	Ameritsy -1	1994	Modulator for injector	Yale University Linac	USA	–	–	3	100
3.	Cracoviak	1996	HF generator for cyclotron	Cyclotron for INP of Krakow	Poland	120	8...27	–	–
4.	Rubin-1	1996	HF generator for CO_2 laser	OPTOMIC laser	Israel	22	40.68	–	–
5.	Phianit	1996	HF generator for CO_2 laser	PI RAS laser	Russia Holland	5	150	–	–
6.	Alexandrite	1997	HF generator for CO_2 laser	ILP laser for LINX	Great Britain	2	81.36	–	–
7.	Ameritsy -2	1998	Modulator for injector	Yale University Linac	USA	–	–	10	300
8.	Kopernik-1	1998	HF generator for CO_2 pulse laser	ILP laser	Japan	2	150	0.1	20
9.	Irinit	1999	HF generator for NIIEFA cyclotron	Abo-Academy Cyclotron	Finland	80	8...27	–	–
10.	Olympus	1999	HF generator for CO_2 laser	ILP laser	China	4	81.36	–	–
11.	Avanturin	1999	Modulator for klystron	Yale University Linac	USA	–	–	100	20
12.	Georgit	1999	HF generator for CO_2 laser	ILP laser for AMADA	Russia	20	40.68	–	–
13.	Kopernik -2	2000	HF generator for CO_2 pulse laser	ILP laser for Bourgun Technology	France	50	150	0.1	20
14.	Kaolin	2000	HF generator for cyclotron	Cyclotron (Dubna)	Russia	30	18.5	–	–
15.	Nadin	2000	HF generator for CO_2 laser	ILP laser	Russia	15	81.36	–	–
16.	Natalit	2001	HF generator for electron accelerator	JINR electron accelerator (Dubna)	Russia	150	100	–	–
17.	Olympus	2001	HF generator for cyclotron	ILP laser	Russia	4	81.36	–	–
18.	Magnetit	2001	Modulator for UHF generator	NIIEFA Linac	Russia	–	–	4	42
19.	Ikebana	2002	HF generator for CO_2 laser	ILP laser for AMADA	Japan	35	40.68	–	–
20.	Pyrit	2002	Modulator for UHF generator	Microtron (Dubna)	Russia	–	–	5.5	50
21.	Ionit	2002	Modulator for endotron	NIIEFA ion accelerator	Russia	–	–	1.35	14 24
22.	Georgit -2	2002	HF generator for cyclotron	NIIEFA Cyclotron for Abo-Academy	Finland	25	38	–	–
23.	Alevit	2004	HF generator for CO_2 laser	ILP laser for Prima Industry	Italy	50	81.36	–	–

The load or feeder voltage sensors and respective transistor amplifier input are used to provide the operation of power stabilization system.

Cooling. The greatest part of generators are water cooled in one-loop or two-loop (water-water or water-air) scheme. The air cooling may be also used, if necessary.

Construction. All the generator equipment is located in Shroff standard cabinets (Fig.1). The high-frequency stages are enclosed in duralumin or brass containers with full high-frequency radiation protection. The output power is transmitted through rigid coaxial feeder provided with directional coupler. The delivery set can include, if necessary, a dummy load for total output power.

REFERENCES

[1] A. Dolgov, O. Kildisheva. New generation of HV pulse modulators for technological accelerators

MICROWAVE FEEDING SYSTEM DEVICES OF LINEAR COLLIDER

B. Yu. Bogdanovich, V.I. Kaminsky, M.V. Lalayan, N.P. Sobenin, D.A. Zavadtsev, Moscow Engineering Physics Institute (State University), Russia
M. Ebert, DESY, Germany

Abstract

The simulations, manufacturing and experimental results for two devices of linear collider RF power distribution system are presented. One of these devices is magic tee with movable choke plungers in E- and H-arms for the tuning the coupling-factor and RF phase of high-power accelerating cavities. The Q_{EXT} of the cavity structures must be tuneable in the range from $0.9*10^6$ to $9*10^6$ to match the RF system under different beam conditions. For matching the waveguide power distribution system to cavities with different quench thresholds, adjustable directional couplers are necessary. These directional couplers with a coupling factor of 3.0 dB and 12.5dB with adjusting range of ±1 dB and directivity better than 30dB in were designed and produced. The adjustment elements of these couplers are movable membrane based plungers in two additional 90^0-bended H-arms opposite the coupling slot. All devices were designed for operation at 1.3 GHz and pulse power 1-5 MW.

INTRODUCTION

The high power RF distribution system of the electron-positron collider TESLA [1] is designed to ensure external Q independent adjustment of each superconducting cavity by a factor of 10 and also independent adjustment of the cavity RF phases. A further demand is the individual adjustment possibility of the cavity power feed. For this item adjustable waveguide couplers are foreseen. For Q and phase adjustment E-H-tuners were constructed [2]. For matching the RF power distribution system to cavities with different quench thresholds, the investigation of adjustable direction couplers is underway. The TESLA machine is feeded 18 cavities with one 5-MW klystron-output. Therefore waveguide couplers having different coupling factors between 1/18 (12.6dB) and 1/2 (3.0 dB) with an adjustment range of ±1 dB are necessary. The directivity D should not be less than 25 dB. At first step adjustable 3dB and 12.5dB hybrid couplers are investigated. Another requirement to adjustable direction coupler is to fit the given space limiting the dimensions: length less than 500 mm and width less than 400 mm.

E-H TUNER

Fig.1 shows a magic tee, matched to reflection factor of 0.001, using inductive irises in the E- and H-arms (3 and 4 respectively). Removable sliding shorting plungers with a range of half a wavelength are connected to these arms. Fig. 2 shows an experimentally measured S11 matrix element vs. plungers' position

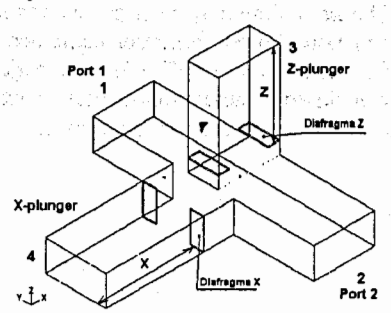

Fig.1: Magic tee, matched using inductive irises

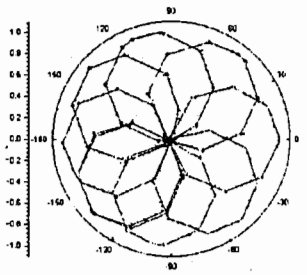

Fig.2: Measured S11

The necessary power capability for the E-H tuner is 280 kW pulse power in a totally reflecting load. This corresponds to 1100 kW to a matched load. Therefore it is important to provide optimum conditions for the short circuit current at the sliding shorts and minimum field strength at sparking endangered locations. Two different variants of choke plungers were considered. Both for 1300 MHz and the waveguide type WR-650 with dimensions 165.1 x 82.55mm^2.[2]

The choke plungers are motorized by stepping motors. In Fig.3 a sketch of the assembly is shown. Positioning the plungers is made by a computer with RS-232 or RS-422 interface. In a calibration mode the computer moves both plungers successively over the full sliding range defined by limit sensors and measures the S-matrix via a network-analyzer. Plunger positions and associated S-parameters are stored in a computer table. In the normal operating mode the user can define desired S-parameters, coupling factors or phases, which are then adjusted automatically by the computer-controlled plungers.

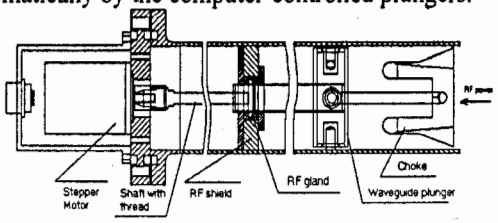

Fig.3.Second design variant of the choke plunger, motorized by a stepping motor

12.5 dB ADJUSTABLE DIRECTIONAL COUPLER

The coupler model is presented in Fig.4. In order to comply the device dimension limitations the 90 grad turn of side waveguides with movable plungers was used.

The side waveguides broad walls length was chosen 276 mm. The simulations show that the side waveguides of reduced width result in dramatic directivity degradation at the plungers displacement from the initial position corresponding to the coupling of C=12.5dB. Enlarged waveguide makes the directivity degradation on the adjustment band sides lesser but moves the entire D vs. C curve down, i.e. decreasing the directivity. So, there is optimal waveguide width value ensures the maximal directivity at adjustment range frontiers (at 11.5dB and 13.5dB coupling)

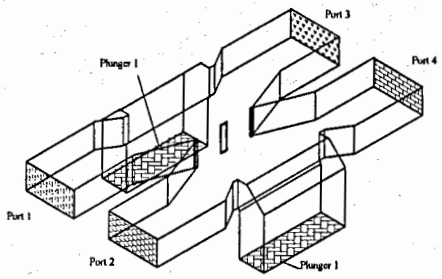

Figure4: 12.5dB directional coupler model

The D vs. C dependence "centering", i.e. directivity maximum shift to the middle of adjustment range C=12.5dB was done by protrusions at the sides of adjusting waveguides dimensions variation. Input waveguide ports matching was done by wedge between 1st / 2nd and 3rd / 4th ports angle variation. Coupling window dimensions define the coupling.

The adjusting waveguide segments at 45 grad allowed matching the bends. The minor segment reduces the electric field overvoltage on the bend edge thus ensuring the coupler electric strength. The model is symmetric and two plungers are displaced simultaneously during the simulation. The results obtained for the coupler with optimized geometry are the following: D exceeding 29dB, reflection R less than –32dB within the full coupling adjustment range 11.5dB to 13.5dB.

Based on the simulation results the coupler design was developed suitable for manufacturing. According to the technological guidelines the coupler has straight waveguide sections just before flanges, latter being of standard shape. The flanges for adjusting waveguides were chosen of increased width keeping the other parameters unchanged.

The coupler parameters computation and its geometry was done by Gradient descent back-propagation method involving 10 dimensions, using HFSS 8.0 code. The main results for optimized device are presented in Fig.5, a. The data show that D is better than 28dB in the coupling adjustment range 11.5dB to 13.5dB. Along with equal plungers positioning the case of independent one was considered. Fig.5, b. shows the surfaces representing the parameters D change with two independent parameters (plunger positions d1 and d2) variation.

The electric strength is one of the most important issues presented by the coupler development. The electric field distribution in the coupler volume was studied for different plunger positions and the field peak values were

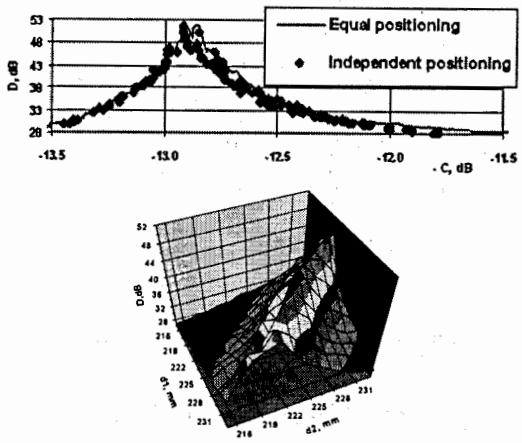

Figure 5: Directivity for 12.5dB coupler vs. coupling dependences (a) and plunger positions (b)

obtained. The adjusting waveguide H-bend corner area being possibly discharge-dangerous is free from overvoltage. Also the field strength in adjusting waveguides is less than one in input waveguides, thus the movable plungers will operate in less strict conditions. The movable plungers design relies on electric time-dependant field distribution in the plunger vicinity. The field distributions are different for two plungers with respect to both time and space. In one waveguide the TE_{10} mode predominantly propagates whereas in the other one TE_{20} mode is distinctive. This means that in case of choke-type plungers they are to be different thus making the coupler design more complicated. The maximum overvoltage factor K, determined as the maximal electric field strength in directional coupler to the traveling wave field strength in attached waveguide, was K=13% at d=233mm corresponding to coupling to C=13.5dB.

3dB ADJUSTABLE DIRECTIONAL COUPLER

The directional coupler with 3dB coupling was designed according to the algorithm used for 12.5dB coupler (see Fig.6.). The main difference in device geometry is in coupling window design. The adjusting waveguides have the same dimensions as for 12.5db device for plunger unification. The optimization was done by gradient descent back-propagation on 7 geometry parameters. The model is symmetric and the plungers' positions are equal for both adjusting waveguides. The directional coupler main parameters after the model optimization are the following: D exceeds 31dB, R less than –35dB inside coupling adjustment range 2db to 4dB. The directional coupler parameters with frequency change

in (1300±5) MHz band were determined for three fixed plunger positions of 211mm, 226mm and 246mm, corresponding to the 2dB, 3dB and 4dB coupling respectively. The data obtained show that the coupler parameters in this frequency band: directivity exceeds 32dB, reflection is less than –32dB and the coupling change is less than 0.15dB.

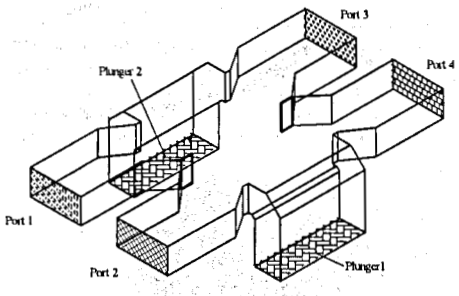

Figure6: 3dB directional coupler model

MOVABLE PLUNGERS

In order to achieve better directivity of the device at the coupling variation within ±1 dB range wide waveguides of 276×82.55 mm^2 cross-sections were chosen. The plunger development was done taking into account two concerns – effective short-circuiting in whole travel range and keeping the fields on the plunger surface below the waveguide fields value.

All the reasons mentioned led to the design of the fits-all-cases plunger based on flexible membrane element. In this design the thin bronze alloy film permanently attached to the waveguide wall and to the plunger body is used to have conductive plane (see Fig.7).

Figure 7:Membrane plunger

This plunger design has the following advantages. High-frequency currents in narrow walls of TE_{10} and TE_{20} modes are perpendicular to the waveguide axis so there will be no high electric field arise between plunger and waveguide (in 9mm slots). Electromagnetic properties of this plunger were determined by HFSS simulation. Electric field maximum was detected at plunger is 20mm displaced from its middle plane towards the coupler. Electric field at 1mm away from membrane edge is 0.07 of the coupler input waveguide field.

Actuating mechanics powered by step motor moves the plungers. Each plunger is equipped with two optical sensors limiting the traveling range.

EXPERIMENTAL RESEARCH

The measurements were done using test stand based on Agilent Network Analyzer 8753ET. Fig.8 presents the directional coupler photo with Network Analyzer connected using waveguide to coaxial transitions.

The controlling, save and recall of the data obtained during measurements are performed by PC. Two controllers by Integrated Motion Systems power the step motors. Network Analyzer connected to PC via GPIB interface measures directional coupler parameters. The computer code is developed using LabView.

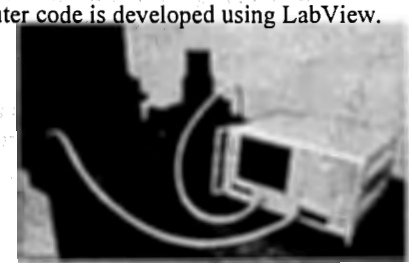

Figure 8: Directional couplers measurement setup

Fig.9 presents the experimentally obtained and simulated by HFSS code parameters comparison. The data include coupling, directivity vs. plungers position. For the same cases directivity vs. coupling dependences are presented.

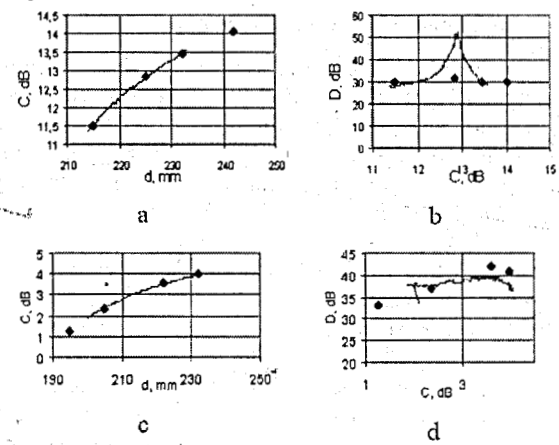

Figure 9: Experimental and calculated using HFSS code data comparison12.5dB (a, b) and 3 dB coupler (c, d): ♦ experiment, – calculation

REFERENCES

[1] R. Brinkmann, G. Materlik, J. Rossbach, A. Wagner, "Conceptual Design of a 500 GeV e^+e^- Linear Collider with Integrated X-ray Laser Facility", DESY 1997–048, ECFA 1997–182, vol.1

[2] B.Yu. Bogdanovich, M. Ebert, M.A. Egorov, V.I. Kaminsky, N.P Sobenin, M.F. Volkov, D.A. Zavadtsev "Design of an E-H–tuner and an adjustable directional coupler for high-power waveguide system", Proc. of the 8-th European Particle Accelerator Conference (EPAC-2002), Paris (France), 2002

RF STATION FOR ION BEAM STAKING IN HIRFL-CSR

V.S.Arbuzov, Yu.A.Biryuchevsky, A.A.Bushuev, N.F.Vajenin, E.I.Gorniker, A.N.Dranichnikov, E.K.Kendjebulatov, A A. Kondakov, S.A. Krutikhin, M. Kondaurov, Ya.G.Kruchkov, G.Ya.Kurkin, L.A.Mironenko, S.V. Motygin, V.N.Osipov, V.M.Petrov, A.M. Pilan, A.M.Popov, V.V.Rashenko, A.N. Selivanov, A.R.Shteinke.

Budker Institute of Nuclear Physics of Siberian Branche of Russian Academy of Sciences, 630090, Novosibirsk, Lavrentiev ave, 11

Abstract

BINP has developed and produced the RF station for Institute of Modern Physics (IMP), Lanzhou, China, for multipurpose accelerator complex with electron cooling. The RF station will be used for accumulation of ion beams in the main ring of the system. It was successfully tested in IMP and installed into the main accelerator ring of the complex.

The RF station includes accelerating RF cavity and RF power generator with power supplies. The station works within frequency range 6.0 - 14.0 MHz, maximum voltage across the accelerating gap of the RF cavity - 20 kV. In the RF cavity the 200 VNP ferrite is utilized. A residual gas pressure in vacuum chamber does not exceed 2,5E - 11 mbar. Maximum output power of the RF generator 25 kW.

The data acquisition and control of the RF station is based on COMPACT – PCI bus and provides all functions of monitoring and control.

INTODUCTION

HIRFL-CSR is the new accelerator complex that nowadays undergoes commissioning at Center for heavy ion study (HIRFL) in Lanzhou city, China. It is a multipurpose accelerator complex, consisting of the main accelerating ring (CSRm) and an experimental ring (CSRe). Bunches of heavy ions with an energy of 10-50 MeV/u will be stored, accumulated, cooled, and then accelerated up to 400 - 900 MeV/u by accelerating ring CSRm.

RF STATION PARAMETERS

RF station №2 is destined for accumulation (RF staking) of ions in CSRm before acceleration cycle. The acceleration station (№1) during this time is to be switched off. Parameters of staking station №2 are given in Table 1.

A newly injected bunch is captured in RF separatrix, and then a frequency of driving oscillator of station is changed in special way to make orbit of newly injected particles motion come closer to the orbit of previously accumulated particles circulating in the ring. RF voltage of the RF station №2 is switched off after that, and the injected bunch is attached to circulating particles with an aid of electron cooling. Then the cycle is repeated.

The injected bunch has a short length but a wide energy spread. In order to capture such a bunch in separatrix a high accelerating voltage is needed.

Table 1: Main parameters of RF station №2

Frequency range		6.0 - 14.0	MHz
RF voltage amplitude		20.0	kV
Harmonic number		16, 32	
Operation vacuum in RF cavity		$< 3.5 \cdot 10^{-11}$	mbar
Ferrite type		200 VNP	
Max. RF power of generator		25	kW
Cycle duration		50	ms
Repetition frequency		20	Hz
Installation length of RF cavity		2300	mm
Height	Orbit plane	1500	mm
Aperture	horizontal	200	mm
	vertical	200	mm

At that time while new injected bunch approaches the circulated particles, and the frequency of RF voltage and circulation frequency become closer, high accelerating voltage would disturb the motion of circulating particles too much.

Moreover, the cooling efficiency will also decrease at large initial energy dispersion of the bunch. That is why the bunch is injected when the gap accelerating RF voltage equals to 20 kV in accepted scheme. The RF voltage is quickly decreased to value 1.0 – 1.5 kV after period of time equal to quarter of synchrotron oscillation (some tens microseconds), when energy spread of particles is minimal. This voltage is sufficient for keeping particles in separatrix and this voltage is maintained constant till the end of cycle.

RF station consists of accelerating RF cavity, RF power generator and control system (see fig. 1).

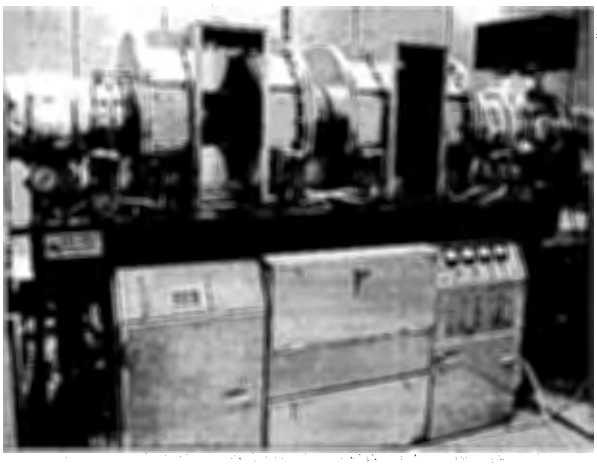

Fig.1: RF cavity and RF power generator of station

RF cavity, RF power generator with power supplies are assembled in single module, the control system is mounted separately in radio rack.

RF CAVITY

RF cavity has two gaps into which a ceramic insulators are welded in (see fig. 2). Maximal voltage on each insulator – 10 kV. This voltages are summed up at single accelerating gap inside vacuum chamber.

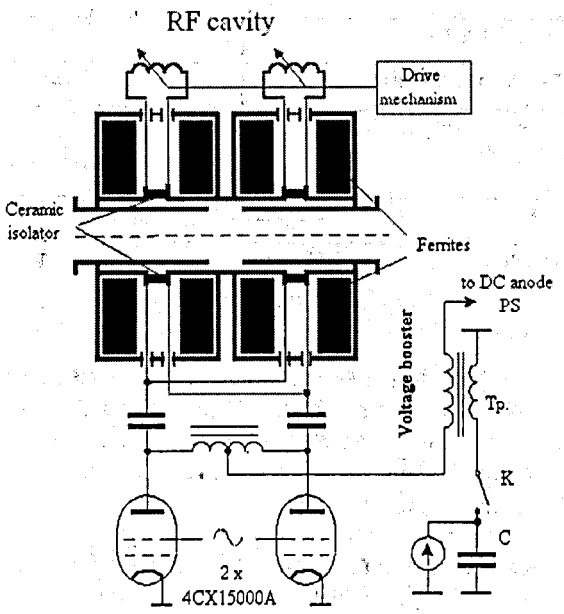

Fig.2: Block diagram of RF station

Resonant frequency of RF cavity is not tuned during operation cycle because the range of generator frequency tuning lies within resonant frequency band of RF cavity for the given type of ions. Change for another type of ions and compensation of the thermal or any other instabilities is accomplished by RF cavity tuning with an aid of electro-mechanically driven variable inductivity (see fig. 2).

The RF cavity is tuned in such a way that it is accurately at resonance when the gap voltage is maximal (20 kV). Later (during cycle) when RF voltage is small, the operation frequency moves away relative to the resonant frequency of RF cavity, and required RF voltage at detuned cavity is maintained by increasing of excitation of output stage of RF generator.

In RF cavity of station the ferrite of 200 VNP type is used. It is produced by "Magnetron" plant, St.Petersburg. Ferrite was delivered from plant in form of tiles, which were than mechanically treated and glued into octagonal rings. Inner diameter of the ring – 340 mm, total length of rings assembly – 500 mm. The heat, dissipated in ferrite, is removed by copper discs inserted between rings. The discs are cooled with water. For improving the thermal contact between ferrite rings and copper plates, mechanical stability of elements as well as for increase of the electric strength of insulation, a free space in the cavity is filled with a sealing compound. Maximal induction in ferrite at 6 MHz and gap voltage 20 kV – 90 Gs.

Vacuum chamber with ceramic insulators was backed at temperature 350°C for achievement of high vacuum $3.5\ 10^{-11}$ mbar.

RF POWER GENERATOR

Two air-cooled vacuum tetrodes 8281/4CX15000A are utilized in output stage of RF power generator. The tubes are connected into push-pull scheme with common cathode, and their anodes are connected directly to accelerating gap via high frequency.

The output stage is fed by 2.5 kV rectifier. Boosting device provides increase of anode voltage up to 6.5 kV during 150 microseconds at the beginning of each operation cycle when RF voltage at cavity gap is 20 kV. The pulse transformer Tp is connected in series to anode power supply circuit for this purpose. The switch K connects storage capacitor C to primary winding for the time ~ 150 mc.

A water cooled broadband preamplifier is based on transistors and drives the tetrodes in the whole frequency range without tuning. Maximum output power of the preamplifier is 0.9 kW in CW mode. The input power of the preamplifier is 0.25W max.

CONTROL SYSTEM

The Control System is based on the Compact PCI bus and provides for a complete control and monitoring of all parameter of RF station. The control system provides regulation of the operating frequency of RF station by a given program, controls amplitude and phase of accelerating voltage of RF cavity and fine tuning of its resonant frequency.

The Main Control Module is installed in the Compact PCI crate and contains the Master Oscillator of RF station using DDS technology, the DACs providing DC reference signals for RF cavity amplitude and ADC for monitoring of RF station parameters during the cycle. The AD9854 DDS is functioned with EP1K30QC208 FPGA in parallel connect mode to achieve high updating of signal frequency. The DDS supplies frequency resolution less then 1 Hz and frequency update less then 1μs. RF system is locked by phase feedback loop to compensate phase deviation between the DDS and cavity voltage. 16 bit of amplitude date and voltage feedback from the cavity are applied to amplitude modulation unit. Digital frequency date through linearization table is also converted to analog signal. This voltage is added with the signal from phase meter between cavity voltage and feeder current and put to unit tuning the cavity.

The RAM section of the module stores the information, which determines the key parameters during the operating cycle: the output frequency of DDS, amplitude of accelerating voltage of RF. The station can be controlled from the Central Control Room of the CSRm through Ethernet or/and from a local monitor and a keyboard.

RESULTS OF RF STATION TEST

After shipment of RF station to Lanzhou it was reassembled there and the required vacuum in the cavity was obtained. The commissioning testing of the cavity was made during 72 hours non-stop. The RF cavity voltage instabilities was measured to be within 0.2%, accuracy of the cavity tuner was inside 5 degree. After successful completion of the test the RF station was moved into CSRm ring, installed there and now is ready for operation.

REFERENCES

[1] J.W. Xia, Y.F. Wang et. al., HIRFL status and HIRFL-CSR project in Lanzhou, APAC'98, KEK, Japan.

[2] W.L. Zhan, J.W. Xia et. al., HIRFL-CSR Project, Cyclotrons 2001, American Institute of Physics, USA

STATUS OF 178.5 MHZ RF SYSTEM FOR THE DUKE FELL STORAGE RING

V.S. Arbuzov, A.A. Bushuev, N.G. Gavrilov, E.I. Gorniker, E.K. Kenjebulatov, M.A. Kholopov, A.A. Kondakov, S.A. Krutikhin, Ya.G. Kruchkov, I.V. Kuptsov, G.Ya. Kurkin, L.A. Mironenko, N.V. Mityanina, S.V. Motygin, V.N. Osipov, V.M. Petrov, A.M. Pilan, A.M. Popov, E.A. Rotov, I.K. Sedlyarov, A.G. Tribendis, V.N. Volkov
Budker Institute of Nuclear Physics, Siberian Branch of the Russian Academy of Science, Novosibirsk, Russia

Abstract

A new RF system for the DFELL (Duke Free Electron Laser Laboratory) storage ring is presented. High power RF generator with a GU-101A tetrode and bimetal cavity with a higher order modes ceramic load are described. Results of the RF system tests are discussed.

INTRODUCTION

About 10 years ago, Institute of Nuclear Physics produced an accelerating cavity and control system for the DFELL storage ring, USA.

The RF system has been successfully operated during almost 10 years. However, the RF system did not allow storing high beam currents because of synchrotron oscillations arising from interaction of the cavity HOMs with the electron beam. Although the cavity was equipped with two HOM tuners, it was practically impossible to set the cavity HOM frequencies so that they did not affect the beam dynamics at high currents and in multibunch mode.

In 2001, DFELL started a machine upgrade project aiming at the FEL experiments in VUV spectrum range [1]. After the upgrade the machine should operate at energy up to 1.2 GeV with average current up to 300 mA and number of bunches from 1 to 64. The storage ring upgrade calls for a new 178.5 MHz RF system with a cavity with HOM-damping. The accelerating voltage across the cavity should be up to 730 kV.

HIGH POWER GENERATOR

A vacuum tube generator for the new RF system was produced on the basis of high power tetrode GU-101A (Fig. 1). BINP has developed and operate generators with output power up to 600 kW [2, 3], containing modules (up to 4) based on GU-101A tetrode. The DFELL RF generator provides up to 140 kW output power in the frequency range

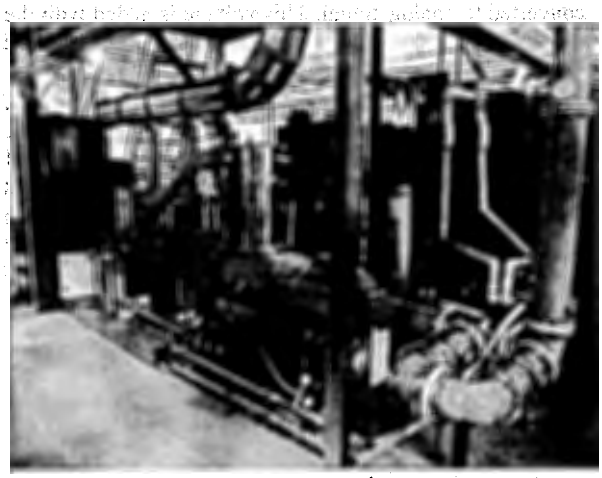

Fig. 1: New DFELL generator

of 178...179 MHz. The generator is a 3 stage power amplifier with an external drive. In two first generator stages, GU-92A tetrodes are used. A high power GU-101A tetrode is used in the output stage. The amplifier is driven by a 100 W solid-state pre-amplifier. The output power is delivered to the cavity via a 75 Ohm rigid coaxial feeder.

In order to increase the reliability of the generator and to extend the lifetime of the tubes, the tubes operate in somewhat relaxed regimes. The voltages of power supplies and dissipated powers are slightly reduced in comparison to values recommended by the manufacturer.

Table 1: Parameters of bimetal cavities for the fundamental (accelerating) mode

	BINP FEL	DFELL Duke-1	DFELL Duke-2
Operation frequency f, MHz	180.4	178.5	178.5
Characteristic impedance R_{acc}/Q, Ohm	110	114	88.6
Transit time factor T	0.903	0.919	0.764
Quality factor Q	41000	42000	39000
Shunt impedance R_{acc}, MOhm *	4.50	4.77	3.46
Accelerating voltage V_{acc}, kV	850	640	730

* Shunt impedance is defined as $R_{acc} = V_{acc} / 2P$, where V_{acc} is the accelerating voltage.

BIMETAL CAVITY WITH HOM DAMPING

BINP has gained a wide experience in production of bimetal RF accelerating cavities [4]. Over 25 bimetal cavities have been produced, tested and now operate in various facilities (BINP, Korean Atomic Energy Research Institute, DFELL).

The RF cavity for the new RF system DFELL, "Duke-2", was developed on the basis of a "standard" bimetal (copper clad stainless steel) RF cavity. Parameters for the fundamental mode of the cavity are listed in Table 1. For comparison, parameters of the "standard" cavity of the BINP microtron FEL and the old DFELL cavity are also presented. Old DFELL cavity had only slight modifications from "standard" one in the geometry to fit the operation frequency of the Duke storage ring.

The appearance of new RF cavity for DFELL is shown on Fig. 2. The cavity is equipped with RF power absorbing load for HOM damping. HOMs are coupled to the RF absorbing load via a large (700 mm) diameter beam pipe. The cutoff frequency of the pipe for the accelerating TM_{01} mode is substantially higher than the fundamental mode frequency, so the fundamental mode is trapped in the cavity, while the HOMs propagate out of the cavity to the absorbing load. The load is within 1200 mm distance away from RF cavity, so it does not cause any considerable influence on the Q-factor of the fundamental mode. Power loss in the load at accelerating frequency is 100 W. The large opening in the cavity wall causes a fundamental mode resonant frequency shift up. A nose cone at the opposite cavity face wall is needed to bring the frequency down to the design value. Also, the transit time factor decreases due to the field pattern distortion. This leads to higher fields in the cavity at the same accelerating voltage.

Cylindrical shell of the cavity has some ports for connection of various units. Coaxial input coupler with a cylindrical ceramic window is installed on top of the cavity. Two ports are used for fundamental mode tuners, noncontact plungers.

The cavity is pumped out by two combined vacuum pumps (each pump includes ion and getter pumps) of PVIG-250/630 type with total pumping speed of 630 l/s each. Pumps are attached at the bottom of the tube connecting the cavity to the HOM load. According to the experience with bimetallic cavities, after manufacturing and assembly the Duke-2 cavity was baked at 300 °C. After an RF processing vacuum in the cavity of $1 \cdot 10^{-10}$ torr was achieved.

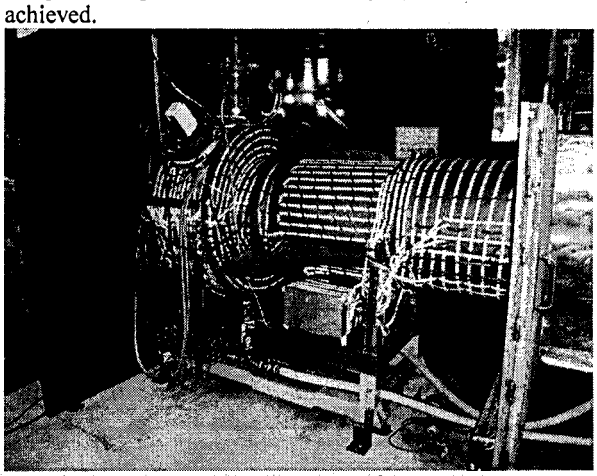

Fig. 2: Duke-2 cavity

A conducting ceramics KT-30 produced by "Start" company, Russia, Fryasino was chosen as an absorbing material for the HOM load. The composition of the ceramics is: TiO_2 – 30 %, A-995 – 70 % (Al_2O_3 – 99.8 %, MgO – 0.2 %). The RF absorber elements are ceramic cylindrical cups with diameter 32 mm and height 45mm. Every absorber is fixed on an internal wall of the load tube with a bolt. The material used and the design of the loads sustain baking of the cavity with the loads at the required temperature.

SUMMARY

Cold measurements of the cavity have shown that the HOMs are indeed well suppressed (Fig. 3 and 4). According to calculations, this should allow storing currents over 300 mA. During hot tests of the cavity, the accelerating voltage of 890 kV was achieved. At present time, the new RF system is tested and installed in the storage ring. Commissioning of the DFELL storage ring with the new RF system is in progress now.

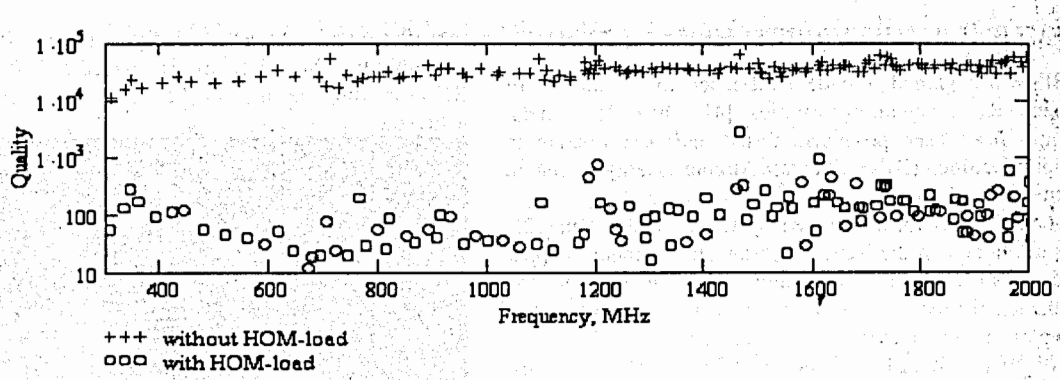

Fig. 3: Calculated Q values for the HOMs (TE_{0mn}, TH_{0mn})

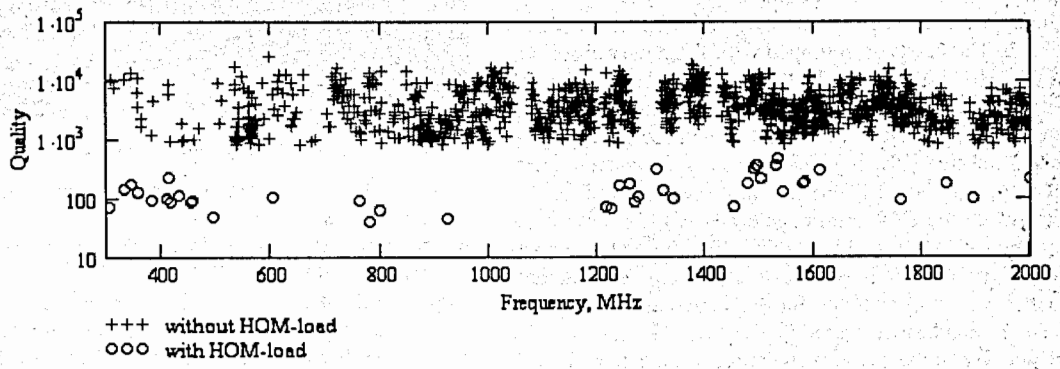

Fig. 4: The measured Q of the HOMs

REFERENCES

[1] S.F. Mikhailov, V.N. Litvinenko (Duke University), Y. Wu (LBNL), "Low Emittance Lattices for the Duke FEL Storage Ring", Proc. of the 2001 Particle Acc. Conf., Chicago, Illinois USA, June 18-22, 2001, vol. 5, pp. 3528-3530,

[2] V.S.Arbusov, A.A.Bushuev, A.A.Kondakov, etc. "Powerful RF generator of a modular design for stores and accelerators", XVI meeting on accelerators of the charged particles, Protvino, October 20-22, 1998.

[3] V.S.Arbuzov, B.A.Baklakov, B.P.Bolotin, etc. "Constructing RF of system of a race-track microtron-recuperator for the high power FEL", The report at XVII Meeting on accelerators of the charged particles. Protvino, October 17 - 20, 2000.

[4] N.Gavrilov et al., "RF Cavity for the Novosibirsk Race-Track Microtron-Recuperator", Budker INP preprint 94-92, Novosibirsk, 1994.

DATA OBTAINING AND PROCESSING SOFTWARE FOR ION-BEAM MONITOR AT THE FRANKFURT 14GHZ ECRIS

A. Kayukov, V. Alexandrov, M. Koryovkina, O. Strekalovsky, K.E. Stiebing

Abstract

A program package for control of the beam monitor, data acquisition and the subsequent processing is developed. BMCM PC20 and PCI300 input-output cards are used for control and data acquisition. The control program is written on VisualC, the processing program is written on LabView. The control program allows to supervise position of a beam in real time and to save data files for two types of monitors. The processing program enables the preliminary analysis of the data and to calculate emittance of the ion beam.

DESCRIPTION OF THE INSTALLATION

The ion beam monitor for definition of x/x ' and y/y ' emittance has been developed and tested at the ERCIS facility in Frankfurt IKF[1]. The monitor consists of a specially shaped screen rotating around the Faraday cup and of a system of two gaps, positioned at an angle of 90°. Gaps are inserted into the beam by means of stepper motors. The monitor is located 1 meter away from the ion source. The step length of gaps moving used is 0,5 mm to achieve a measurement accuracy of emittance about 102 π mm mrad. The typical kind of pulse current is shown in Fig. 1a, which is measured in each position of x-and y-gaps with the aid of Faraday cup. The differentiated signal looks like that shown in Fig. 1b.

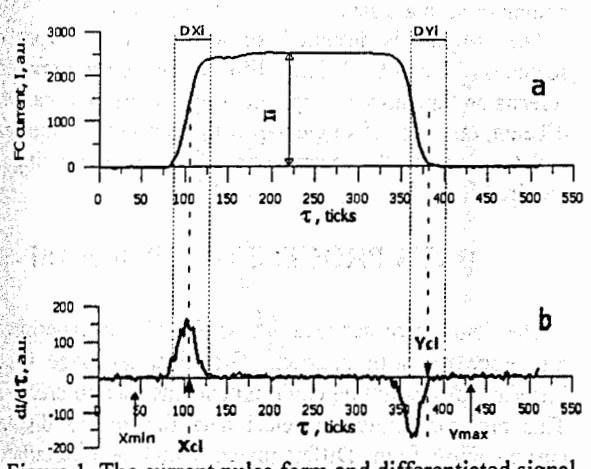

Figure 1. The current pulse form and differentiated signal.

Processing of the signal yields; current amplitude I_I, coordinates of the mass centre (X_{cl}, Y_{cl}) and sizes D_{xl} and D_{yl} of the beam portion cut out by gaps.

BEAM MONITOR CONTROL PROGRAM

Controls

The beam monitor contains the following controls:

- step motors No. 1 and No.2, which move gaps for 0° beam
- step motor No.3, which move gaps for 90° beam
- direct current motor, which rotates the screen for 0° beam
- direct current motor, which rotates the screen for 90° beam

Each direct current motor also rotates a disk fixed on the same pulley, where the screen is fixed. A part of such disk circle arch is marked in black color that means the "Stop" signal of measurement. The light part of the disk circle arch activates the "Start" signal.

I/O Cards

There are 2 I/O cards used in the control system: PC20 with bus ISA and PCI300 with bus PCI. Each card contains 12-bit ADC, DAC and digital I/Os. ADCs are used to obtain a signal from the Faraday cup, digital I/Os – to control stepper motors and to receive the "Start" signal. Access to I/O cards ports is realized by means of drivers delivered by the company BMCM as a part of the complete delivery set.

The Program Structure

It is possible to divide the beam control program into the following blocks conditionally:

- The synchronization block
- The data read-out block
- The visualization block
- The data saving block
- The step motors control block
- The automatic beam scanning block with consecutive moving of step motors

All blocks forms a single whole and executes according to beam scanner work algorithm.

The Interface

The program is based on the Dialog application.

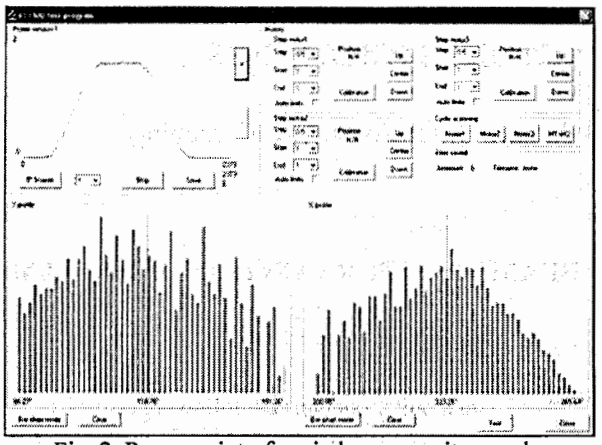

Fig. 2: Program interface in beam monitor mode.

In the beam monitor mode (Fig. 2), the top window displays a signal received from Faraday cup during the signal "Start". The ADC input voltage is displayed on 0Y axis , and the angle of the beam screen turn is shown on axis 0X. Derivatives of signal front and recession within the top window limits are displayed in right and left bottom windows in the beam monitor mode. The signal recession derivative is inverted with respect to OY axis.

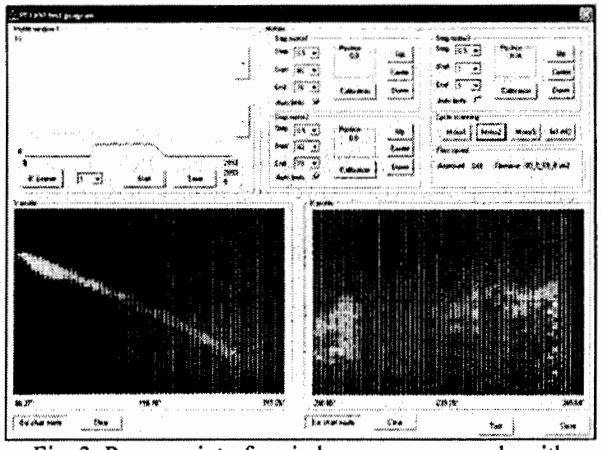

Fig. 3: Program interface in beam scanner mode with consecutive gaps moving.

Pseudo-three-dimensional histograms of derivative levels of corresponding pulse fronts and recessions are displayed in bottom windows in beam scanner mode with consecutive moving of gaps (Fig.3) where value ranges are shown in different colors. The quantity of histogram lines corresponds to the quantity of gap steps from the beginning to the end of scanning. The dialog elements located in the right top part of a window are used for the start of scanning and control of gaps, adjustment of their position and lengths of steps.

Principle of Program Functioning

By default, the program works in beam monitor mode (Fig. 2). About 15000 readouts from Faraday cup are received during signal "Start" at frequency of beam screen rotation of about 1 Hz. Before the work begins the synchronization block defines speed of rotation and the readouts quantity for summation of average values to reduce the array size up to 2500-3000 readouts. The synchronization block is called also at each change of disk rotation speed. Further the read-out block is started for the data, which are displayed in corresponding windows by the block of visualization. This operation mode is used for beam form adjustment. Current data can also be saved to a file manually using the data saving block.

Before the work with step motors begins their calibration on all length of gaps moving is carried out, the motor steps quantity, necessary for moving a gap for 1mm is calculated. Then initial and final position of gaps and a step of their moving must be selected. It's possible to set a standard range of measurement. Beam scanning with consecutive gaps moving starts after translation the derivative display mode to the pseudo-three-dimensional mode. Gaps move as follows: the gap No.1 moves for 1 step, then the gap No.2 moves from the beginning to the end of the scanning range with a set step. Further the gap No.1 moves for 1 step and the gap No.2 moves from the end to the beginning of the scanning range with a set step. Then the movement proceeds until the final position is reached by the gap No.

After each gap moving the data are displayed in corresponding windows (Fig. 3) as a diagram of the signal received from Faraday cup and derivatives histograms of pulse front and recession. Also the data are saved in a file. Files are organized in the directories named according to scanning beginning time and date. Also the pulse diagram window image before the beginning of scanning and images of derivative pulses histograms windows after the ending of scan are saved.

The program is designed for work with two types of scanners: 0 ° and 90 °. They differ in the configuration of screens and quantity of gaps, i.e. step motors. To scan the 0°beam, one pass of single gap with a set step is required, and to scan the 90° beam, consecutive gaps moving is required.

DATA PROCESSING PROGRAM

The data which are received as a result of experiment are processed with program. Graphical language G of LabView programming environment was used to create it. This program allows to select data file and to display current pulse form. Differentiated signals are calculated and represented as diagrams. It is possible to select and delete erroneous data, to determine the data field for subsequent processing. Three cursors are used for it. The zoom button, the cursor movement tool and panning tool are used to make data look more convenient.

The color palette is used for three-dimensional representation of differentiated signals (X-direction – X slit coordinate, Y-direction – number of channels, Z-direction – value of differentiated signal). Every specified value interval has its defined color. The following values are calculated in the program: the characteristics of phase ellipse, angle of inclination of beam axis to channel centerline, displacement of beam centre of mass on the scanner Δxcm relative to its position Xcm in slit area, mean-square emittance, 100% emittance. Calculated data and experimental values are visualized on the graphs. Programm allows to convert data from binary format to spreadsheet format.

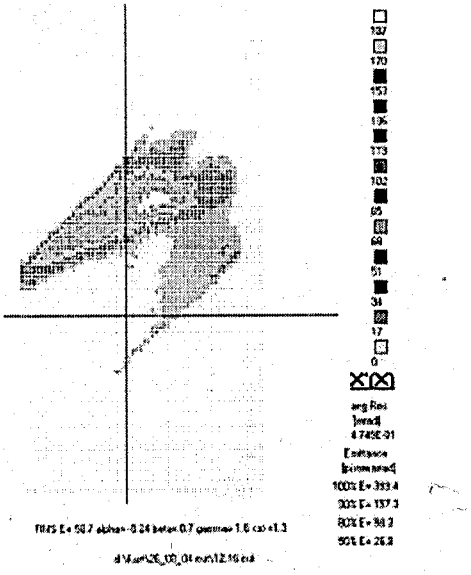

Fig. 4: Result of work of data processing program for the 0° beam scanner

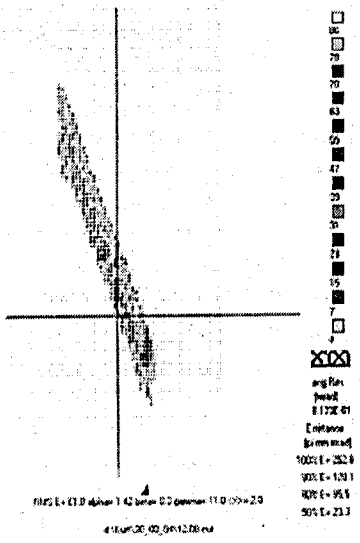

Fig. 5: Result of work of data processing program for the 90° beam scanner

CONCLUSION

The program complex developed fully automates control of the beam monitor for its adjustment and emittance calculation. The control program combines blocks of step motors control both in manual, and in an automatic mode. Synchronization with beam screen rotation frequency occurs automatically at change of rotation speed. Results of an automatic scanning session are displayed in a form convenient for a preliminary emittance estimation. All data are saved in directories structured by date and time of the measurement beginning. The files received are processed by the emittance calculation program which results of work are diagrams and emittance values on axes.

REFERENCES

[1] Kurt E. Stiebing, J.D.Meyer, O.Strekalovsky, V.Alexandrov, A.Kayukov, G.Shirkov In Proc of the 10th International Conference on Ion Sources, JINR, Dubna, September, 2003

OPTICAL DIAGNOSTIC OF THE VEPP-4M COLLIDER

O. I. Meshkov#, V.F. Gurko, A. N. Zhuravlev, E. I. Zinin, P. V. Zubarev, N. Yu. Muchnoi, Yu. A Pahotin, A. N. Selivanov, M. G. Fedotov, A. D. Khilchenko, BINP, Novosibirsk, Russia

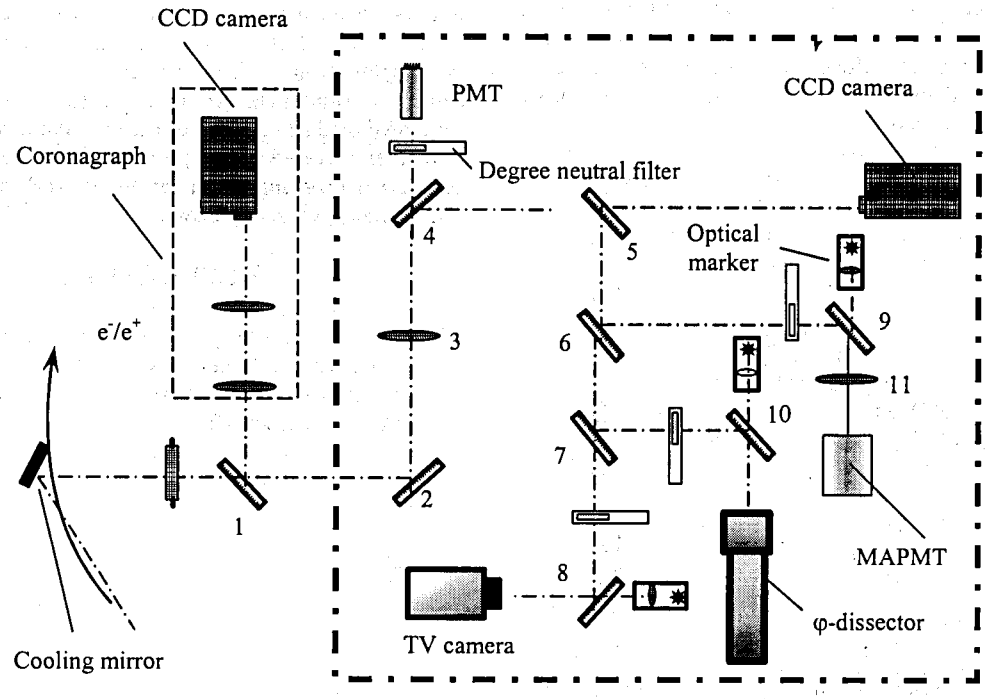

Figure 1: Layout of the optical diagnostic. 3,11 – lenses, 4÷10 – mirrors

Abstract

The upgraded optical diagnostic of the VEPP-4M collider is described. The system abilities are improved sufficiently in comparing with [1]. Now the diagnostic supplies the data about electron/positron beam transversal and longitudinal size, shape and position. It is applied to study the electron beam "tails" and turn-to-turn beam profile dynamics. The system is used to tune of the beam pass-by from the VEPP-3 booster to the VEPP-4M collider and to measure of the synchrotron and betatron frequencies.

INTRODUCTION

VEPP-4M [2] is an electron-positron collider at the energy up to 6 GeV. This collider consists of 2 semi-rings with the average radius R of 45.5 m, which are connected by two linear segments. Computed dimensions of the beam at the point of the optical diagnostic location are: $\sigma_z \approx 0.1$ ìì , $\sigma_r = 0.5$ ìì , $\sigma_\varphi = 2.5$ cì (E = 1550 MeV, $U_r = 0.5$ MeV). The current physical program of the facility is directed at the energy area of J/ψ meson and τ lepton (up to 2×2 GeV).

LAYOUT OF THE OPTICAL DIAGNOSTIC

Optical diagnostic provides the following data:

- transversal and longitudinal beams sizes;
- XY Beams coordinates at the points of SR outlet;
- Electron beam tails distribution;
- Electron beam profile with one-turn temporal distribution during 2^{17} turns;
- Electron beam synchrotron and betatron frequencies.

Two channels of SR output are located in the bending magnets of the semi-rings and separated by a linear segment. Each channel outputs a radiation of electron or positron beam only. Each channel is equipped with practically identical diagnostic systems (Fig. 1).

#O.I.Meshkov@inp.nsk.su

The optical component of SR is reflected from cooled metallic mirror and outlets from the vacuum chamber through a quarts window. Mirror 1 reflects a part of light to the optical coronagraph, which is applied for beam tails study. Mirror 2 matches the light with an optical axis of the system. The beam image is set up on lens 3 on all the optical detectors simultaneously. A remote controlled switchable neutral filters expand the dynamic range of the system.

A part of light reflected from the semi-transparent mirror 7 is used for measurement of a longitudinal size of the beam. The φ-dissector with electrostatic focusing and deflection is employed for this purpose [3]. It has FWHM of instrumental function at 40 ps.

CCD-CAMERA WITH 100 MBIT ETHERNET INTERFACE

CCD-cameras [4] are employed for measurements of

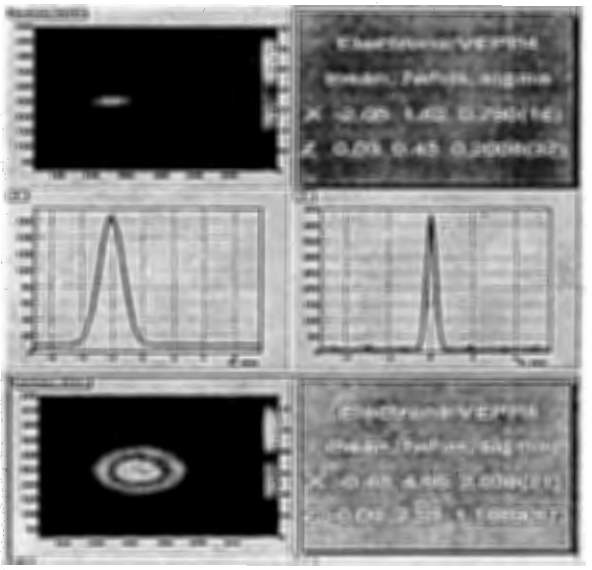

Figure 2: CCD camera results. Upper image is the current view of the electron beam. Down image is the first 100 turns of electrons after pass-by from VEPP-3 to VEP-4M. Data refreshing frequency is nearly 0.3 Hz.

transversal beam dimensions and position. Value of σ_Y of the electron and positron beams is permanently displayed on the monitor, what is convenient, in part, for tuning of luminosity of the collider (Fig. 2). Camera has an external trigger with jitter of 100 mcsec. This is enough for quality control of the process of beam transport from the booster VEPP-3 to the collider VEPP-4M. Camera is applied also for image acquisition of the tails of the electron beam at distances over $5\,\sigma_Y$.

OPTICAL CORONAGRAPH

The ability of on-line measurements of the tails is sufficient for the accelerator tuning. Two methods are widely applied for that nowadays: scraping collimator [5] and a wire scanner [6]. Both methods interact with beam, change its properties and destroy it. Moreover, scraper application takes long term and poor combine with another experiments carried on the machine. The advantage of both diagnostics is a wide dynamic range, up to 10^6.

The development of non-disturbing method that enables on-line fast study of the beam distribution function within the limit of $5\,\sigma$ seems relevant. We have applied the optical coronagraph for this purpose [7]. The coronagraph is intended for study of beam-beam effects and polarization experiments. We tested the device on VEPP-3 preliminary. The coronagraph was applied for study of the beam scattering on the atoms of residual gas. This process can be theoretically simulated [8] and comparison with experimental data is possible (Fig. 3) [9]. The first results obtained with coronagraph at VEPP-4M are presented at Fig. 3.

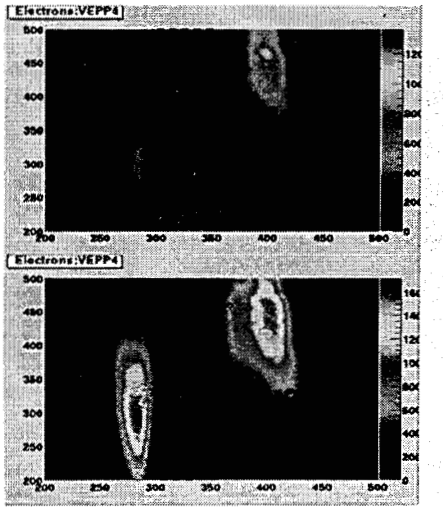

Figure 3: The first results from VEPP-4M coronagraph. Upper figure: the beams aren't converged in the interaction point. Down figure: the beams are converged in the interaction point. The tails appearing is seeing.

FAST MULTI-TURN BEAM PROFILE MEASUREMENT

The interest to study of beam distribution within development of fast instabilities the same, as beam-beam effects always existed in the physics of accelerators. The corresponding diagnostics should provide a one-turn distribution during tens thousand turns of beam. For this purpose we have designed the device based on the multianode photomultiplier R5900U-00-L16 HAMAMATSU, Fig. 4, [10]. This device is capable to record a transversal

profile of a beam at 16 points at one turn during 2^{17} turns of a beam. Some features of the diagnostic are listed in the Tab. 1.

Table 1: The technical data of the beam profile monitor.

Size	250 x 100 x 100 mm
Interface	100Mb ethernet
Internal memory	~4 M (2^{17} beam profile at 16 points)
Discontinuity of record	$1 \div 2^8$ turns
Analyzable frequency range	10 Hz ÷ 1 MHz
Single anode size	0.8 × 16 mm

Fig. 4 represents a typical beam profile. Fig. 5 shows a process of electron and positron beam convergence in the interaction point. The total duration of the process is about 0.4 sec., or nearly $3 \cdot 10^5$ of the beam turns. Time

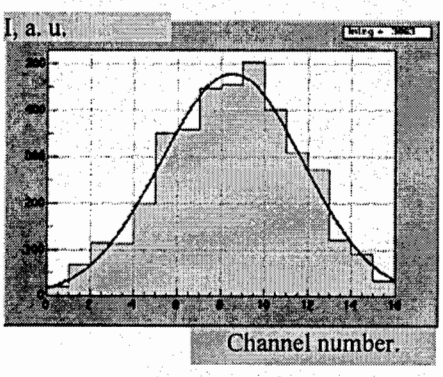

Figure 4: Typical beam profile, recorded of the device. Gauss approximation is realized for each turn.

of the single turn is 1220 ns. Channel constant is 0.12 mm. The instability, caused of beam-beam interaction is clearly seen.

CONCLUSION

The upgraded optical diagnostic of VEPP-4M has been described. Spatial and temporal resolution of the diagnostic corresponds to the demands of the current VEPP-4M experiments. The diagnostic provides a simultaneously data of the beams size, position and frequency oscillations. This information is effectively used for machine tuning and running.

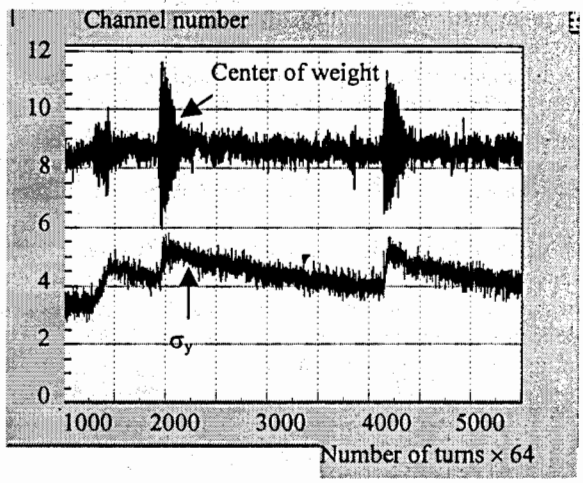

Figure 5: The position of center-of-weight of electron beam (black line) and σ_y behavior (red line) after the beams convergence in the interaction point.

REFERENCES

[1]. E. I. Zinin, S. E. Karnaev, V. A. Kiselev, O. I. Meshkov, N. Y. Mutchnoi, N. Selivanov, E. A. Simonov, A. A. Valishev, M. G. Fedotov, Proc. of PAC-01 Conference, Chicago, 2001, p. 2438-2440.

[2] V.V. Smalyk et. al. Accelerator physics issues of the VEPP-4M at low energy. This conference.

[3] Coppens J., Luijckx G., Zinin E. Proc. of the EPAC 96, Barcelona, 10 - 14 June 1996, Vol. 2, p. 1704 - 1706.

[4] N.Y. Mutchnoi et al., EPAC02 Conference Proc., Paris, 2002, pp. 2040-2043.

[5] H. Burkhardt et al, Proc. Of the 5th Europe Particle Accelerator Conference, v.2, pp. 1152-1154, 1996

[6] J. D. Gilpatrick et al., DIPAC 2001 Proc. – ESRF, Grenoble.

[7] Koomen M. J. Et al., Appl. Opt., 14, p.743, 1975. K.

[8] Hirata and K. Yokoya, Particle Accelerators, 1992, Vol. 39, pp. 147–158

[9] O. I. Meshkov et al. Study of beam tails with the optical coronagraph, EPAC04 Conference Proc., Lucerne, 2004, THPLT108

[10] O.I. Meshkov et al. VEPP-4M optical beam profile monitor with one-turn temporal resolution, EPAC04 Conference Proc., Lucerne, 2004, THPLT107

THEORETICAL AND EXPERIMENTAL STUDY OF BEAM ENERGY SPREAD DIAGNOSTICS WITH VAVILOV – CHERENKOV RADIATION AT OPTICAL AND RF WAVELENGTH

K.A. Trukhanov, IMBP RAS,
V.V. Poliektov, V.I. Shvedunov, SINP MSU, Moscow, Russia

Abstract

Use of Cherenkov radiation (CR) in the optical and in the microwave ranges for the accelerator beam energy and the energy spectrum measurements is described. The methods are based on the radiation intensity dependence on a phase velocity of an electromagnetic wave in Cherenkov radiator medium. The details of a mathematical procedure to extract the energy spectrum from the measured intensity are given.

INTRODUCTION

The development of the non-intercepting methods for the electron beam energy and the energy spectrum measurements with high accuracy in the energy range 1-20 MeV and above is of great importance for irradiation process control in industry and medicine.

We consider methods of the electron beam energy and the energy spectrum measurement based on the dependence of the CR intensity (CRI) and its spectral distribution on the phase velocity of the electromagnetic waves in the optical and microwaves ranges.

The methods are practically non-intercepting and can be used for the energy and energy spectrum measurements of high intensity electron beams.

OPTICAL RANGE

CRI Dependence on Refraction Index

For the first time the possibility of average electron velocity determination in the electron accelerator beams with the measurements of the CRI dependence on a radiator refraction index n in an optical range was demonstrated in [1-2].

The gases, which refraction index varies with pressure p as $n(p) = 1 + kp$, if $kp \ll 1$, are natural choice of the CR medium in this method. The CRI grows nonlinearly with kp between the thresholds of Cherenkov radiation for a maximal and minimum electron velocity in beam in the detector ($1/\beta_{max} \le n(kp) \le 1/\beta_{min}$), but for $n(kp) > 1/\beta_{min}$ the dependence is linear.

The intersection of the extrapolated CR (CRI) linear part with a background level corresponds to the average electron velocity in the beam [1]. The same method was proposed 15 years later [3] without reference to [1-2]. No nonlinear part in I(n) dependence was noted.

In [4-6] it was shown that the nonlinear part of the intensity curve can be used for obtaining the velocity distribution and the energy distribution of the particles in the beam.

If the same fraction of the CR light is registered with the photodetector independently of the position and the direction of a particle passing through the radiator (as for example in the spherical Cherenkov detector) then the velocity distribution and the energy spectrum can be obtained for the arbitrary angular distribution of the particles. In the case under consideration (the accelerator monitoring) this condition can be easily fulfilled.

Following [6] a number of the CR photons $N_{ph}(n(\nu))$ in a unit frequency band reaching the photodetector can be written as:

$$g \int_{\max\left\{\frac{1}{n},\beta_{min}\right\}}^{\beta_{max}} \left(1 - \frac{1}{n(\nu)^2 \beta^2}\right) f(\beta) d\beta = N_{ph}(n(\nu)) \qquad (1)$$

where $f(\beta)$ is a particle velocity distribution; $g = 2\pi\alpha N_e k L$, where α is the fine structure constant, N_e – the number of the electrons, L- the length of particle path in detector, k – the photon collection factor and ν is a photon frequency.

The equation (1) is Volterra integral equation of the first kind with the right part having experimental errors. Although it is ill - posed task the several methods for solution of such equations have been developed during the past decades. These methods can be used to extract the particle velocity distribution from the measured dependence of N_{ph} on the refraction index n

The equation (1) can be reduced to equation of convolution type [6]. Let us change variables:

$$\beta = y^{1/2}; \quad \Psi(y) = \frac{f(y^{1/2})}{2y^{3/2}}; \quad \frac{1}{n(\nu)} = z^{1/2} \qquad (2)$$

Then

$$g \int_{z}^{z_{max}} (y - z(\nu)) \Psi(y) dy = N_{ph}(z(\nu)) \qquad (3)$$

By successively differentiating (3) we obtain the solution as:

$$\Psi(z^{1/2}) = \frac{1}{g} \frac{d^2 N_{ph}(z)}{dz^2} \qquad (4)$$

The first derivative of the N_{ph} in (3) is an integral spectrum, i.e. the number of particles above some energy. In this case the CR monitor can be used at the accelerators as the threshold sensor producing a signal when the beam energy exceeds some prescribed value.

To avoid the gas dissociation by the electron beam usage of the single atomic gases is preferable. For the narrow energy spectra typical for the microtron beams or the beams from the high brightness accelerators, the required change of the pressure will not exceed several percents. The narrow band filter installed in front of the photodetector and measurement of gas refraction index with a build-in interferometer can decrease sufficiently

the experimental errors. The instant gas expansion by high power beam pulse can be neglected if a pulse is very short ($\leq 10^{-8}$ s.)

The yield of the CR near the threshold for the most electron accelerators is more than sufficient for the reliable intensity registration with the photodetectors (photomultipliers). The energy loss fluctuations in the CR detector should be taken into account at the determination of a device resolution power.

Experimental Results

Experiments were conducted with the beam of 35 MeV race track microtron [7]. The beam with an energy in the range 4.8 – 34.2 MeV, an energy spread ~200 keV can be extracted from the different orbits with a step ~2.4 MeV. The beam pulses following with the repetition frequency 50 Hz have a duration ~5 ns with a charge ~ 1 nC/pulse. The experimental set-up is shown in Fig. 1. The electron beam from the accelerator produces CR on its path "AB" in the chamber (1) filled by a gas which pressure is regulated by a membrane (5) and controlled by the manometer (6). A light pulse reflected by a mirror (3) is registered by a photomultiplier (4). The beam pulse charge is controlled by Faraday cup (2).

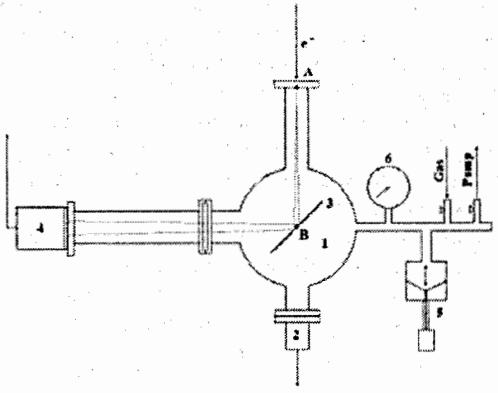

Figure 1: Experimental set-up.

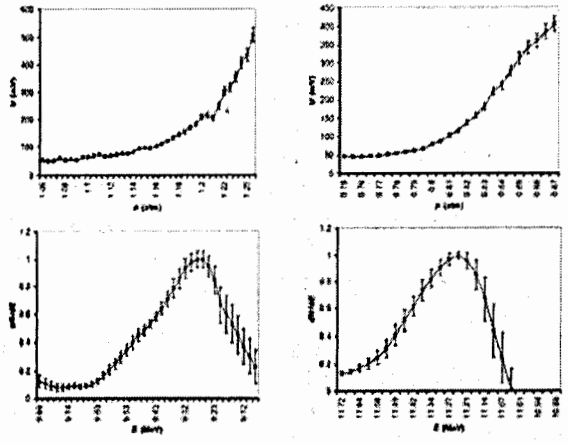

(a) (b)

Figure 2: CRI measured for (a) 2^d and (b) 3^d RTM orbits and corresponding energy spectra.

In Fig. 2 we show CRI measured depending on Freon R-12 gas pressure and corresponding the energy spectra extracted using formula (4) with regularization algorithm.

CRI Dependence on Wavelength

Dependence of the refraction index on the wavelength requires some precautions when measuring the particles energy spectra by the changing gas pressure as described above. Dispersion of light causes some trouble in Cherenkov counter methods in general. However it becomes "friendly" phenomena in another proposed method, the essence of which consists in following. CR from the radiator output is directed to a spectral device (grating, prism etc.) for spectral decomposition and CR intensity dependence on wavelength is registered with the line of photodetectors. Because of refraction index for any medium depends on a wavelength, the CR threshold depends on a wavelength also. Thus, the measurements at the different wavelengths are analogous to the measurements with variable gas pressure or to measurements with a large number of the threshold counters with different thresholds.

In the visible light range the refraction index decreases with the wavelength increase. Thus, the higher is electron velocity the longer wavelength CR threshold is. At threshold wavelength for some specific energy a number of the emitted CR photons is equal to zero but increases systematically as the wavelength of the registration is deceased.

The number of the CR photons having a wavelength λ in the unit wavelength range may be written as:

$$N_{ph,\lambda} = g \int_{\beta_\lambda}^{\beta_{max}} f(\beta)(1-\frac{\beta_\lambda^2}{\beta^2})\lambda^{-2} d\beta \qquad (5)$$

(β_λ is the threshold velocity at the wavelength λ, g is as in (1).)

Using Cauchy formula $n(\lambda) \approx a + b\lambda^{-2}$, where a and b are the constants individual for different gases, we obtain the threshold wavelength for given β_λ:

$$\lambda^{-2} = (\beta_\lambda^{-1} - a)/b \qquad (6)$$

Substituting (6) into (5) after some transformations we obtain:

$$f(\beta_\lambda) = \frac{\beta_\lambda^2}{2g}\frac{d}{d\beta_\lambda}\left(\frac{1}{\beta_\lambda}\cdot\frac{d}{\beta_\lambda}\left(\frac{b}{\beta^{-1}-a}\cdot N_{ph,\lambda}\right)\right) \qquad (7)$$

The equation (5) can be reduced similar to equation (3) to convolution equation (the designations are the same):

$$\int_z^{z_{max}} (y - z(\lambda))\Psi(y)dy = \frac{\lambda^2}{g} N_{ph,\lambda}(z(\nu)) \qquad (8)$$

which can be solved by successive differentiation.

Thus, to get the beam velocity distribution it is necessary to measure the number of photons in the different wavelength ranges and to get their first and second derivatives with respect to the wavelength. The number of photons is known with error and this procedure is ill -posed task, so appropriate methods to obtain stable solution must be applied too.

The proposed method will be convenient for the accelerator monitoring especially in the case of the

narrow energy spectra. As an example, at the beam energy 30 MeV and the energy spread of 0.5 MeV the spectral interval for Xenon is in the range from 400 nm to 600 nm.

MICROWAVE RANGE

For continuous beam energy control during an accelerator operation it is desirable to have a monitor with a vacuum beam channel excluding the ionization and the radiation electron energy losses. A charge when passing through the vacuum channel in a dielectric radiates in the same manner as in a continuous medium if the next conditions are fulfilled [8]:

$$b << \frac{\lambda_C \beta}{2\pi\sqrt{1-\beta^2}}, \quad b << \frac{\lambda_C \beta}{2\pi\sqrt{\varepsilon\mu\beta^2 - 1}} \tag{9a}$$

where b – is a radius of the vacuum beam channel in a dielectric with the permittivity ε and the magnetic conductivity μ, λ_C –the CR wavelength. It is supposed that conditions for the CR in a dielectric are fulfilled: $\varepsilon\mu\beta^2 > 1$. In practice a beam channel radius should be not less than 5 mm, so a radiation will take place at mm and cm wavelength, i.e. in the RF range.

For the beam channel radius not satisfying the conditions (9a) the analytical solution for a radiation field distribution and a radiated power exists [8]. It should be noted that a radiated power is cut in the short wavelength range at:

$$\lambda << \frac{4\pi b\sqrt{1-\beta^2}}{\beta} \tag{9b}$$

In the RF accelerator particles are grouped in the bunches with the length $l << \lambda_{RF}$, where λ_{RF} – is the free space wavelength of the accelerating field. For $\lambda_C > 2\pi l$ the amplitudes of the field radiated with the particles within the bunch add coherently and the radiated power is enhanced by the factor approaching to N_e, i.e. by many orders of magnitude.

To provide vacuum at the beam path and to arrange the conditions for the radiated power collection and registration dielectric with a beam channel should be placed inside a conducting metal tube. The main feature of the radiation generated by the charge in this case is that it takes place at the discrete frequencies which values are determined by the waveguide and the beam channel radii, the dielectric properties and the particle velocity. The charge passing along the beam channel axis will excite with a highest amplitude TM_{01} mode wave with a longitudinal electric field on axis. Thus, if the conditions (9a) are fulfilled, then a frequency of the excited TM_{01} mode wave is connected with a particle velocity by [8]:

$$\nu_{01} \approx \frac{\beta c x_{01}}{2\pi b\sqrt{\varepsilon\mu\beta^2 - 1}} \tag{10}$$

where $x_{01}\approx 2.405$ – is the first root of zero order Bessel function J_0. The power radiated in this mode is:

$$p_{01}(\beta) \approx \frac{2e^2\beta c}{b^2\varepsilon\varepsilon_0 J_0'(x_{01})} \tag{11}$$

From (10) it follows that when approaching the Cherenkov effect threshold ($\varepsilon\mu\beta^2 = 1$) a generated wave frequency goes to infinity, but in reality limit for a frequency will be defined by the condition (9b). For a beam channel radius not satisfying to (9a) the analytical expressions for a radiation frequency and a power are available [8].

Strong dependence of the generated radiation frequency on the particle velocity and absence of the sharp boundary for a RF signal appearance make difficult to use the method for the energy and energy spectrum determination developed for an optical wavelength range and described above. So, we propose to use for the beam energy and energy spectrum control in the microwave range strong dependence of the generated wave oscillation frequency on the particle velocity. The generated wave oscillation frequency is uniquely connected with the particle velocity via (10) and for the relativistic particles according to (11) a radiated power is nearly independent of the velocity. Thus measurement of the generated radiation spectrum is a direct method for the beam energy spectrum control not requiring a solution of the inverse task.

Energy resolution of proposed method is connected with frequency resolution by:

$$\frac{\Delta E}{E} \approx \frac{(\varepsilon\mu\beta^2 - 1)\beta}{1-\beta^2} \times \frac{\Delta\nu}{\nu} \tag{12}$$

The quite simple RF measurement methods (e.g. using a high quality factor tunable cavity) provide a frequency resolution $\Delta\nu/\nu \approx 10^{-3}$. For the beam energy ~ 10 MeV (the industrial and medical accelerators) and $\varepsilon\mu \approx 1.1$ (aerogel) energy resolution will be about 4%, and for a circular waveguide radius ~ 10 mm radiation will take place at ~8 mm wavelength range.

ACKNOWLEDGEMENTS

Authors would like to thank B.M. Bolotovsky and A.V. Serov for useful discussions.

REFERENCES

[1] M.R. Bhiday, R.E.Jennings, P.I.P.Kalmus, Proc. Phys. Soc., **72**, 1958, p.973.

[2] R.E. Jennings, P.I.P. Kalmus, Nucl. Instr. Meth., **6**, 1960, p.209.

[3] C.E. De Almeida, P.R. Almond, Phys. Med. Biol., **19**, N 4, 1974, p.476.

[4] K.A. Trukhanov, V.N. Grebenev, V.M. Shlapak, in Proc. IV Int. Cong. Int. Rad. Protection Assoc. Paris, 24-30 April 1977, p. 119.

[5] E.A. Vainer, K.A. Trukhanov, in Proc.3th meeting on charge particle accelerator use in economics", Leningrad, 26-28.06.1979, V. III, p. 345.

[6] K.A. Trukhanov, in Proc. Seminar "Cherenkov detectors and their applications in science and technics" (1984), M. Nauka, 1990, p. 380.

[7] V.I. Shvedunov, R.A. Barday, D.A. Frolov, et al., Nucl. Instr. Meth. **A531**, 2004, p. 346

[8] B.M. Bolotovsky, Usp. Fiz. Nauk, **125**, 1961, p. 295.

STATUS OF VEPP-5 INJECTION COMPLEX

M.S.Avilov, A.V.Akimov, A.V.Antoshin, P.A.Bak, Yu.M.Boimelshtein, D.Yu.Bolkhovityanov, A.R.Frolov, R.Kh.Galimov, R.G.Gromov, K.V.Gubin, S.M.Gurov, E.A.Gusev, N.S.Dikansky, I.V.Kazarezov, V.D.Khambikov, S.N.Klyuschev, E.S.Konstantinov, N.Kh.Kot, V.I.Kokoulin, A.A.Korepanov, R.M.Lapik, N.N.Lebedev, P.V.Logatchev, A.I.Lobas, P.V.Martyshkin, L.A.Mironenko, V.M.Pavlov, I.L.Pivovarov, O.V.Pirogov, V.V.Podlevskikh, S.L.Samoylov, Yu.I.Semenov, B.A.Skarbo, A.N.Skrinsky, A.A.Starostenko, S.V.Shiyankov, A.S.Tsyganov, O.Yu.Tokarev, A.G.Chupyra

BINP RAS, Novosibirsk, Russia.

Abstract

VEPP-5 injection complex is an intensive source of electron and positron bunches with energy of 510MeV (see Table 1), which will fulfill all the needs of existing and building colliders in BINP RAS. The complex consists of a 285MeV electron linac, 510MeV positron linac, and a damping ring with transport channels (see Fig.1). During last two years an intensive work on production, assembling and tuning of positron system was carried out. As a result, in May 2004 it was put into operation. This allowed to accelerate a single bunch of $2*10^8$ positrons to 75MeV. Results of preliminary tests of VEPP-5's regular positron system are presented in this article.

Table 1: Beam parameters at the output of injection complex

Energy	510 MeV
Maximum number of electrons in a bunch	$2.0\ 10^{10}$
Maximum number of positrons in a bunch	$2.0\ 10^{10}$
Repetition rate	1 Hz
Energy spread of the bunch	0.07 %
Longitudinal size of the bunch (FWHM)	0.4 cm
Vertical emittance	0.005 mm·mrad
Horizontal emittance	0.023 mm·mrad

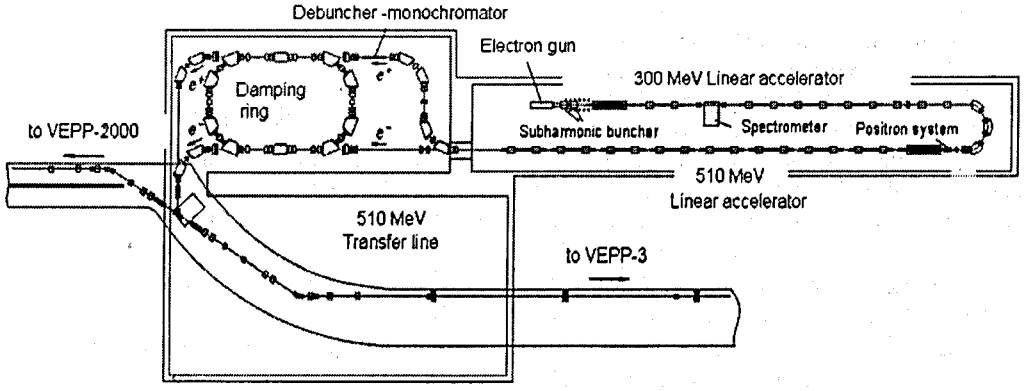

Fig.1: VEPP-5 layout

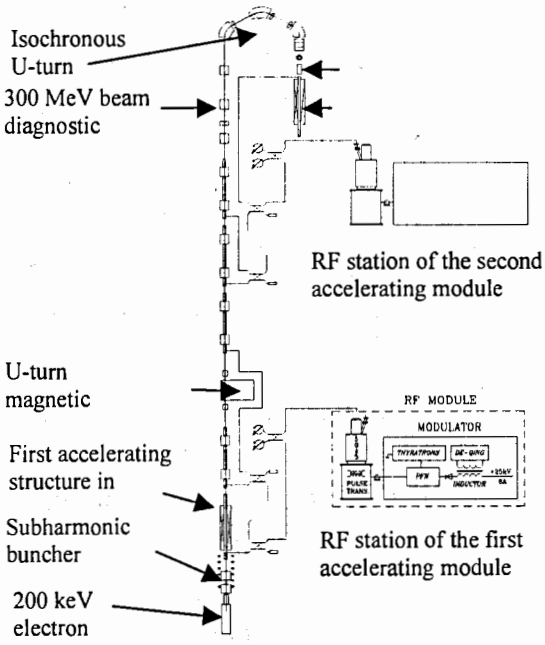

Fig.2: Currently operating part of injection complex

DESCRIPTION OF CURRENTLY OPERATING PART OF THE FACILITY.

Accelerator consists of two equally RF-fed accelerating modules. Each one includes a klystron (5045, SLAC), SLED-type power compression system, and three accelerating structures with a constant impedance incursion of $2\pi/3$ per cell, operating on a running wave. System operating frequency is 2856Hz. Accelerating structure has a length of 3m and is a round diaphragmatic waveguide, at ends coordinated with a rectangular waveguide of 72×34mm. Through this rectangular waveguide the structure is fed with impulse RF-power of 60–120MW and length of 0.5μs. Duration of input impulse is equal to a wave propagation time in a 3m accelerating structure. RF power, passed through the structure, is completely absorbed by a matched load.

Acceleration of the beam is performed at the moment when RF power reaches the load, accelerating structure is filled, and absorption of the energy by the beam is maximal. Forming of the feeding RF impulse occurs in power compression system, which works as a storage of RF energy, collected during the main part of klystron impulse (3μs duration), and sends all the energy, collected during last 0.5μs of RF impulse, to accelerating structures. Energy sending process is initiated by a quick (in several nanoseconds) 180° change in phase of a wave from klystron. As a result, at the output of the power compression system a 1.5μs, 240MW RF impulse is formed, which is than divided between module's three accelerating structures in a 2:1:1 ratio. Acceleration structures are identical. One such module at klystron power of 60MW accelerates the beam to 180MeV. Each module also includes a magnetic focusing system, a beam diagnostic system and a thermostabilization system.

285MeV electron linac includes electron source, grouping system, the whole 1st accelerating module and two lowered-rate acceleration structures from the second module. Pulse-fed electron gun forms a beam of 2.2ns duration, with a current of 2.5A at 200kEV energy. For effective seize of a beam by linac the duration must be reduced from 2200ps to 20ps. It is achieved via longitudinal compression of the bunch by two RF cavities, operating at 178MHz (16th harmonic of main frequency), and by a buncher at a main frequency. In order to preserve transverse beam size the bunching process is performed in increasing magnetic field.

Layout of linac's two first modules is presented on Fig.2. The 3rd structure of the 2nd module is located after isochronous turn and is used to accelerate positrons. A temporary diagnostic channel is located after this structure and is being used for positron beam parameters measurement. Directly after the isochronous achromatic turn a tripled is located, which focuses the beam onto tantalum conversion target.

Beam transverse profile monitors, located in the turn, provide measurement of energy and energy spread in the beam. Secondary-emission wire sensors of beam's transverse profile located before and after the turn, control loss of particles in the turn. Single-bunch mode (see Table 2) is primary for injection complex's linacs. It provides accumulation of intensive electron and positron bunches in a damping ring with subsequent transport into VEPP-4M and VEPP-2000 colliders.

Table 2: Main parameters of injection complex's linacs

Energy	510 MeV
Maximum number of electrons in a bunch	1011
Maximum number of positrons in a bunch	109
Repetition rate	50 Hz
Energy spread of the electrons bunch	1 %
Energy spread of the positrons bunch	3 %
Emittance	15 mm·mrad
Longitudinal bunch size (FWHM)	0.4 cm
Acceleration structure operational frequency	2856 MHz
Klystron output power	63 MW
Number of klystrons	4

OPERATION OF POSITRON SYSTEM.

In the mode reviewed below, $2 \cdot 10^{10}$ electrons in one bunch with energy of 270MeV are focused on tantalum conversion target into a spot with 1mm diameter. Target's thickness is 2.5 radiation lengths, which provides maximum positron output at a given beam energy. Besides the target itself, positron system includes a pulse concentrator magnet of the flow, a system of solenoids which form constant magnetic field, and the first positrons' accelerating structure. Pulse magnet coordinates phase volume of a positron bunch, emitted from the target, with acceptance of the accelerating structure. Measured and calculated dependencies of number of accelerated positrons from magnetic field value are presented on Fig.3. Energy spectrums of positrons and electrons, passing through the 1st positron structure with pulse magnet turned on and off, are presented on Fig.4.

Spectrums were measured with a sectioned Faraday cup, located at the output of a separating magnet, at the end of diagnostic positron channel. Two central sections of Faraday cup are positively charged due to secondary electron emission, caused by high energy photons, emitted from conversion target at low angles. These measurements were performed for $2 \cdot 10^{10}$ electrons, falling onto tantalum target in one bunch, with flow concentrator magnet turned on. The conversion ratio of electrons into positrons, accelerated and delivered to Faraday cup, was 0.01.

Now, in parallel with testing of positron system, production of missing components of positron linac is being done. Currently a 510MeV transport channel to VEPP-2000 collider is being constructed.

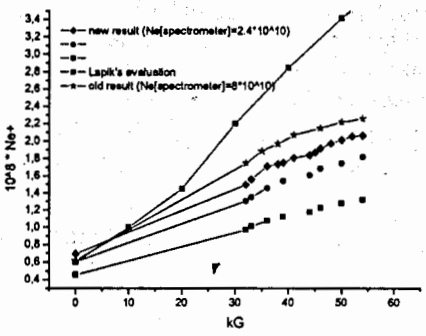

Fig.3: Dependency of accelerated positrons on a maximum field in a concentrating magnet

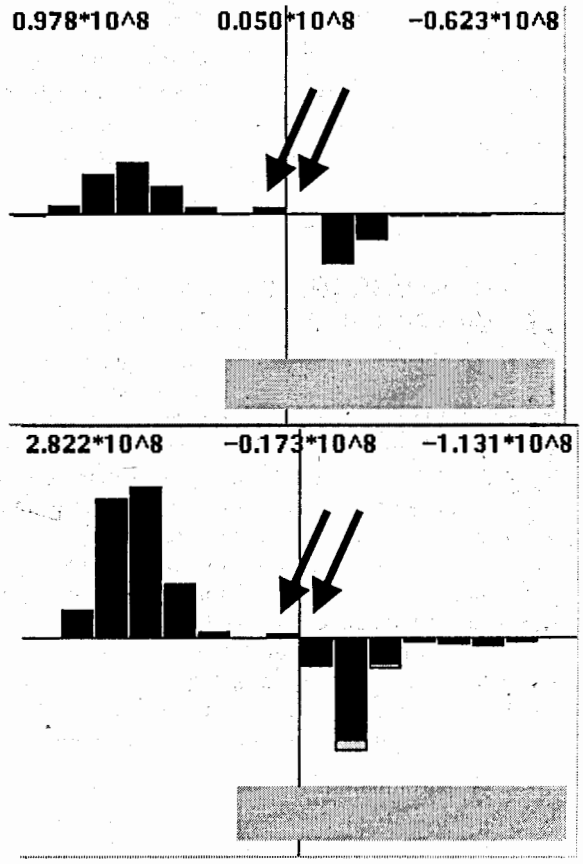

Fig.4: Energy spectrum of electrons and positrons at the output of the 1st accelerating structure

PRELIMINARY TESTS OF THE DECRIS-SC ION SOURCE

A.Efremov, V. Bechterev, S. Bogomolov, P.Bondarenko, S.Dmitriev, A.Lebedev, M.Leporis, A.Nikiforov, S.Paschenko, Yu.Smirnov, B.Yakovlev, N.Yazvitsky, FLNR, JINR, Dubna, Russia
N.Anischenko, V.Datskov, V.Drobin, V.Seleznev, G.Tsvineva, Yu.A.Shishov, LHE, JINR, Dubna, Russia
H.Malinowski, Electrotechnical Institute, Warsaw, Poland

Abstract

A new "liquid He-free" superconducting Electron Cyclotron Resonance Ion Source DECRIS-SC, to be used as injector for the IC-100 small cyclotron, has been designed by FLNR and LHE JINR. The main feature is that a compact refrigerator of Gifford-McMahon type is used to cool the solenoid coils. For the reason of very small cooling power at 4.2 K (about 1 W) our efforts were to optimize the magnetic structure and minimize an external heating of the coils. The maximum magnetic field strength is 3 T and 2 T in injection and extraction region respectively. For the radial plasma confinement a hexapole made of NdFeB permanent magnet is used. The source will be capable of ECR plasma heating using different frequencies (14 GHz or 18 GHz). To be able to deliver usable intensities of solids, the design is also allow axial access for evaporation oven and metal samples using the plasma sputtering technique. Very preliminary results of the source test are presented.

INTRODUCTION

The new ECR ion source is dedicated to be used as an injector for the IC-100. IC-100 is the small cyclotron with the pole diameter of 100 cm. It is intended for researches in solid state physics, materials science and new industrial technologies. After modernization the cyclotron will be able to accelerate ions such as Kr^{15+}, Xe^{22+} and, in the future, Kr^{20+}, Xe^{30+} up to energy about of 1 MeV/n and about of 2 MeV/n correspondingly. With this in view, the liquid He-free superconducting ECR ion source DECRIS-SC has been designed in FLNR JINR in collaboration with the cryogenic group of LHE JINR. The main feature of this source is the use of compact refrigerator to cool solenoid coils instead of liquid He. This method of cooling allows us to avoid the complicated operation of ordinary SC magnetic system using liquid He. Another feature is the use of a permanent magnet hexapole together with the SC solenoid coils. It leads to the essential simplification of the cryostat construction.

There were few reasons to choose this type of magnetic structure for the new ECRIS:

- It is clear now that the large mirror ratio and strong magnetic field are the essential points to produce the intense beams of highly charged ions [1];
- The cyclotron together with their subsystems consumes less than 150 kW of electric power. The power consumption of the ion source should be few times less.
- According to the LNS group results, values of $B_{radial} = 2\ B_{res}$ and $B_{axial} = 3\ B_{res}$ are enough to improve the plasma stability and to produce high charge state ions [1].
- Two liquid He-free superconducting ECRIS, RAMSES and SHIVA were successfully built and tested in Japan [2].

DESIGN CONSIDARATION

The design parameters of the source are collected in Table 1.

Table 1: Design parameters of DECRIS-SC

UHF frequency	14 GHz or 18 GHz
Mirror field on the axis: Extraction side Injection side	 2 T 3 T
Mirror to mirror space	390 mm
Max. coil current	60 A
Radial field at the wall	1.2 T
Plasma chamber internal diameter	74 mm
Max. extraction voltage	30 kV

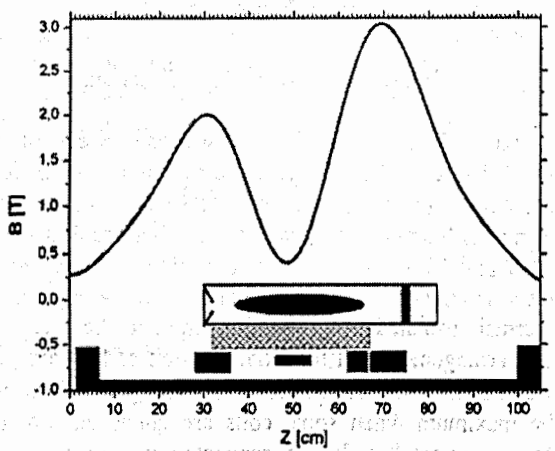

Figure 1: The axial magnetic field distribution and soft iron screen position

The axial magnetic field is created by a set of four solenoid coils. At nominal excitation, this magnetic system allows to rich peak mirror fields on the axis of 3 T

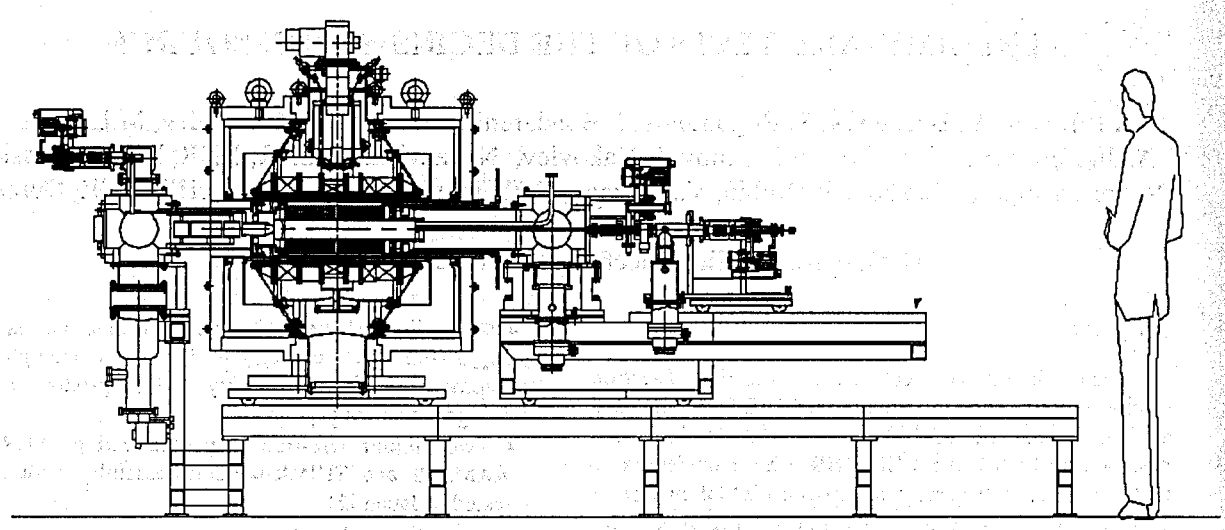

Figure 2: The cross sectional view of the DECIS-SC

at the injection and 2 T at the extraction region. Parameters of solenoid coils are collected in Table 2. Figure 1 shows the axial magnetic field distribution with the nominal current of 60 A.

Table 2: Main parameters of solenoid coils

Parameter	Coil 1	Coil2	Coil 3	Coil4
D_{in} mm	281	280	280	281
D_{out} mm	397	397	296	350
L mm	80	81	50	80
I_{nom} A	60			
N turns	9333	9333	5227	52500
Material	NbTi/Cu			

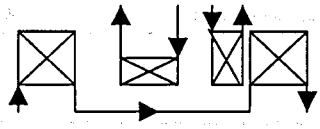

Figure 3: Electrical coil connection.

Figure 2 shows the cross sectional view of the DECRIS-SC. The compact refrigerator of Gifford-McMahon type is used to cool the solenoid coils. When using small power refrigerator with a small cooling power (1 W at 4.2 K), it is necessary to minimize an unbalanced electromagnetic force which must be supported by thermal insulated supports. To minimize the force, the coil arrangement and the axial position of the iron yoke was carefully optimized. The electromagnetic force will be maximum when some coils are quenched. For this reason external coils are connected in series and the central one is working with a reverse current to ensure a required minimum level (Fig. 3). According to our calculations the unbalanced electromagnetic force does not exceed of about 10 kN for any kind of quenches. To minimize the resistance, we use the high-temperature super conducting material current leads placed between 40K and 4.2 K region. The detailed design of the axial magnetic system is described in ref. 3.

The hexapole for radial confinement of plasma consists of 24 pieces of NdFeB permanent magnet (see Fig. 4). The inner diameter, the outer diameter and the length of

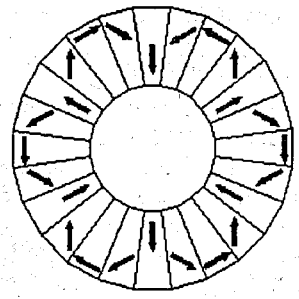

Figure 4: The hexapole cross section

the hexapole are 80 mm, 200 mm and 350 mm, respectively. The desired radial magnetic field strength on the plasma chamber wall is 1.3 T. When solenoid coils are excited with the nominal current, the hexapole became to be dipped to the very strong external magnetic field which has both axial and radial components (see Fig. 5). To protect hexapole magnets from demagnetization by external and internal magnetic field, magnets with corresponding values of B_r, H_{cB} and H_{cJ} were used. The adopted permanent magnets are collected in Table 3. The hexapole magnet was successfully manufactured by VACUUMSCHMELZE GmbH according to our design. The results of the magnetic field measurements along the 3 of 6 poles at the radius 36 mm are presented in Fig. 6. The field strength on the plasma chamber surface reaches about of 1.35 T.

Table 3: Characteristics of permanent magnets

VACODYM	B_r T	H_{cB} kOe	H_{cJ} kOe
745	1.44	14	15
677	1.18	11.5	31
655	1.28	12.4	23
633	1.35	13.1	18
335	1.3	12.3	13

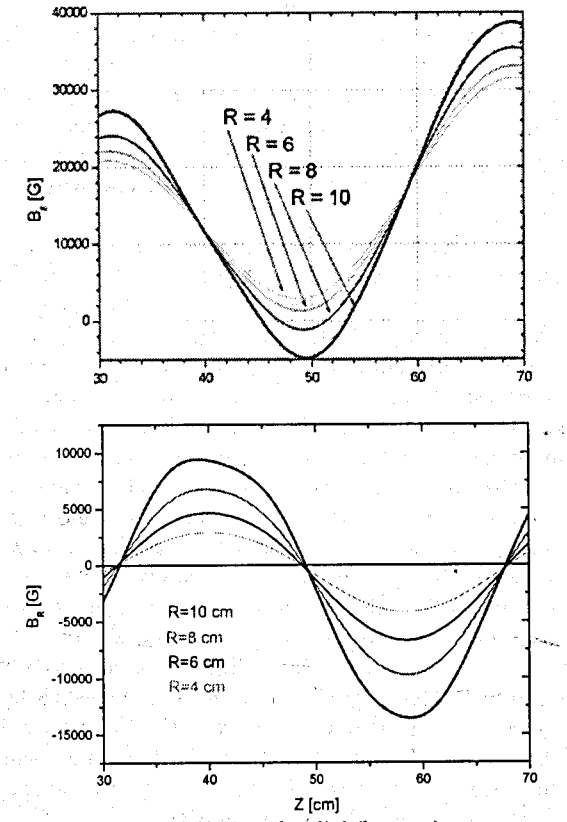

Figure 5: Axial (top) and radial (bottom) components of the magnetic field produced by solenoid coils.

To protect the hexapole magnet from demagnetization by high temperature, a water-cooled plasma chamber (internal diameter is 72 mm, external diameter is 80 mm) has been constructed. A single 18 GHz klystron supplies the UHF power to the source chamber. For vacuum system two turbo-molecular pumps are mounted on the injection side to rich the residual vacuum about of 10^{-8} Torr. All feedthroughs for gas, solids and UHF are done along the axis, avoiding any radial opening. The puller and einzel lens are movable by external manipulation.

PRELIMINARY TESTS

The preliminary tests of the ion source were carried out in May. For cooling the solenoid coils down to 4.2 K from room temperature, we need about of 200 hours when only cooler is used. When cooler is used in combination with the liquid nitrogen the cooling time can be

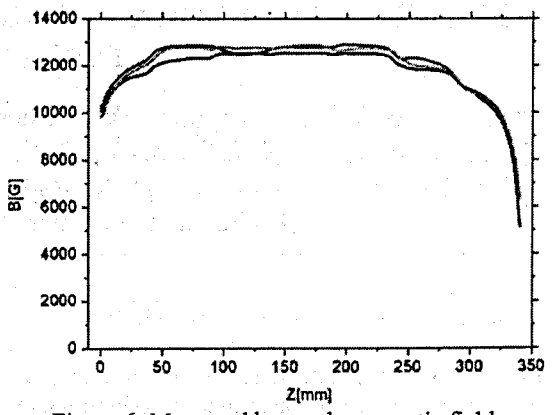

Figure 6: Measured hexapole magnetic field.

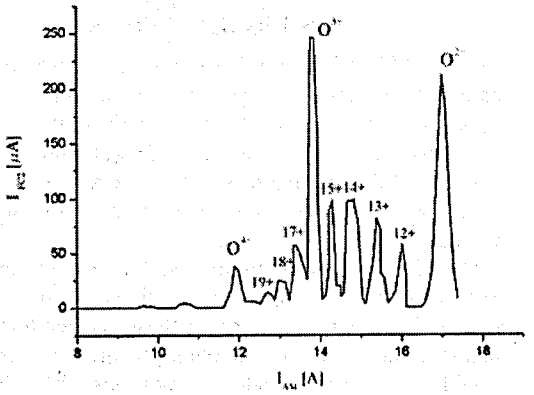

Figure 7: Kr spectrum.

shortened to about of 120 hours. Because of the Kr^{15+} and Xe^{22+} are the most important ions for this cyclotron, the first test was done with Kr. One of the first Kr spectrums is shown in Fig. 7. The current of Kr^{15+} reaches about of 100 μA with the injected microwave power 350 W only. When the required Kr beam was successfully produced, the ion source was completely busy to tune the cyclotron itself. We are planning to continue our tests of the ion source for the production of higher charged ions with Kr and Xe in the nearest future.

REFERENCES

[1]T G.Ciavola et al., Proc. of the 14th Int. Workshop on ECR ion sources, Geneva, 1999, (CERN 1999), p5

[2] T.Nakagawa et al., Rew. Sci. Instr., V73, N2, 2002, p.513

[3] V.I.Dackov et al., this Proceedings.

ELECTRON ACCELERATOR FOR ENERGY UP TO 5.0 MEV AND BEAM POWER UP TO 50 KW

V. L. Auslender, A. A. Bryazgin, V.G. Cheskidov, I.V. Gornakov, B.L. Faktorovich, E.N. Kokin, M.V. Korobeynikov, G.I. Kuznetsov, A.N. Lukin, I.G. Makarov, S. A. Maximov, V. E. Nekhaev, G.N. Ostreiko, A. D. Panfilov, V.M. Radchenko, N.D. Romashko, A.V. Sidorov, M.A. Tiunov, V. O. Tkachenko, A.F. Tuvik, L.A. Voronin, BINP, Novosibirsk, Russia

Abstract

The report describes the industrial electron accelerator ILU-10 for electron energy up to 5 MeV and beam power up to 50 kW specially designed for use in industrial applications. The operation regime is a pulsed regime, the maximum pulse repetition rate is 50 (60) Hz, a pulse duration is 0.4-0.5 ms.

1 INTRODUCTION

Since 1970, BINP SB RAS has been developing and manufacturing the ILU-type electron accelerators for the work in the research and industrial radiation-technological installations. The design and schematic solutions of the installations envisage a continuous round-the-clock operation under conditions of industrial production.

The ILU-type accelerators overlap the energy range from 0.7 to 5 MeV at an accelerated beam power of up to 50 kW. The intrinsic features of these accelerators are the simple design, ease in maintenance and the long term reliable operation under conditions of industrial production. Table 1 shows the basic parameters of the ILU-type accelerators produced by BINP [1,2,3].

Table 1: Basic parameters of the ILU-type accelerators

Parameters	ILU-6	ILU- 8	ILU-10	ILU-12 Project
Energy of electrons, MeV	1.2-2.5	0.6-1.0	2.5-5.0	4.0-5.0
Average beam power (max), kW	20	25	50	300
Average beam current (max), mA	20	30	15	60
Power consumption, kW	100	80	150	700
Accelerator weight, tons	2.2	0.6	2.9	5
Weight of local protection, t	-	76	-	-

The basic model of the ILU accelerators is the ILU-6 accelerator [1]. The base model of the family is ILU-6 This machine has rather high parameters at modest dimensions and can be used for wide spectrum of technological processes. The protected hall with inner dimensions 3*4*5 m is big enough for its placement. The necessary volume of concrete for construction of such hall is about 180 m^3 (the required wall thickness is of about 1.5 m).

The model ILU-6 is widely used as in our country and abroad. A principle of high-voltage acceleration is used in majority of modern accelerators, i.e., the energy of electrons corresponds to the voltage generated by the rectifier. The industrial accelerators type ILU are the exception of this rule. A principle of acceleration of electrons in the gap of HF resonator is used in the ILU machines. Such accelerator does not contain details, potentials of which in respect to the ground is comparable to accelerating voltage. So the complex high-voltage units (accelerating tubes, sections of rectifiers and etc.) which are damaged by the occasional discharges are not used in ILU machines. And so there is also no necessity to use insulating gas and high-pressure vessels.

Use of a principle of high-frequency acceleration has allowed to create rather simple design of the machine having modest dimensions and weight. As a result the machine can be placed inside the hall of the smaller dimensions comparing with the halls for high-voltage accelerators having the same parameters.

The pulse nature of electron beam generated by ILU machines enables one to direct the beam into various channels of the beam extraction device without beam losses. Hence, there is the opportunity to create the extraction devices forming an irradiation zone according to the form of a treated product, that permits to increase efficiency of beam usage.

The model ILU-8 is the result of its further development. It is designed mainly for processing of cables and tubes. This accelerator does not require construction of a special protected premise (hall) and can be placed in usual industrial shop. It can work inside the local biological shielding. The local shielding of the accelerator is a kind of a box made from steel plates. Inside the box is divided into two parts. The top part is used to place accelerating system with HF resonator, spallation vacuum pumps and forevacuum system. The beam extraction device, air pipes of ventilation system and technological equipment are placed in the bottom part of the shielding. The back wall of the shielding has the channels (labyrinths) for input of cables, air and water

pipes. The removable front wall serves as a door of a protective box. The thickness of radiation shielding in side walls part is 330 mm and in top is 240 mm. Gross weight of shielding is 76 tons. The reduction factor for brake radiation (Bremsstrahlung) at electron energy 1.0 MeV is not less than $5*10^7$.

On the base of the ILU-6 accelerator, the ILU-10 accelerator was developed to satisfy the needs of technological processes requiring the energies up to 5 MeV. This report describes the ILU-10 machine.

2 GENERAL DESCRIPTION OF ILU-10 ACCELERATOR

The basic component of the accelerator is a toroidal copper cavity with an operating frequency of 116 MHz with axial protrusions forming the accelerating gap having length of 270 mm. The protrusion shape was chosen from the conditions of the formation and focusing of an electron beam in the processes of its injection, acceleration and further passage through the extraction system with minimum losses.

The cavity 2 is placed into the vacuum tank 1 (Fig.1). The electron injector 5 is formed by the cathode unit and the grid mounted in the upper protrusion. The lower electrode and injector form a triode accelerating system. The beam current of accelerated electrons is controlled by varying the value of the positive bias at the cathode with respect to the grid.

Under the lower electrode of the cavity there is a magnetic lens shaping an electron beam in the accelerator channel and the extraction device 6.

Two RF autogenerators 9 based on powerful triodes type GI –50A are installed directly on the vacuum tank. Generators 9 assembled according to the common grid circuit are working at frequency about 116 MHz that is near the specific frequency of the cavity. Anode circuits are coupled to cavity through the inductance loops. The coupling rate is determined by the square of loop and the tuning of the anode circuits. The generator feedback is provided by the additional capacitance made in the form of a disk inserted between the tube's anode and cathode. The value of capacitance is about 20 pF. The fine tuning of the feedback value and its phase is made by the cathode short-circuited tail with a movable shortcut contact moved by a servodrive. The coupling rate of generator with cavity is tuned during the accelerator's preliminary adjustment by varying the capacity of the vacuum capacitor 8 and the square of the coupling loop by varying the position of its support 7.

The measuring loop is installed on the upper flange of the tank. Its signal proportional to the cavity gap voltage is used for measuring the energy of accelerated electrons. For stabilization of the leading front of the high frequency voltage pulse when applying the pulse voltage to the tubes anode, an additional excitation of the generator by the direct voltage of 0.9 - 1.5 kV is used. The cavity is placed into the vacuum vessel made of stainless steel. The high vacuum pumping is done by four spallation pumps placed at the cylindrical surface of the tank. The forevacuum pumping is provided by the forevacuum aggregate through the nitrogen trap. All the sealings in the vacuum vessel are made of metal (copper and indium). The operating vacuum is of 10^{-7} Tor. In the normal operation of the accelerator intervals of about two days do not require the forevacuum pumping for switching on the spallation pumps. The vacuum tank pressure is measured by the current value in the spallation pumps.

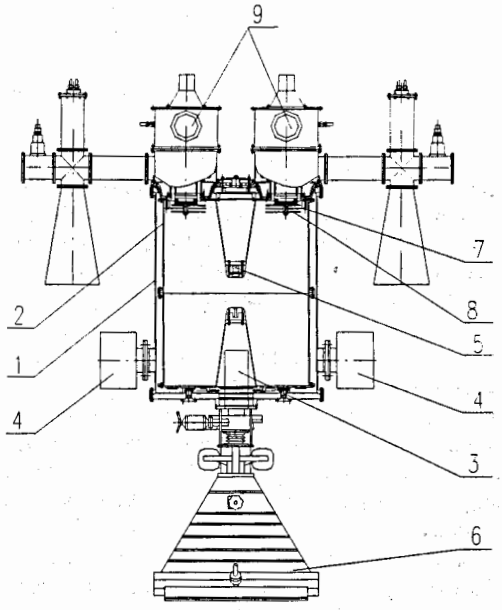

Figure 1: ILU-10 accelerator. 1 – vacuum tank, 2 – copper toroidal cavity, 3 – magnetic lens, 4 – ion pumps, 5 – grid-cathode unit, 6 – beam extraction device with linear scanning, 7–coupling loop support, 8 – vacuum capacitor, 9 – RF generators

3 BEAM INJECTION

As mentioned above, use of the internal injection, when the cathode with the control grid is placed directly at the accelerating gap entrance, is the ILU-type accelerator's feature. The opposite electrode of the cavity acceleration gap is used as an anode.

The grid-cathode unit is located on the upper electrode directly at the accelerating gap entrance (see Fig. 2). The triode gun consists of the cathode, control grid, and lower accelerating gap electrode in the role of the anode. The grid and upper electrode are the united peace made of copper. The cathode unit is installed on the insulator ahead of the grid. The 16 mm diameter cathode tablet is made of lanthanum hexaboride (LaB_6). 20 amperes current flows at a voltage of 12–15 V through the cathode heater which is a cone helix made of tungsten wire of 0.6 mm diameter. The anode hole has 30 mm diameter. A magnetic lens is installed inside the lower electrode allowing the beam transverse size at the output device entrance to be controlled. At this injection method, the current is formed by RF field penetrating into the grid-

cathode gap from the accelerating gap and is determined by the grid penetration factor.

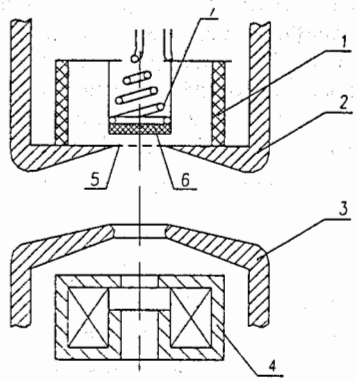

Figure 2: Accelerating structure with grid-cathode unit. 1 - cylindrical ceramic insulator, 2 - upper protrusion (electrode) of resonator, 3 - lower protrusion (electrode) of resonator, 4 - focusing lens, 5 – grid, 6 – cathode (electron emitter), 7 - cathode filament

The maximal current micropulse value is obtained practically at maximum of the accelerating voltage in the cavity gap. The injected current micropulse phase duration together with accelerated beam energy spread may be somewhat changed by varying the constant stopping potential on the grid. Here, there are no backing electrons.

The ILU-10 accelerator is the RF machine and so the initial energy spectrum of electrons in beam is not monochromatic but has the certain energy spread. To increase the X-ray power the energy spectrum of electrons ought to be made more narrow and the part of electrons with maximum energy ought to be increased because the electrons of the low energy part of spectrum do not make the input into the X-ray power, and their energy is transformed into the heating of target. It is possible to improve the energy spectrum of electron beam (to decrease the part of low energy electrons) by applying the high frequency bias voltage on the grid-cathode gap of the accelerator's electron gun.

4 ELECTRON BEAM EXTRACTION

The pulse nature of electron beam generated by ILU machines permits to design the beam extraction devices for radiation technologies forming the irradiation zones for multilateral irradiation of objects having the various forms. It enables one to increase beam usage efficiency and in some cases to reduce the electron energy required for irradiation, or to expand the nomenclature of treated products.

Beam extraction device for extraction of electrons into air, is attached to the vacuum tank's lower flange through a separating valve. The electron beam extracted into the air through foil. Usually three types beam extraction device can be used; linear scanning device for treatment of flat product, 3-window extraction device for 4-side tube or cable irradiation and beam extraction device with X-ray converter.

In the linear scanning device each pulse of the beam is scanned along the length of extraction window (Fig.1). In the 3-window extraction device beam pulses are scanned sequentially along its upper windows and along the left and right parts of lower window.

Scanning magnets, installed on scanning chambers, are used for scanning of the beam. The magnets are fed by current stabilizer, providing initial beam position at the start of beam pulse, and by a pulse transformer, providing scanning of beam along the window.

The irradiation of wires, cables and tubes ought to be made at least from two sides. Bilateral irradiation is acceptable for miniature or flat multi-strand wires, bands, etc. But in case of bilateral irradiation of thick cables and pipes the inhomogeneity of a dose all over the perimeter of a product occurs to be too high. Moreover, the usage of usual irradiators with linear scanning of a beam and underbeam transportation device ensuring bilateral irradiation of cable on one level does not give good results due to twist of a product around its longitudinal axis during rewinding. The irradiation scheme is convenient for radiation processing of cables and tubes if it is free from changing of the direction of bending of the treated product during rewinding, i.e., in such scheme the product is irradiated on two levels and at least from two sides. Such organization of irradiation process is realized by means of the 3-window extraction device for 4-side tube or cable irradiation (Fig.3).

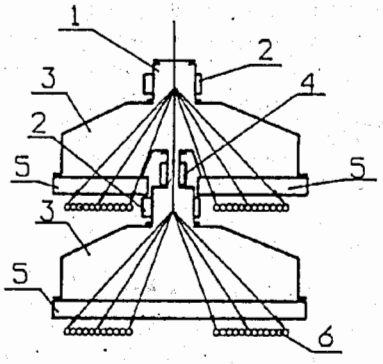

Figure 3: Beam extraction device for 4-sided irradiation. 1-beam deflection unit, 2-core of the deflecting magnet, 3-body of the device, 4-focusing lens, 5-extraction windows, 6-treated objects

In recent years, in the majority of countries the beam technologies are being developed aiming at their use for irradiation products in the food industry. However, in the use of the electron-beam technology one should take into account that the electron beam permeability is rather small thus putting limitation to the amount of the irradiated material. A reasonable alternative seems to be the use of powerful fluxes of X-rays. To generate this radiation the electron beam can be directed to the X-ray converter. The technological process of the product

treatment requires the certain type of the extraction device. For example, the beam bent at an angle of 90 grades enables a substantial simplification in the design of the conveyor system for subjecting the treated product to two-sided irradiation.

General view of the bending system design is given in Fig.4 [4]. The beam from the accelerator reaches the bending channel and is turned there throgh an angle of 90 grades and hits vertical long optimized X-ray converter, which is an aluminum plate coated by the layer of tantalum.

The channel is an electron optical system having two 45 grades bending magnets with the parallel ends, quadruple lens with a large radial aperture, two adjustable lens doublets, scanning magnet and correcting magnet. The scanning magnet in a period of 500 mks scans the beam from above to down along the converter of 1 m in length. The scanning angle is ranging from -25 to +25 grades.

For the formation of the technologically optimum dose field, an electron beam should be incident at the converter edges at an angle close to 90 grades. This is provided by the use of the correcting magnet located at distance of 15 cm from the converter.

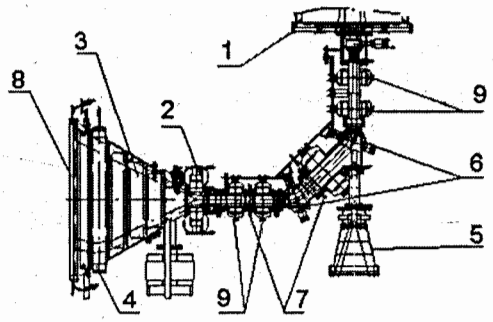

Figure 4: Beam extraction device with X-ray converter. 1-vacuum tank, 2-scanning magnet, 3-extraction device, 4-correcting magnet, 5- direct extraction device, 6-bending magnets, 7-pick-up stations, 8-converter, 9-quadruple lenses

All the components of the beam channel have the water cooling systems enabling to remove totally of up 5 kW heat in a continuous regime. The system of vertical extraction of a beam through titanium foil is kept for expanding the technological capabilities of the accelerator.

The ILU-10 accelerator is a pulse machine, the maximum pulse repetition rate is 50 Hz, the pulse duration is 400-500 mks. In the work with the tantalum converter, a rather homogeneous dose distribution on the irradiated material surface was obtained. At the scanning width of 60 cm, the average dose value was 17 kGy with the conveyor equivalent speed of 1 mm/s. Dose distribution along the beam window is presented in Fig.5.

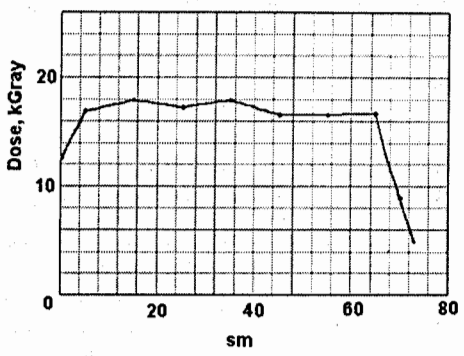

Figure 5: Dose distribution along the beam window

5 TECHNOLOGIES

The important direction in works of Institute of Nuclear Physics are medical, biological and pharmacological applications of our accelerators. The sterilization technology for medical single use products with the use of the beam of accelerated electrons is well studied and widely used both in our country and abroad [1]. This technology appeared as an alternative to the gamma irradiation by the installations with isotopes Co and Cs. Table 2 shows the X-ray applications and dose values collected by IAEA.

The ILU-10 machine that can reach maximum energy of 5.5 MeV ideally suites for the irradiation centers purposed for treatment of wide spectrum of goods. The electron energy of 5 MeV permits to treat the products that can have the surface density up to 3 g/cm^2 if the two-sided irradiation is organized. It means that the products can be treated in the packed form – in the cartoon boxes containing the several sets of products.

The maximum beam power of ILU-10 machine is 50 kW, so the productive rate of the irradiation facility can be up to 300-700 kg per hour assuming the sterilization dose of 25 kGy.

The project of the irradiation facility purposed for radiation synthesis of the new medical preparations and sterilization of the medical, pharmacological and other product is now on the final stage of development. The irradiation installation will start to work in nearest time – the planned date is year of 2006.

Now one ILU-10 machine in BINP is regularly used for sterilization of single use medical dressing sets and sets of instruments. The treated products are packed in the cartoon boxes having dimensions of 420mm*500 mm and height up to 150 mm (up to 10 sets in box), the weight of the box usually does not exceed 3 kg. The market for sterilization services is now actively growing and the demand for the irradiation of different products is constantly increasing. The phytogenous raw materials (herbs, ground roots, etc.) are efficiently sterilized by electron beam treatment without loosing of their medicinal action.

Table 2: X-ray Applications and dose values collected by IAEA

Benefit	Dose (kGy)	Products
Inhibition of sprouting	0.05-0.15	Potatoes, onions, garlic, root ginger, yam etc
Insect disinfestation and parasite disinfection	0.15-0.5	Cereals and pulses, fresh and dried fruits, dried fish and meat, fresh pork, etc.
Delay of physiological processes (e.g. ripening)	0.25-1.0	Fresh fruits and vegetables.
Extension of shelf-life	1.0-3.0	Fresh fish, strawberries, mushrooms etc.
Elimination of spoilage and pathogenic of food	2.0-7.0	Fresh and frozen seafood, raw or frozen poultry and meat, etc.
Improving technological properties of food	2.0-7.0	Grapes (increasing juice yield), dehydrated vegetables (reduced cooking time), etc.
Industrial sterilization (in combination with mild heat)	30-50	Meat, poultry, seafood, prepared foods, sterilized hospital diets.
Decontaminatio n of certain food additives and ingredients	10-50	Spices, enzyme preparations, natural gum, etc.

The electron beam power generated by ILU-10 machine can be up to 40-50 kW at energy of 5 MeV so this accelerator can be used as powerful X-ray source.

The usage of X-ray mode permits to widen the range of the treated products, but the economical efficiency of this treatment is sufficiently lower (in 50 times) comparing with the electron beam treatment.

REFERENCES

[1] V.L. Auslender. ILU-type electron accelerator for industrial technologies. Nuclear Instruments and Methods in Physical research, B 89 (1984), 46-48.

[2] V.L. Auslender, A.A. Bryzgin, L.A. Voronin, G.A. Vasiliev, V.A. Gorbunov, M. Korobeinikov, V.N. Kokin, S.A. Maximov, V.E. Nekhaev, A.D. Panfilov, V.M. Radchenko, V.O. .Tkachenko, A.A. Tuvik, B.L. Factrovich. ILU-type electron accelerators with energies higher than 5.0 MeV and power over 50 kW, Abstracts of Proceedings of XVII Workshop on accelerators of charged particles, Protvino, 2000.

[3] Auslender, R.A. Salimov. Electron accelerators of INP SB AS USSR for national economy, Atomnaja energija, v.44, issue 5, 1978. – pp. 403–408.

[4] V.L. Auslender et al. Electron Accelerator for Energy up to 5.0 MeV and Beam Power up to 50 kW with X-ray Converter, in XVIII Int. Workshop on Charged Particle Acc. Proc., Alushta, 2003.

LINEAR ELECTRON ACCELERATORS FOR RADIATION PROCESSING. CURRENT STATUS.

M.F. Vorogushin, Yu.N. Gavrish, M.I. Demsky, A.P. Klinov, O.L. Maslennikov, S.F. Naumov, V.M. Nikolaev, A.M. Fialkovsky, L.P. Fomin, Yu.P. Shchepin, FSUE "D.V. Efremov Scientific Research Institute of Electrophysical Apparatus", St. Petersburg, Russia

Abstract

NPK LUTS NIIEFA has been developing linear accelerators for industrial applications during about 30 years. More than 150 linear accelerators for different applications have been manufactured by this company and installed in different regions of Russia and abroad. The linear accelerators for radiation sterilization developed in NPK LUTS NIIEFA are reviewed in this report.

For more than 30 years the D.V. Efremov Scientific Research Institute of Electrophysical Apparatus, NIIEFA designs, manufactures and delivers linear accelerators for radiation processing. In machines of the 1st generation manufactured in the '70-80s (ten in number) a long-anode magnetron operating at a frequency of 3 GHz was used as a source of RF power. The accelerators produced electron beams with a kinetic energy of 8 MeV and beam power up to 5-6 kW. Some machines offered a wide range of energy variation and were used both as pilot installations and for production of electron flows under commercial operation. Some of the machines are still in operation nowadays, e.g. at Dunashrink Kft., Anglo-Hungarian Heat Shrink Product Manufacturing and Trading Ltd. in Hungary, Budapest (the accelerator has been operating since 1980); at the Co Rad firm in St. Petersburg; at Radient Nord in France; at a firm in province Shanghai, China and at the the Kurgan joint-stock company of medical preparations and utensils "Sintez" (since 1975).

In 1971 a linear accelerator for electron energy up to 18 Mev and beam power of 10 kW (at 10 MeV) was designed and delivered to the Institute of Nuclear Chemistry and Technology, Warsaw, Poland. A klystron operating at a frequency of 1.818 GHz was employed in the machine. At present it is used for electron beam sterilization and treatment of foodstuffs not only on the territory of Poland but also in other countries of European Union.

In the 1980s the accelerators for radiation processing of the 2nd generation were designed on the basis of a multi-beam klystron generating at a frequency of 2.45 GHz a pulse power of 6 MW at an average power of 25 kW. Such a machine has been operated at the Kurgan joint-stock company of medical preparations and utensils "Sintez" since 1992.

The development of powerful electron accelerators of the 3rd generation was started in 2000 and is continued nowadays. The accelerators operate in the "S" band of wavelengths and apply a multiple-beam KPA-147A klystron generating at a frequency of 2.856 GHz.

In the accelerating device of the first accelerator of the 3rd generation – UELV-10-15S a 2100 mm long combined accelerating structure is used. The initial part of the structure is a standing wave buncher, and its main part is a traveling wave disk-loaded waveguide. The accelerating device also includes a three-electrode electron gun and an injection device with a short-focus lens.

The current of accelerated electrons is controlled by an induction current monitor with a feedback applied to the magnetic lens of the injection device. This feedback provides the necessary stabilization of the beam current at the accelerator outlet.

A special ionization chamber is used for monitoring the energy of accelerated electrons, dimensions and characteristics of the scanned electron beam The chamber is equipped with two rows of collecting electrodes and one raw of measuring probes installed along the scanning length between the collecting electrodes [1]. Energy is periodically checked from the current measured in an Al barrier. For this purpose, as well as for periodic check of the induction current monitor, a two-plate beam absorber, installed directly behind the above ionization chamber, is used.

The energy of accelerated electrons is controlled by varying the current of accelerated electrons, RF power at the inlet to the accelerating structure and frequency of RF oscillations.

Table 1: UELV-10-15S Beam Parameters

Nominal energy of accelerated electrons, MeV	10
Range of energy variation, MeV	5-12
Average beam power in the nominal mode, kW	14
Pulse current of accelerated electrons in the nominal mode, A	0.33
Beam current pulse length, μs	14
Pulse repetition rate, l/s	300
Injection energy, kV	50
Pulse injection current in the nominal mode, A	up to 0.5
Irradiation field sizes 10 cm from the extraction window foil:	
Scanning line length, mm	500
Scanning line width (at 10 MeV and 80 μm Ti-foils) mm	about 25

Table 3: Main Performances of the Facility

Parameters of Accelerated Electron Beam	
Nominal average energy, MeV	3
Nominal average current, mA	up to 1
Nominal average power of the beam extracted to the atmosphere, kW	2.5
Nominal pulse current, A	0.4
Current pulse duration,μs	8 or 6.5
Pulse repetition rate, pulse 1/s	300 or 360
Beam diameter at the scanning system output window (90% of electrons), mm	20
Maximum scanning length (scanning in the vertical plane), mm	400
Dose variation along the scanning length, %	± 5
Radiation leakage-X-ray dose rate on the facility surface, μSv/h	1
Parameters of the Irradiation, Scanning and Transport Systems	
Sizes of irradiated objects: Depth, mm Height, mm Length, mm	 200 350 500
Scanning frequency, Hz	1-10
Speed of an irradiated object transport in the process of scanning ,m/min	about 1
Under two-sided irradiation, the cassette with an irradiated object is turned through 180° by the transport system	
Dimensions and Weight of the Facility	
Length, mm	4500
Width, mm	2400
Height, mm	1800
Weight, t	up to 35

The equipment of the UEL-3-2.5S is given in Fig. 2.

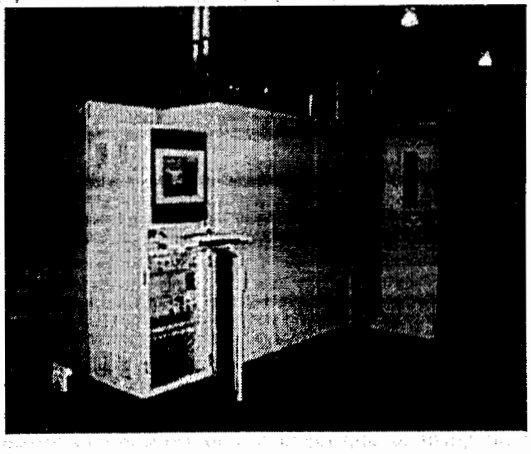

Figure 2: UEL-3-2.5S accelerator-based facility

The KPA-168 klystron operating at reduced pulse power is a source of RF power.

A combined-type accelerating structure and a double-electrode gun with a short-focus lens are applied in the accelerator.

The facility based on the UEL-3-2.5S accelerator is developed in two modifications. In the first version cassettes with packages to be irradiated are placed on the transport system in the irradiation chamber one by one (discrete process). Such a modification of the facility has been manufactured and delivered to the customer (the Kasel Associates Industries Inc, USA) and is successfully operated nowadays; all design parameters are provided.

The second modification of the machine is intended for continuous irradiation of a large batch of products, which are put into the irradiation chamber on the transport system through a labyrinth with an additional radiation shielding. The development of such a machine is still in progress.

In all the machines of the 3rd generation the computer control system is built on the basis of Octagon Systems 6000 controllers and an Advantech host computer. The control system is updated as far as the machine is updated and can be modified at the customer's request.

Nowadays, works on the updating of systems for variation of energy of electrons are underway.

S-band accelerators for a beam power up to 25-30 kW are under design.

Works on increasing the beam diameter at the scanning system output are also in progress.

REFERENCES:

[1] A.A. Volzhev, M.I. Demsky et al., "Beam Extraction System for Linear Electron Accelerators Applied to Industry", XVII Conference on Charged Particle Accelerators, Protvino, Collected reports, v. 2, pp. 374-375.

[2] M.F. Vorogushin, Yu.N. Gavrish et al., "3 MeV Linac Based Facility for Electron Beam Processing", Atomnaya Energiya, v. 95, №1, p. 44

SIMPLE PLANAR SYSTEM

M.Kats, B.Druzhinin
(ITEP, Moscow)

Abstract

Simple Planar System SPS(F) was suggested instead of GANTRY in 2002 [1-5] as compromise between price and properties of equipment for proton or ion beam transport to horizontally fixated patient from many spatial directions. It used bend of the beam by one immovable magnet in vertical plane only just near to the patient and suitable change of vertical position of treatment coach with patient. Beam can be bend on any angles to horizontal plane in interval -F≤ angle ≤F.

Selection of Maximal and Suitable Angle F

Spatial schemes of SPS for proton and ion beams (0.7 and 1.9GeV/c) are shown on Fig.1 for F=30, 60, 90 degrees at maximal field in magnet 1.8Tl. Scheme of possible directions for irradiation for simplest systems with fixated directions, for SPS(60) and GANTRY(90) are shown on Fig.2.

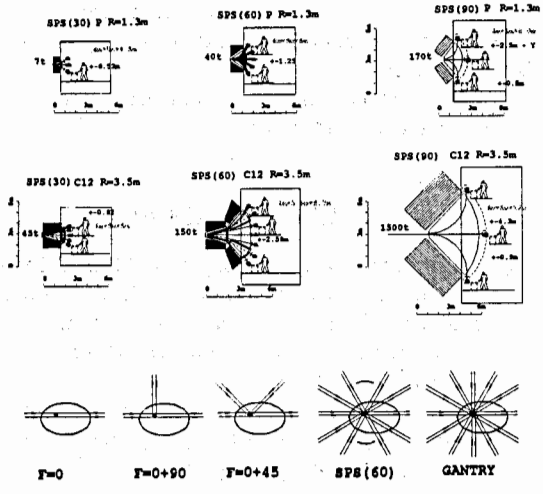

Fig. 1: Spatial schemes of SPS for transport of proton and ion beams and comparison of possible directions of irradiation for different equipment

After comparison of possibility of irradiation, weights and power of magnet, mechanical problems with treatment coach displacement maximal value of F was choose as 60 degrees.

Using of Super Conductive Magnet

Possibility of using super conducted magnet was reviewed. Few spatial schemes of SPS(60) for proton and ion beams are shown on Fig.3 for hot magnets with B<1.8Tl and super conducted magnets with B=1.8Tl.

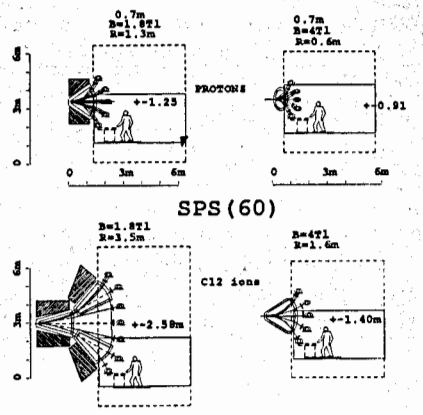

Fig. 2: Spatial schemes of SPS for proton and ion beams with B<1.8Tl and B<4Tl

It can see that using super conductive magnet for proton beam is usefulness, but it can be useful at field like 5Tl for transport ion beam both for decreasing size of treatment room and for decreasing of linear dispersion at the target, and for decreasing displacement of treatment coach.

Adaptation Condition of Treatment Room with SPS(60) to Usual Condition

Next step was devoted to adaptation condition of treatment room with SPS(60) to usual condition in room with horizontal beam or with GANTRY. It was suggested to move vertically all treatment room with its treatment coach and all devices.

Floor of treatment room is joined with permanent floor by a stair with hinged steps.

Patient transportation and installation at treatment coach can be performed only during the horizontal position of the stair.

Displacement of the treatment room can be performed only between irradiations from different directions. Speed of displacement is near 3 cm/sec only.

Beam pass through iso-center with precision ±0.2mm.

Access to the treatment room is possible independent on room displacement and independent on electricity.

Beam monitor and multi leaf collimator can be moved at the beam direction simultaneously with room displacement.

Schemes of treatment room with horizontal beam or with SPS, scheme of patient transport and preliminary design of treatment room are shown on Figs. 3-5.

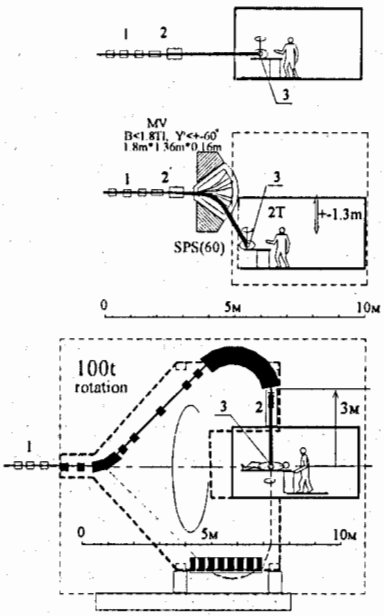

Fig. 3: Spatial schemes of treatment room with horizontal beam, with SPS(60) and with GANTRY

1. last part of transport channel – part of SPS(60).
2. scanning magnets.
3. center of the target.

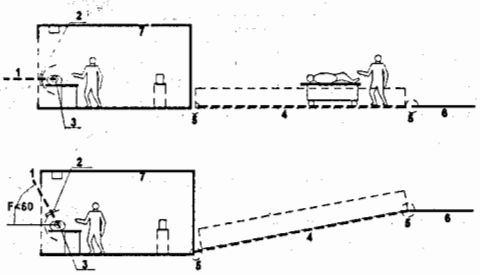

Fig. 4: Scheme of the patient transport in treatment room.

1. beam direction.
2. monitor of the beam and multi leaf collimator.
3. center of the target.
4. stair with changeable shape (depend on its direction).
5. hinged steps.
6. permanent floor.
7. treatment room with vertical displacement.

It is evident, SPS(60) is much simple, smaller and cheaper in comparison with any versions of rotating GANTRY. Preferences of SPS in size and price are especially significant at transport of ion beam and at using many treatment rooms near one accelerator.

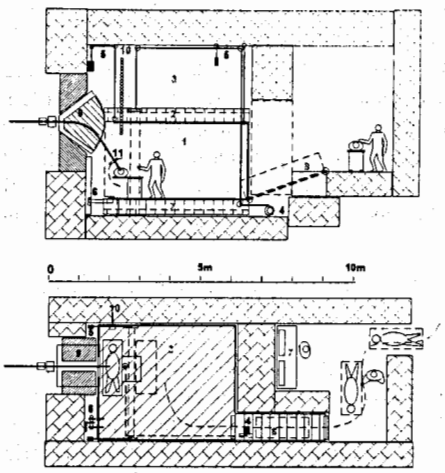

Fig. 5: Spatial and mechanical schemes of treatment room with SPS(60) for proton beam

1. Internal volume of treatment room (4m×5m×3m) with usual treatment coach, with all usual devices for precision patient installation** and beam monitoring and collimation, with thin wall in beam directions.
2. Rigid spatial frame of treatment room.
3. Free entrance for treatment room displacement (4m×5m×3m).
4. System of room displacement (motor, steel rope transmission).
5. System of counter-weights.
6. System of radial fixation.
7. Control room.
8. Stair between treatment room and permanent floor.
9. Vertical magnet.
10. Optical position measurement.
11. Monitor and multi leaf collimator.

**For centers of treatment with high productivity it would be better to install the patient with precision in additional room [6].

Optical Solution of Transport Channel and SPS(60)

It was suggested to use magnetic optics of transport channel as a part of SPS(60). Examples of such optical solutions at scanning of target volume by pencil beam are shown on Fig.6 for two values of F.

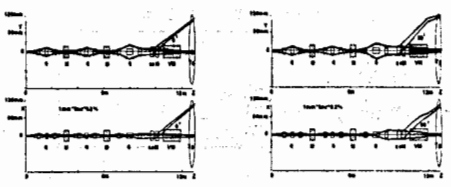

F=0 F=60

Fig. 6: Optical schemes of beam transport to treatment room and to the target through of the SPS(60).

At quick extraction beam spreading through the target volume can be done by optics of SPS(60) or by using of scatters before vertical magnet.
It was shown that SPS(60) can transport successfully at scanning beam with significant phase volume (XX' =10mmmr) and small momentum spread (dP/P<±0.2%). Such beam can be prepared after slow extraction from any synchrotron or after cyclotron – degrader – ESS system, but in the last version useful part of extracted beam will be smaller.

Comparison of Properties SPS(60) and GANTRY

For the beginning doses distribution in depth (of water) was calculated by TRIM for mono energetic protons with correction on nuclear interactions and straggling [4,7]. Then were calculated doses distributions for different size and depth of targets with corrections on initial beam parameters and distance of scanning, on elastic scattering, for maximal range 30cm.
"Physical" criteria of quality of irradiation C was used as relation useful part of the beam energy to average level of doses in healthy parts of the body K
The quality of irradiation C increased with quantity of directions of irradiation N and with F, but there are plateau in F dependants after 60 degrees at any conditions. Thus, "physical" quality of irradiation at using of SPS(60) will be comparable with "physical" quality of irradiation at using of GANTRY (90) ([3, 4, 5].
"Medical" comparison of equipment with different F was made by using 11 different examples of real tomographs. Those examples were in practices of Proff. E.Khmelevskii (MCRR). It was shown, optimal directions of irradiation were the same for SPS(60) and GANTRY for most of localizations (breast, prostata, liver, pancreas body and head, thick intestine, throat, esophagus, mediastinum).
Thus, by "medical" point of view any targets can be irradiated with using SPS(60) successfully and most of targets can be irradiated with using SPS(60) with the same results, as with using GANTRY [5].

Improving Treatment Rooms Equipped with Horizontal Beam

It was suggested to improve treatment rooms with horizontal beams by using SPS(30) with additional small magnet just before the patient and with using vertical displacement of horizontally fixated patient by usual treatment coach (see Fig.7).

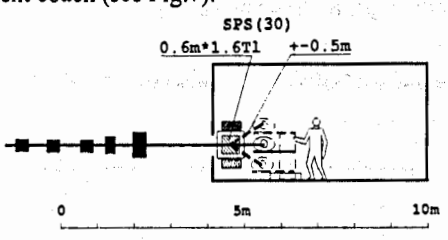

Fig.7. Scheme of treatment room with SPS(30) instead of horizontal beam.

Using of SPS(60)

For increasing quantity of treatment in each future center of therapy by proton or ion beams [6,8] it is necessary to use near each accelerator many treatment rooms and time of irradiation must be short (like 15 min per one patient per day, or per fraction). It was shown in this text that quantity of directions for the best irradiation must be near 6. It means, that time of irradiation from each one direction and time of changing of direction of irradiation must be near 1 min. Such time of irradiation can be received by 3-d scanning without any mechanical movement, or after quick extraction by scanning in depth only with using multi leaf collimator near to patient. It was shown in [6] quantity of treatment room at one direction of extracted beam for their effective work must be less 5. For increasing of efficiency of therapy center it was suggested to use two independent directions of extraction from synchrotron (with its own energy and intensity) and 4 treatment rooms with SPS(60) in each direction. Scheme of such treatment center is shown on Fig.8.

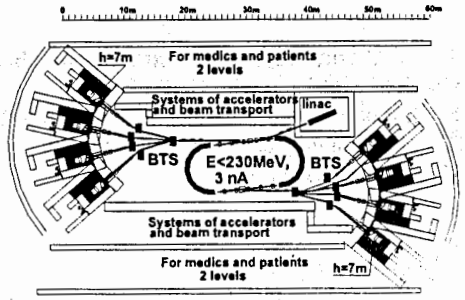

Fig. 8: Scheme of proton synchrotron with two directions of extraction and with 8 treatment rooms with SPS(60) in each.

CONCLUSIONS

Introducing of SPS(60) and SPS(30) in all new projects of therapy by proton and ion beams is suitable and actual.

ACKNOWLEDGMENTS

Authors thanks Yu.Antipov (IHEP), E.Khmelevskii (MCRR), T.Ratner(MOC) and all scientists of ITEP and IBA who support of this work.

REFERENCES

[1]. M. Kats IET, v.45, 2, 2002, p.272-276
[2]. M. Kats TERA report 2002/3 FAS 11. 2.2002.
[3]. M.Kats Report at RUPAC, 10.2002,
[4]. M.Kats, B.Druzhinin Atomic Energy, 2, 2003.
[5]. M.Kats Report on PTCOG40, Paris, 06.2004.
[6]. G.Kraft, U.Weber A proton and ion-beam facility for Rhou-Klinikum AG, Report on PTCOG39, San Francisco, 10.2003.
[7]. J.P. Biersack, J.F. Ziegler Calculation from TRIM HHH> Version - 95.xx 1989, 1992, 1995
[8]. M.Abe Hyogo Ion Beam Medical Center Prospect 2004.

DC HIGH POWER ELV ACCELERATORS FOR INDUSTRIAL AND RESEARCH APPLICATION

Yu.I. Golubenko, N.K. Kuksanov, P.I. Nemytov, R.A. Salimov,
S.N. Fadeev, M.E. Veis, V.V. Prudnikov
Budker Institute of Nuclear Physics SB RAS Lavrentyev av. 11, Novosibirsk, 630090, Russia

Abstract

Beginning from 1971, the Budker Institute of Nuclear Physics Siberian Branch of Russian Academy of Science (SB RAS) started its activity in the development and manufacturing of electron accelerators of the ELV-type for their use in the industrial and research radiation-technological installations. The ELV-type accelerators were designed with use of the unified systems and units enabling thus to adapt them to the specific requirements of the customer by the main parameters such as the energy range, beam power, length of extraction window, etc.. INP proposes a series of electron accelerators of the ELV-type covering the energy range from 0.3 to 2.5 MeV with a beam of accelerated electrons of up to 400 mA and maximum power of up to 400 kW. The design and schematic solutions provide the long term and round-the - clock operation of accelerators under the conditions of industrial production processes. The ELV accelerators are most popular accelerators not only in Russia, but in China, Korea, and etc.

INTRODUTION

The main features of ELV-accelerators are as follows:

1. High power of electron beam in wide energy range, it means high productivity of EB processing;
2. High efficiency of conversation of electricity power to electron beam power. The efficiency is limited by frequency converter and in case of transistors frequency converter efficiency is increased up to 85-92%;
3. Simple procedure of accelerator control by operator due to control system based on IBM compatible computer. It allows operating accelerator in on-line mode.
4. Accelerator control system comprises a set of software and hardware covering all the accelerator units required an operative control and diagnostics.
5. Accelerator itself has simple design and high reliability. If some troubles appear our customers repair accelerator by themselves with our consulting by phone, as a rule.
6. After warranty service. It means we delivery spare parts or parts with limited lifetime or make any accelerator service after warranty period by separate contracts with the low price.
7. A set of additional equipment (such as transportation line, ring or double side irradiation system, 4-side irradiation system) increases the accelerator possibility.
8. ELV accelerators are stable in operation. The energy and beam current instabilities practically do not exceed +/-2%.

Basic parameters of the ELV-type accelerators are given below at the Table1. and ELV-4 is sown at Fig1.

Table1:

	Energy range, MeV	Beam power, kW	Max. beam current, mA
ELV-0.5	0.4 - 0.7	25	50
ELV-1	0.4 - 0.8	25	50
ELV-2	0.8 - 1.5	20	25
ELV-3	0.5 - 0.7	50	100
ELV-4	1.0 - 1.5	50	50
ELV-6	0.8 - 1.2	100	100
ELV-8	1.0 - 2.5	90	50
ELV-6M	0.75 - 0.95	160	200
ELV-12	0.6 - 1.0	400	500

By now, over 90 accelerators had been delivered inside Russia and abroad and the total operation time exceeds 800 accelerator-years. .

50 accelerators were delivered inside of former USSR
20 accelerators were delivered in China
8 were delivered in Korea
2 accelerators were delivered in Japan
2 accelerators were delivered in Poland
1 accelerators was delivered in Germany
1 accelerators was delivered in Chech Republic
1 accelerators was delivered in Bulgaria, etc.

On international market we have strong competition with other firms producing accelerators. The number of delivered ELV accelerator during last 5 years is more than any others delivered accelerators. Very often the firms already have one or two accelerators in operation prefer to buy new ELV. So there are some places were ELV accelerators are operating at same place and conditions with NHV and RDI accelerators.

Separate units and systems of ELV accelerators are widely used in installation for scientific research.

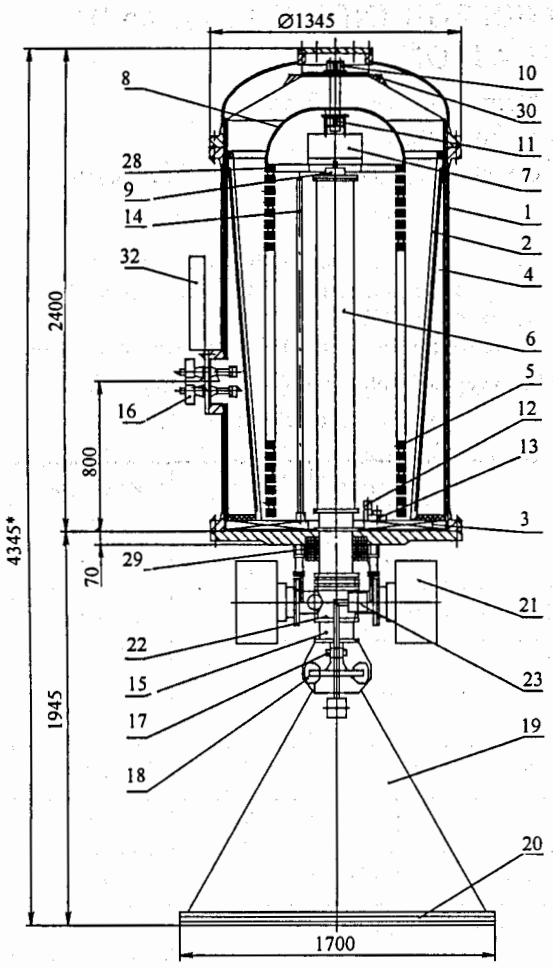

Fig.1: General view of ELV-4 accelerator

1 - vessel, 2 - primary winding; 3,4 - magnitoguides; 5 - rectifier sections; 6 - accelerating tube; 7 - injector control unit; 8 - high voltage electrode; 9 - injector; 10,11 - optical channels for injector control; 12 - section divider; 13 - capacitor unit; 14 - energy divider; 15 - vacuum gate; 16 - primary winding terminals; 17,18 - scanning coils; 19 - extraction device; 20 - extraction window frame; 21 - vacuum pumps; 22 - cross head; 23 - vacuum gate; 28 - base of high voltage electrode; 29 - magnetic lens; 30 - high voltage shield; 32 - clamp set.

APPLICATION OF ELV ACCELERATORS

ELV accelerators are used practically in all technologies where electron beam is needed.

1. The main application of ELV-accelerators is modification of polyethylene insulation of cable and wires. The irradiation allows changing the properties of insulation: to make it thermo-, fire-, oil-, radiation- resists or with combined resistivity to these agents. The square of wire treated by ELV accelerator is from 0.1 to 120 mm.sq. The productivity (depended on composition and properties) is up to 500 m/min.
   We developed the system of 4-side irradiation for cable and pipes. This system increases the quality of irradiation, because improves the azimuth homogeneity of absorbed dose. Simultaneously it decreases required energy for irradiation, i.e. increase efficiency of treatment. 4-side irradiation system is especially effective for treatment of big diameter cables. Now we equip with such system both new accelerators, and delivered before also
2. Another profitable application of ELV accelerators is production of thermoshrinkable pipes, films and bands. The productivity can be up to 1000 kg per hour. As a rule the accelerators for cable and thermoshrinkable irradiation operate round-o-clock (24 hours per day).
3. The production of artificial leather. It means the polymerization by EB the several compounds for manufacturing leather-like material with heat-, fire-, oil-, cool, and etc. resistance. Radiation-chemical technology allows obtaining both non-base material and coats on the substances of different type. This material is for shelters, overalls, shoes, and bags. Productivity is up to 1000 m.sq. per hour.
4. The production of self-adhesion bands and rubberizing items. It is also the polymerization by electron beam.
5. Composite material for soft roofing. Intended for making roofs of residential, public and industrial buildings and structures. It is a roll polymerfabric formed of rubber mix based on rubbers of general application with subsequent vulcanization by EB.
6. 1 accelerator is used for manufacturing of polyethylene-oxide gel.
7. 1 accelerator is used for production of pre-pregs based on carbon fiber fillers and polymer binders.
8. Curing lacquer-paint coatings on different bases for the building industry with productivity of up to 500-m.sq./per hour. 2 accelerators for this purpose are in Russia (but they are not operated now).
9. Desinsectization of grain with productivity 200T/hour per each 20 kW power of accelerator.
10. Waste water treatment.
11. Purification of flue gases of thermal station from Sulfur oxide and Nitrogen oxide. For this purpose we develop high power accelerator ELV-12. It's design adapted to environmental application.
12. ELV accelerators can be equipped by system for extraction to atmosphere the concentrated electron beam. It allows using accelerator for other kind of application such as: production of catalysts for the ammonia synthesis; evaporation of any materials for producing super fine powders; surfacing and hardening of metals; welding, melting and cutting of metals, producing the special types of ceramics and etc. Unfortunately such extraction device did not use in industry.

13. The 8 accelerators are installed in research and irradiation centers. Accelerator here is not connected with determined technology but is used as multifunction device. ELV accelerator is very convenient for this purpose due to wide range and high stability of beam parameters and irradiation fields, simplicity of control. Practically, researchers (chemists or others specialists) operate with accelerator themselves without special training. Set of software allows obtaining required doze with high accuracy and repeatability.

Also in BINP we have special accelerator for investigation and developing of radiation processing. Our potential customer can make experiments with electron beam here. This accelerator has power up to 100 kW.

In accordance with parameters and possibilities for users ELV accelerators are one of the best in the world.

RADIOLOGICAL CENTRE BASED ON INR PROTON LINAC

S.V.Akulinichev, L.V.Kravchuk, V.A.Matveev,
Institute for Nuclear Research,
Moscow 117312, Russia

Abstract
The radiological centre based on INR proton linac is now going to be built in Troitsk. The unambiguous variation of proton energy and average beam current will allow to irradiate many types of tumors. On the first stage, one treatment room with fixed proton beam, as well as another treatment room with medical electron 6 MeV accelerator, will be put in action. Some perspectives of the centre are discussed.

PROTON THERAPY AND INR LINAC

It is known that about 20% of all the oncological patients die because of their primary tumors without metastases. In many of these cases, the loco-regional treatment with the help of surgery and conventional radiotherapy is complicated by difficult localizations of tumors when neighbor critical organs prevent the application of conventional methods.

The hadrontherapy alone or in combination with conventional methods may allow us to significantly reduce the above number. The principal advantages of radiotherapy with proton beams, as a particular case of hadrontherapy, are due to physical properties of proton beams in matter: 1) protons, as all ions, have a unique inverse dose profile (the Bragg peak) and loose a large fraction of their initial kinetic energy in a narrow region near the end of their path in matter, 2) protons do not produce any irradiation behind the Bragg peak, which has an energy-dependent position, 3) protons have a relatively small range and lateral scattering, 4) protons, as all charged particles, can be steered by magnetic fields allowing precise shaping of the treatment volume by means of dynamic scanning of the beam. Although these advantages of proton beams are known since 1946, technical difficulties prevent a wide application of hadrontherapy. By now about 30000 patients have been treated using this method in the world and about 4000 - in Russia. Each year, only 1% of patients with prescriptions for proton therapy will have a chance to get this kind of treatment. Since proton and heavier ion accelerators (as well as beam delivery, monitoring and control systems) are quite complicated facilities, all working hadrontherapy centres, except LCUMC in Loma Linda, are based on physical research institutes. For example in Germany, the Pilot project for proton therapy was realized in GSI on a basis of research synchrotron prior to construct the Heidelberg ion beam medical centre. In Russia, three proton therapy centres are now in action in nuclear research institutes (see Table 1) and the fourth is now under construction in INR.

Table 1: accelerators for proton therapy

institute	beam energy, MeV	beam pulse, μsec	pulse frequency, Hz	patients treated
ITEP, Moscow	70-200	0,14	< 1	3500
PINP, St.Peter.	1000	300	40	1200
JINR, Dubna	660	30	250	200
INR, Troitsk	70-250	50-200	50-100	-

In order to irradiate targets at different depths, the beam energy must be variable in the range 70 – 250 Mev. From the other side, for the purposes of beam monitoring and scanning, the pulse duration and the pulse frequency (the duty cycle) must be as large as possible. From the Table 1 it follows that only the INR linac may fulfill these requirements and may be used for the development and application of such new techniques as beam scanning and beam rotation with the help of ganry . The selected beam energy is obtained by a simple switching of a necessary number of accelerator sections. Though the linac was designed for higher beam intensities with average current in the range of several μA, the necessary therapeutic currents of about 1 nA are simply obtained with the help of collimators in the initial part of accelerator. Moreover, the additional injector for H^--ions, which is now under construction, will allow to simultaneously produce two different beams: one low-intensity beam for therapy and another high-intensity beam for other applications.

PRESENT STATUS OF THE CENTRE

The first stage of the Centre, which may be built and completed by the equipment in the end of 2005, includes one treatment room with horizontal fixed proton beam and one treatment room with 6 MeV medical electron accelerator SL-75-5-MT. The patient positioning system in the proton treatment room, as well as control systems, are designed in a way to allow the irradiation of any targets from small eye tumors up to large deep-sited tumors of the body. This means that a patient may be fixed in a sitting and lying positions. However, the passive dose formation system, which

will be initially realized in the Centre, gives an upper limit for the target size of the order of 8-10 cm because it is difficult to provide an accurate dose delivery for larger targets. The electron accelerator, which will be in action by the end of 2004, will increase the effectiveness of the Centre. For many reasons, the proton beam time is quite expensive, in particular for research accelerators. The fact that for larger tumors the number of irradiation fractions may exceed 20 significantly reduces the perspectives of large application of proton therapy. On the other hand, the so called *boost*-method of tumor irradiation, when more than half of the dose is delivered using conventional radiotherapy and only the remaining part of the dose will be delivered by a more expensive proton beam, makes the perspectives of the Centre more promising. In average, the *boost*-method reduces the number of proton irradiation fraction by more than 50% without reducing the effectiveness of the treatment. For the needs of the Centre, the ambulatory with modern engineering equipment, including air conditioning and other supply systems, was constructed in the main experimental building of the Institute. This ambulatory will allow the treatment of more than 50 patients per day. The radiological section of the Troitsk hospital, which will provide the clinical support of patients, is now being organized.

PERSPECTIVES OF THE CENTRE

The first stage of the Centre will not be able to provide the application of some new achievements in hadrontherapy, in particular of beam scanning and rotation. However, as it was already mentioned, the parameters of the accelerator allow us to further develop the irradiation techniques. For example, the beam scanning equipment may be installed already in the existing treatment room. The main experimental hall of the INR Meson factory complex, where both present treatment rooms were installed, is a unique building, which allow to install without huge investments such additional systems as a proton gantry and/or a treatment room with fixed vertical proton beam. Another perspective of the Centre is connected to isotope production at the INR linac. At present, several isotopes for medical application are produced or can be produced at INR. Among them are Pd-103, Sr-82, Cu-67, Sn-117 and other isotopes. In the domain of isotope production, INR is one of the leading accelerator centres in the world. The new laboratory for isotope extraction from irradiated samples, whose project is now approved, will allow to complete the technology of medical isotope production. In this case, the INR Radiological centre may become an universal radiological centre, where most modern methods of radiology may be developed and applied.

MAIN TENDENCIES OF DEVELOPMENT OF RUSSIAN ONCOLOGY RADIOTHERAPY SYSTEM EFARAD

M.F. Vorogushin, V.A. Shishov, S.F. Naumov, A.V. Sidorov, O.M. Anouchin,
FSUE "D.V. Efremov Scientific Research Institute of Electrophysical Apparatus",
St. Petersburg, Russia
S. V. Kanaev, The N.N. Petrov Scientific Research Institute of Oncology, St. Petersburg, Russia

Abstract

The EFARAD complex incorporates therapeutic irradiators-linear medical electron accelerators LUER-20M and SL75-5-MT; TSP-100-anatomic and topometric device which provides necessary information in the form of digital projection images of patient at different angles; "Scan-plan"-treatment-planning system and computerized dose field analyzer with water phantom.

The EFARAD complex is integrated into a processing line with the help of a flexible information computer system comprising, in addition to the above components, local systems for the treatment verification, physicists' and physicians' workstations, files and data bases for various applications, patient tracking system, etc. When applying the conformal beam therapy technologies and wider arsenal of beam-forming devices, the requirements for the volume of topometric information necessary for treatment planning, for the treatment planning system, beam forming devices and accelerator systems, procedures for treatment simulation and verification becomes more stringent. The concept of EFARAD application for solution of problems both of conventional and conformal radiotherapy has been worked out in NPKLUTS.

At this point a problem of radiotherapy quality guaranty is successfully resolved in USA and in a number of western countries. In Russia the problem of radiotherapy quality guaranty is very far from resolving in routine clinical practice because of inadequate provisions of radiotherapy equipment. Experience of world-advanced radiotherapy centres shows that required quality level could be achieved only by implementation of integrated computer-based technology, which covers all stages of radiotherapy treatment.

Computer-based radiotherapy system EFARAD is being developed at Scientific and Production Complex of Linear Accelerators and Cyclotrons (NPKLUTS) of the FSUE "D.V. Efremov Scientific Research Institute of Electrophysical Apparatus" (NIIEFA).

The system is built as per module principle. This allows flexible distribution of functions between the system hardware and upgrading the system by additions of new modules. The system modules are integrated through standard interfaces; they form flexible adjustable automated information system.

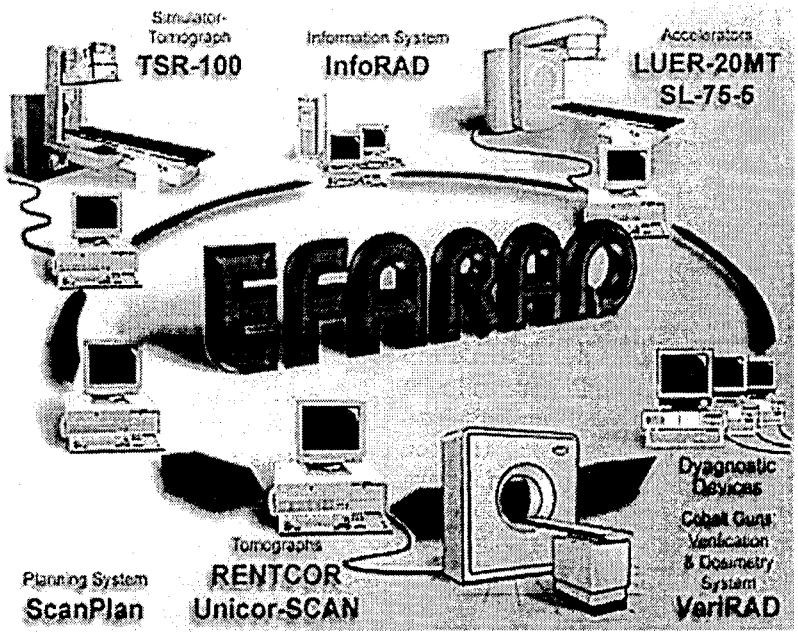

Figure 1: Computer-based radiotherapy system EFARAD

The EFARAD system (see Fig. 1) contains the following:

- Irradiators: linear medical accelerators LUER-20M, which generate 5 to 20 MeV electron and photon beams, and 6 MeV photon linear accelerators SL75-5-MT;
- Anatomic & topometric preparation equipment: radiotherapy topometric system TSR-100;
- Treatment planning system ScanPlan;
- Information system InfoRad: this system contains computer-based work stations for doctors and radiology physicists which are connected with the treatment system units, with databases and archives;
- Treatment verification system VeriRad, which contains dosimetric equipment and devices for comparison of factual and prescribed treatment plan.

Preparations of treatment prescriptions include collection of anatomic data with topometric system TSR-100 and calculations of dosimetric plans with treatment planning system ScanPlan using transversal X-ray computer tomograms. Topometric system TSR-100 performs functions of either digital simulator or computer tomography.

Anatomic & topometric images, generated by TSR-100, are transferred to the treatment planning system ScanPlan. The information system InfoRad supports operation of database and operation of clinic personnel with information of earlier made diagnostic procedures and about current treatment process.

NPKLUTS NIIEFA looks into alternatives of realisation of conformal treatment technique. Multi-leaf collimator with computer control system for the LUER-20M accelerator is being designed. Opportunities for expansion of TSR-100 capacities for supporting topometry and verification of conformal treatment are investigated.

Linear electron accelerator LUER-20M (Fig.2) is intended for distance radiotherapy with photon beams and electrons in static and arc modes.

Figure 2: LUER-20M linear accelerator

Linear electron accelerator SL75-5-MT (see Fig. 3) is basic therapy machine, which is intended for radiotherapy with photon beam in static and arc modes. Control system of the SL75-5-MT accelerator is being up-graded.

Figure 3: SL75-5-MT linear accelerator

Both linear electron accelerators are integrated in general information system.

New radiotherapy technology approaches and new radiotherapy equipment with advanced capabilities in the world market leads to reviewing role and place of various equipment for treatment preparations and for treatment verification.

Leading experts of radiation physics from Canada estimated suitability of the following four types of equipment for realisation of various radiotherapy technologies of treatment preparations and their functional parameters:

- Standard X-ray simulator;
- Computer diagnostic X-ray tomography system (CT);
- Computer X-ray tomography & simulator (CT-simulator);
- X-ray simulator with computer X-ray tomography option.

Results of the analysis indicate tomography & simulator on the top position. Simulator with tomography option takes the second place; Standard simulator and tomography are on the third place. The analysis also indicates that the main drawback of the simulator with tomography option is low capacity and poor quality of tomograms. Operation speed in the tomography mode should be increased to a level of routine tomography. Quality of the tomograms should be equal to quality of routine tomograms.

The X-ray topometric system for radiotherapy TSR-100 (Fig. 4) is intended for package solution for biometry of oncology patients and for verification of treatment plans. The system provides either projection images of a patient body in geometry of radiotherapy machine with contouring radiation field or transversal computer tomograms at required levels. Thus, the system combines X-ray simulator and CT. Operation principle is based on digital system for radiation registration which equipped by movement mechanism and collimators for fan-shaped X-ray beam scanning. The system sensor is array of solid detectors of scintillator-photodiode type.

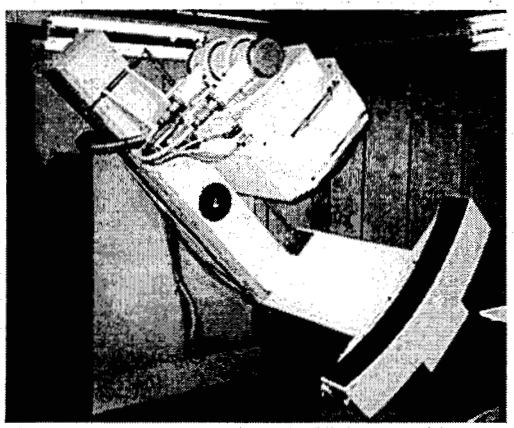

Figure 4: TSR-100 topometric system for radiotherapy

TSR-100 allows the following:

1. Localisation of tumour and healthy tissues. Determination of size/configuration of a tumour and adjacent critical organs.
2. Collection of topometric information for treatment planning with possibility to create transversal slices of patient body and projection images without patient re-setting.
3. Treatment simulation. On the base of its result the treatment plan is approved or some required corrections of the treatment plan would be made.
4. Verification of treatment plan, which allows radiographic confirmation of correct covering of target and minimum radiation of healthy tissues. This procedure is mandatory when treatments plans are realised which are calculated with use of limited topometric information (from one or two slices).
5. Treatment monitoring for control of repeatability of treatment plan using reference marks of the patient body. Monitoring of dynamics of growing/regressing the tumour, change of the patient's weight, swellings, etc.

Standard procedure of application of EFARAD system for conventional radiotherapy is developed in the N.N. Petrov Scientific Research Oncology Institute. Implementation of conformal radiotherapy techniques and use of wide range of beam forming accessories (such as shaped shadow blocks, individual shaped diaphragms, etc.) require increasing volume of topometric information. For example, implementation of multi-leaf collimator (MLC) even in static modes from different directions treatment planning is required with 3D presentation of anatomic structures and targets. Implementation of MLC also requires dramatically more complicate techniques of treatment simulation and verification and more accurate anatomic & topometric data. This problem should be resolved with technique of conformal treatment preparations based on multi-slice computer tomography with 3D object reconstruction virtual simulation of radiation beam edges.

Direct verification of treatment plans would require too complicate design of X-ray simulator. Therefore advanced approaches to the simulation tend toward virtual technologies.

TSR-100 can operate in conventional radiotherapy system with two linear accelerators SL75-5-MT and with distance gamma-therapy machine. With implementation of individual treatment plans and conformal radiotherapy capacity of equipment become very critical. Slow collection of topographic data impedes treatment-planning process considerably.

To improve technology of topometry a prototype of topometric system with two gantries was developed in the N. N. Petrov Scientific Research Oncology Institute in 1995 &1996 (Fig. 5).

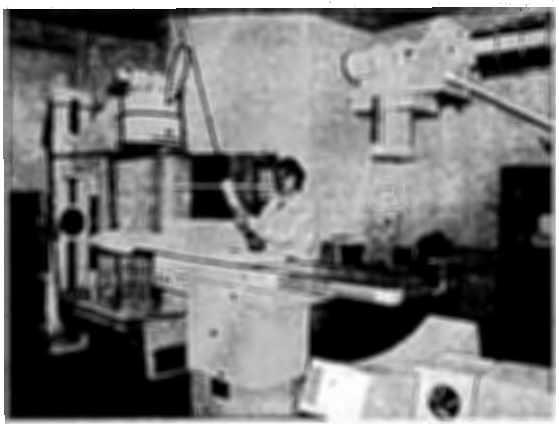

Figure 5: Prototype of two-gantry topometric system

The second unit is topographic X-ray option whish was based of principle of computer tomography system of the 3rd generation. Time of data collection for reconstruction of one tomogram is 10 second. Experience of the N.N. Petrov Institute shows that capacity of two-gantry simulation & tomography system can be very close to capacity of specialized tomography system with virtual simulation function.

At this point the EFARAD system is equipped with ScanPlan treatment planning system, which provides treatment planning of conventional radiotherapy therapy with photon beams.

For implementation of conformal radiotherapy the EFARAD system should be equipped with 3D treatment planning system. Implementation of conformal radiotherapy will allow assuring quality guaranty of radiotherapy when the most complicate treatment techniques are used.

HIGH POWER TRANSISTORS FREQUENCY CONVERTER FOR SUPPLY UP TO 500 KW DC ELECTRON ACCELERATORS

P.I. Nemytov*, Yu.I. Golubenko, N.K. Kuksanov, R.A. Salimov, S.N. Fadeev, M.E. Veis
Budker Institute of Nuclear Physics SB RAS Lavrentyev av. 11, Novosibirsk, 630090, Russia

Abstract

In this work, the generalized experience in the development of powerful (500 kW) frequency converters based on JGBT modules designed for feeding industrial electron accelerators of the transformer type is presented. The problems related to the matching of the converter output with the primary winding of the high voltage transformer are considered and recommendations on the converter design are given.

INTRODUTION

The industrial electron accelerators of ELV type are constructed on the base of the cascade generator with a parallel feed of cascades. These accelerators are manufactured in the Budker Institute of Nuclear Physics.

A many tens of accelerators of this series are being operated successfully at the industrial and research institutions of various countries around the world. They are mainly used for the treatment of cable products, for producing thermoshrinkable tubes and films, for waste water treatment and many other technological processes.

The electron beam power for ELV-type accelerators is up to 400 kW. Beam energy range is 0.3 MeV...2.5 MeV.

The design and parameters of the ELV-accelerators are given in many publications (see, for example, [1]).

DESIGN OF ELV-12 ACCELERATOR

Schematically configuration of the high-voltage rectifier of accelerator ELV-12 is shown on fig. 1. The source of a high voltage consists of a primary winding of transformer PW and a column of high-voltage rectifier HVR. The column of the high-voltage rectifier consists of several tens consistently connected rectifying sections. Everyone section contains a secondary winding, rectifying diodes and filtering capacitors. The primary winding feeds by AC voltage of the increased frequency (400 ... 1000 Hz).

Distinctive features of configuration of accelerator ELV-12 (400 kW) are as follow: the presence of two primary windings and two columns of the high-voltage rectifier. Columns of high-voltage rectifiers are installed one above another so the high potential applied to accelerating tubes, appears in the center.

*P.I.Nemytov@inp.nsk.su

ELV-12 accelerator has three accelerating tubes and three extraction devices: one tube is located inside bottom rectifying column, and two another tubes are installed in remote modules. The high voltage for remote tubes are passed through a gas high-voltage feeder.

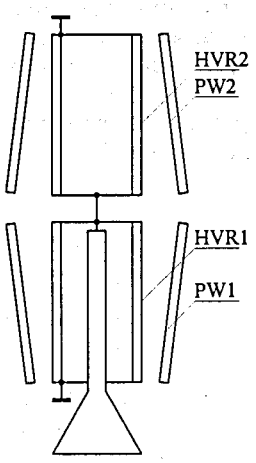

Fig. 1: Configuration of the high-voltage rectifier of accelerator ELV-12

As against the usual transformer the given configuration has essential differences. Extremely simplified linear equivalent circuit is shown on fig. 2.

For ELV-type accelerators inductances L_S and L_μ are approximately the same.

It is related to the fact that the gap between the primary and secondary windings (designed for the total accelerator voltage) is large. The large value of the scattering inductance leads to «sagging» of the output voltage under the load and to the change in the resonance frequency of the power supply-accelerator system.

In addition, inductance values are small (typical value is of 0.4 mH). It means that the primary winding current is high (it may reach a kiloampere and higher). The primary winding voltage can reach 1 kV.

These facts force to insert the circuit for the compensation for the reactive power between the frequency converter and the primary winding of the high voltage transformer.

On fig. 2 the linear equivalent circuit of the high-voltage rectifier together with the circuit of compensation of reactive power is shown.

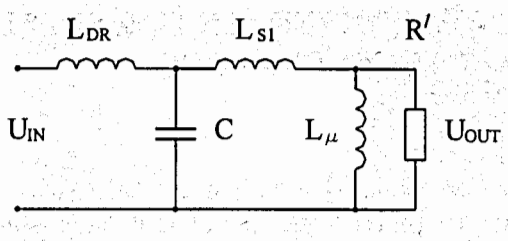

Fig. 2:
L_{S1}- transformer leakage inductance;
L_μ- magnetizing inductance;
R- load resistance reduced to the magnetizing;
L_{DR}, R, C – compensation circuit

The analysis of amplitude-frequency characteristics of an equivalent circuit allows us to define values of parameters of the circuit of compensation (L_{DR}, C). It is obvious, that the given circuit provides maximal coefficient of efficiency if the phase of an input current is equal to zero.

Graphs of amplitude-frequency characteristics of an equivalent circuit are shown on fig. 3.

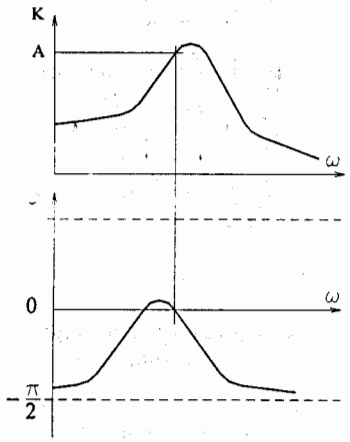

Fig. 3

On the top graph it is the amplitude-frequency characteristic of the circuit, and on bottom - the phase characteristic are shown.

Required value of transfer constant (A) is defined by a necessary a primary winding voltage.

Thus, for a finding values of inductance and capacitor in the circuit of compensation of reactive power we should solve the system of the equations shown below relatively L_{DR} , C. It is necessary to set frequency of the inverter preliminary. The conclusion of these expressions is bulky and not shown here:

$$\begin{cases} \dfrac{k}{\sqrt{(1-T^2\omega^2)^2+(2\xi T\omega)^2}} = \left|\dfrac{U_{OUT}}{U_{IN}}\right| = A \\ \operatorname{arctg}\dfrac{\omega^4 T_1^4+\omega^2(T_2^2-T_1^2-k_1T_1^2)+k_1}{\omega T_2(1-k_1)} = 0 \end{cases}$$

Constants and variables in the given system of the equations can be determined from the expressions shown below.

$$k=\frac{L_{\|}}{L_{DR}} \qquad L_{\|}=\frac{LL_{DR}}{L+L_{DR}} \qquad T=\sqrt{L_{\|}C}$$

$$R=\frac{D^2+M^2}{D} \qquad \xi=\frac{L_{\|}}{2R\sqrt{L_{\|}C}}$$

$$D=\frac{\omega^2 R' L_\mu^2}{(R')^2+\omega^2 L_\mu^2}$$

$$M=\frac{\omega(R')^2(L_\mu+L_S)+\omega^3 L_\mu^2 L_S}{(R')^2+\omega^2 L_\mu^2}$$

$$k_1=\frac{L_{DR}+L}{L_{DR}}$$

$$L=\frac{D^2+M^2}{\omega M} \qquad T_1^2=LC \qquad T_2=L/R$$

FREQENCY CONVERTER CIRCUIT

For operation with such loading has been developed a frequency converter based on IGBT half-bridge modules.

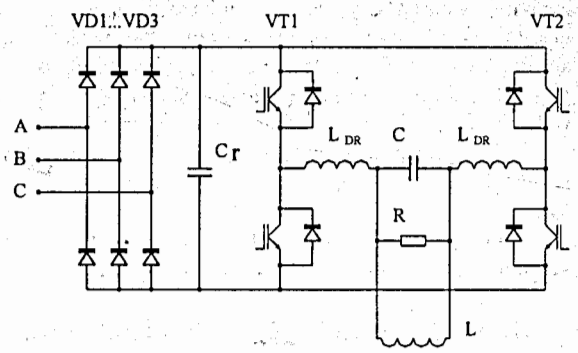

Fig. 4: Simplified power circuitry of converter.
L1, L2, C_P – compensation circuit.

The capacitor bank C_{DC} on the rectifier output composed on film capacitors is installed on the rectifier output. This bank is used for reducing down to acceptable value the overvoltages occurred during reswitching the bridge transistors.

The transistor bridge combines functions of the inverter, output voltage control and also it provides the emergency de-energizing of the accelerator in case of, for example, the high voltage breakdown.

Main Technical Parameters of Converter.

- Accelerator beam power is up to 150 kW;
- For increasing beam power up to 500 kW it is necessary to connect 4 this converters in parallel.
- Coefficient of power efficiency - 95%;

- Output frequency – 400...1000 Hz;
- Range of regulation on the first harmonic of an output voltage of the transistor bridge – 0 ... 400 V.

By the operation principle, the frequency converter belongs to the voltage inverters based on the bridge transformer-free scheme with powerful IJBT modules of half-bridges with built-in inverse diodes. The control of primary winding voltage is realized by the variation of the width of output pulse.

Forms of the voltage and current of the primary winding are close to sinusoidal.

For obtaining the maximum voltage on the accelerator primary winding the resonant frequency of the contour formed by the circuit of compensation for the reactive power and the primary winding of the accelerator should correspond to the operating frequency of the converter.

DESIGN OF CONVERTER

Let us note some important moments to be taken into account when designing and arranging the module: rectifier, capacitor bank C_{DC}, transistor bridge VT1, VT2.

In order to provide the switching of the inverter from the short-circuit mode, one should limit overvoltages occurred at the transistor collectors.

At the moment of transistor switching off, the current stored in unductances L1, L2 moves through inverse diodes to the capacitor bank C_{DC}. On the design inductance of wires (buses) connecting C_{DC} with the bridge the voltage increases jumpingly. The computer simulation shows the already of the order of a microhenry the overvoltage pulse value during switching on exceeds much the admissible collector voltages of the transistor bridge, which is inadmissible.

In order to reduce the design inductances to minimum, the inverter design is based on the plane-parallel buses. Capacitors should have very small stray inductance. Calculations show, that the value of capacity C_{DC} should make not less than 10 mkF/kW of output power.

For the beam power more than 100...150 kW one inverter module is not enough for feeding of accelerator. In this case it are possible to use the circuits of addition of power of several modules. The principle of addition of power is shown on fig. 5.

As it was specified earlier the high-voltage power supply of powerful accelerators of ELV type (ELV-6M and ELV-12) has two HV rectifiers. Each of columns has own primary winding. Similar configuration allows, using the biphase inverter to organize a biphase feed for reduction of high voltage pulsations value.

Four described the modules of inverter through reactors DR1 ... DR8 are connected in pairs in parallel, forming two independent inverters. Outputs of inverters are connected to the primary windings of high-voltage rectifier PW1 and PW2. Master clock generator G makes two sequences of the rectangular pulses. Shift of phases between these pulses makes a quarter of the period.

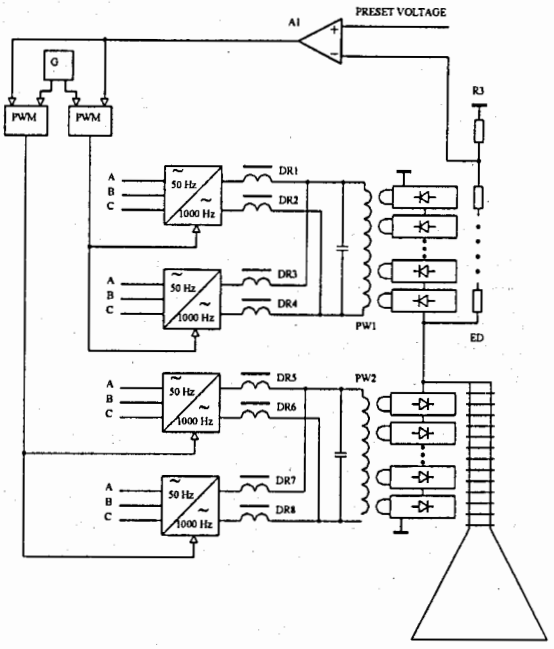

Fig. 5

The energy stabilization system controls the width PWM-signal on an output of the transistor bridge. The loop of a feedback of system includes inverters, high-voltage rectifiers, measuring high-voltage divider ED, the error amplifier A1, pulse-width modulators.

The developed frequency converter was tested together with ELV-12 accelerator for beam power up to 500 kW and has shown high reliability, both at normal operation, and in emergency operation (short circuit on an output of inverter).

If to compare the developed converter with same power electromachine, it is possible to mark, that weight of a transistor converter is tens times less than electromachine one, and its efficiency more than 20% higher in comparing with electromachine one.

Due to small dimensions and weight of a transistor converter all power systems of accelerator are placed in one cabinet. The additional possibilities are opened by simple turning over a wide range frequency of output voltage. The simplicity of the control circuit, high efficiency and convenience of operation allow to hope that the converter will make a worthy competitiveness to the traditional circuits of a power supply of industrial accelerators.

REFERENCES

[1]. Salimov RA, Cherepkov VG, Golubenko JI, Krainov GS, Korabelnikov BM, Kuznetsov SA, Kuksanov NK, Malinin AB, Nemytov PI, Petrov SE, Prudnikov VV, Fadeev SN and Veis ME. Radiat. Phys. and Chem. 2000;57:666.

DEVELOPMENT OF COMPACT CYCLOTRON FOR EXPLOSIVES DETECTION BY NUCLEAR RESONANCE ABSORPTION OF GAMMA-RAYS IN NITROGEN

L.M. Onischenko, Yu.G. Alenitsky, A.A. Glazov, G.A. Karamysheva, D.L. Novikov, E.V. Samsonov, A.S. Vorozhtsov, S.B. Vorozhtsov, N.L. Zaplatin, JINR, Dubna, Russia

Abstract

The inspected object is scanned by a beam of 9.17 MeV gamma-rays, which represents on-resonance flux capable of being absorbed by nitrogen nuclei. The resonance gamma-rays are generated in reaction of the proton capturing by C-13 and the following irradiation of gamma-rays by the appeared N-14 nucleus.

To produce the 1.747 MeV protons the compact isochronous cyclotron with external injection of H^- ions is under consideration. Computer simulation of beam dynamics in such a cyclotron confirms a possibility to produce on the target the proton beam with intensity of some milliamp. The paper describes the main cyclotron parts – injection line, magnetic, acceleration and extraction system.

INTRODUCTION

The maximum cross-section of the resonant 9.17 MeV γ-ray production via $^{13}C(p,\gamma)^{14}N$ reaction is equal 2.1 barn. It occurs at the proton energy 1.747 MeV and the thick target. Reaction yield into 4π is calculated to be $\sim 6\cdot10^{-9}$ γ/proton. Since the life time of the 9.17 MeV level ($5\cdot10^{-18}$ s) is very short compared to ion stopping time (typically $\sim 1\cdot10^{-12}$ s) the emission of γ-ray occurs during the recoil of the exited ^{14}N nucleus, resulting in Doppler-shifting of the γ-ray. At the resonant angle $\theta_R = 80.66^0$ with respect to the proton beam, the nuclear recoil energy losses that occur during emission and absorption of the γ-ray by the ^{14}N nucleus are precisely compensated by the Doppler-shifted energy component [1]. The resonant photons are emitted with axial symmetry relative to the proton beam forming an angular cone of width $\Delta\theta$ centered around the resonant angle θ_R. The gamma-rays resonant absorption crossection for ^{14}N nuclei near the 9.17 MeV level is equal 2.4 barn with the total energy width of the level 128 eV. Hence we need the proton source with intensity of some milliampers with the as small as possible energy spread and the angular divergence [2]. To produce the proton beam with energy 1.747 MeV and with intensity of some milliampers we consider the compact isochronous cyclotron with an external injection of H^{-35}

ions. The full scheme of the γ-rays production is shown in Fig. 1.

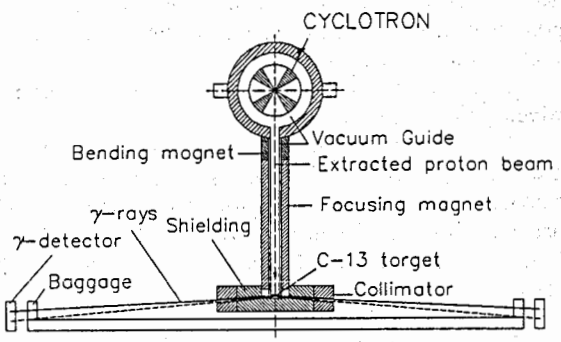

Figure 1: General layout of the explosive detection.

PARAMETERS OF THE CYCLOTRON

Main cyclotron parameters are showed in the following Table 1.

Table 1.

Type of ion		H^-
Injection energy	(keV)	30
Extraction energy	(MeV)	1.8
Average magnetic field	(T)	0.64
Number of sectors		4
Number of dees		2
Betatron frequencies	ν_r, ν_z	1.1, 0.85
Angular span of dees	(°)	45
RF voltage	(kV)	60
Orbital frequency	(MHz)	9.76
Harmonic number		4

The choice of the magnetic field level (0.64 T) is a compromise between the next considerations.

From one side the higher field level has to be chosen to provide the small cyclotron sizes. At the same time the higher field level provides higher space charge limit due to higher axial focusing strength.

From the other side the higher field demands the higher injection energy, hence the higher voltage on the spiral inflector. At the same time the turn separation is smaller at this case and the extraction efficiency goes down.

Main systems of the cyclotron will be described in the papers which will be reported at this conference. Here the short theirs description will be done.

MAGNET

The 4-fold type magnet with all-round yoke is chosen for the cyclotron [3]. The cyclotron vacuum chamber for this design is shaped by the magnet poles and yoke.

Table 2.

Magnet height	89 cm
Magnet outer radius	70 cm
Pole outer radius	35 cm
Final orbit radius	30 cm
Hill field at final radius	1.35 T
Valley field	0.2 T
Number of sectors	4
Hill gap	3 cm
Valley gap	40 cm
Sector angular width	$10\text{-}30^0$
Power consumption	10 kW

Sketch of the magnet is shown in Fig. 2. The dees and spiral inflector are shown schematically at the same picture.

Figure 2: Magnetic structure, inflector, dees, deflector.

In Fig. 3 the plan view of the cyclotron is shown with the particle trajectories [4].

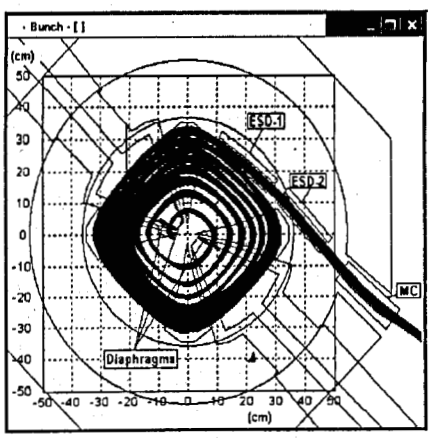

Figure 3: Plan view on cyclotron with extraction system.

ACCELERATION SYSTEM

High frequency system is formed by two resonators, consisting of the two 45-degree dees, which are located in opposite valleys (Fig. 2); of two resonance lines with the systems of feed, the voltage and phase stabilization and control.

The radiofrequency f=39 MHz corresponds to 4^{th} harmonic of the orbit frequency; amplitude of accelerating voltage U=60 kV, peak energy gain per turn $\Delta W=4U$. The dissipated power in each resonator is near 5 kW.

EXTRACTION SYSTEM

The extraction system consists of two electrostatic deflectors (Fig. 3) ESD-1 and ESD-2 with the electric field strength 22 kV/cm in the center of their radial aperture. The voltage on the high-voltage electrode is equal 60 kV. To compensate the beam horizontal defocusing the electrostatic field in deflectors has gradients – 4.6 and – 12.2 kV/cm in ESD-1 and ESD-2, respectively. The electrostatic deflectors are followed by the passive magnet MC (Fig. 3) with the gradient magnetic field. Extraction efficiency calculated to be near 80%.

ION SOURCE

It is supposed to use for the cyclotron the TRIUMF type H^- Volume-Cusp Ion Source produced by DHL (Dehnel Consulting Ltd). This Ion Source will have next parameters: beam energy – 30 keV; beam continuous current – 15 mA. At this beam current the normalized 4 rms emittance is 1.0 mm*mrad. General view of ion source is shown in Fig. 4.

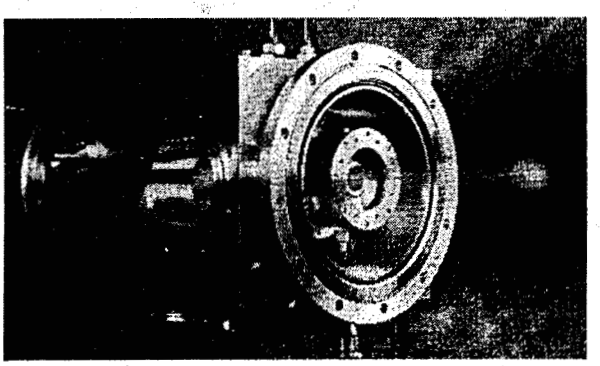

Figure 4: General view of ion source.

INJECTION SYSTEM

The injection system consists of a double-drift beam bunching system, a spiral inflector, beam analysis diagnostics, focusing and adjustment elements [5]. A layout of the injection system is shown schematically in Fig. 5. We plan to use a double-drift buncher design (the buncher gap is 5 mm and the distance between 2 gaps is $3/2\beta\lambda$ (92 mm)) with sinusoidal waveform. The position for the buncher is 0.4 m from the cyclotron median plane.

Quadruple doublet is used for injection line focusing, quadruple field gradient less than 300 Gs/cm, effective length of the quadruples - 10 cm, aperture diameter – 15 cm. The spiral inflector for ion bending from axial to median plane is used. The spiral inflector view is presented in Fig.6. A spiral inflector consists of coaxial, spirally twisted electrostatic deflection plates placed in a magnetic field. The chosen electric field of 24 kV/cm is restricted by breakdown limit. Height of the inflector is limited by cyclotron magnet center design and equal to 25 mm. The 10mm gap between electrodes was chosen to ensure bending of beam with emittance 100 ÷ 150 π mm mrad. The aspect ratio between the width and the spacing of the electrodes is taken equal 2 to avoid the fringe field effect and to tolerate shifts in beam trajectories inside the inflector. Computer modeling confirmed the possibility of high-intensity beam transmission, bunching and bending from axial to median plane with losses less than 10 % at an injection voltage of 30 KeV.

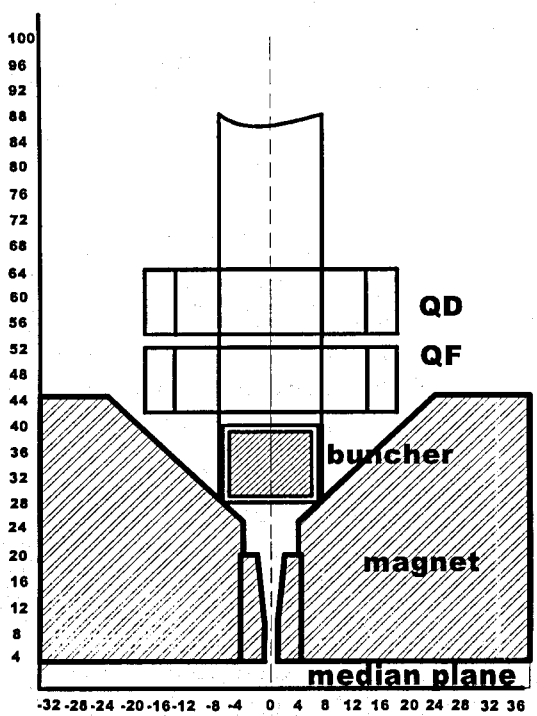

Figure 5: Layout of the injection system.

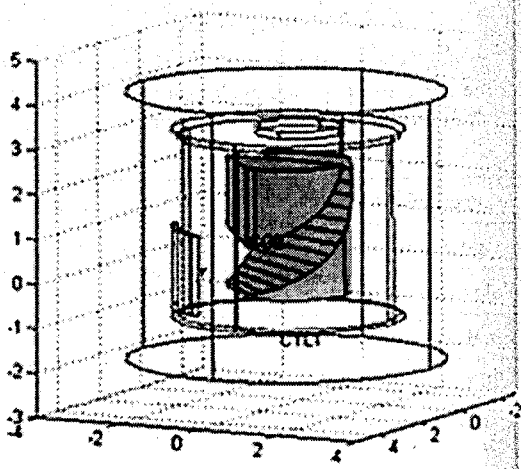

Figure 6: The spiral inflector.

REFERENCES

[1] D. Vartsky et al, A method for Detection Explosives based on Nuclear Resonance Absorp of Gamma-rays in ^{14}N, SPIE Conference Substance Detection Systems, Proc. SPIE Vol. 2 Insbruck, Austria, October 1993, p. 307 – 313.

[2] R.E. Morgado et al, The effects of proton b quality on the production of gamma-rays for nuc resonance absorption in nitrogen, ibid. 1 p. 503 – 513.

[3] A.S. Vorozhtsov, S.B. Vorozhtsov, Magnetic Simulation in the Customs Cyclotron, this confere

[4] E.V. Samsonov, L.M. Onischenko, Computatio beam dynamics with space charge in com cyclotron on energy 1.8 MeV, this conference.

[5] G.A. Karamysheva, Injection system of cust cyclotron, this conference.

PROJECT OF THE U400R CYCLOTRON AT THE FLNR JINR

Yu. Ts. Oganessian, G.G. Gulbekyan, B.N. Gikal, I.V. Kalagin, S.L. Bogomolov, I.V. Kolesov, G.N. Ivanov, V.V. Bekhterev, M.V. Khabarov, O.N. Borisov, I.A. Ivanenko, J. Franko, S. Kralek*
Flerov Laboratory of Nuclear Reaction, Joint Institute for Nuclear Research,
Dubna, Moscow reg., 141980 Russia
*DNPT FEI Slovakian Technical University Bratislava, Slovakia

Abstract

The U400 cyclotron diameter is 4 m, the K-factor is 625. The U400 has been put in operation since 1978. The stripping foil method is used to extract ion beams. The axial injection system with the ECR ion source and two bunchers (Sine and Line types) was created in the period of 1996-1998.

At present time, some cyclotron parameters can be improved. First of all it is concern of the total acceleration efficiency and possibility to vary ion energy fluently at factor 5 for every mass to charge ratio A/Z by means of changing the RF frequency and the magnetic field. The width of ion energy region will be from 0.8 to 27 MeV/nucleon. The project of U400 modernization intends decreasing the magnetic field level at the cyclotron center from 1.93÷2.1T to 0.8÷1.8T. One intends changing the construction of the axial injection. For ion extraction out of the U400, both the stripping foil and deflector methods are considered. Also, the project intends changing the U400 vacuum, RF and power supply systems.

INTRODUCTION

The isochronous U400 cyclotron has been in operation since 1978 [1]. Today, the main accelerating particle at U400 is the rare $_{48}Ca$ isotope [2] The intensity of $_{48}Ca^{+5}$ ions with energy of 260 MeV at extraction radius is about 4.3 pμA (21.5 μA). After extraction by means of the stripping foil at charge exchange rate of $Z_{out}/Z_{in}=3$, the intensity of the main spectrum line of $_{48}Ca^{+18}$, that is mainly used for physical experiments, is about 1.4 pμA (25μA). The U400 allows us to vary ion energy fluently (without decreasing the ion intensity at U400 output) at about 8% around the standard energy for given A/Z. This variation is carried out by means of changing the stripping foil position, or changing the RF frequency and the magnetic field level. Nevertheless, for some experiments the depth of the fluent energy variation is not enough.

Modernization has been suggested to improve the cyclotron parameters. The cyclotron parameters before (U400) and after (U400R) the modernization are shown in Tab.1.

The aims of the modernization are:

1. Decreasing the magnetic field level at the cyclotron center from the region of 1.93÷2.1 T to 0.8÷1.8 T, that allows us to decrease the electrical power of the U400R main coil power supply in four times.
2. Providing the fluent ion energy variation at factor 5 for every mass to charge ratio A/Z at accuracy of $\Delta E/E=5\cdot10^{-3}$;
3. Increasing the intensity of accelerated ions of rare stable isotopes at factor 3.

Table 1:

	U400	U400R
Parameters	**Value/Name**	
Electrical power of magnet power supply system	850 kW	200 kW
The magnetic field level in the magnet center	1.93÷2.1 T	0.8÷1.8 T
The hill angular width at the external radius	42°	43.7°
The hill gap at the external radius	42 mm	56 mm
The valley gap	300 mm	300 mm
The number of trim coils	8, radial 1, azimutal	14, radial 4, azimutal
The number of dees	2	2
The dee voltage (amplitude)	80 kV	80 kV
The A/Z range	5÷12	4÷12
The frequency range	5.42÷12.2 MHz	5.42÷12.2 MHz
Harmonic modes	2	2÷6
The ultimate extraction radius	1.72 m	1.8 m
K- factor	305÷625	100÷506
Vacuum level	$(1\div5)\cdot10^{-7}$ Top	$(1\div2)\cdot10^{-7}$ Top
Ion extraction method	Stripping foil	Stripping foil Deflector
Number of directions for ion extraction	2	2

MODERNIZATION OF MAGNETIC SYSTEM

As it was mentioned above, the modernization project intends to decrease the U400 magnetic field level from the region of 1.93÷2.1 T to 0.8÷1.8 T. Construction of the main magnet and the main coils will not be

changed, but the cyclotron hills and the trim coils will be modernized.

The working diagram and energy range of possible accelerated ions for the U400R are shown in Fig. 1 and Fig. 2.

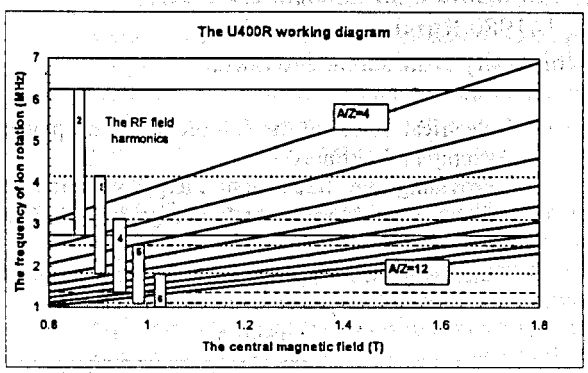

Fig. 1: The U400R working diagram

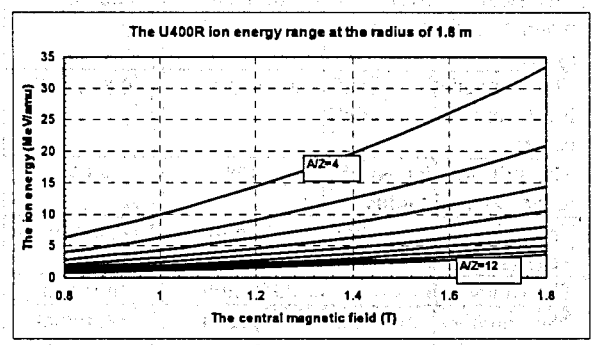

Fig. 2: The energy range of possible accelerated ions

Realization of the diagram requires to create isochronous magnetic field up to the radius of 1.8 m. For the purposes, the 3-D computer model of the U400 magnet system was created in the "Syntez" NIIEFA, St-Peterburg and magnetic field calculations has been carried out. On the base of the model, step-by-step optimization of the magnetic structure and construction of trim coils has been made. The final construction of the U400R magnetic system includes plate hills with azimutal shimmes and chamfers of 45°(50×50 mm×mm) at the outer radius. The trim coils will be situated under the hills in the gap of 28 mm. The total power of the trim coil power supplies will be about 20 kW.

MODERNIZATION OF AXIAL INJECTION SYSTEM

The beginning modernization of the U400 axial injection that has been undertaken in 2002 included sharp shortening the injection canal horizontal part [2]. As the result, the distance from the ECR to the AM90 bending magnet became equal to 730 mm (Fig. 3). The changes allows us to increase the $_{48}Ca^{+18}$ ion intensity at the U400 output from 0.9 to 1.4 pμA. Further modernization intends decreasing ion losses by means of increasing the SL solenoid inner diameter from 68 to 100 mm and the AM90 banding magnet horizontal aperture from 70 to 94 mm.

In according to calculation results, decreasing the U400 magnetic field demands to install three S1, S2,S3 solenoids in the top part of the channel and one extra S4 solenoid in the bottom part to provide ion focusing at the inflector input. The S1, S2, S3 solenoids will have total magnetic field of 0.2 T at the total effective length of 812 mm. The S4 will have the magnetic field of 0.45 T at the effective length of 134 mm.

In the future, we are planning to search possibility increasing the injection voltage from the range of 13÷20 kV to 30÷50 kV. As we estimated, the changes can give us increasing the U400R accelerating efficiency in 1.5÷2 times, it is particularly important for $_{48}Ca$ ions.

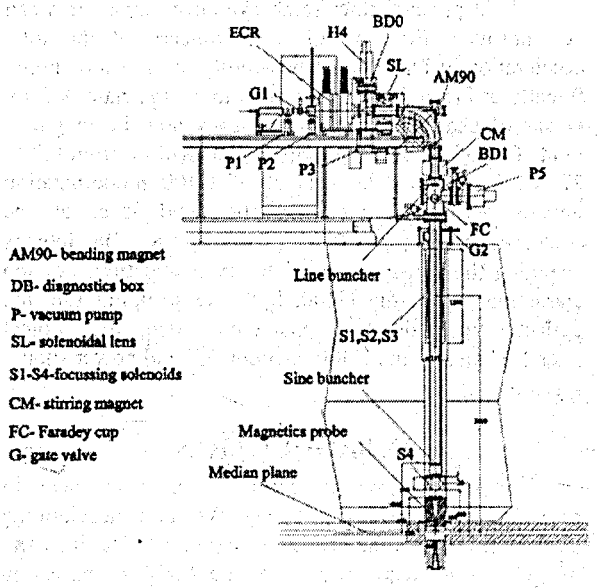

Fig. 3: The U400R axial injection

MODERNIZATION OF ION EXTRACTION SYSTEM

To extract ions out of the U400R we suppose to use two ways: electrostatic deflector and stripping foil method. To estimate the extraction possibility, the numerical calculation has been carried out for ions with A/Z=4÷12. In the calculations, the magnetic field maps were used. The maps were calculated in the "Syntez" NIIEFA, St-Peterburg, the calculated results are in good accordance with experimental data.

The results of calculation the ion trajectories for the electrostatic deflector (ESD) are shown in Fig. 4. It was supposed, that the average radius of the final orbit is Rav=180 cm. To deflect ion beam the deflector with the asimutal longitude of 40° (Θ=70°÷110°), situated in the vale V1 is used. The strength of the ESD electrical field is not more than 100 kV/cm. The calculation results give us two directions of extracted ions with A/Z=4 at maximal

energy: with the angle between the vale axis and the extraction trajectory of ≈52° for the ion energy of Wmax=22.4 MeV/amu at the ESD field strength of Edef=94 kV/cm and with the angle of ≈83° for Wmax=25.55 MeV/amu and Edef=98 kV/cm. In the method, providing the extraction efficiency up to 80% requires the magnetic field stability at the level of $\Delta B/B=5\cdot10^{-6}$, the RF amplitude stability of $\Delta U/U=2\cdot10^{-4}$. Besides that it is necessary or to provide the beam bunching in the faze of 5° or using the flat-top system to decrease the ion momentum spread.

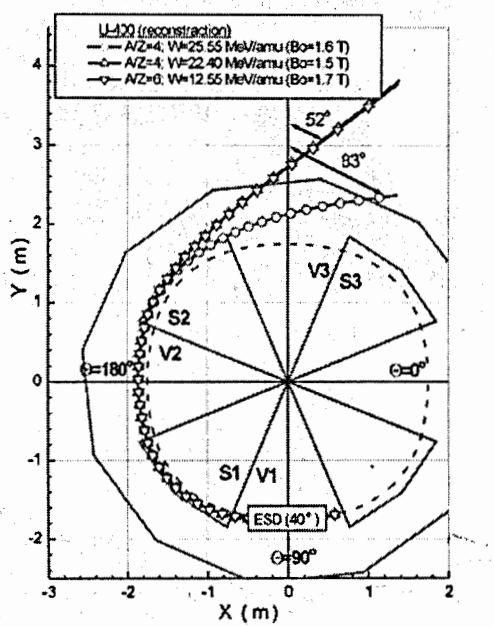

Fig. 4: The scheme of the ion beam extraction by deflector in two extraction regimes

The results of numerical simulation of ion extraction by the stripping foil method shown in Fig. 5. The calculations have been carried out for ions with A/Z=8, at the magnetic field levels of Bo=0.8÷1.2÷1.8 T and the charge exchange coefficients of Z_{out}/Z_{in}=2,0÷2,5÷3,0÷3,5. The beam emittances after the stripping foil taken equal to E_x=5÷10 π mm×mrad; E_z=4 π mm×mrad at the energy spread of δW=1.5%. After analyzing of the results, we decided to extract ions by means of two separate foil probes. The first probe will extract ions with Z_{out}/Z_{in}=2,5÷3,0÷3,5 and the second one will extract ions with Z_{out}/Z_{in}=2,0÷2.5. Correspondingly, the total number of the foil probes to extract ions in two opposite directions will be 4 (2+2) pieces. The extracted efficiency of the method depends on the ion type, ion energy and extracted line in extracted ion spectrum. For heavy elements the efficiency is not more than 40%.

Both the methods allow us to extract ions in the directions of existing ion transport channels.

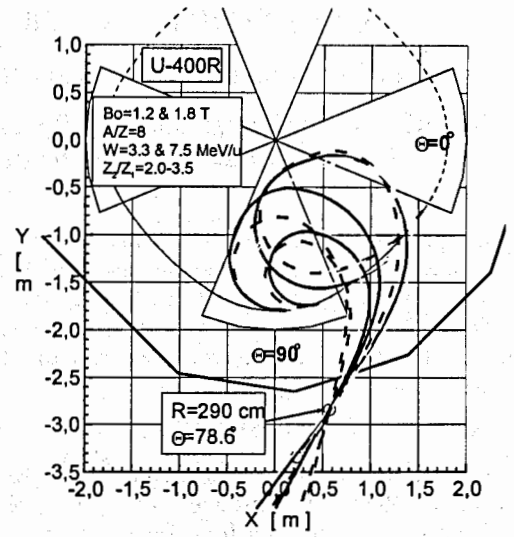

Fig. 5: The scheme of the ion beam extraction by stripping foils with two separate foil probes. For B0=1,2÷1,8 T, W=3,3÷7,5 MeV/u, Z2/Z1=2÷3,5

MODERNIZATION OF RF SYSTEM

The RF system of U400R will consists of two RF generators that will excite two separated RF dee resonators. The RF resonators will be made from iron with copper coating to decrease the outgasing rate from the vacuum surface.

MODERNIZATION OF VACUUM SYSTEM

The modernization of vacuum system will include changing five diffusion pumps VA-8-7 with N_2 pumping rate of Q=4250 l/s each to five cryopumps with Q=3000 l/s each and two turbopumps with 1900 l/s each. In addition the materials of the cyclotron vacuum chamber and RF resonators will be changed to decrease their outgasing rate. The given changes allow us to improve vacuum in the cyclotron chamber from $(1.5\div2)\times10^{-7}$ Torr to 10^{-7} Torr.

REFERENCES

[1]. Gulbekian G. and CYCLOTRONS Group, "Status of the FLNR JINR Heavy Ion Cyclotrons" in Proc. of 14th Int. Conf. On Cyclotrons and Their Applications, Cape Town, South Africa, p. 95-98,1995

[2]. Yu. Ts. Oganessian, G.G. Gulbekyan, B.N. Gikal, I.V. Kalagin et al. "STATUS REPORT OF THE U400 CYCLOTRON AT THE FLNR JINR", in Proc. of APAC2004 Int. Conf, Gyeongju, Korea, 2004, to be published

CYCLOTRON RIC-30: 10 YEARS OF THE OPERATION

Eliseev I.A., Kaplun V.G., Rogozev B.I., Stepanov A.V., Suzikov A.G., Jagol'nikov S.V.

MD RF Second Central Scientific Research Institute, SPA "V.G. Khlopin Radium Institute ", SPA " D.V.Efremov Scientific Research Institute of Electrophysical Equipment"

Abstract

An operating experience of cyclotron RIC 30 is represented. Its sufficient reliability and possibility of operation in the regime of radionuclides production is confirmed. The basic unresolved question is obtaining the current of external and internal beams, close to the certified values.

CYCLOTRON DESCRIPTION

Cyclotron RIC-30 (development of SPA" D.V.Efremov Scientific Research Institute of Electrophysical Equipment" is in operation from 1993. Accelerator it is placed in the specially designed building, in rooms of which are established basic, general technical and accessory equipment (Fig. 2), including: cyclotron RIC-30 (Fig. 1); control system of accelerator; the extraction system and transport of beam to the remote targets with the beam extraction into the atmosphere and vacuum chamber; the set of internal target devices and system for the installation of external targets; means and devices for providing the radiation safety, monitoring-measuring equipment, the means of storage and information processing, other technical equipment. Accelerator RIC-30 - the isochronous sector-focusing one-dee cyclotron with pot electromagnet is intended [1] for the production of radionuclides on the internal and external beams with the aid of the appropriate target devices. The proposed and achieved characteristics of the cyclotron are given in Table 1.

Table 1:

	Proposed	Achieved
Current External (mkA) Internal (mkA)	 200 1000-500	 60 (5-10) 500(250)
Proton energy (MeV)	28	28 (28,5)
RF frequency (MHz)	17,6	17,5(17,4)
Dee voltage (kV)	50	50
Magnetic field (T)	1.2	1.2
Current of main coil (A)	480	480
Extraction radius (mm)	650	650
Deflector angular width (°)	40	40
Deflector voltage (kV)	65	60
Pressure in vacuum chamber (torr).	$2\ 10^{-5}$	$2\ 10^{-5}$
Power consumption (kW)	300	300 (200-250)

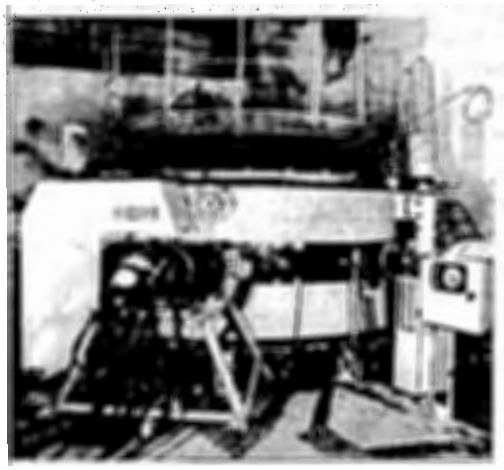

Figure 1: Cyclotron RIC-30

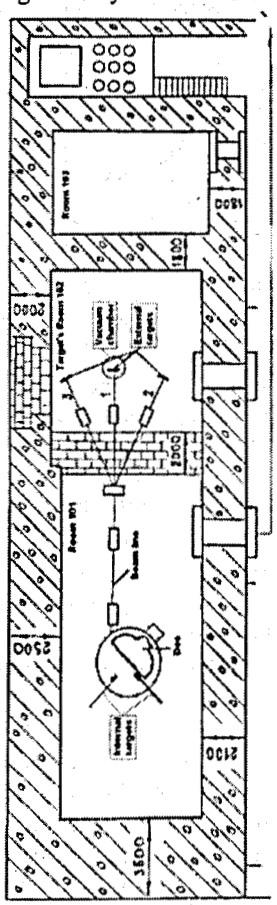

Figure 2: Plan view of the RIC-30 arrangement

Structure of the magnetic field of cyclotron - four-sector with the weak spirally. Four concentric coils with the independent supply are used for the precise fine

adjustment of field. Azimuthal magnetic bumps are corrected by two groups of the harmonic coils.

The ion source of slit type with the hot cathode is introduced into the accelerating chamber vertically through the hole in pole.

The diagnostic equipment of cyclotron includes 3 probes (basic, in dee and in deflector), the collimators and sensors of the beam profile, and also Faraday's cylinders, which provide control of the parameters of internal and external beams. Channel of beam extraction - electrostatic.

To fulfill the program of applied-scientific studies, mainly, on the study of the yields of radionuclides in different nuclear reactions and the operating time of the isotopes of scientific and technical and medical purpose, first of all with Co-57, GA-67, Cd-109, Tl-201, the work on equipping of cyclotron additionally by the internal target, made on the base of main probe, was carried out. The calculated approach angle of beam to the fixed water-cooled target is -5°. In this case the length of beam trace is 40 mm, the width of track ~ 6... 8 mm is determined by the vertical size of the beam (see Fig. 3). Target is located in the valley of magnetic system, i.e., in the region of the maximum value of a radius of the orbit of protons. Target equipment ensures the automated (input-output) and extraction of the target. In the initial stages of operation the current of internal beam did not exceed 50 mkA, which proved to be insufficient for the implementation of the program of the radionuclides production. In the course of studies it was revealed, that the limitations of current were caused by the design features of dee, which give to it insufficient high quality factor, i.e. to the complexity of obtaining high accelerating voltages and to the significant losses of beam on initial radii. In connection with this the solution about the replacement of dee was accepted. The project of new dee with the aperture 50 mm with the increased quality factor and by the improved water cooling was made with the help of the colleagues from Dzelepov Laboratory of JINR. As a result the current of internal beam was increased to 250 mkA with duty factor 2.5. In this case the task of reduction in the power density on the target, up to the tolerance levels, arose. For its solution on the cyclotron RIC -30 for the first time was realized vertical scanning of the beam [3] due to the variable radial component of magnetic field, obtained by supplying the harmonic current to the concentric winding, located in the region of target alignment. An increase in the uniformity of the power density of beam on the target in the vertical plane is achieved by the selection of phase of scanning voltages relative to the phase of accelerating voltage. Radiography of standard beam trace on internal target during the switched on regime of scanning is given in fig. 4. The dependence of a relative increase in the dimensions of beam trace on the value of current of scanning is represented in fig. 5. The operating range of the currents of scanning lies within the limits 6.0 – 9.5 A.

As a result of the introduction of thee/conditions of the scanning beam regime the dissipated power on the internal target was increased to ~5.5 kW.

For expanding the test possibilities of cyclotron, first of all, with an increase in the beam current in more than 250 mkA was designed and prepared the second target, installed on the place of deflector probe. A basic difference in the second target – increasing to ~ 7 kW dissipated power, which makes it possible to carry the radionuclides production with the current up to 300 mkA.

At present the losses of beam on initial radii of acceleration (to 170 mm), lead to the significant warming-up of the central region. In connection with this the attempts to increase the current of internal beam to the proposed value of about 500 mkA lead to the development of breakdown phenomena.

For the purpose of the optimization of the electric field structure in the central region and to decrease of losses SPA" D.V.Efremov Scientific Research Institute of Electrophysical Equipment" was carried out the calculation of the dynamics of particle motion in the central region and formulated recommendations regarding the correction of field due to the special electrodes in the form of cover plates to the dee lips. However, preliminary tests did not yield positive results.

While performing of setup work by developer the current of external beam up to 10 μA was obtained. In this case the coefficient of extraction composed less than ~10%, which led, if to increase internal current, to the significant warming-up of deflector and to the development of breakdowns. Tuning of the extraction regime by the correction of deflector position and change of the currents in harmonic coils did not lead to the desired result.

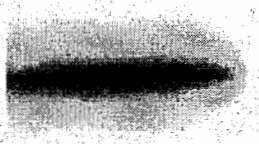

Figure 3: Radiography of beam on the target without the vertical scanning

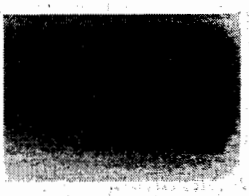

Figure 4: Radiography of beam on the target with the vertical scanning

In the course of conducting the tests on cyclotron RIC-30 the number of the deficiencies, which hamper its operation was revealed.

1. Power of the cooling system of cyclotron is insufficient for the maintenance in the summer time of the operating temperature of the heat-transfer agent of internal outline within the permissible limits, which significantly limits the operational capabilities of cyclotron.

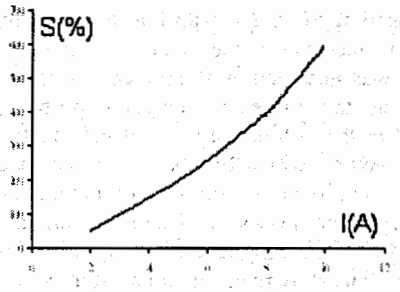

Figure. 5: Dependence S of a relative increase in the area of beam trace versus the current I of scanning

The connection of the cooling system of the electro and RF devices to the external cooling circuit of cyclotron, led to the disturbance of heat withdrawal because of the precipitation of salts and suspensions in the zones of heat exchange and the failure of the elements of radio-electronic equipment. In connection with this the alteration of the cooling system of these devices by salt-free water was required.

2. Possibility of an increase in the internal current due to the decrease of duty factor was limited due to the development of breakdown phenomena as a result of the excessive heating of the walls of resonator from RF losses and forming the local region insufficient high vacuum. Vacuum pumps, installed at the maximum distance from the position of resonator, do not ensure effective evacuation from this region. The installation of additional pump in immediate proximity of the resonator made it possible to solve this problem.

3. Realized regime of the work of the oscillator tubes (tetrode GU-92A - penultimate cascade and triode GU-66'A - the final stage) of power-supply RF system leads to the high currents of rest and as consequence to the excessive energy consumption (according to our estimation - 30 kW). In connection with this question the modernization of high-frequency generator is examined.

4. Elements of the tanks for cooling the lamps of the terminal and penultimate cascades of RF supply, which are located under the potential 10 kV and 6 kV, in view of the special features of their design concept are subjected to intensive electrochemical destruction, which contributes to the appearance of sudden flows of water and to the failure of lamps.

Radiological Situation.

In the course of operating the cyclotron the system of providing radiation safety, developed at the stage of design, provides for the following basic forms of radiation monitoring:

• the operational monitoring of the rate of the neutrons dose and gamma-radiation, surface pollution by in β-active radionuclides, the volumetric aerosol activity of air and volumetric activity of water of the internal cooling circuit of cyclotron;

•the stationary monitoring of the rate of the dose of gamma-radiation and rate of the dose of neutrons in the technological rooms (hall of cyclotron, halls of peripheral target devices);

•individual personnel monitoring.

The results of radiation monitoring, obtained in the course cyclotron running, for the parameters of beam given above, give the following fundamental characteristics of radiological situation and dose loads of operational personnel during the operation RIC-30:

1. Dose characteristics of the fields of neutron and gamma-radiation outside the biological protection do not exceed background values.

2. During the work RIC-30 on internal beam (standard regime) in the hall the rate of the dose of neutrons is from 50 to 150 mZv/h, and the rate of the dose of gamma-radiation - from 30 to 60 mZv/h.

3. In 0.5 hours after the disconnection of cyclotron the rate of the dose of gamma-radiation in the hall is from 10 to 50 mkZv/h in the places of performing work on the prompt service of the systems of cyclotron (target devices, RF system, the source of ions). The values of the rate of the dose of gamma-radiation from the induced activity in vacuum chamber of cyclotron after prolonged (> month) stoppage RIC-30 lie in the range from 0,5 to 10 mZv/h.

4. Average value of the annual individual dose of personnel in the last 5 years composes ~3 mZv, which indicates a sufficient level of providing radiation safety during the operation of cyclotron.

Operational Indices.

yclotron RIC-30 is characterized by a comparatively small energy consumption. In the operating mode on internal beam the energy consumption does not exceed 250 kW·h. The indices of average annual operating time in the last 5 years are represented in Table 2.

Table 2:

Years	1999	2000	20001	2002	2003
Working time (h)	1520	1850	1710	1930	2150

As a whole, work experience on the cyclotron RIC-30 showed its sufficient reliability and possibility of operation in the regime of radionuclides production. Work on an increase in the internal beam current to 500 mkA with a simultaneous increase in the power of target is planned. Obtaining the external beam current, close to the proposed value, remains the basic unresolved question.

REFERENCES

[1] Design parameters of radioisotope cyclotron RIC. Proceedings of All-Union Conference on the charged particle accelerators. JINR, Dubna, 1979.

[2] Cyclotron RIC-30. Technical documentation. 1986.

[3] Method of increasing the reliability of target. Patent №64675 from 25.07.77.

[4] State of works on the cyclotron RIC-30. Proceedings of 10th International Conferences on the Application of Charged Particle Accelerators in the Industry and Medicine. S- Petersburg, 2001.

DYNAMICAL PROPERTIES OF THE ELECTROMAGNETIC FIELD OF THE CUSTOMS CYCLOTRON

S.B.Vorozhtsov, E.E.Perepelkin, A.S.Vorozhtsov JINR, Dubna, Russia

Abstract

The compact isochronous cyclotron is considered as a source of 1.75 MeV protons for detection of explosives using the gamma–ray resonant absorption technique.

Dynamical properties of the so-called Customs Cyclotron magnetic and acceleration fields were estimated analytically and digitally for the set of ion closed equilibrium orbits and by computer simulation of the beam acceleration process.

The acceleration of the injected bunched beam was attempted first. Axial beam profile shows that no axial losses are visible with axial aperture in the low intensity limit. But the final beam quality does not completely meet the requirements.

The results of the space-charge dominated beam acceleration revealed the axial losses. The transmission at ~5 mA injected beam intensity is less than ~30% making ~1.5 mA in the output beam only. Calculation of the 30 mA CW beam motion through the cyclotron gave a ~6 mA beam accepted in the acceleration regime. Several methods to improve the quality of the output beam were proposed.

INTRODUCTION

Requirements to the output beam [1] are summarized in Table 1.

Table 1: Required output beam parameters

Parameter	Value	Comments
Type of emerging particles	Proton	
Peak beam current	40mA	
Macro pulse width	Variable	
Pulse repetition rate	Variable	
Duty factor	25%	
Average beam current	> 10 mA	> $6.2 \cdot 10^{16}$ pps
Mean beam energy	1.747 MeV	
Energy spread	< 2 keV	
Beam spot at the target	10 mm^2	
Divergence at target	3 mrad	

The compact cyclotron, shown in Fig. 1, was selected to fulfill the requirements.

Dynamical properties of the cyclotron magnetic [2] and acceleration fields were estimated analytically and digitally for the set of ion closed equilibrium orbits (EO) and by computer simulation of the beam acceleration process. At the initial stage of the study, an analytical approximation of the spatial electrical field in the Dee-anti-Dee structure was assumed. The 3D electrical field simulation was provided for the further calculation (see Fig. 2).

Given the above mentioned marginal requirement for the beam intensity and quality, H^- ions were selected for acceleration in the cyclotron aiming at the high efficiency extraction either by stripping at the 1st stage or by ESD (Electrostatic Deflector) attempting to meet the output beam specifications.

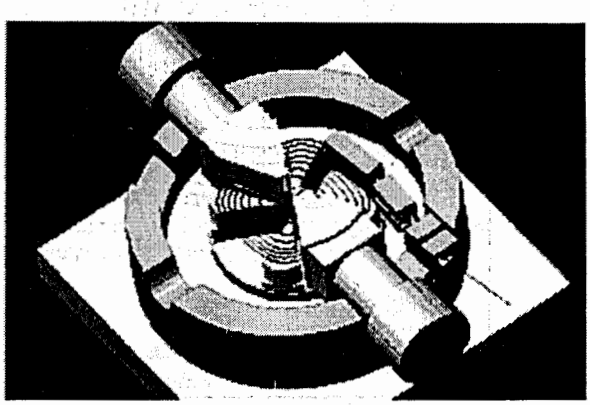

Figure 1: Cyclotron with the Upper Part of the Magnet Removed.

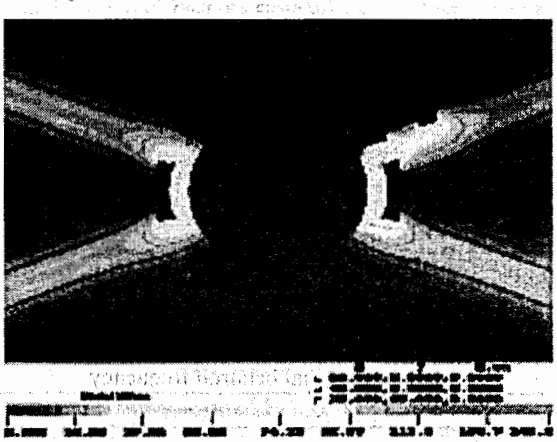

Figure 2: Central Region Acceleration Field Distribution.

EQUILIBRIUM ORBIT PROPERTIES

Main Acceleration Radial Region

Assuming 60 kV dee voltage amplitude with two ~45° dee structure and h_{rf}=4 acceleration mode harmonic, one can estimate the maximal energy gain per turn ~ 240 keV. Injecting H^- ions with energy ~ 30 keV, the energy of the beam after passing the 1st acceleration gap would be ~ 90 keV. Fig. 3 shows several EOs starting from the EO with the energy = 67 keV (somewhere inside the 1st acceleration gap) with the step 240 keV and the final orbit with energy = 1.747 MeV.

So, Fig. 3 depicts an accelerator turn structure in the case of maximal energy gain per turn.

Fig. 4 and Fig. 5 show particle betatron frequencies for the so-called "smooth" simulated magnetic field in the whole radial range 6 ÷ 29 cm.

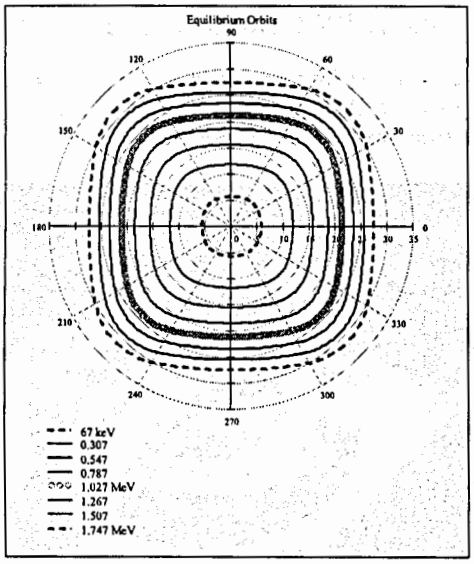

Figure 3: Closed Equilibrium orbits.

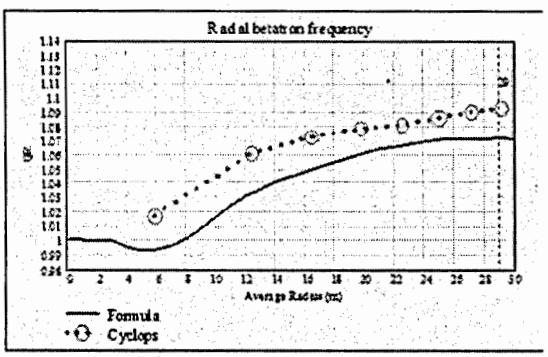

Figure 4: Radial betatron frequency.

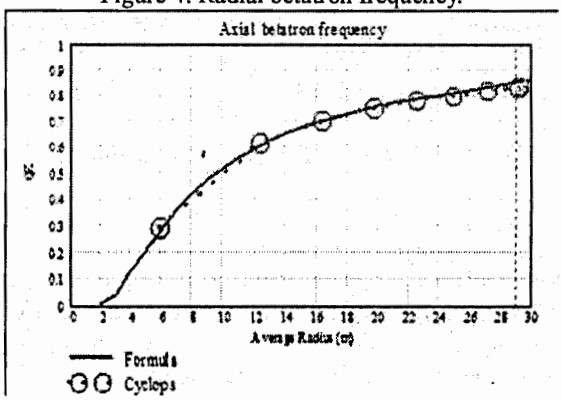

Figure 5: Axial betatron frequency.

The axial betatron frequency Q_z is equal to 0.3 at 1st EO and is greater than 0.5 at the rest of the acceleration range, which is close to the focusing condition of the separated sector magnet machine. No crossing of the dangerous resonances occurs during the acceleration. Orbital frequency differs from the reference value 9.7462 MHz no more than by ~ 15 kHz, which is quite sufficient for isochronous acceleration of the beam. The obtained result means that the average magnetic field is an isochronous one within the tolerance of ~ 1 mT.

BUNCHED BEAM ACCELERATION

Checking dynamical properties of the magnetic field at EOs is not sufficient for the full investigation. So, acceleration simulation was attempted. In Table 2 characteristic beam dimensions (2σ, i.e. 2 standard deviations of the particle distributions) are given.

The injected beam has rather arbitrary parameters defined by the emittance matching, since at that moment no information of the beam coming from inflector exit was available. No axial losses are visible with axial aperture of the cyclotron = 30mm (air gap between sectors).

The final beam parameters are also shown in Table 1. It is evident that the output beam quality does not completely meet the requirements formulated in Table 1, and some additional "gymnastics" with the beam should be performed either inside or after extraction outside cyclotron.

Table 1 Beam parameters.

Motion	Parameter	Initial	Final
Radial	Displacement (mm)	8	5
	Momentum spread (mrad)	50	16
	Emittance (π·mm·mrad)	100	
Axial	Displacement (mm)	4	4
	Momentum spread (mrad)	29	5
	Emittance (π·mm·mrad)	100	
Longitudinal	RF phase range (° RF)	14	4
	Energy spread (keV)	2	11

CONTINUOUS INJECTED BEAM

with the space-charge effects included was performed by new CBDA code, recently announced in [3].

The high-intensity beam self field leads to fattening of the beam, and under certain conditions (high particle volume density) would cause axial losses of ions, in particular at the low energy region. The particle-to-particle method with the field experienced by each macro-particle is the sum of the field of all other macro-particles at the position of the given macro-particle was used for the self-field calculations.

The initial beam emittance coming out of the inflector [4] was presented by the coordinates and velocity components and energy of the particles.

Calculation of the beam motion through the cyclotron is shown in Fig.6. The axial losses, which are ~66% of the

total intensity, are marked by black color, radial losses of ~14% – by violet making in total ~80% of lost particles with only ~20% being accepted in the acceleration regime, which corresponds to ~6 mA under hypothetical CW injected beam of 30 mA.

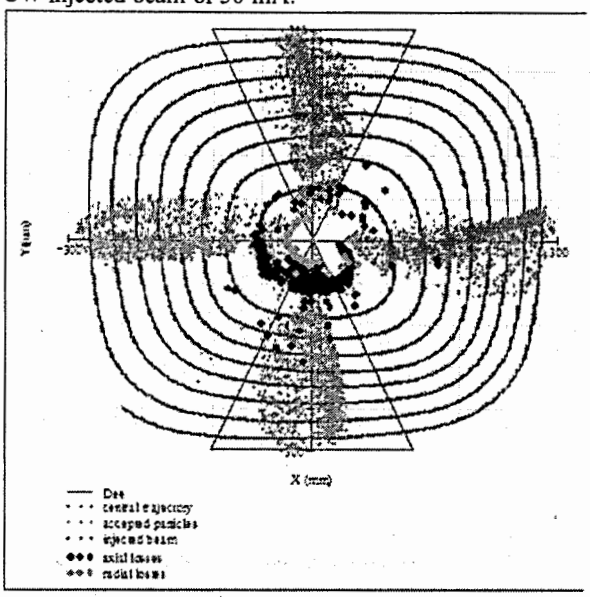

Figure 6: Continuous beam injection and acceleration.

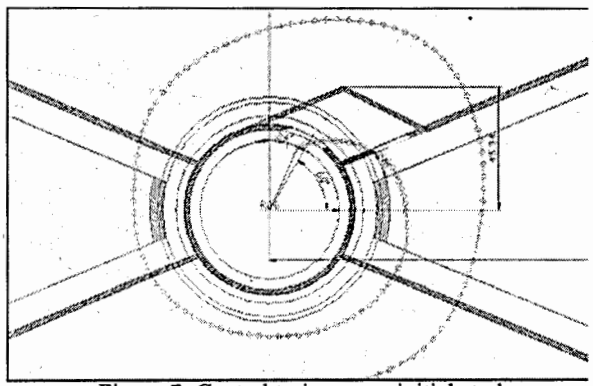

Figure 7: Central trajectory – initial study.

ELECTRICAL FIELD ANALYSIS

Acceleration field map in the central region of the cyclotron, shown in Fig. 2, was used in the orbit centering process when injecting the beam from the spiral inflector to the acceptance area of the 1st cyclotron orbits (Fig. 7).

Electrostatic field distributions in the ESD deflectors was simulated by the MERMAID 3D code and applied for the beam extraction process (see Fig. 8).

OUTPUT BEAM QUALITY

Rather large energy spread in the final beam is of primary concern. The remedy would be:

- Flat topping with longitudinal space charge compensation. But it looks complicated and not efficient in this energy range.
- Energy degrader at the exit. Factor of ~ 10 can be obtained in the energy spread improvement

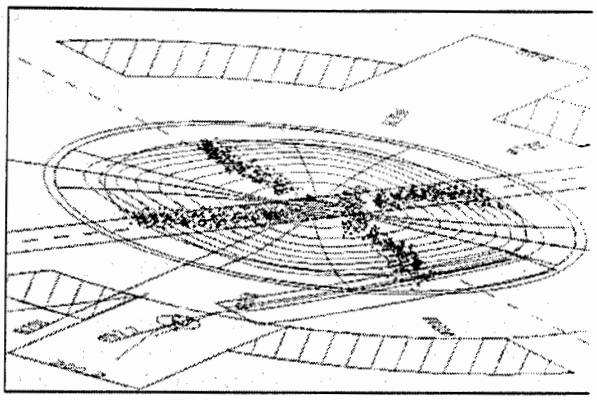

Figure 8: Extraction by ESD. 60 kV, aperture=21 mm.

- Debuncher at the extracted beam
- Cooling ring to inject the cyclotron beam in. it looks promising and presently is under investigation.

CONCLUSIONS

- Main parameters of the cyclotron related to the beam acceleration were selected.
- Dynamical properties of the magnetic and acceleration field, assessed at the equilibrium orbits and by simulation of the ion acceleration process, were found satisfactory.
- Preliminary estimation of the beam intensity at the final radius taking into account the space charge effects gave ~ 1.5 mA in the best quality case and ~ 5 mA otherwise.
- Initial analysis of the beam transport through the spiral inflector, central region and electrostatic deflector was performed.
- More scrutinized investigation of the beam dynamics with the space charge is presented elsewhere [5].

REFERENCES

[1] V.A.Mashinin et al. Review of the Possibilities of Gamma-Resonance method of HE Detection.

[2] A.S.Vorozhtsov, S.B.Vorozhtsov. Magnetic Field Simulation in the Customs Cyclotron. This conference.

[3] E.E. Perepelkin, S.B. Vorozhtsov, A.S. Vorozhtsov. New features of the Cyclotron Beam Dynamics Analysis (CBDA) code. Internal report, Belgrade, March 2004.

[4] G.A.Karamysheva. Injection Line for Customs Cyclotron. This conference.

[5] E.V.Samsonov, L.M.Onischenko. Computation of Beam Dynamics with Space Charge in Compact Cyclotron on Energy ~1.8 MeV. This conference.

MAGNETIC FIELD SIMULATION IN THE CUSTOMS CYCLOTRON

A.S. Vorozhtsov, S.B. Vorozhtsov, JINR, Dubna, Russia

Abstract

The compact isochronous cyclotron is considered as a source of 1.747 MeV protons (H-ions) for the detection of explosives using gamma–ray resonant absorption technique.

Selection of the so called Customs Cyclotron magnetic system parameters and 3D magnetic field simulation are presented in the report. The major input parameters for selecting magnetic structure were the final H^- ion energy and the final average radius ~30cm. The beam axial size defines the minimum available axial aperture comprised by the axial air gap between the sector = 30mm. The idea was to provide the maximum axial betatron oscillation frequency > 0.5 at all radii except probably the central region. This is very important to copy with the beam space charge repulsion at the required average beam intensity ~ 5mA [1].

INRODUCTION

Selection of the cyclotron magnetic system parameters and 3D magnetic field simulation are presented.

MAGNET STRUCTURE

General view of cyclotron magnet configuration and interface with RF and extraction systems is shown in (Fig. 1).

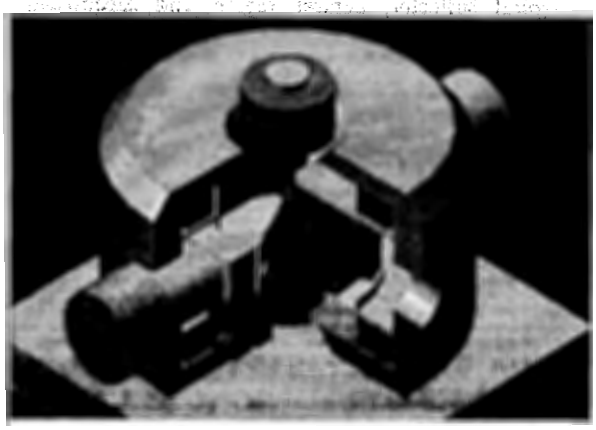

Figure 1: Magnetic structure, dees, extraction system.

Magnet cross sections is given in (Fig.2-Fig.4). Shaping of the azimuthally averaged magnetic field was performed with the help of the sector angular width variation along radius in accordance with (Fig.5).

The major input parameters for selecting magnetic structure were the final H^- ion energy = 1.747 MeV and the final average radius ~30cm. Those parameters will automatically define the central magnetic field =0.64 T and consequently the ion orbital frequency = 9.7462 MHz.

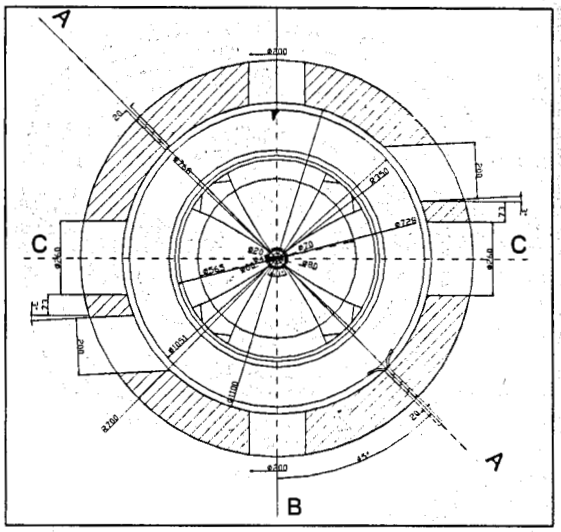

Figure 2: Magnetic system median plane layout

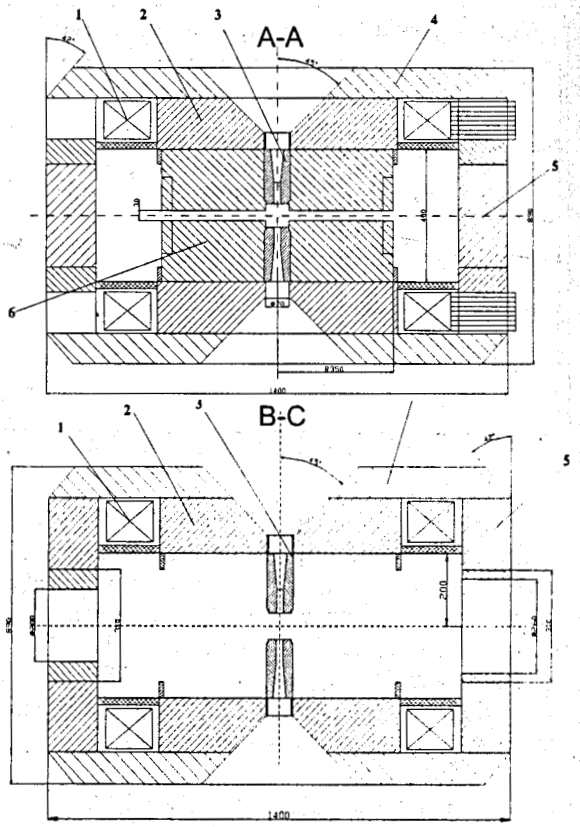

Figure 3: Magnet cross sections. 360° return yoke. Upper frame – sector symmetry plane, lower frame – valley symmetry plane. 1 – Coil, 2 – Pole, 3 – Plug, 4 – Horizontal yoke, 5 – Vertical yoke, 6 - Sector

Harmonic mode = 4 was selected to provide a maximum energy gain per turn with two ~45° dees installed in 2 opposite valleys of the 4-fold symmetry magnetic structure.

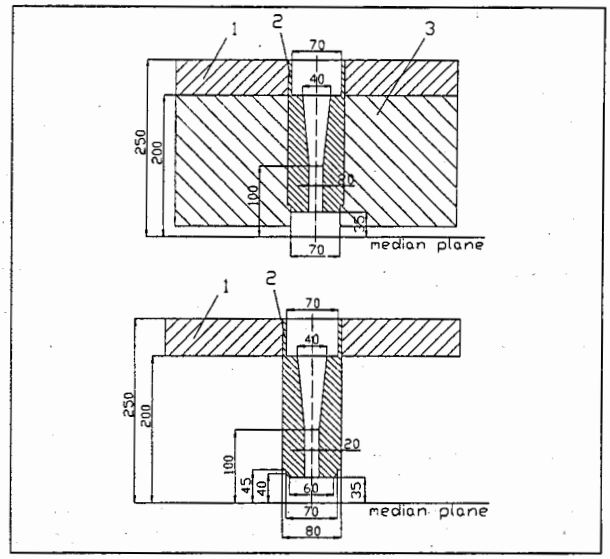

Figure 4: Central region cross-sections. Upper frame – sector symmetry plane, lower frame – valley symmetry plane. 1 – Pole, 2 – Plug, 3 - Sector

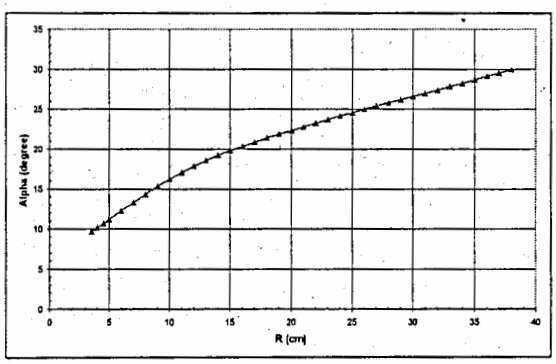

Figure 5: Sector angular width variation with radius

The beam axial size defines the minimum available axial aperture comprised by the axial air gap between the sector = 30mm. The valley gap = 400mm has been selected having in mind obtaining of the maximum possible flutter with still tolerable increase in Ampere-turns of the magnet coil for the given average magnetic field. The idea was to provide the maximum axial betatron oscillation frequency > 0.5 at all radii except probably the central region.

The final sector radius was selected to provide a good field radial range beyond the maximal radius of the final closed equilibrium orbit (EO) ~ 32cm

The coil shape and axial gap between the coils was selected taking into account the consumed magnet power and the need to release the space for the RF system.

Table 1 presents the selected system parameters defined as described above.

Table 1: Selected magnetic system parameters

Field	
Central magnetic field	0.640 T
Final average magnetic field	~0.613 T
Hill field at final radius	~1.35 T
Valley field at final radius	~0.2 T
Flutter at final radius	~0.65
Average radius of the final equilibrium orbit	~29 cm
Cyclotron radius	489.6 cm
Core	
Number of sectors/pole	4
Diameter of the pole	728 mm
Hill gap	30 mm
Valley gap	400 mm
Sector angular width	10° - 30°
Core weight	4.5 ton
Coil	
Ampere turns per magnet	58 kA*turns
Nominal coil current	362.5 A
Current density	3.2 A/ mm^2
Cu conductor dimensions	12.5×12.5×7.5 mm
Voltage	~28V
Power	~10 kW
Conductor weight	0.5 ton
Magnet	
Diameter	*1.4 m*
Height	*0.89 m*
Weight	*5 ton*

MAGNET CORE FIELD DISTRIBUTION

Magnetic field distributions in the magnet median plane (XOY) and in the cross-sections through the sector symmetry planes (ROZ) are presented in (Fig. 6-Fig. 7).

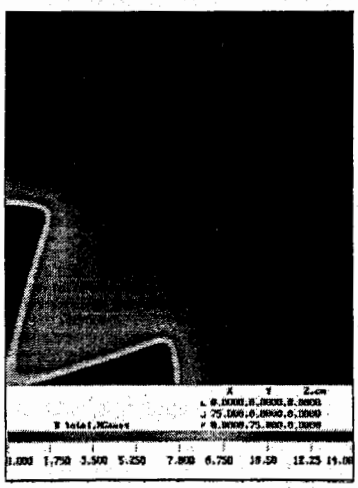

Figure 6: Midplane field map

The return yoke design reflected in the Figures showed that at the selected midplane field level the sector are highly saturated where as the magnet yoke passes through the magnetic flux without excessive Ampere-turns losses.

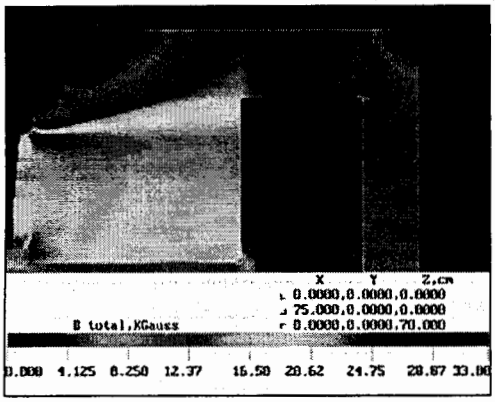

Figure 7: Magnetic field distribution in sector cross section

MIDPLANE FIELD

Isochronous Field

Azimuthal shimming of the sectors as it was mentioned above after several iterations provided the required isochronous field within the tolerances.

One of the most difficult problems to solve is the magnetic field shaping in the central region of the machine. Optimization of the central plug gap affects both the vertical sparking probability and the beam dynamics. The following limiting conditions should be met:

- Sufficient space for placement of the inflector and central region electrode structure.
- Requirements from the magnetic field measurement system.

The central region shimming was performed with the special form of the plug, shown in (Fig. 4).

Central Bump

The major problem with the beam space charge effects is related with insufficient axial focusing in the central region. The obvious method for increasing an axial focusing in the central region is introducing of falling with radius average magnetic field in such a way as to keep the RF phase only slightly changed (Fig. 8).

The attempts with calculated bump show that Q_z could be increase from 0.3 up to 0.45 at the 1st orbit without essential modification of the particle RF phase. The beam acceleration simulation in the bump field performed in [2] showed that the axial focusing would not change essentially as far as the axial particle losses concerned. Nevertheless, it was decided to retain the bump field shape for future usage of its potential capability to limit the beam axial dimension applying better matching of the injected beam and having in mind minimization of some possible magnetic midplane distortions impact on the beam quality and transmission efficiency.

The result of computational shimming is shown in (Fig. 8-Fig. 9). The analysis of the dynamic properties of the field shows that the obtained map meets the requirements formulated above.[2]

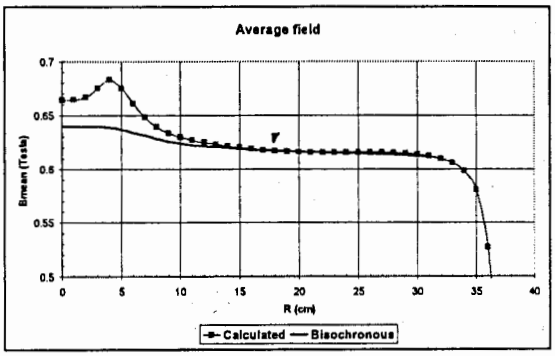

Figure 8: B-averaged with the bump

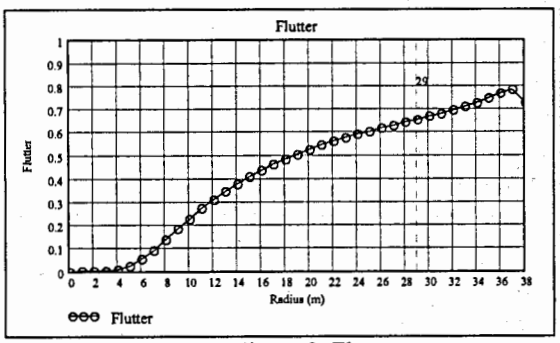

Figure 9: Flutter

CONCLUSIONS

- Magnetic structure parameters were obtained by the 3D computer simulations of the magnetic field.
- Some optimization study of the parameters selected has been performed.
- The space available for the axial injection system was released for axial injection design.
- The magnetic field maps along axial injection line, inside the cylinder comprising the spiral inflector and in the working radial range of the magnet midplane were produced for axial injection design and beam dynamics analysis.
- The obtained by simulation fringe magnetic field map was used for extraction system studies

REFERENCES

[1] V.A.Mashinin et al. Review of the Possibilities of Gamma-Resonance method of HE Detection.

[2] S.B.Vorozhtsov, E.E.Perepelkin, A.S.Vorozhtsov Dynamical Properties of the Electromagnetic Field of the Customs Cyclotron This conference.

COMPUTATION OF BEAM DYNAMICS WITH SPACE CHARGE IN COMPACT CYCLOTRON ON ENERGY ~ 1.8 MEV

E.V.Samsonov, L.M.Onischenko, JINR, Dubna, Russia

Abstract

A project of isochronous 4-fold compact type cyclotron to the energy of the H^- ions ~1.8MeV with an intensity of about several milliamperes is developed in the JINR. An external source of ions and axial line of injection with spiral inflector is assumed to be used in the cyclotron. The results of calculations of the beam dynamics taking into account the effects of space charge are examined beginning from an exit of inflector. The final parameters of beam - transverse emittances, energy spread, and value of maximal accessible intensity of the beam are given.

PARAMETERS OF THE CYCLOTRON

Main cyclotron parameters are shown in the following table.

Type of ion		H^-
Injection energy	(keV)	30
Extraction energy	(MeV)	1.8
Average magnetic field	(T)	0.64
Number of sectors		4
Number of dees		2
Betatron frequencies	ν_r, ν_z	1.1, 0.85
Angular span of dees	(°)	45
RF voltage	(kV)	60
Orbital frequency	(MHz)	9.76
Harmonic number		4

CODE DESCRIPTION

Code PHASCOL [1] has been adopted for the particle dynamic computations in the cyclotron. Full differential equations describing the particle dynamics in an electromagnetic field of cyclotron are integrated inside the PHASCOL.

We have used two ways for the computation of beam electric field: (I) - method of direct summation of the Coulomb's field created by each macroparticle (PTP method) and (II) - method of fast Fourier's transform (PIC method). PIC method assumes a calculation of beam electric field on a 3D grid that covers bunch. Both methods gave close results, but the second method worked faster, if the number of macroparticles composed several thousand. Therefore we have used mainly PIC method in the calculations.

RESULTS OF COMPUTATIONS

Ideally Injected Beam

In the first stage of computations we examined the conditions of ideally injected beam. We wanted to answer a question: is it possible, in principle, to accelerate 5 mA current in the cyclotron, without worrying in this case how this current would be injected into a central region?

The effects, which appear in the line of injection, were considered partially at this point of calculations. We took into account only the effects induced by a buncher. It is well known that an action of spiral inflector on the beam leads to some negative factors:

1. Large axial divergence of the beam.
2. Increase in the phase width of bunch.
3. Miss of the beam in an accelerated equilibrium orbit.

At this moment we assumed that the spiral inflector did not have these negative qualities and that it could transfer beam into the required region of phase space in the center of cyclotron.

Selection of the beam initial parameters was carried out taking into account minimal bunch phase width ensured by the buncher action depending on the beam intensity. A set of 5000 particles was chosen around an accelerated equilibrium orbit at radius 5.6 cm (Figure 1).

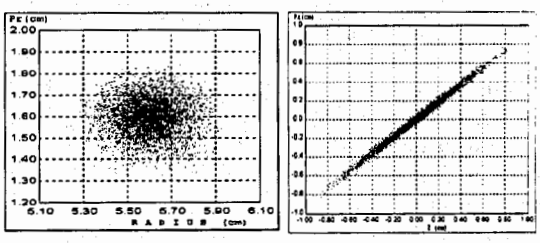

Figure 1: Initial parameters of ideally injected beam with I=5 mA. Emittances $\varepsilon r = \varepsilon z = 125\ \pi$ mm.mrad, energy W=30±6 keV, phase length $\Delta\varphi$=15*4=60°RF.

Figure 2 shows a layout of the cyclotron with the trajectories of 5000 particles at initial beam intensities 0 and 5mA.

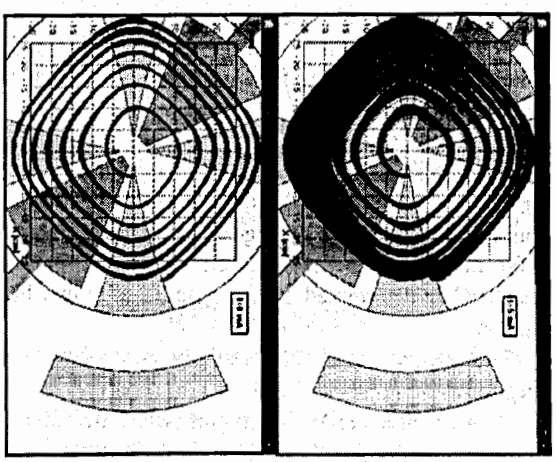

Figure 2: Particle trajectories at different initial current. To the left I=0 mA, to the right I=5 mA

Axial particle motion is shown in Figure 3. Approximately 15% of the beam with initial current 5 mA were lost on the dees plates during first 2 turns (dee aperture is 3 cm).

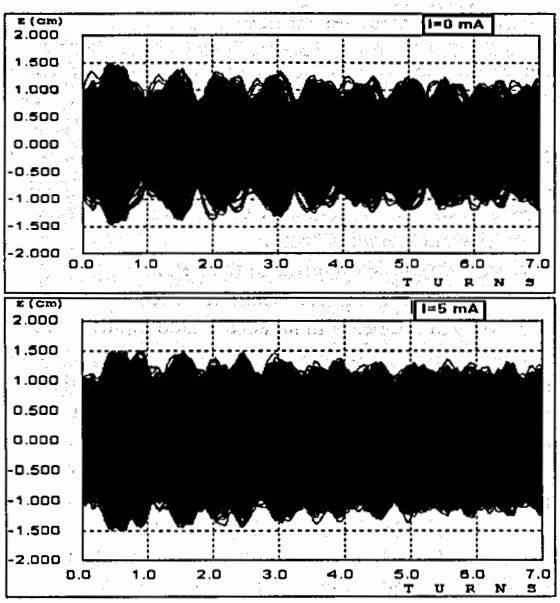

Figure 3: Axial trajectories at different initial current. Above I=0 mA, below I=5 mA.

Some conclusions were made on the base of computations for ideally injected beam:

- the focusing properties of the cyclotron magnetic field make it possible to accelerate beam with the current approximately 5 mA.
- radial width of beam with current 4.3 mA on the last turn equals 18-25 mm depending on azimuth;
- final root-mean-square ($\pm 2\sigma$) emittances of beam are following :εr=170 π mm mrad, εz =130 π mm mrad.

Not Ideally Injected Beam

At the second stage of calculations we used the more realistic initial conditions [2], which corresponded to the passage of the beam through the injection line ended by the inflector. Selection of the beam initial parameters was done in a range 1-20 mA. As an example, in Figure 4 one can see position of 2000 macroparticles inside 6D phase volume at injection current 5 mA. Here we can see an increase in the particle density as the result of acting the buncher, and the axial divergence of beam, which reaches 200 mrad. The energy spread of the injected beam (± 10%) is determined by the space charge and buncher action.

The calculations of acceleration were performed in two regimes:

1. With three radial diaphragms (width ΔR=20 mm) installed inside the dees on the first turn.
2. Without radial diaphragms.

Three types of losses were simulated in the calculations. Particle was removed from the computations if:

1. Axial coordinate of particle was greater than half of vertical aperture (Z>15 mm).
2. Particle did not pass the window of diaphragm.
3. Particle went to the center of cyclotron because of bad phase motion.

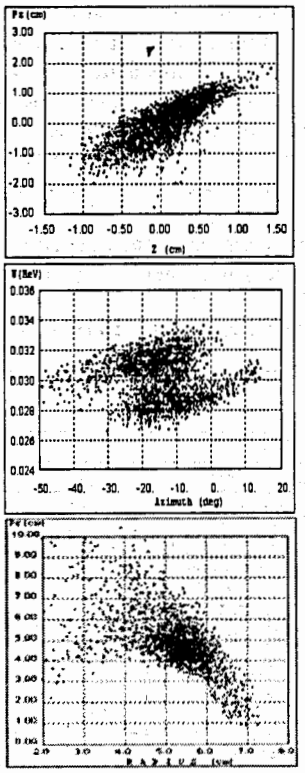

Figure 4: Initial position of 2000 particles on three phase planes. Above –axial plane, below -radial plane, in center - (azimuth-energy) plane (I=5 mA).

Computations have shown (Figure 5) that axial losses were greater in 2 – 4 times than radial ones. There are two main reasons of axial losses: large initial beam axial divergence and bad RF phase for a part of the beam when it passes through the 1-st accelerating gap. The last occurs due to large phase width of the bunch.

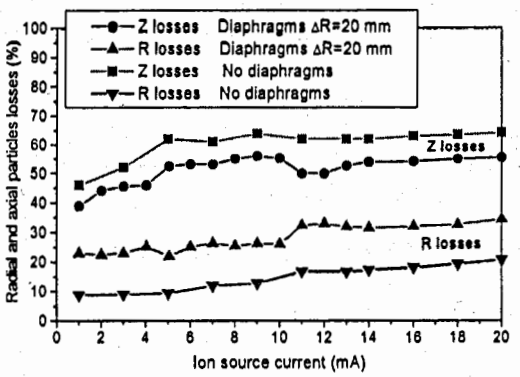

Figure 5: Radial and axial particle losses versus injection current

Interpretation of results (Figure 6) shows that beginning from the current of injection 12 mA an increase in the internal current of cyclotron practically stops. At this moment the current of cyclotron reaches approximately 2 mA.

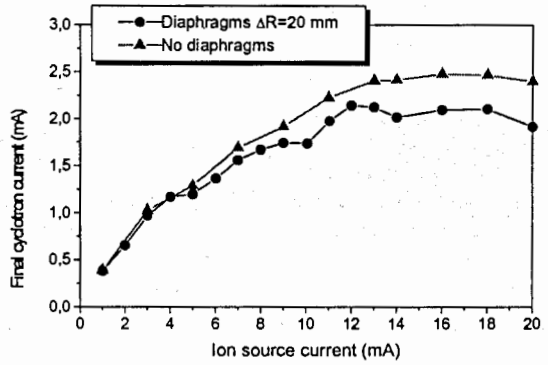

Figure 6: Cyclotron current at the end of acceleration versus injection current

Remarkable deterioration in the radial beam quality is observed (Figure 7) when injection current becomes greater than 10 mA. The axial emittance of beam weakly depends on intensity, since it is determined mainly by the vertical aperture of dees.

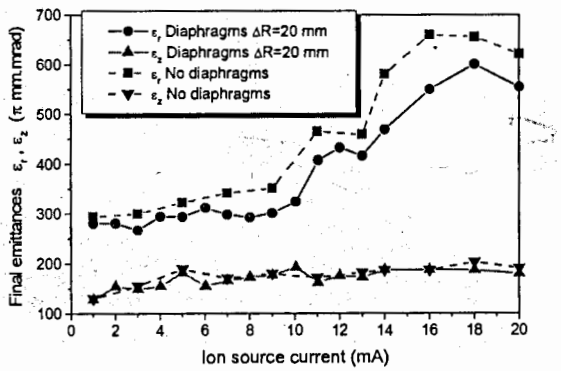

Figure 7: Transverse emittances at the end of acceleration versus injection current

Extraction System

Two types of the system of beam extraction from the cyclotron were examined: on the base of stripping foil and with the aid of the electrostatic deflectors. Since the possibility of guaranteeing the sufficiently long time of the foil life at the beam intensity ~ 2 mA causes doubts, then basic efforts were concentrated during the development of the electrostatic system of extraction.

The system of extraction consists of two deflectors ESD-1 and ESD-2 (Figure 8) with the strength 22 kV/cm of electric field at the center of their aperture. Voltage 60 kV on the high-voltage electrode corresponds to the value of the horizontal aperture of deflectors 2.5 cm. For compensating the beam defocusing in the horizontal plane by the action of edge magnetic field the necessary gradients of electric field in the deflectors ESD-1 and ESD-2 are -4.6 and -12.2 kV/cm^2, respectively.

Electrostatic elements are supplemented with the turning passive magnet MC with the field at the center of its aperture -0.2 T and with a gradient in the horizontal plane 0.02 T/cm.

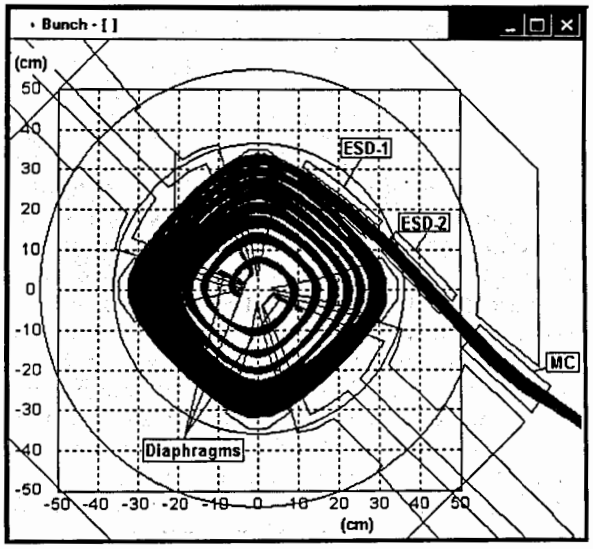

Figure 8: Layout of the cyclotron with particle trajectories. Only particles accelerated to final energy are depicted. Position of the diaphragms and extraction system are drawn schematically.(I=1 mA)

Computations showed that extraction efficiency is ~80%. The basic losses of particles are observed at the entrance into the first deflector of the extraction system. Losses inside the extraction system are insignificant since horizontal size of the beam cross section remains less than deflectors' aperture.

CONCLUSIONS

Maximally accessible current of cyclotron is 2 mA with the diaphragms ΔR=20 mm and 2.5 mA without the diaphragms.

Particles are lost mainly on the vertical plane because of the bad axial motion. Radial (phase) losses are several times less than axial ones.

Noticeable deterioration in the quality of cyclotron beam is observed if the current of injection exceeds 10 mA.

Final cyclotron parameters that correspond injection current 10 mA are: current 1.75 mA; angular divergence of beam ± (15-30)mrad; beam energy spread ± 8%; emittances εr,z=300, 150 π mm mrad.

REFERENCES

[1] L.M.Onischenko et al, Numerical simulation of space charge effects in the sector cyclotron, Nukleonika, 2003, 48 (Supplement 2), p.45-48.

[2] G.A.Karamysheva, Injection line for the customs cyclotron, this conference.

AXIAL INJECTION CHANNEL OF THE DC-72 CYCLOTRON

G.G. Gulbekyan, S.L. Bogomolov, V.V. Bekhterev, I.V. Kalagin*, N.Yu. Kazarinov,
M.V. Khabarov, V.N.Loginov, M.Leporis
Flerov Laboratory of Nuclear Reaction, Joint Institute for Nuclear Research,
Dubna, Moscow reg., 141980 Russia

Abstract

Axial injection channel of the DC-72 cyclotron consists of two horizontal part placed at the opposite side of the vertical analysing magnet and common vertical part from the magnet to median plane of the cyclotron. The first part is intended for transportation of H^-, $^2H^{1+}$ and $^4He^{1+}$ ions obtained from the multi-cusp ion sources. The second part is used for transportation of the heavy ions from Li to Xe obtained from the ECR-ion source. The focusing in the beam line is produced by solenoidal and quadrupole lenses. The sinusoidal buncher installed in the vertical part of the channel is used for increasing of the accelerating efficiency. The beam diagnostics placed in the special boxes consists of the Faraday caps and the scanners. The scanners are used for beam profile monitoring and emittance measurements. The first experiments at H^-, $^2H^{1+}$ and $^4He^{1+}$ part of the channel were performed.

GENERAL LAYOUT OF THE CHANNEL

The scheme of DC-72 axial injection channel is shown in Fig.1. The vertical channel height is 5.2 m. The magnetic focusing elements were made by NIIEFA, St.Peterburg, Russia. The vacuum elements were made by Vacuum-Prague, Prague, Czech Republic.

ION SOURCES

The heavy ions from He to Xe are obtained from 14 GHz electron cyclotron resonance ion source (IECR) [1]. The H^- and the $^2H^{1+}$ ions are obtained from two identical "multi-cusp" ion sources produced by Université catholique de Louvain, Centre de Recherches du Cyclotron.

BEAM FOCUSING

The focusing of the H^- and the $^2H^{1+}$ ions beam is produced by magnets IM60 and IM90 fringe fields and solenoidal lenses IS2,3,4. The set of quadrupoles IQH,2,3 are used for the formation of the axial symmetric beam between quad Q3 and the middle plane of the cyclotron. The solenoidal lenses IS2,3,4 are used for matching of the optical functions with the acceptance of the cyclotron inflector. The computed trajectories of the particles of the $^2H^{1+}$ ions beam with kinetic energy 16.83 keV and current 500 μA are shown in Fig.2.

The focusing of the heavy ion beams is produced by magnet IM90 fringe fields and solenoidal lenses IS1,2,3,4. Solenoidal lens IS1 decreases the beam divergence just after IECR ion source. As in the H^- and $^2H^{1+}$ part of the channel the set of quadrupole lenses Q1,2,3 forms the axial symmetric beam just after Q3 quad. The solenoidal lenses IS2,3,4 are used for matching of the optical functions with the acceptance of the cyclotron inflector. The computed trajectories of the particles of the argon beam with kinetic energy Z×13.5 keV (Z is ion charge) and current 160 μA are shown in Fig.3.

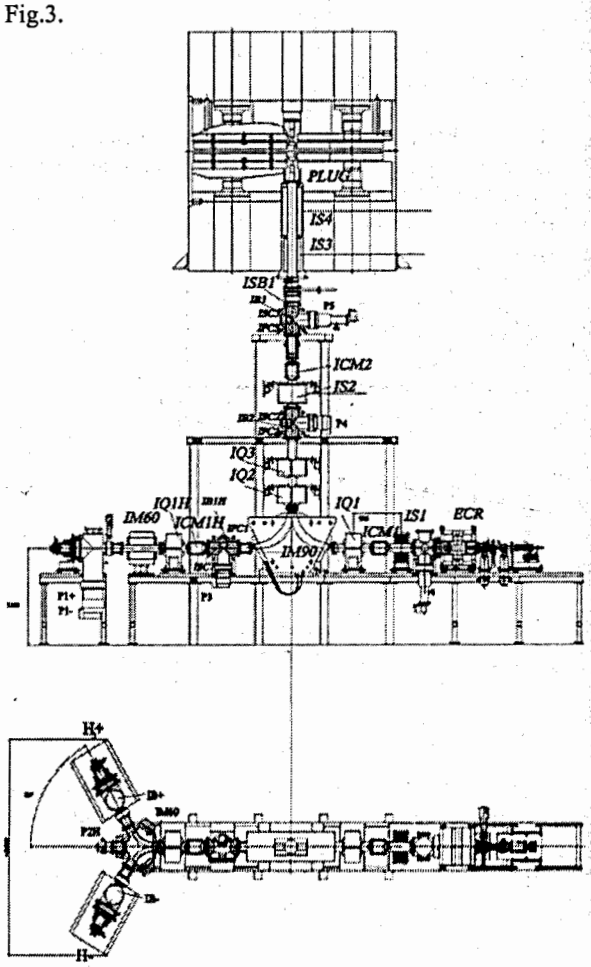

Figure 1: The scheme of the axial injection channel.

Where IECR – electron cyclotron resonance ion source; H^-, H2+ – multi-cusp ion sources; IM60 – 60° horizontal magnet; IM90 – 90° vertical magnet; IQ1H, IQ1,2,3 – quadrupoles; IS1,2,3,4 – solenoidal lenses; IB1H,IB1,2,3 – diagnostic boxes; ISC1,2,3 – scanners; ISB1 – sinusoidal buncher; IFC1H, IFC2,3 – Faraday caps.

* kalagin@nrmail.jinr.ru

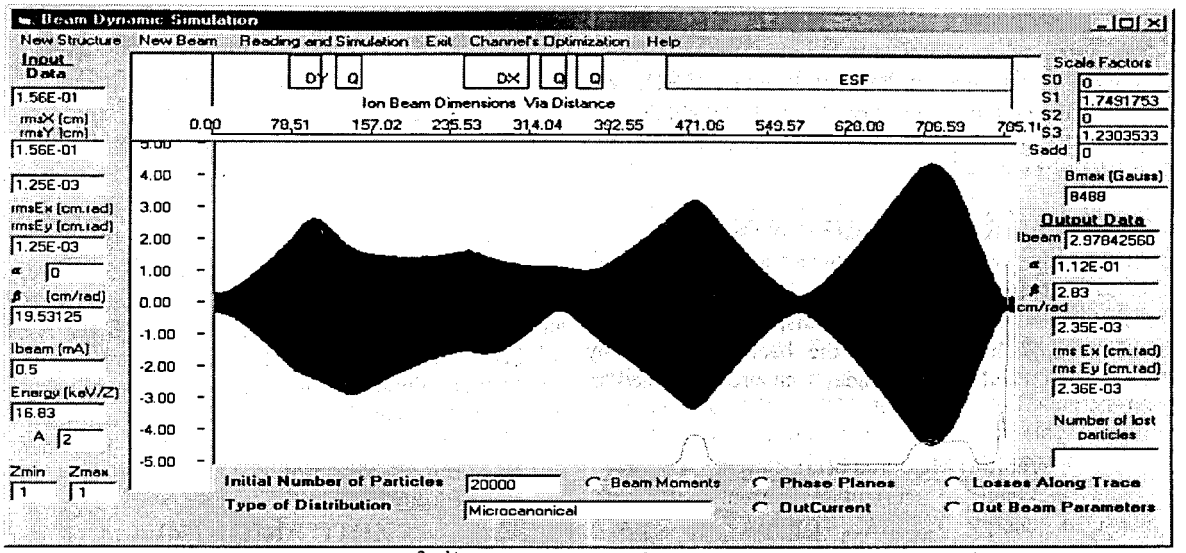

Figure 2: $^{2}H^{1+}$ ion trajectories. Beam current 500 μA.

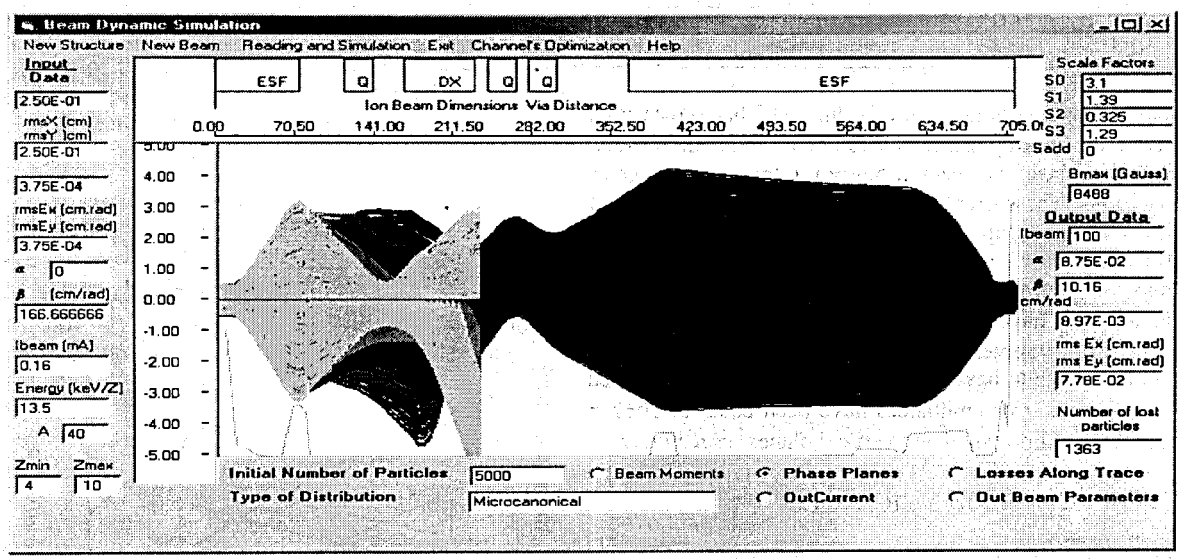

Figure 3: Argon ion trajectories. Beam current 160 μA.

SINUSOIDAL BUNCHER

The sinusoidal buncher ISB1 installed in the vertical part of the channel at 190 cm from the median plane of the cyclotron is used for increasing of the accelerating efficiency. The simulation has shown that longitudinal beam density will be increased at about 5 times.

VACUUM SYSTEM

The vacuum system of the injection channel consists of 4 sections. The extraction boxes of two multicusp ion sources are pumped by turbopumps with the pumping speed of 1400 l/s. The horizontal part of the channel is pumped by two turbopumps with the pumping speed of 500 l/s, and the vertical part of the channel is pumped by two cryopumps with the pumping speed of 800 l/s. In static mode the pressure in the extraction boxes is about 10^{-7} Torr, about $6 \cdot 10^{-8}$ Torr in the chamber of IM60 magnet, and about $3 \cdot 10^{-8}$ Torr in the diagnostic box IB3. During the operation with the $^{2}H^{1+}$ and $^{4}He^{1+}$ ion beams the pressure in the extraction box consists of about $2 \cdot 10^{-6}$ Torr, and about $2 \cdot 10^{-5}$ Torr in operation with H^{-} ion beam. The vacuum monitoring is provided by using combination of Pirani and Penning gauges.

SYSTEM OF DIAGNOSTIC

The beam diagnostics placed in the special boxes IB1H, IB1, IB2, IB3 consists of the Faraday caps IFC1H, IFC2, IFC3 and the wire scanners ISC1, ISC2, ISC3. The scanners are used for beam profile monitoring and emittance measurements [2]. The diagnostics elements were made by the Laboratory for Technical Development in Physics of Bulgarian Academy of Science, Sofia, Bulgaria.

SYSTEM OF CORRECTION

The system of the center of beam correction consists of two-plane dipole steering magnet ICM1H, ICM1, and ICM2. This system gives possibility to eliminate the displacement and angle of the beam center just after the steering magnet ICM2.

FIRST EXPERIMENTS

All elements of the channel have been manufactured and tested. During the first experiments the beams of H^-, $^2H^{1+}$and $^4He^{1+}$ ions have been transported up to IFC3 Faraday cup. The current of the beam measured by IFC1H, IFC2 and IFC3 Faraday cap are contained in Table1.

Table 1: Measured beam current

beam	kinetic energy keV	current μA IFC1H	current μA IFC2	current μA IFC3
H^-	16.83	356	301	321
$^2H^{1+}$	16.83	643	530	552
$^4He^{1+}$	15.39	587	286	500

The maximal currents of the H^- and $^2H^{1+}$ beam measured at IFC1H Faraday cap have been equal to about 750 μA. The $^4He^{1+}$ beam has been produced in the same source as $^2H^{1+}$ ions. The currents at IFC2 are less than currents at IFC3 Faraday cap because of the beam dimensions at IFC2 are greater than diameter of the cup (60 mm). The maximum current of the $^4He^{1+}$ beam measured at IFC1H Faraday cap have been equal to about 700 μA.

The measurements of the H^- beam emittance by gradient method have been performed [3]. The measured values of the rms emittances have been equal to 19±2 π mm·mrad in horizontal and vertical planes respectively.

REFERENCES

[1] Vladimir N. Loginov, Vladimir V. Bekhterev, Sergei L. Bogomolov, Andrei A. Efremov, Alexander N. Lebedev, Marek Leporis, Nikolai Yu. Yazvitski, Andrej Zelenak - First beam from the DECRIS 14-2m ion source for Slovak republic, NUKLEONIKA 2003;Volume 48(Supplement 2), p. S85-S88

[2] N.Yu. Kazarinov, B.I. Kazacha, I.V.Kalagin, A.Gall, "Method of the Ion Beam Emittance Measurement in Injection Beam Line of DC-72 Cyclotron in the presence of its space charge using the scaner to determinate beam dimensions", in Communication of JINR, P9-2002-266

[3] N.Yu. Kazarinov, V.I. Kazacha, I.V. Kalagin, V.V. Aleinikov, A.I. Krylov, "Measurement of H^- Beam Emittance in Axial Injection Channel of DC-72 Cyclotron", in Communication of JINR, E9-2004-146

DC-72 CYCLOTRON MAGNETIC FIELD FORMATION

G. Gulbekian, I. Ivanenko, J. Franko, J. Keniz, E.Samsonov, JINR, Dubna, 141980 Russia

V.P.Kukhtin, E.V.Lamzin, S.E.Sytchevsky, ERIEA, St. Petersburg, 189631, Russia

Abstract

The isochronous cyclotron DC-72 is intended to accelerate the ions from H- (A/Z=1, W=72MeV/u) up to 129Xe18+ (A/Z=7.167, W=2.7MeV/u). The cyclotron magnet has the pole of 2.6м diameter and provides the working magnetic fields at the range of 0.9T - 1.51T for the given modes of acceleration. The preliminary design of a magnetic field has been accomplished with the model of a magnet (scale 1/5) and 3D code COMPOT. The results of magnetic field final formation are presented.

INTRODUCTION

The DC-72 Cyclotron is an isochronous cyclotron with azimuthally varying field. The working diagram of the DC-72 cyclotron is presented at the figure 1. The wide diapason of the accelerated ions and their energy's sets the stringent conditions on the formation of the magnetic field distribution at the cyclotron working area.

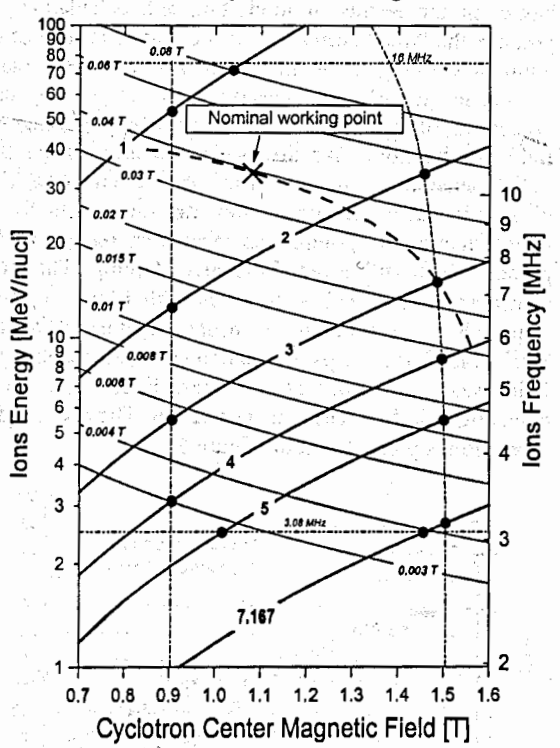

Figure 1: The working diagram of the DC-72 cyclotron.

The azimuthal variation of the magnetic field is achieved by four straight sectors per pole. The sectors have a variable axial profile at the side of the median plane of the magnet. This method of the sectors shimming give the optimal behaviour of the mean field radial growth function, dB=f(Bo) and satisfy the conditions of the working diagram [1]. At the figure 2 the area of dB(Bo) values (according to the DC72 cyclotron working diagram) and dB(Bo)-function of the cyclotron magnet (the magnetic field behaviour without using of correcting coils) are presented by the points and dash line respectively. At the figure 1 the same dB(Bo)-function of the cyclotron magnet is presented by the dash line too. The regime of Bo=1.08T and dB=400Gs were chosen as the nominal working point. The shimming of magnet structure was carried out to produce the isochronous field at this point.

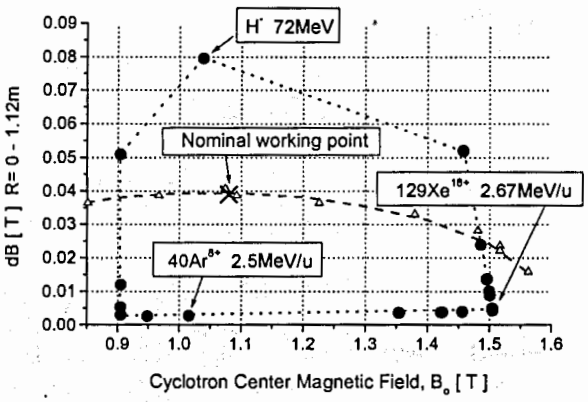

Figure 2: The working diagram area of dB(Bo) values and dB(Bo)-function of the cyclotron magnet.

Table 1: DC-72 cyclotron magnet parameters.

Magnet type	H – type
Working magnetic field diapason	0.9 – 1.52 T
Yoke length, width, height	5,6×2,7×3,1 m
Diameter of the pole	1.6 m
Gap between the poles	280mm
Minimal gap between the sectors	90mm
Gap between the pole and sector	20mm
Number of sectors per pole	4
Angular span of the sector (spirality)	45° (0°)
Extraction radius	1.118 m
Number of radial correcting coils	10
Number of azimuthal correcting coils	4
Maximal power consumption	70 kW
Maximal current at the main coils	340A

DC-72 CYCLOTRON MAGNET

Table 1 shows the general cyclotron magnet parameters. The peculiarity of the cyclotron magnet structure is the presence of holes for resonators, vacuum pumping and power supply wires of correcting coils. These holes are placed at each "valley" and distort the magnetic field. The effect of the valley holes is considered at the form of required isochronous fields. Ten pairs of the radial correcting coils gives necessary freedom for selection the dB(Bo) function value according working diagram. They are located in the space between the sectors and the pole and provide the additional correction of the working magnetic field to obtain the isochronous distribution for the given modes of acceleration. Four pairs of the azimuthal correcting coils provide the operative correction of the beam orbit centering, see figure 3. Both radial and azimuthal correcting coils have a 40 turns per pole and maximum current 35A.

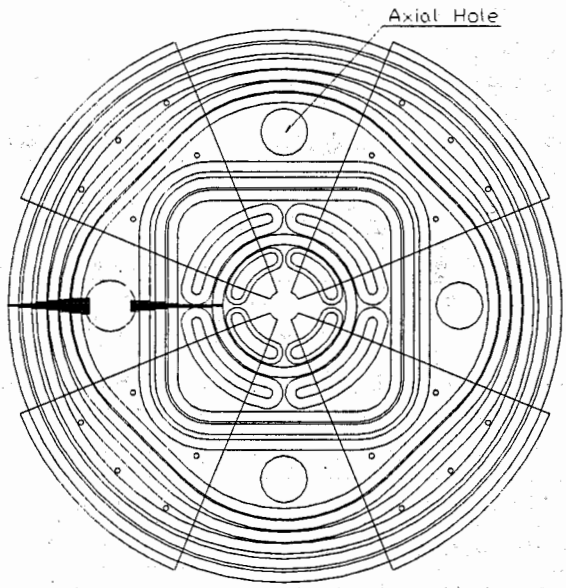

Figure 3: The position of the ten radial and four azimuthal correcting coils on the magnet pole.

MAGNETIC FIELD COMPUTATION AND MODELING

The preliminary researches of the magnetic field behaviour for the given modes of acceleration are conducted on the model of the DC-72 cyclotron magnet, scale 1/5. The research of the different methods of the sector shimming has been carried out on this model. The method of the "top" axial shimming (the sectors are processed at the side of the median plane of the magnet) was chosen as the main one [1]. Simultaneously, the magnetic field simulation was performed with the help of 3-D computer code KOMPOT [2]. The measured magnetic characteristics of the magnet yoke elements were taken into account at the calculation. The actual axial profile of the sectors as a result of modelling and computation are presented at the figure 4.

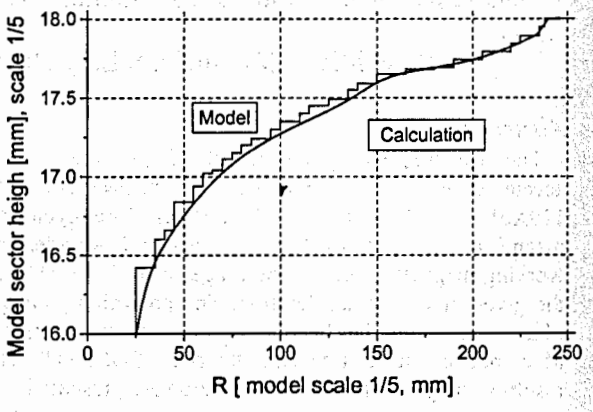

Figure 4: Sector axial profile, scale 1/5, from the modelling and the computation.

FORMATION OF CYCLOTRON MAGNETIC FIELD

The DC-72 cyclotron magnet was manufactured based on the results of modelling and calculation. To produce the "thin" correction of the magnetic field at the nominal working point the 10mm azimutal wide plates are placed at the both sides of each sector. The axial processing of these plates allows correcting the magnetic field first harmonic and the local unlinearity of the field radial behaviour. The measuring of the magnetic field distribution at the median plane was carried out by the unique measured system. The magnetometer has 8 Hall probes placed with a radial distance 200mm. The radial measured distance is 0 ÷ 1600mm with 10mm or 20mm steps. There are azimuthal measured regimes of 90° and 360° with 1° or 2° steps. Formation of cyclotron magnetic field was carried out at 3 stages. First stage was a magnetic field first harmonic correction. The result of this correction is presented at the figure 5.

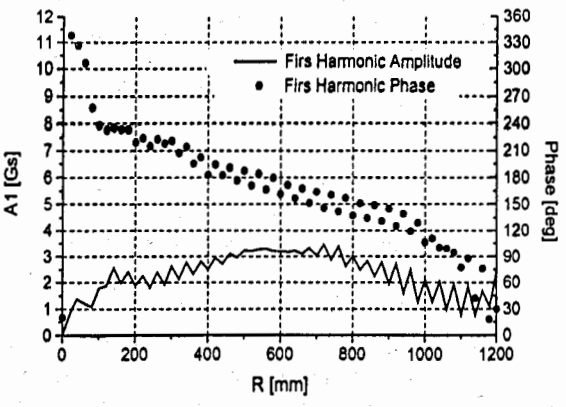

Figure 5: First harmonic amplitude and phase after correction.

At the second stage the formation of the field at the nominal working point was carried out. The form of this field must be suitable for the subsequent formation with the radial correcting coils the most important regime H- (72MeV). At the figure 6 the measured nominal working point field is presented. At the same figure the regimes of H- (72MeV) and 40Ar+5 (3.2MeV) are presented by the calculated isochronous fields and fields, formed with correcting coils (simulation version).

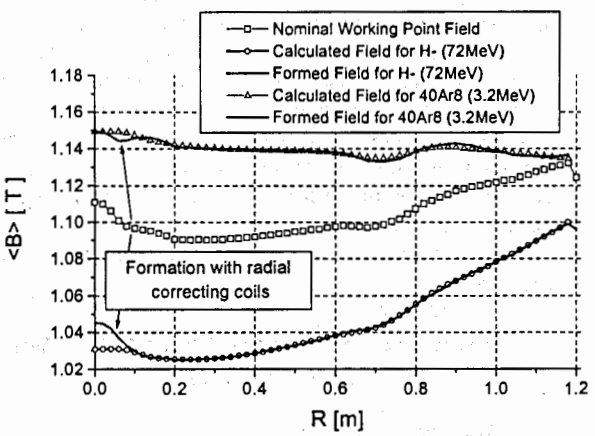

Figure 6: Formation of isochronous field for H- (72Mev) and 40Ar+5 (3.2 MeV) regimes by means of radial correcting coils.

At the third stage the contributions of radial and azimuthal correcting coils fields were measured at 7 levels of main magnetic fields.

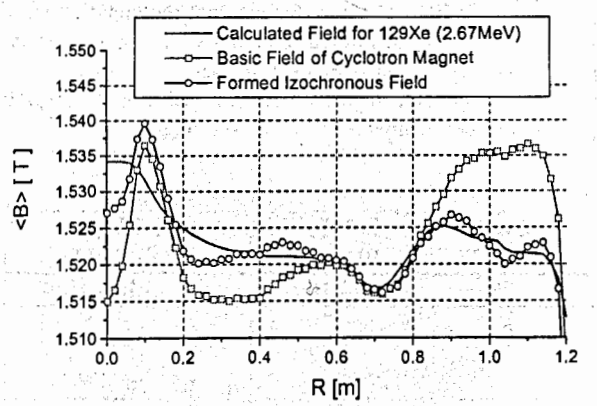

Figure 7: Formation of isochronous field for 129Xe+18 (2.67Mev) regime by means of radial correcting coils.

The forms of contribution of radial coils are different when they are turned on positively or negatively regarding to the main magnet field. The smaller the levels of main field the more this difference. For the correct formation of isochronous field for H- (72Mev) one have had to measure both positive and negative radial coils contributions. At the higher-level magnetic field, 1.5T, the positive and negative contributions are practically identical. At the figure 8 the positive contribution of 10 radial coils at 1.1T main field are presented. The coils current is 35A. Based on the measured magnetic fields of main magnet and correcting coils the main regimes of cyclotron working diagram (H- (72MeV), 129 Xe+18 (2.67MeV), at all.) were calculated and then measured, figures 6 and 7.

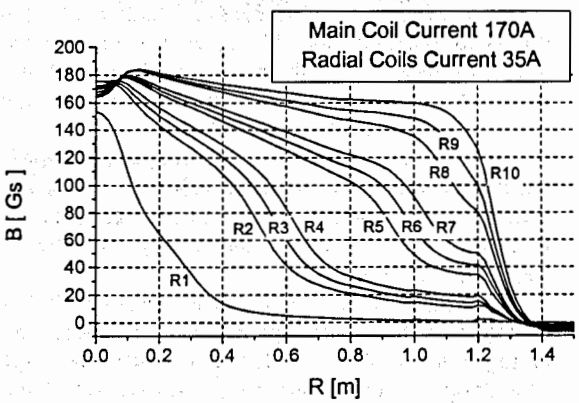

Figure 8: Fields of the ten radial correcting coils.

CONCLUSION

The formation of DC-72 cyclotron magnetic field was carried out. The modelling and 3D computer simulations of the magnet elements were used for preliminary choice of the cyclotron magnet structure. For exact isochronous magnetic field forming at the nominal working point and correction of the field first harmonic the side sectors shims were used. The measured magnetic fields of main magnet and correcting coils at the different levels are used at the computer program to forming any regimes of the working diagram. The following calculations of the beam dynamics at the chosen working regimes with the appropriate magnetic fields, formed with correcting coils and then measured, show the satisfying results.

REFERENCES

[1] I. Ivanenko, G. Gulbekian, J. Franko, A. Semchenkov, "The model of DC72 cyclotron magnet. The research of the sector shimming methods for obtaining the working magnetic field for light and heavy ions acceleration," EPAC2002.

[2] G. Gulbekian and all., "A method of the magnetic field formation in cyclotron DC-72," NUKLEONIKA, Vol. 48, number 4 - 2003, pp. 207-210.

CYCLOTRON FOR BEAM THERAPY APPLICATION

Yu. G.Alenitsky, S.B.Vorozhtsov, A.A.Glazov, G.V.Mytsyn, A.G.Molokanov, N.L.Zaplatin, G.A.Karamysheva, S.A.Kostromin, L.M.Onischenko, E.V.Samsonov,
DLNP, Joint Institute for Nuclear Research, Dubna, Russia

Abstract

The proton beam for radiation therapy application in Russia for the first time [1] was created in 1967 on the base of Phasotron (Laboratory of Nuclear Problems JINR). Now an energy of extracted proton beam is Ep=680 MeV, intensity Ip=3 mkA [2].

A six–cabin medical facility has been developed and put into operation on this beam [3]. Now in practice of treatment on medical beam LNP JINR the most frequently used beam has the energy 170 MeV and current Ip ~ 0.1 mkA [4, 5].

We suppose that it is more rational to create a new cyclotron with required parameters of beams and to arrange it in the LNP JINR for use in a medical complex. The design proton beam energy is: Ep~200 MeV[6]. Cyclotron is proposed on the basis of compact fore sectors magnet with ring opposite yoke having a diameter of poles Ø=3 m. Two dees accelerating system is located in valleys.

THE BASIC PARAMETERS OF CYCLOTRONS FOR MEDICAL APPLICATION

Now IBA and SHI firms create the project [7] of the cyclotron on energy of protons 235 MeV especially for the therapy and some such accelerators already were put into operation. Firm ACCEL Instruments GmbH [8] develops superconducting cyclotron on energy of protons 250 MeV.

In the table 1 some parameters of cyclotrons C- 235 (IBA) [7], C-250 (ACCEL)[8], C190 (H-) [6] and C200p are given. Cyclotrons given in the table 1 differ by a level of the used magnetic field and by correspondent technical parameters. The most important characteristics of the installation are the size and technology of manufacturing of the project (cost), and operational conditions – energy consumption and cost of service. We consider, for our conditions, that the offered project C200p is optimum because of the installation will be able to be manufactured inside our institute, and will have a pretty low cost.

THE BASIC PARAMETERS OF C200p CYCLOTRON

Magnetic System

Isochronous cyclotron for proton therapy application is supposed to be created on the basis of a compact four sectors magnet with ring opposite yoke having an outer diameter 5.2 м and height 2.4 m.

A computer modeling of cyclotron magnetic system was carried out with the help of the code Radia [9], which works in the system of Mathematica and calculates the magnetic field of three-dimensional magnetic systems by a method of the integral equations. A plane view on the various cyclotron systems is shown in figures 1.

A general view of mathematical model of a bottom part of the magnet is shown in figure 2.

Table 1: Main parameters of cyclotrons

PARAMETER	C – 235 IBA	C-250 ACCEL	C-190(H⁻) JINR LNP	C-200p JINR LNP
Energy of protons (MeV)	235	250	70-190	~200
Average magnetic field (T)				
At center	1.739	~4	0.77	1.33
At extraction radii	2.165	~4	0.92	1.64
Extraction radius (m)	1.08	~0.9	~2.1	1.4
Magnetic field at extraction radius (T)	3.09	4.0	0.6	2.65
hill	0.985	1.6	1.1	0.95
valley				
Gap (mm) valley	600		380	400
hill	96-9	-	140	50
Number of sectors	4	4	4	4
Main coil ampere turn (kA)	525	-	150	340
Power consumption (kW)	190	40(cooling)	120	170
Weight of magnet (T)	210	90	400	300

alen@nusun.jinr.ru

The magnetic system consist of sectors (1), poles (2), ring top and bottom horizontal yokes (3), coils (4) and vertical yoke (5) (see figs. 1). The required configuration of the magnetic field is formed using a spiraled and angular extent of sector shims depending on radius.

The complete angular extent of one sector on a pole composes 55°, thus there is an opportunity to place two 42° resonators in valley.

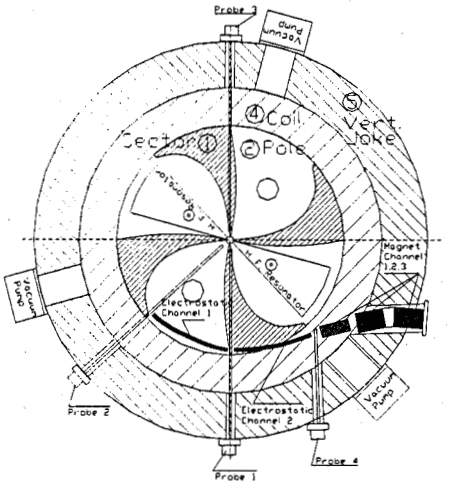

Figure 1: Plane view of the magnetic system of proton cyclotron C200p

Beam Dynamics

In figs. 4 -7 the dynamic characteristics of beam in the magnetic field are given. The betatron frequencies of axial and radial motion (fig. 4) are in allowable limits

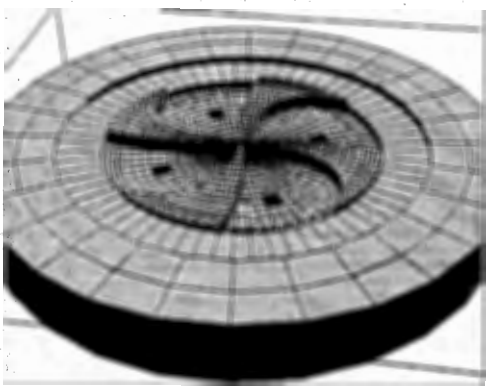

Figure 2: Computer model of the magnetic system of C200p (bottom part of the magnet, hole for coaxial line of RF system can be seen)

Working point diagram along the acceleration in C200p is presented in figure 5. The point to point distance is 10 MeV. The most dangerous resonance Q_r-Q_z=1 is crossed two times at energies 130 and 170 MeV. Modeling of particle dynamics showed that no axial amplitude increase observed after the resonance (see below) if no skew harmonics presented in magnetic field map. Further computations have to define permissible limits of such harmonics.

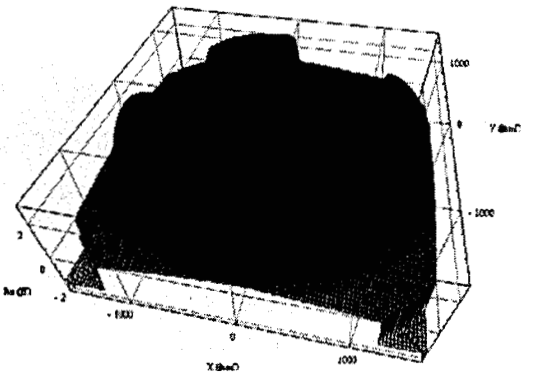

Figure 3: Magnetic field map computed by the RADIA code

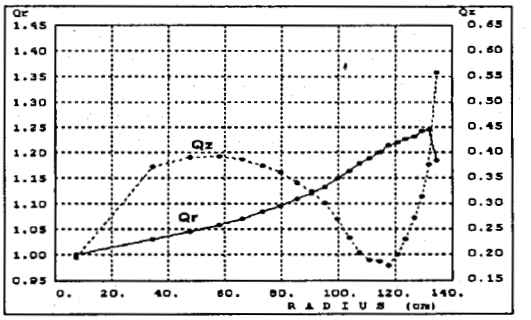

Figure 4: Free betatron frequencies along radius

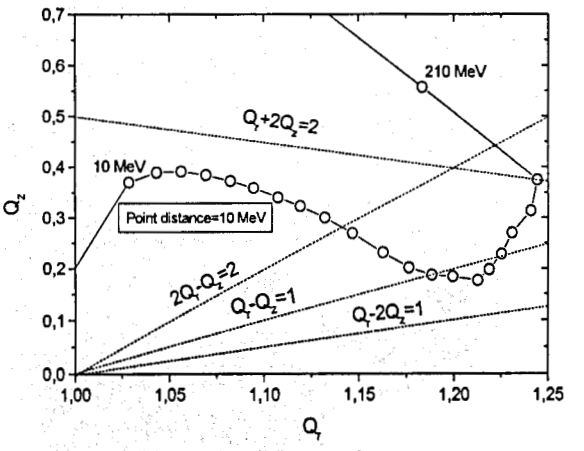

Figure 5: Working point diagram of C200p

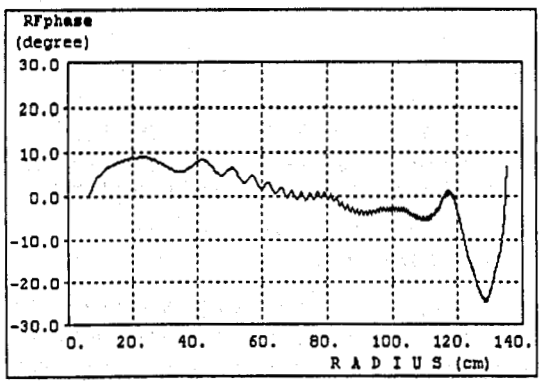

Figure 6: Phase motion of central particle

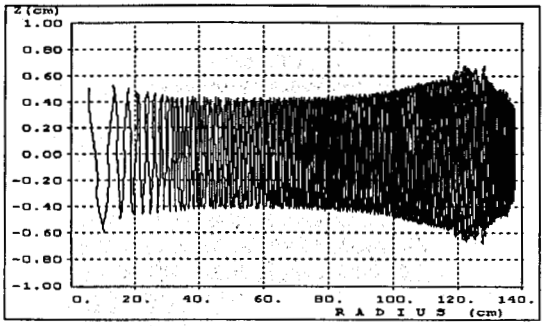

Figure 7: Axial motion of one particle

Phase motion of central particle computed along the acceleration (see fig. 6) shows good accuracy of a isochronous field. Particle resonance orbital frequency is 20.4545 MHz. Axial particle motion along acceleration in magnetic field with no skew harmonics is shown in fig. 8. Amplitude of particle radial oscillation was 5 mm during this computations. Changing of axial oscillations amplitude corresponds to the dependence of axial betatron frequency on the radius.

Radiofrequency System

Rectilinear on radius the accelerating resonators and dees have angular extent 42° and 30°, respectively. They are located in valleys between sectors (see figure 1), where the gap between poles is 400 mm. The adjustment and excitation of resonators is carried out through coaxial lines. The central rods used for dees support are located above and below them. A view of high-frequency cyclotron system is given in fig. 8. The basic parameters of high-frequency system designed by a three-dimensional program ANSYS are given in the table 2.

Figure 8: RF system with coaxial lines above and bellow

For excitation of accelerating system it is expedient to use a standard high-frequency generator on a suitable power and frequency working on a linkage feeder.

Extraction System

A general view of extraction system is shown in fig. 1. It consists of beam radial enhancement system, electrostatic sections, deflecting and focusing magnetic sections. In the present work the preliminary result of computation of extraction trajectory is shown. To define the parameters of radial enhancement system and the extraction channel the additional efforts are needed. The energy of the extracted beam in the table 1 is given approximately. The exact value of energy will be determined after corresponding computation of the extraction system.

Table 2: The main parameters of accelerating system

Resonance frequency (MHz)	81,8
case dimensions	
Radial (Rmax) (mm)	1500
Height (mm)	400
Azimuth span (°)	50
dimensions Δ-electrod (dee)	
Max.rad.(Rmax)(mm)	1400
Height (mm)	50
Aperture (mm)	30
Azimuth span (°)	30
Accelerating gap (°)	6
Coaxial line dimensions	
Between clothe contact plates (mm)	800
Radius of coaxial line	
inner (mm)	100
outer (mm)	180
From center of cycl. to axes (mm)	750

CONCLUSIONS

The physical substantiation for proton cyclotron on energy of the beam E_p ~200 MeV is given. This cyclotron will supply performance of all scientific and medical programs on the medical beam of Dzhelepov Laboratory of Nuclear Problem, Joint Institute for Nuclear Research.

The creation of cyclotron for the medical centers in other interested organizations is possible on the basis of proposed project.

REFERENCES

[1] V.P.Dzhelepov, V.I.Komarov, O.V.Savchenko. Preprint JINR 16-3491, Dubna, 1967; Med. Radiology 1969, №4.

[2] V.P.Dzhelepov, V.P.Dmitrievsky, L.M.Onischenko, Preprint JINR , P9-85-358, Dubna, 1985.

[3] Abazov V.M.et al, Radiation therapy with JINR Phasotron Beams, Dubna, Second Edition,JINR- 9-96-387, 1996.

[4] Abazov V.M. et al, Medical facility for radiation therapy with JINR Phasotron beams, E18-94-112, Dubna, 1994.

[5] Stopping Powers and Ranges for Protons and Alpha Particles, ICRU Report 49, Bethesda, USA, ISRU (1993).

[6] Yu.G.Alenitsky at al, Variable energy cyclotron for proton therapy application. Preprint JINR P9-2004-32, Dubna, 2004.

[7] http://www.shi.co.jp/quantum/index.html; http://www.iba-worldwide.com/root_hq/index.html

[8] M. Schillo. The ACCEL Superconducting Cyclotron: A Driver for Proton Therapy. Abstracts of PTCOG-38, Chester, UK, 2003, p.10.

[9] P. Elleaume, O. Chubar, J. Chavanne, "Computing 3D Magnetic Field from Insertion Devices", Proc. of the PAC97 Conference May 1997, p. 3509-3511.

CONTROL SYSTEM FOR IC-100 CYCLOTRON

Aleinikov V.V., Bondarenko P.G., Krylov A.I., Nikiforov A S., Pashchenko S.V.

JINR, FLNR, Dubna, RUSSIA

Abstract

The control system for IC-100 cyclotron has been designed and developed at the Flerov's Laboratory of Nuclear Reactions. The control of the accelerator is realized from a remote machine through the local area network. The software for the QNX operating system and SCADA FLEX CONTROL is developed. The application of the universal controller produced a flexible and simple system that has shown high operational characteristics. The structure of the control system and its specialized modules are described in present article.

INTRODUCTION

As we begin to apply totally integrated automation solutions from industry automation [1] to the control of accelerators, we are faced the question of procurement and development of specialized modules. For example, the development of filtering modules of current signal with current magnitude as little as one micro Ampere and the modules for the control and management of high frequency signals presents in our tasks. The development and manufacturing of control systems with a mixture of standard and custom made modules was acknowledged by us to be a wrong approach. The main reason of this is the induced difficulty in operation and repair of the equipment. A collection of integrated controllers of SMARTBOX series along with all the necessary specialized modules was developed in the Laboratory of Nuclear Reactions. The new system have already used in the control of accelerators DC-72, EA10-10, and IC-100. Works to modernize control systems of U-400 and MC-400 are being carried out. The present article describes the control system of IC-100.

CONTROL SYSTEM

The structure of control system is shown in figure 1. The control system is mounted in five 19" racks. Management of all equipment is carried out through serial communication channels. The system deploys RS-232, RS-422, RS-485, IEEE 802 protocols and universal controllers of type SMARTBOX-4. 14 controllers are used in the system. Management of controllers is executed through a serial interface RS-485. The protocol of exchange with the computer is PROFIBUS. Each controller has the unique address, which is defined, by its installation site in the system by means of crosspieces on the plug in crate. A controller address is determined once the power is switched on.

Management of all equipment is carried out in the following way. An Industrial 4 port RS-232/RS-422/RS-485 of the serial board produced by Moxa Technologies is used for management on communication channels in a personal computer. The interface IEEE 802 is used for remote control of the accelerator and for other operational needs.

For the management of the equipment that takes place under potential ECR source (up to 30 kV); two converters RS-485 are installed to fiber optic, providing isolation of the controller on communication line RS-485.

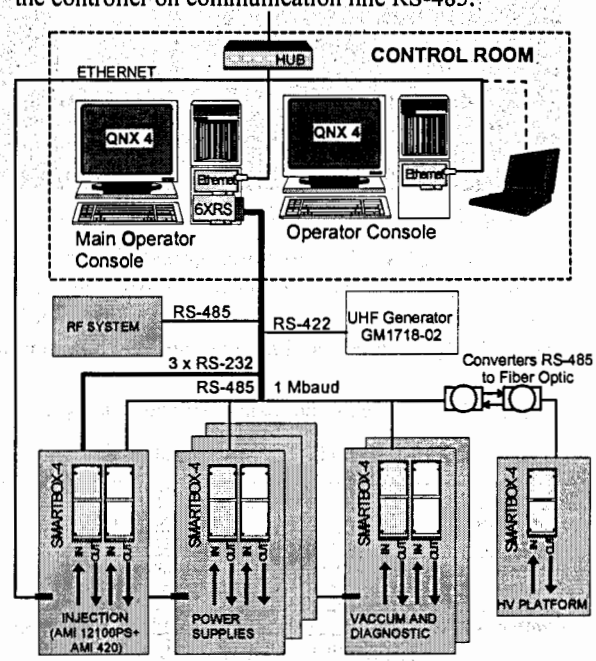

Fig. 1: The structure of control system.

For the management of magnetic elements of beam lines current sources of series ES, SM firms DELTA ELEKTRONIKA BV, Netherlands with 10V analog interface are used.

A collection of current-to-voltage transformers is developed to measure signals from current samplers. All converters are constructed under the three-cascade circuit inverting «current to voltage» with input protection, the active low frequency filter of the second order with Ku = 1, the inverting cascade with Ku = 10.

Modules are 7TE, 6HE Euro-19" size. Input : 24 VDC.

CVC-01. Module is designed for converting profile meter current signal in range of 1 mkA to voltage 10 V. Number of input channels - 32.

CVC-02. Module is designed for converting aperture diaphragms current signal in range of 20 mkA to voltage 10 V. Number of input channels - 12. A range of controllable resistance of a source of a signal 50 whom – 5 MOhm

CVC-03. Module is designed for converting Faraday cup current signal in ranges of 1 mkA, 10 mkA, 100 mkA, 1000 mkA to voltage 10 V. Number of input channels – 16, output channel - 1 A range of controllable resistance of a source signal 10 kOhm – 100 MOhм

SMARTBOX-4.

The functional diagram of SMARTBOX-4 module is shown in figure 2.

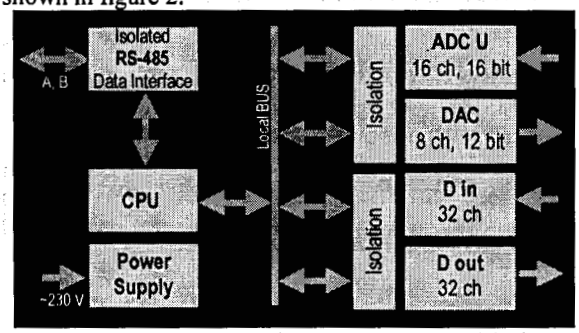

Fig. 2: The SMARTBOX-4 functional diagram

The SMARTBOX series microprocessor controlled device is designed as fully enclosed data acquisition module with built-in industrial bus interface. Mechanically modules can be integrated into a system by way of a crate.

SMARTBOX-4 technical data is shown in table 1.

Table. 1. SMARTBOX 4 technical data

CPU	Type	MSC-51
Communication	Type	EIA RS-485
	Communication speed	921600 baud
Power	Power supply type	Built-in, Analog
	Input voltage	~230 V, 12VA
Construction	Type	Euro 19", crate mount
	Dimension	6U, 10HE, 188mm
	Operational humidity	From 65% ±15% at 25°C
Analog INPUT	ADC type	Σ-Δ ADC
	Voltage Channels	16 channels, 16 bit
	Voltage Range	±10 V
Analog OUTPUT	Channels	8 channels, 12bit
	Output Range	0 – 10V
	Output Current	±5 mA
Digital INPUT	Channels	32 (4*8) Isolated channel
	Logic level 0	0 – 5 V
	Logic level 1	10 – 24 V
	Isolation voltage	250 V AC
Digital OUTPUT	Channels	32 (8*4) Isolated channel
	Open collector	To 30 V max.
	Output current	200 mA per channel
	Isolation voltage	250 V AC

SOFTWARE

The control system for IC-100 cyclotron uses commercial SCADA FlexControl running under RTOS QNX 4 [2]. QNX is UNIX-style scalable, multi-user, multi-tasking, real-time, network and POSIX-compliant operating system. FlexControl [3] is a process control system for the automation of technological processes. It is modular and scalable. We have developed a library of functions, which we have built into application to control the screen and the keyboard. It uses Photon Application Builder as graphical editor, object configurator and application compiler. In order to manage message queues for HMI client in the network we have developed Visualization Server. HMI allows analyze process data in real-time trend, store and retrieve a set of variables to repeat important system modes. Alarm server controls faulty operations and signalizes by means of ringing bell, message and/or printing. Reports can be hard copied and exported in text file.

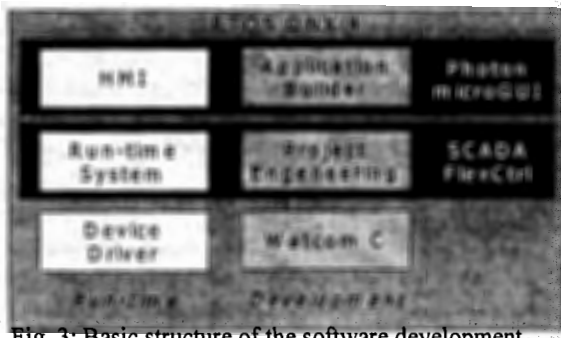

Fig. 3: Basic structure of the software development

It was developed device drivers for 3rd party equipment with unique remote control protocols (via RS-232):

- UHF synthesizer GM1718-02,
- UHF Power amplifier Neptun-18,
- Power supplies AMI-420 for superconductive magnets.

Data flow diagram [5] is shown on fig. 4.

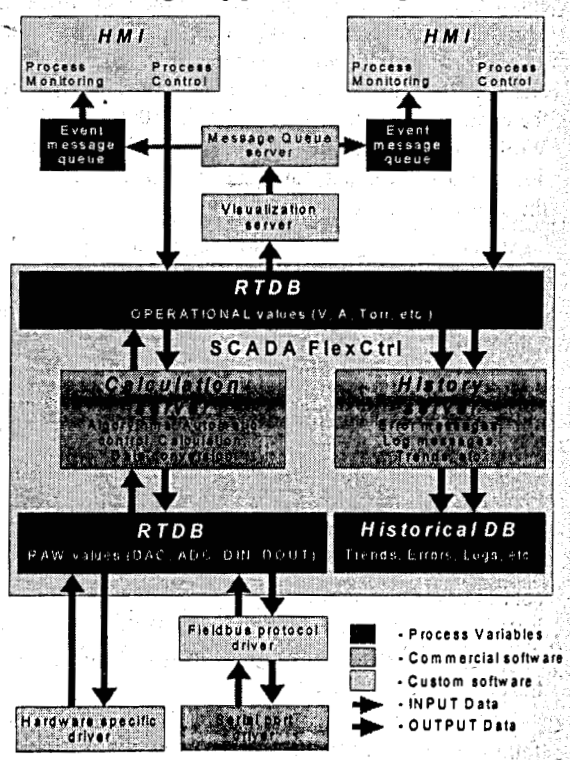

Fig. 4: Data flow

Basic structure of the software development [4] is shown on fig. 3. HMI for IC-100 cyclotron systems were designed as follows:

- Vacuum system (axial injection, see fig. 5, cyclotron, extraction and beam line)
- Beam transport magnets and beam diagnostics system
- ECR source and superconductive magnets diagnostics
- RF system
- Cooling system

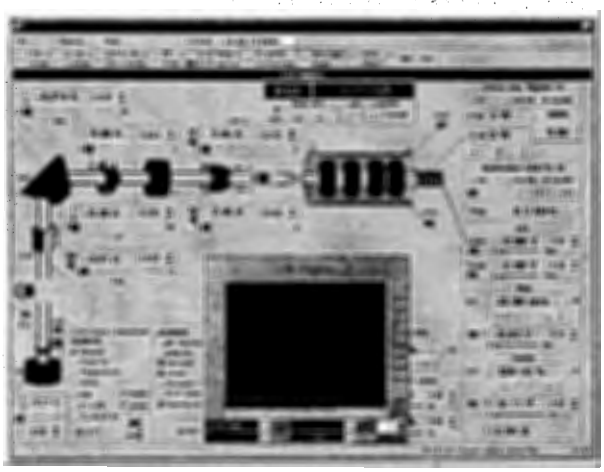

Fig. 5: IC-100 Axial injection HMI

Using commercial SCADA for a control system decreases total project development time, unifies data processing and allows concentrating more on visualization and automation algorithms. It also increases reliability and endurance of the software since the core of the system is well optimized and tested.

REFERENCES

[1] SIMATIC Controllers. http://www.ad.siemens.com

[2] Rob Krten, "Getting started with QNX 4. A Guide for Realtime Programmers". PARSE Software Devices, 1998.

[3] FlexControl - System Architecture Manual. BitCtrl GmbH. October 1998.

[4] V. Aleinikov, S. Paschenko, "Using commercial SCADA in control system for ECR CyLab." PCaPAC 2000. Hamburg.

[5] V. Aleinikov, A. Nikiforov, "Integtrating custom software and commercial SCADA." NEC 2003. Varna

HIGH-FREQUENCY SYSTEM OF THE CYCLOTRON DC - 72

G. Gulbekian, Dubna, FLNR, 141980 Russia
M. Hudak, Dubna, FLNR, 141980 Russia, On leave from the Slovak University of Technology

Abstract

The basic parameters of a RF system of a cyclotron DC-72 are presented in the given article. The results are obtained by virtue of numerical calculations using the software package POISSON SUPERFISH and are checked in the series of measurements using the resonator model with the scale 1:1.

INTRODUCTION

The azimuthally varying field cyclotron DC – 72 accelerates ions from H to Xe over an energy range 2.5 MeV per nucleon for heavy ions like Xe^{+18} to 72 MeV for protons. The orbital frequency of ions ranges from 3.08 to 16 MHz. The ions are accelerated by two independent resonators with an acceleration voltage up to 60 kV in the 2nd; 3rd, 4th, 5th or 6th harmonic mode. This requires a frequency range of 18.25 - 32 MHz for the RF system.

RESONATORS

The resonators are coaxial λ/2-cavities, which are symmetric with respect to the median plane and are located up and down in the yoke magnet. Dees are located in the valleys of the magnet poles.
The calculated main RF and mechanical characteristics are summarized in Table 1.

Table 1: Resonator characteristics

frequency range	[MHz]	18.25 - 32
cavity type:		coaxial λ/2
cantilever length	[mm]	2x2070
electrode angle	[°]	40
accelerating gap width	[mm]	10 at injection 40 at extraction
vertical aperture	[mm]	30 (20 at injection)
inner line diameter	[mm]	106
outer line diameter	[mm]	400
coarse tuning system		sliding short
sliding short displacement	[mm]	1200
fine tuning system		adjustable plate
coupling system		stable plate and variable capacitor
extraction radius mm	[mm]	1120
peak voltage range	[kV]	up to 60
Q factor		about 6000
maximum RF power	[kW]	19
RF probes		4 capacitives

RF CALCULATIONS AND MEASUREMENTS USING THE RESONATOR MODEL

RF calculations were performed with the software package POISSON SUPERFISH [1].

Drawing of the resonator model and the dee are shown on Figure 1.

For calculations we used equivalent scheme where dee was replaced with a cylinder. The capacitance of the equivalent cylinder and of the dee is the same.

Figures 2 to 4 show the calculated and measured resonant frequencies at different position of sliding shorts and Q factor and power dissipation at different frequencies respectively.

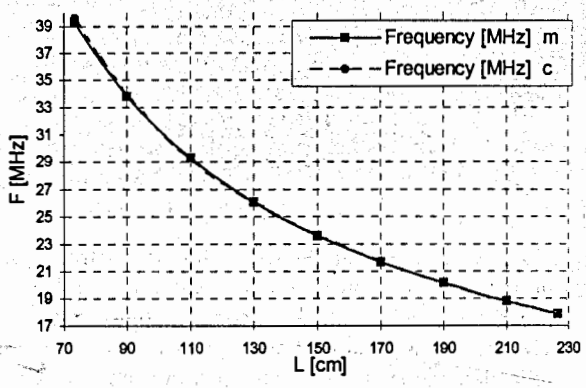

Figure 2: Calculated and measured resonant frequencies at different position of sliding shorts.

For variable sliding shorts at the distance of 735 to 2265 mm from median plane a resonant frequency range from 39.091 to 17.759 MHz for calculated and from 39.260 to 17.855 MHz for measured values.

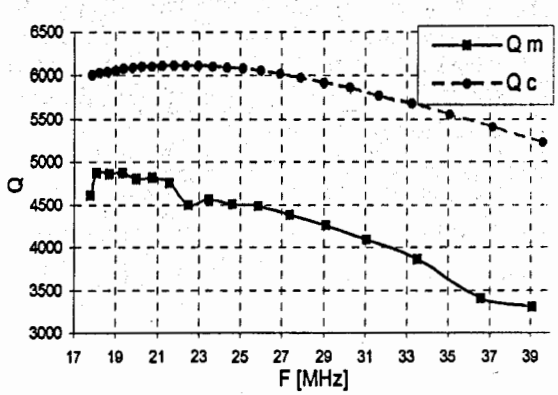

Figure 3: Calculated and measured Q factor at different frequencies.

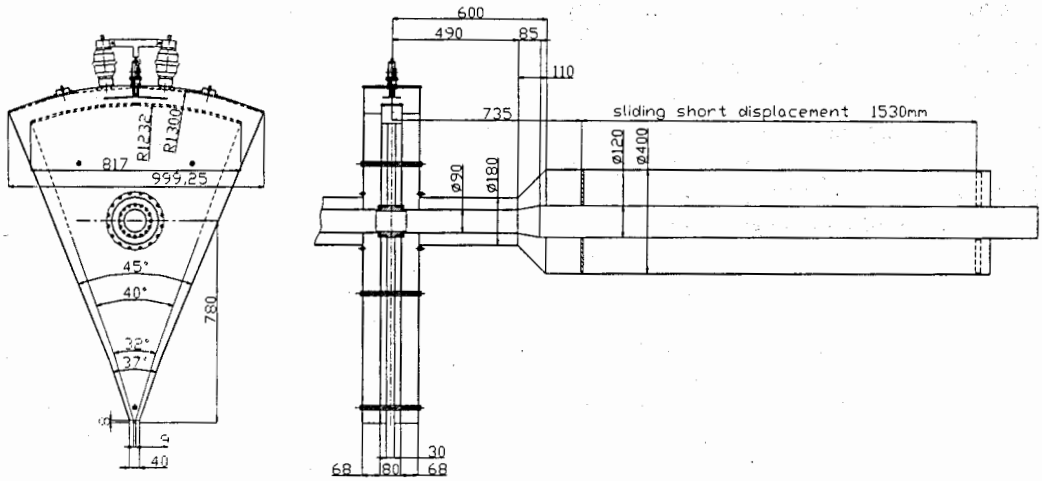

Figure 1: Drawing of resonator model with the scale 1:1.

Q factor was measured with a delta mode method (see Eq. 1). Q factor is 6115 to 5225 in the case of calculation and 4875 to 3310 for measurement at different frequencies.

$$Q = \frac{F_r}{F_2 - F_1} \tag{1}$$

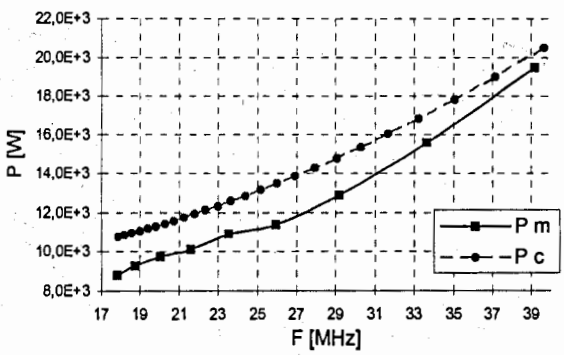

Figure 4: Calculated and measured power dissipation at different frequencies.

The value of measured power dissipation was calculated with an equivalent capacitance of resonator and Q factor (see Eq. 2, 3, 4).
Equivalent capacitance is:

$$C_{eq} = \frac{F_r \cdot \Delta C}{2 \cdot \Delta F}, \qquad \Delta F = F_r - F_{rC}, \tag{2}$$

where ΔC is a appended capacitance, F_r is a resonant frequency and F_{rC} is a resonant frequency with an appended capacitor set on the dee at maximum value voltage.
Shunt resistance is:

$$R_{Sh} = \frac{Q}{2 \cdot \pi \cdot F_r \cdot C_{eq}}. \tag{3}$$

Power dissipation is:

$$P = \frac{U_{dee}^2}{2 \cdot R_{Sh}}. \tag{4}$$

Power dissipation is calculated for U_{dee} = 60 kV and range from 10.75 to 20.50 kW for calculation and from 8.6 to 19.5 kW for measurement at different frequencies.

COMPARISON OF CALCULATIONS WITH MEASUREMENTS

Frequency Range

In the case of calculation two-dimensional cylindrical equivalent gives the best results compared with measured values.

Q Factor

Q factor depends on quality of electrical contacts and material properties of resonator. Difference between measured and calculated values was mainly due to ideal electrical contacts used in equivalent scheme.

Power Dissipation

Indirect method measurement of the power dissipation results in an accumulation error consisted of Q factor measurement and equivalent capacitance measurement.

CONCLUSIONS

RF system of a cyclotron DC – 72 was designed by virtue of computer simulation and measurements using

the resonator model with the scale 1:1. In the near future series of cold measurements and the first power tests for the RF system will be carried out in resonators.

REFERENCES

[1] James H. Billen and Lloyd M. Young, POISSON, SUPERFISH LA-UR-96-1834, The Regents of the University of California. Copyright, 1985-2001

APPLIED LOW-ENERGY CYCLOTRON

M.F. Vorogushin, Yu.N. Gavrish, A.V. Galchuk, L.I. Korolev, V.G. Mudrolyubov, A.V. Stepanov, A.P.Strokach, FSUE "D.V. Efremov Scientific Research Institute of Electrophysical Apparatus", St. Petersburg, Russia

Abstract

Design parameters of the cyclotron intended for the acceleration of protons at an energy ranging from 0.2 to 2.5 MeV at an extracted beam current of 200 μA are presented in the paper. The features of the cyclotron are its small overall sizes and low energy consumption. The cyclotron is equipped with a computer control system. The machine can be applied for studies of the radiation resistance of radio-electronic components and structural materials as well as for the element express analysis using such methods of nuclear physics as PIXE, RBS and resonance nuclear reactions.

In addition, energy variable over a wide range allows profile distribution studies of implanted materials. With this aim in view, the cyclotron can be equipped with a beam transport line with a scanning system and a chamber for material irradiation.

INTRODUCTION

A source of accelerated protons with energies ranging from 200 keV up to 2.5 MeV with a beam current of 120-150 μA and energy spread of no more than 0,5 % (FWHM) is of obvious interest for the research into the radiation resistance of structural materials and radio-electronic components. Irradiated objects are up to 30×30 cm in sizes, and in this view the accelerator should be equipped with a beam transport line and a system for beam scanning along the surface of an inspected object.

Important requirements are: simple and reliable operation, low energy consumption and computer control of the machine. Nowadays, high- voltage accelerators are used to produce beams with the characteristics mentioned above. The machines offering such advantages as high energy stability, low emittance of the beam extracted from the ion source and continuous mode of operation, however, suffer from such serious drawbacks as large dimensions and high cost.

Cyclotrons are known to be widely applied in the research into the radiation resistance of the structural materials of nuclear reactors as well as for studying the wear of units under stress. For these purposes beams of protons, deuterium ions and multi-charged high energy ions (10-30 MeV/nucleon) are used. In the Karlsruhe Laboratory, 26 MeV proton beams are extracted through a thin foil into the atmosphere and transported into a special chamber with samples under study. Similar works were done on the U-150 cyclotron in Obninsk.

In modern isochronous cyclotrons allowable significant reduction of the accelerating voltage amplitude and, correspondingly, air gaps of the electromagnet makes possible reduction of the weight, sizes and energy consumption of the whole facility. The RF system operates in the continuous mode, and there are no problems in the production of a 100-200 μA (and higher) beam of protons. Thus, cyclotrons can be considered as a potential source of accelerated protons with energy of several MeV.

CHOICE OF CYCLOTRON PARAMETERS

In late eighties a DC-3 cyclotron was designed and manufactured in NIIEFA for the acceleration of deuterium ions up to a fixed energy of 3 MeV. When the amplitude of the voltage across the 180° dee was 14 kV, the beam current at the final radius was 500 μA, and that at the external target amounted to 150 μA. The machine weight was 5 tons, energy consumption – 35 kW [1]. The cyclotron was used for activation analysis – to determine the content of light elements in the matrices of heavy metals.

The new cyclotron project is distinguished with a comparatively low energy of accelerated protons and energy variation over a range of 0.2-2.5 MeV.

The acceleration process on this cyclotron can be schematically divided into three stages. The first is the motion of ions in the center, which is characterized with changes in the position of orbit centers and grouping of the phases captured in the process of acceleration. Usually up to the 6-10th turns, the position of orbit centers is stabilized, which points to the beginning of the 2nd stage – the acceleration of ions in the isochronous mode. The duration of this stage depends on the cyclotron energy and amounts to from several tens up to several hundreds of turns. At the 3rd stage the beam is deflected from the final radius and extracted to external target (1-2 turns); thus the acceleration process is finished.

In the considered case at a minimum energy of the cyclotron of 0.2 MeV, the energy gain is reduced, as the number of turns in the process of acceleration should be not less than 20-25. Consequently, the energy gain per turn should not exceed 8-10 keV. At a maximum energy of 2.5 MeV, the energy gain can be increased up to 25-30 keV, and the number of turns in the process of acceleration can be respectively increased up to 80-100.

In connection with the above-said, the choice of the accelerating structure parameters should be grounded on the practical feasibility of minimum energy gain per turn, ΔW. As is well known, $\Delta W = 2nU_d Sin(q\vartheta/2)$, where n is the dee number, U_d is the amplitude of the accelerating

voltage across the dee, q is the harmonic mode of the accelerating voltage frequency, ϑ is the dee azimuthal length. Thus, the minimum energy gain occurs in an accelerating structure with a single 180° dee. Unfortunately a single dee with the angular length different from 180° cannot be used because of the microtron effect resulting in the drift of orbits and loss of radial stability. The values of energy gain given above take place when the amplitude of voltage across the dee is chosen from 4 up to 15 kV and the minimum amplitude value corresponds to low magnetic field induction, that is important when centering orbits and for detouring the ion source head.

In the energy range between 0.2 and 2.5 MeV the magnetic rigidity of protons is varied from 0.0646 up to 0.2284 Tm. If the magnet pole diameter is taken to be 600 mm, the final acceleration radius is ~260 mm. The magnetic field strength should vary from 0.248 up to 0.879 T, and the proton rotation frequency- from 3.79 up to 13.42 MHz. The machine can operate at q = 3, and taking this fact into account, the frequency range must be 3. The smaller possible value of the frequency band lower boundary is preferable, however, this results in larger sizes of the resonance system. The frequency band of 8-24 MHz is a reasonable compromise.

Low magnetic induction and weak relativistic effect of accelerated protons (β_{min} = 0.0206 at W = 0.2 MeV, β_{max} = 0.073 at W = 2.5 MeV) make much easy the formation of required magnetic field. In the design range of energy variation the radial increase of the average magnetic field is from 0.05 up to 2.3 mT (0.5-23 G). The azimuthal variation applied in the magnetic field at a level of 10-15% from the average value is sufficient for effective beam focusing in vertical direction.

An electrostatic deflector and radically-focusing magnetic channel will be used for beam extraction. In the beam extraction area turns are separated due to precession of orbit centers by introducing the controlled first harmonic of the magnetic field. Comparatively low strengths of the deflector electric field (50-80 kV/cm) are sufficient for effective beam extraction. No difficulties are expected to emerge with the septum cooling, as its heat losses will amount to no more than 200-300 W. The septum activation will be also low, and therefore no problems with repair/maintenance works in the vacuum chamber of the cyclotron are anticipated.

From the known voltage across the dee, the air gap of the electromagnet can be found. It is formed by: the dee aperture – 10 mm, thickness of the dee covers – 6×2 = 12 mm, high-frequency gap – 12.5×2 =25 mm, sectors with liners – 10×2 = 20 mm; totally – 67 mm in the "hill" and 87 mm in the "valley". The "valleys" house low–power gradient coils, which can be also used for the correction of the first harmonic of the magnetic field azimuthal instability.

Main Parameters of the Cyclotron:

- Accelerated ions.....H^+
- Energy (variable), MeV.....0.2-2.5
- Energy spread (FWHM), %.....0.5
- Current, μA.....200
- Irradiation field sizes, mm2.....300×300
- Proton flux density on target, nA/cm^2.....0.1-100
- Beam current instability for 1 h, %.....not worse than 5
- Flux density inhomogeneity on irradiated surface, %.....no more than 20
- service life of the ion source cathode, h.....200 (can be replaced within 20 minutes)

Power Consumption

- Stand-by condition, kW.....<15
- Beam on target, kW.....35

Magnetic Structure

- Shielding type magnet
- Pole diameter, cm.....60
- Number of sectors (per pole).....4
- Average induction, T.....0.3-0.9
- Gap (hill/valley), mm.....70/90
- Overall dimensions, mm:
  - outer diameter.....1300
  - height.....1000
- Magnet weight (Fe/Cu), t.....5/0.6
- DC power in coils, kW.....5

Radio-frequency System

- Number of dees.....1
- Dee angle.....1800
- Harmonic mode.....1 and 3
- Frequency range, MHz.....8-24
- Dee voltage amplitude (max), kV.....15
- Dissipated RF power per dee, kW.....7
- RF oscillator output power, kW.....10

Ion Source

- Type of source.....PIG
- Location.....internal
- Arc power, kW.....1

Beam Extraction and Diagnostics

The beam is extracted with an electrostatic deflector with radially focusing magnetic channel. A water-cooled internal probe with remote control is used for the cyclotron adjustment.

Pumping System

- Number of diffusion pumps.....2
- Pumping speed, l/s.....3500
- Mechanical pump with pumping speed, l/s.....10
- Operating vacuum, torr.....$(1\text{-}2)\cdot10^{-5}$

Beam Transport Line and Scanning System

The beam of accelerated protons via the beamline is transported from the cyclotron to the target chamber where samples up to 300×300 mm are irradiated. The beamline is equipped with an independent pumping system, electromagnetic devices for correction of the beam position, beam focusing, measuring the beam parameters and beam scanning across an irradiated sample.

Control System

The control system of the cyclotron is based on a programmable controller with a computer. The control system includes a control rack, a control console of table-top type with a computer and keyboard.

CYCLOTRON LAYOUT

The cyclotron may have a standard layout (Fig. 1), similar to that of the DC-3 cyclotron, with the only difference-the resonance system with a triple frequency range. The dee in the chamber can be mounted on the insulator, and in this case the device for adjustment of the resonance system frequency can be located at atmospheric pressure.

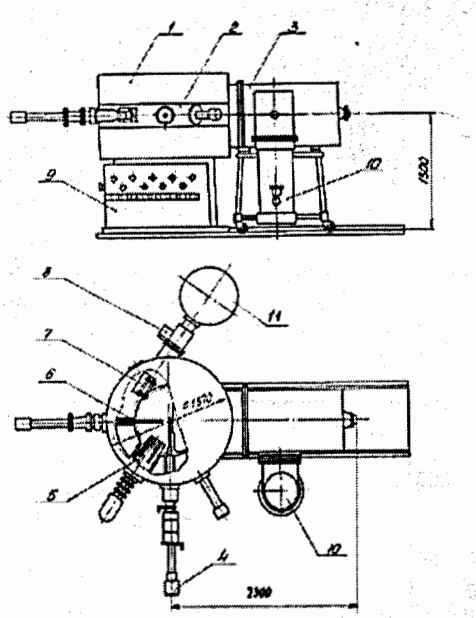

Figure 1: General view of the cyclotron.
1 – magnet, *2* – accelerating chamber, *3* – resonance system, *4* – source, *5* – deflector, *6* – probe, *7* – magnetic channel, *8* – gate valve, *9* – water distributing board, *10* – vacuum pump, *11* – target chamber.

REFERENCES

[1] A.N. Galaev, A.V. Galchuk, P.V. Bogdanov et al. Compact deuteron cyclotron for activation analysis, 6th All-Union Conference on Applied Charged Particle Accelerators. L., 1988; M-TSNIIatominform, 1988, p. 211-212.

INJECTION SYSTEM OF THE COMPACT CYCLOTRON

G.A. Karamysheva, L.M. Onischenko, JINR, Dubna, Russia

Abstract

Compact Cyclotron will be equipped with the external ion source. Since the injection system will transport space charge dominated, high-intensity beams, the injection energy must be as high as practically achievable (limited by the voltage holding capability spiral inflector). Ions energy from ion source will be equal 30 keV.

The injection system consists of a double-drift beam bunching system, a spiral inflector, beam analysis diagnostics, focusing and adjustment elements.

The design and optics characteristics for the injection line (buncher-qudrupole doublet-inflector) are described and the results of the computer simulations taking into account space charge effects are presented.

The injection axis is vertical, while the cyclotron's acceleration plane is horizontal.

BEAM DYNAMIC COMPUTER SIMULATIONS

Numeric simulations are carried out for 500 particles using code for calculation of particle dynamics by integration of differential equations in Cartesian coordinate system written in MATLAB. Direct Coulomb particle-to-particle method is used to take into account space-charge effects. 3D electrostatic field calculations are performed for particle motion simulation through the inflector. 3D magnetostatic calculations of the qudrupole doublet are also made. Calculated electric and magnetic field maps are used for beam dynamic simulations.

First of all particle dynamic modelling in buncher and inflector is carried out. Finally the beam motion in different variants of injection line (including focusing elements, buncher and inflector) is simulated.

THE AXIAL BUNCHER

To guarantee 100% beam bunching efficiency beam-bunching system should use an ideal saw-tooth waveform. However, a high-power, high frequency saw-tooth wave generator is expensive and quite difficult to realize in practice. Generally, bunchers use sinusoidal waveform generators with a few higher order harmonics.

In our simulations we use a double-drift buncher design (the buncher gap is 5 mm and the distance between 2 gaps is $3/2\beta\lambda$ (92 mm)) with sinusoidal waveform. The main advantages of sinusoidal bunching system are simplicity in structure and low cost. Initial transversal emittances were equal to $5\times20 = 100\ \pi$ mm mrad, initial phase extension – 360° RF. Voltage amplitude on the sinusoidal buncher was 1500 B, providing focus location from buncher – 40 cm.

Fig. 1 and Fig. 2 demonstrate beam bunch creation along z-axis after sinusoidal buncher (z = 0 corresponds to the beginning of the first accelerating gap). Figure 1 – without space charge effects, Fig. 2 – taking into account space charge effects (DC beam intensity I = 5 mA).

Number of particles in one histogram bin corresponds to number of particles within bunch width 36°RF thus one can estimate efficiency of the buncher.

Sinusoidal buncher efficiency totals 60% for I = 0 mA and about 50% for I = 5 mA (bunching efficiency is the ratio of the number of particles within the bunch width (60°RF) to the total number of particles in an rf cycle). Energy spread induced by sinusoidal buncher is equal to ±3 keV. Such energy spread is required to compensate Coulomb forces in space charge dominated beam.

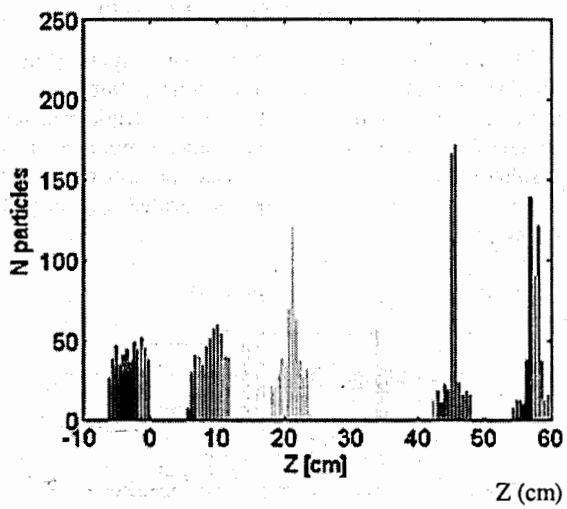

Figure 1: Sinusoidal buncher, without space charge effects, (number of particles in one histogram bin corresponds to the number of particles within bunch width 30°RF).

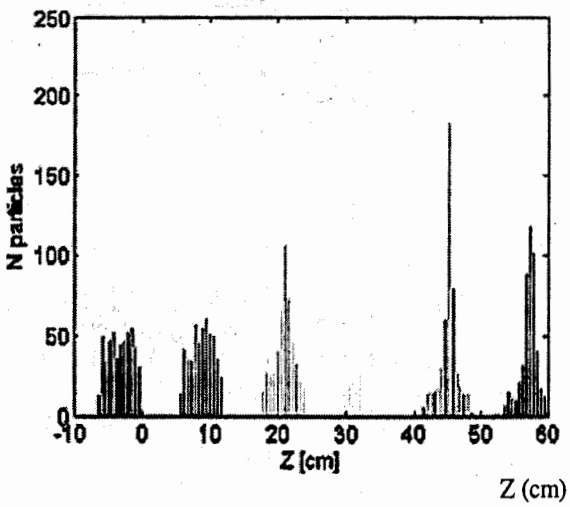

Figure 2: Sinusoidal buncher (taking into account space charge effects).

Fig. 3, 4 show beam energy variation vs time. One can see energy spread narrowing induced by space charge.

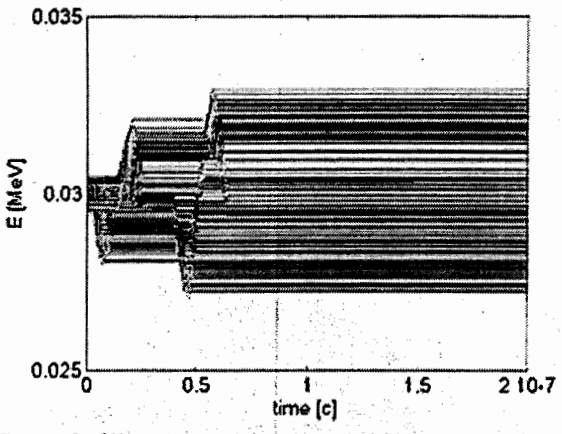

Figure 3: beam energy vs time (without space charge effects).

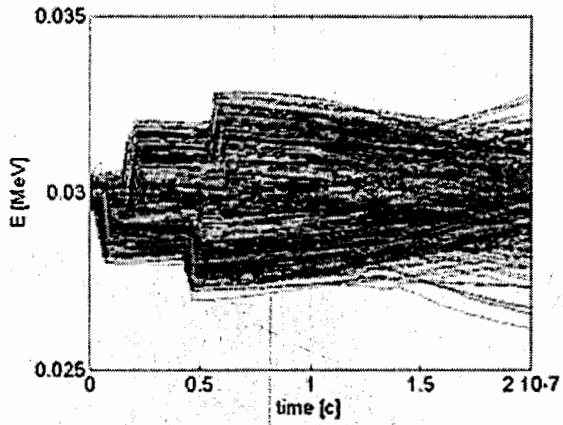

Figure 4: beam energy vs time (taking into account space charge effects).

Thus space charge effects decrease efficiency of the buncher. For a 5 mA unbunched circulating beam, 30 kV injection energy, h = 4 the optimum position for the buncher less than 0.40 m from focus location.

For more accurate results it is necessary to perform 3D-numeric simulation of the buncher gap field to take into account fringe field effects.

QUADRUPLE DOUBLET- BUNCHER – INFLECTOR.

Quadrupole doublet is used for injection line focusing. The quadrupole doublet rotation with respect to the inflector ensures an optimal matching capability. Computer model of the inflector is described in [1]. View of the quadrupole doublet computer model is presented in Fig. 5. A layout of the injection system is shown schematically in Fig. 6.

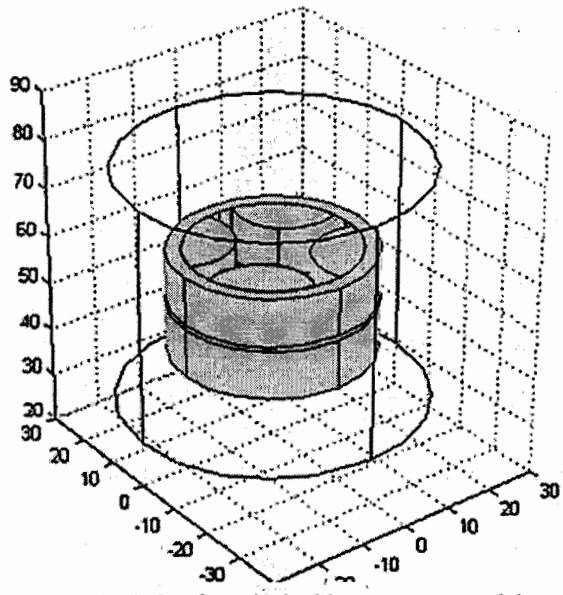

Fig.5: Quadrupole doublet computer model

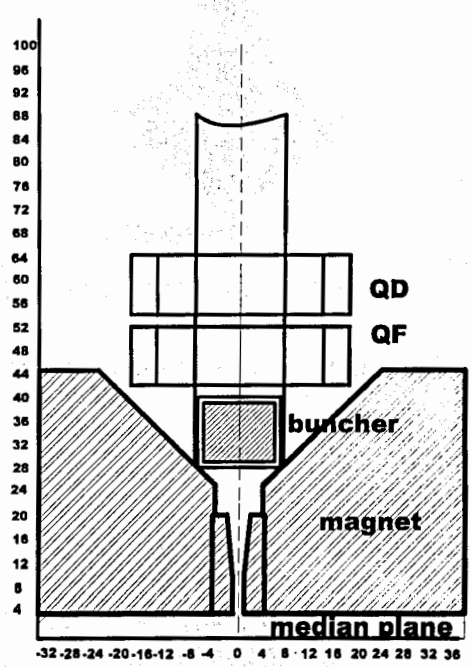

Figure 6: Layout of the injection system.

Quadruple field gradients less than 30 mT/cm, effective length of the quadruples – 10 cm, aperture diameter – 15 cm.

The position for the buncher is 0.4 m from the cyclotron median plane. Beam trajectories in axial injection line are demonstrated in x-z and y-z axis (z – along the injection line) in Fig. 7, Fig. 8.

In Fig. 9 beam axial emittance at the exit from inflector is shown.

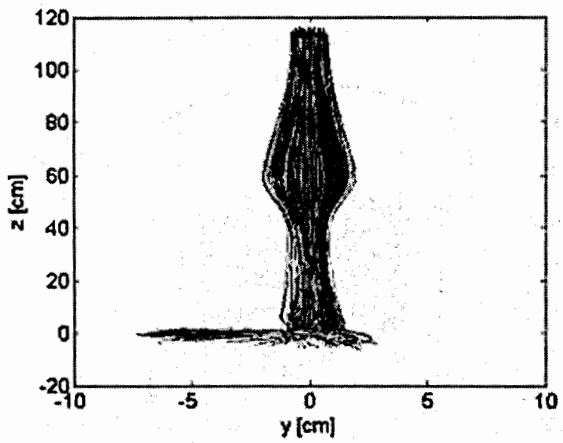

Figure 7: Beam trajectories in axial injection line in Z-Y axis.

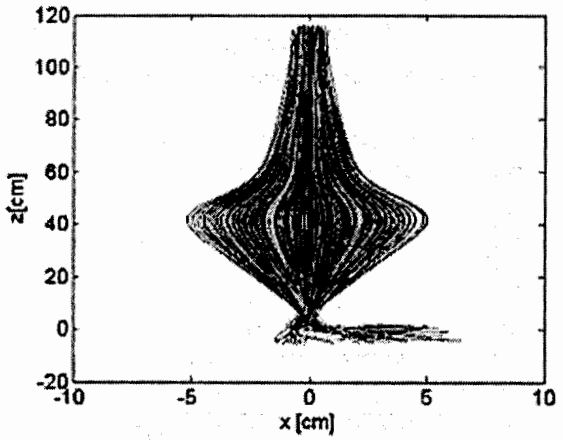

Figure 8: Beam trajectories in axial injection line in Z-X axis.

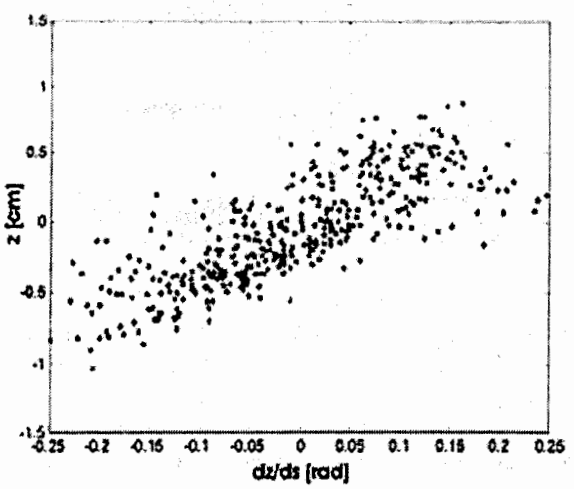

Figure 9: Beam axial emittance at the exit from the inflector.

The beam losses totaled ~ 10 %. The axial divergence of the beam (see Fig. 8) can cause additional losses in the center of cyclotron. Bunch azimuth distribution in the first accelerating gap is presented in Fig. 10. Efficiency of the buncher is about 50%. It is necessary to perform additional simulations paying particular attention to the matching between the injection line and the cyclotron central region. Fig. 11 shows beam energy distribution in the first gap. It is clear that accurate estimation of the beam losses in the cyclotron center may be done after realization integrate modelling of the central region.

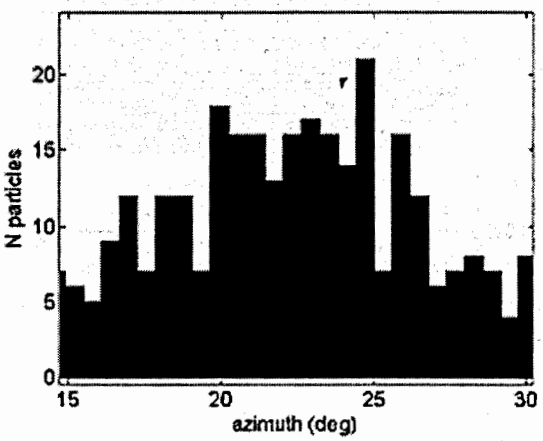

Figure 10: Bunch azimuth distribution in the first accelerating gap.

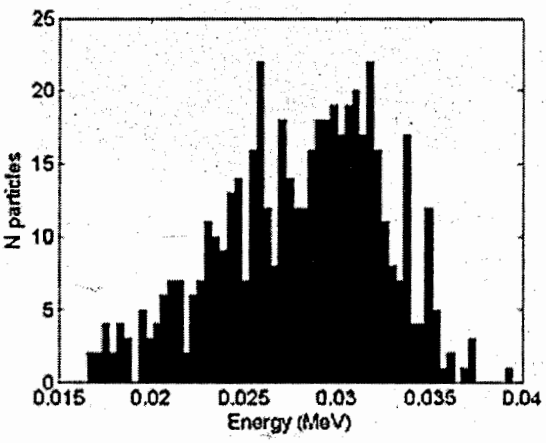

Figure 11: Beam energy distribution in the first gap.

CONCLUSION

Computer modelling confirmed the possibility of high-intensity beam transmission, bunching and bending from axial to median plane with losses less than 10 % at an injection voltage of 30 KeV (DC beam intensity I = 5 mA). Bunching efficiency is about 50%. Precise estimation of beam losses in the cyclotron center may be done after realization 3D modelling of the central region and computer simulation of beam matching to the acceptance of the cyclotron.

REFERENCES

1. G.A.Karamysheva, L.M.Onischenko, Spiral inflector for compact cyclotron, this conference.

Russian Particle Accelerator Conference (RUPAC'2004) (19; 2004; Dubna).

R95 Proceedings of the XIX Russian Particle Accelerator Conference (RUPAC'2004) (Dubna, October 4–8, 2004). — Dubna: JINR, 2005. — 176 p.

ISBN 5-9530-0079-0

The Proceedings of the XIX Russian Particle Accelerator Conference (RUPAC'2004) include oral and invited reports. The conference took place at the Joint Institute for Nuclear Research on 4–8 October 2004 in Dubna, Russia. About 300 participants from scientific, educational and industrial centers of Russia and leading accelerating laboratories of the world took part in the conference. The scientific programme included 79 oral and 129 poster reports devoted to modern status of acceleration science and technique.

The Proceedings are of interest to scientists and engineers specializing and working in the field of accelerator physics and techniques.

Всероссийская конференция по ускорителям заряженных частиц «RUPAC'2004» (19; 2004; Дубна).

Труды XIX Всероссийской конференции по ускорителям заряженных частиц «RUPAC'2004» (Дубна, 4–8 октября 2004 г.). — Дубна: ОИЯИ, 2005. — 176 с.

ISBN 5-9530-0079-0

В сборнике представлены доклады XIX Всероссийской конференции по ускорителям заряженных частиц «RUPAC'2004», прошедшей в Объединенном институте ядерных исследований с 4 по 8 октября 2004 г. В работе конференции приняло участие около 300 специалистов из научных, образовательных и промышленных центров России и ведущих ускорительных лабораторий мира. Программа конференции включала 79 устных и 129 стендовых докладов, дающих достаточно полное представление о современном состоянии ускорительной науки и техники.

Сборник представляет интерес для научных работников и инженеров, специализирующихся и работающих в области физики и техники ускорителей.

УДК 621.384.6(063)
ББК 22.381.1я.431

Научное издание

XIX Russian Particle Accelerator Conference (RUPAC'2004)

Proceedings of the Conference

XIX Всероссийская конференция по ускорителям заряженных частиц «RUPAC'2004»

Труды конференции

E9-2005-43

Сборник отпечатан методом прямого репродуцирования
с оригиналов, предоставленных оргкомитетом.

Ответственная за подготовку сборника к печати *Е. Э. Ширкова.*

Получено 12.05.2005. Подписано в печать 12.05.2005.
Формат 60 × 84/8. Бумага офсетная. Печать офсетная.
Усл. печ. л. 20,46. Уч.-изд. л. 31,46. Тираж 150. Заказ 54869.

Издательский отдел Объединенного института ядерных исследований
141980, г. Дубна, Московская обл., ул. Жолио-Кюри, 6.
E-mail: publish@pds.jinr.ru
www.jinr.ru/publish/